Title
Selection and scaling of ground motions for nonlinear response history analysis of buildings in performance-based earthquake engineering

Author
Kwong, Neal Simon

Publication Date
2015

Peer reviewed|Thesis/dissertation

Selection and scaling of ground motions for nonlinear response history analysis of buildings in performance-based earthquake engineering

by

Neal Simon Kwong

A dissertation submitted in partial satisfaction of the

requirements for the degree of

Doctor of Philosophy

in

Engineering – Civil and Environmental Engineering

in the

Graduate Division

of the

University of California, Berkeley

Committee in charge:

Professor Anil K. Chopra, Chair
Professor Stephen A. Mahin
Professor Douglas S. Dreger

Spring 2015

Selection and scaling of ground motions for nonlinear response history analysis of buildings in performance-based earthquake engineering

Abstract

Selection and scaling of ground motions for nonlinear response history analysis of buildings in performance-based earthquake engineering

by

Neal Simon Kwong

Doctor of Philosophy in Engineering – Civil and Environmental Engineering

University of California, Berkeley

Professor Anil K. Chopra, Chair

This dissertation investigates the issue of selecting and scaling ground motions as input excitations for response history analyses of buildings in performance-based earthquake engineering. Many ground motion selection and modification (GMSM) procedures have been developed to select ground motions for a wide variety of objectives. In this research, we focus on the selection and scaling of single, horizontal components of ground motion for estimating seismic demand hazard curves (SDHCs) of multistory frames at a given site.

In Chapter 2, a framework is developed for evaluating GMSM procedures in their ability to provide accurate estimates of the SDHC. The notion of a benchmark SDHC is introduced, enabling biases caused by GMSM procedures to be isolated from other sources of bias. More importantly, the ability to quantify bias facilitates the identification of intensity measures (IMs) that are sufficient [1]. However, this approach is limited by the availability of recorded ground motions and of prediction models for engineering demand parameters (EDPs) of structures.

The framework developed in Chapter 2 is applied to synthetic ground motions in Chapter 3, where biases in estimates of SDHCs caused by GMSM procedures can be estimated for any structural system and any EDP. However, the use of synthetic ground motions gives rise to the issue of developing *benchmark-consistent* ground motion prediction models. Based on the results from Chapters 2-3, it is hypothesised that the potential bias in any SDHC estimate is caused directly by two important properties of the particular selection of ground motions: (i) hazard consistency, and (ii) IM sufficiency.

A novel ground motion selection procedure, rooted in the theory of Importance Sampling, is developed in Chapter 4 that allows: (i) hazard consistency of the selected motions to be directly enforced for a user-specified collection of IMs, and (ii) SDHCs of a structure to be estimated from a single ensemble of ground motions, with the option of avoiding record scaling altogether. This procedure, together with two other contemporary GMSM procedures – (i) "exact" Conditional Spectrum and (ii) Generalized Conditional Intensity Measure – are

[1] Strictly speaking, only IMs that are *insufficient* may be identified.

evaluated in Chapters 5-6 for a variety of structural systems and EDPs at a specified site. In these chapters, the amount of effort involved in implementing these procedures for estimating SDHCs is summarized in a step-by-step form, and the magnitude of biases caused by these procedures are documented.

To the loving memory of my grandmother.

Contents

List of Figures

List of Tables

Acknowledgments

The research in this dissertation is supported primarily by the National Science Foundation Graduate Research Fellowship Program under Grant No. DGE 1106400. Additional support is provided by the Popert fellowships from the SEMM program at UC Berkeley and by funding from the US Geological Survey (USGS). These sources of support are gratefully acknowledged. In addition, any opinions, findings, and conclusions or recommendations expressed in this work are those of the author and do not necessarily reflect the views of these sponsors.

I wish to thank Prof. Cosmas Tzavelis for encouraging me to pursue graduate studies in structural engineering and Dr. Erol Kalkan for helping me get started on research in earthquake engineering. I also wish to thank the faculty of the SEMM program (in particular, Professors Anil Chopra, Filip Filippou, Stephen Mahin, Jack Moehle, Khalid Mosalam) and of the statistics department (in particular, Professors Haiyan Huang, Jon McAuliffe, Nathan Ross, Bin Yu) at UC Berkeley for their incredible dedication towards teaching and their influence on my professional development.

I am grateful to Dr. Robin McGuire, Prof. Jack Baker, and Prof. Brendon Bradley for their valuable feedback on many parts of this research; to Dr. Yoshi Yamamoto, Prof. Norman Abrahamson, Prof. Yousef Bozorgnia, and Prof. Ting Lin for fruitful discussions related to various pieces of this research; to Dr. Yoshi Yamamoto and Prof. Curt Haselton for providing the computer models of the multistory buildings used in this dissertation; and to Dr. Frank McKenna for helping me improve the efficiency of performing dynamic analyses with the structural models.

Thanks to all of the staff and students at UC Berkeley who have made this doctoral program an enjoyable experience. In particular, I wish to acknowledge: Grigorios Antonellis, Ahmed Bakhaty, Gerd Brandstetter, Marco Broccardo, Mayssa Dabaghi, Panos Galanis, James Goulet, Christie Hale, Pardeep Kumar, Jiang Jun Lee, Yuan Lu, Mohamed Moustafa, Ahmet Tanyeri, and Tea Višnjić. Additionally, I am grateful to the UC Berkeley Handball team for all of the valuable lessons I've learned from the athletic competitions.

Words cannot express how much I am indebted to my mother and to my family for always having faith in me no matter what I do. I am fortunate to receive emotional support and encouragement from my girlfriend Cecilia Dao, my housemate Greg Wilson, and my friends in New York: Carl Dennis, Harold Mtonga, Kunal Oak, David Poon, Vikas Sathyaprakash, and Jeffrey Tan. I am also grateful to Helen Choe, Andrew Ma, and Charlotte Wong for their friendship and their occasional feedback on my research from a practical perspective. Last but not least, I wish to express my sincerest gratitude to my research advisor Prof. Anil Chopra. Thank you for always believing in me and serving as a role model; I am truly blessed for the opportunity to work with you and will never forget all that you have taught me.

Chapter 1

Introduction

Nonlinear response history analyses (RHAs) play a major role in performance-based earthquake engineering (PBEE) of buildings. By performing RHAs of a computer model of the building subjected to an input ground motion [1], seismic demands can be computed to determine seismic demand hazard curves (SDHCs). In PBEE of buildings, the computed seismic demands are used as inputs to fragility functions for predicting (both structural and nonstructural) damage [2]; e.g., SDHCs can be integrated with fragility functions to provide annual rates of damage exceedance. By predicting damage as a function of the seismic demand instead of the ground motion intensity (e.g., peak ground acceleration, etc.), the resulting estimate of damage is more informative because the variability in the estimate is reduced. Similarly, losses due to earthquakes (e.g., repair costs, business downtime, casualties, etc.) may be better predicted (through consequence functions) with knowledge about the damage in buildings (see e.g., Section 3.9 in [3]). Thus, nonlinear RHAs of building models are an important step in the estimation of losses due to earthquakes.

However, one of the key challenges in this approach is the selection and scaling of ground motions to serve as input excitations for nonlinear RHAs. Researchers have proposed many different ways to select ground motions. Some have proposed to select on the basis of matching seismological parameters for a given earthquake scenario ([4, 5, 6]) whereas others have suggested to select on the basis of spectral shape ([7, 8, 9]). In fact, many different intensity measures (IMs) have been investigated and/or developed for selection purposes ([10, 11, 12, 13, 14]). With such a wide variety of parameters to choose from, how does one identify those that are most desirable?

Regardless of the selection approach, ground motions are often scaled by factors of varying degrees before RHAs are performed. Although scaling offers the advantage of reducing the variability in the resulting demands ([15]), such modification of data raises many questions. For example, some researchers have argued that there is no need to limit the scale factors ([16, 17]) and that scaling does not cause bias in the demands ([18]). On the other hand, some have found that scaling may induce bias, depending on how ground motions were

[1] In this dissertation, the phrase "ground motion" refers to ground acceleration as a function of time, or ground motion time series.

selected ([19, 20]). Moreover, other researchers have suggested that the usefulness of results from scaling is questionable, providing limited if any information ([21]).

The objectives of this dissertation are as follows:

1. To develop a rigorous approach for evaluating SDHCs of a structure from any ground motion selection and modification (GMSM) procedure.

2. To understand the underlying reasons why bias in the demands is observed in some cases but not in others, leading to conflicting conclusions in the literature.

3. To develop a rigorous procedure for selecting ground motions with the option of avoiding record scaling altogether.

4. To comprehensively evaluate contemporary GMSM procedures in their ability to provide accurate estimates of the SDHCs of a structure at a given site.

In Chapter 2, various objectives for performing RHAs are organized, leading to the objective of estimating SDHCs as the appropriate choice for rigorously evaluating GMSM procedures. The notion of a *benchmark* is introduced and its importance in the context of evaluating GMSM procedures is discussed. It is found that the potential bias in any SDHC estimate is directly caused by hazard inconsistencies in the specific selection of ground motions with respect to IMs that are influential to the response. As long as ground motions are selected to be hazard-consistent with respect to a vector-valued IM that is sufficient, then the resulting SDHC estimates are unbiased, irrespective of the level of record scaling.

The framework developed in Chapter 2 is applied to synthetic ground motions in Chapter 3, in order to evaluate GMSM procedures for any structure and any response quantity of interest. Equipped with a rigorous benchmark, the relationship between SDHC bias, hazard consistency, and IM sufficiency is confirmed. Most importantly, the benchmark SDHC enables us to distinguish IMs (e.g., spectral shape, etc.) that are *insufficient* from those that are *approximately sufficient* for the response quantity of interest. Additionally, the issue of benchmark consistency arises for the first time as a consequence of evaluating GMSM procedures with synthetic ground motions; this issue is thoroughly addressed in this chapter.

In Chapter 4, an Importance Sampling based ground motion selection procedure is developed to take advantage of unscaled yet intense ground motions for estimating SDHCs. This procedure permits hazard consistency of the selected motions to be *directly* enforced for a wide range of IMs and exceedance rates, through different choices of the Importance Function. Furthermore, the procedure enables SDHCs of a structure to be estimated from a *single* ensemble of ground motions. The chapter concludes with recommendations for inputs to this procedure: (i) vector of IMs for ground motion selection **IM**, (ii) sample size n, (iii) maximum acceptable scale factor SF_{max}, and (iv) target fraction of scaled ground motions γ.

Using the concept of a benchmark, developed in Chapters 2-3, two state-of-the-art GMSM procedures – (i) "exact" Conditional Spectrum, and (ii) Generalized Conditional Intensity

Measure (GCIM) – are comprehensively evaluated in Chapter 5. First, the implementation of each procedure for estimating SDHCs is summarized in a step-by-step form. It is shown that the implementation can be quite involved, requiring several ensembles of ground motions to be iteratively selected until they are consistent with the target over a wide range of IMs. Second, the procedures are evaluated in their ability to accurately estimate SDHCs for a variety of structural systems and response quantities at a given site. It is found that spectral shape can be insufficient for estimating the annual rate of collapse and or for estimating floor accelerations. Furthermore, it is found that even a vector of IMs that includes spectral accelerations, peak ground measures, spectrum intensities, and cumulative effects, can be insufficient for estimating floor accelerations. Finally, the limitations of the bias-checking procedure in GCIM are identified, where it is shown that misleading conclusions may be obtained from the bias-checking procedure.

The evaluation of the Importance Sampling based procedure from Chapter 4 is the subject of Chapter 6. For the cases considered, the SDHCs from the Importance Sampling procedure are demonstrated to be unbiased for all systems and all response quantities, when ground motions are not scaled. When the procedure is implemented with scaled ground motions, the resulting SDHCs are unbiased for most, but not all, of the cases considered. The epistemic uncertainty in the SDHC estimates from the Importance Sampling procedure is controlled primarily by the Importance Function and secondarily by the number of ground motions. Given a judiciously chosen Importance Function, the procedure greatly simplifies the problem of selecting ground motions for estimating SDHCs; the selection of the Importance Function is discussed in this chapter.

Each of the chapters is written in a self-contained fashion. However, it is advisable to read Chapters2-3 first because the subsequent chapters borrow heavily on the material in these two chapters.

Chapter 2

A framework for the evaluation of ground motion selection and modification procedures

2.1 Abstract

This study develops a framework to evaluate ground motion selection and modification (GMSM) procedures. The context is probabilistic seismic demand analysis (PSDA), where response history analyses (RHAs) of a given structure, using ground motions determined by a GMSM procedure, are performed in order to estimate the seismic demand hazard curve (SDHC) for the structure at a given site. Currently, a GMSM procedure is evaluated in this context by comparing several resulting estimates of the SDHC, each derived from a different definition of the conditioning intensity measure (IM). Using a simple case study, we demonstrate that conclusions from such an approach are not always definitive; therefore, an alternative approach is desirable. In the alternative proposed herein, all estimates of the SDHC from GMSM procedures are compared against a benchmark SDHC, under a common set of ground motion information. This benchmark SDHC is determined by incorporating a prediction model for the seismic demand into the probabilistic seismic hazard analysis (PSHA) calculations. To develop an understanding of why one GMSM procedure may provide more accurate estimates of the SDHC than another procedure, we identify the role of "IM sufficiency" in the relationship between (1) bias in the SDHC estimate and (2) "hazard consistency" of the corresponding ground motions obtained from a GMSM procedure. Finally, we provide examples of how misleading conclusions may potentially be obtained from erroneous implementations of the proposed framework.

2.2 Introduction

Ground motion selection and modification (GMSM) procedures determine the necessary input ground motions for response history analyses (RHAs) of structures. RHAs of a structure are often performed in order to estimate the seismic demands, for one or more engineering demand parameters [1] (EDPs), resulting from a given ensemble of ground motions. The modification of ground motions can be classified into two approaches: (1) amplitude scaling, and (2) spectrum matching in the time or frequency domains. The framework developed in this document applies primarily to the former and secondarily to the latter.

Many different GMSM procedures are available in the literature. Some select and scale on the basis of scalar intensity measures (IMs). For instance, the spectral acceleration [2] at the fundamental period of the structure, $A(T_1)$, is a popular choice as an IM for record scaling (e.g., [17, 15]). Alternative choices for such scalar IMs include the peak deformation of inelastic Single-Degree-of-Freedom (SDF) systems (e.g., [24, 12, 14]). Several procedures select and scale ground motions on the basis of vector-valued IMs. For example, selecting records whose response spectra most closely matches a target spectrum is a common approach (e.g., [8, 25]). A review of various GMSM procedures is provided in Appendix A of [26] and in [27].

There has been much interest in evaluating GMSM procedures. For example, the Pacific Earthquake Engineering Research (PEER) GMSM working group [26], Heo et al [28], and Hancock et al [29] all compared estimates of the median demand of a structure, from RHAs for ground motions determined by GMSM methods, against a 'benchmark' that is defined differently in each of these studies. In the first study, the benchmark is derived from a regression model of the EDP as a function of IMs and the regression is applied to both scaled and unscaled ground motions; this benchmark is referred to as the Point-Of-Comparison [30, 26]. In the study by Heo et al, the benchmark is also derived from a regression model of the EDP as a function of IMs; however, the regression is applied to only unscaled ground motions. Hancock et al derive the benchmark from a regression model of the EDP as a function of seismological parameters (i.e., earthquake magnitude, distance, etc.), and the regression is applied to only unscaled ground motions.

In order to meaningfully evaluate GMSM procedures, the objective of the associated RHAs of the structure must be clearly stated. For example, researchers have been interested in probability distributions of the demand for a given:

1. Earthquake scenario;

2. Ground motion scenario;

3. Intensity level; and

[1] 'Engineering demand parameter' is a synonym for 'response quantity'.

[2] In this document, "spectral acceleration" refers to the pseudo-acceleration [22] for 5% damping corresponding to the arbitrary horizontal component of ground motion [23].

4. Time frame.

The PEER GMSM working group considers the estimation of the median and the complete distribution of 1 and 2 as four separate objectives of GMSM methods [26]. They define an *earthquake scenario* as an earthquake with a specific magnitude, M, distance, R, and rupture information (e.g., style of faulting, dip angle, shear wave velocity of the site, etc.) and a *ground motion scenario* as an earthquake scenario with a specified value of $A(T_1)$. We will use *rupture scenario* as a synonym for earthquake scenario.

The estimation of distributions 1 and 3 above are referred to as a scenario-based assessment and an intensity-based assessment, respectively [3, 31]. In an intensity-based assessment, the IM may be defined as a scalar or a vector; for example, it may be defined as the spectral acceleration at one vibration period or at several periods (i.e., a response spectrum). The estimation of distribution 4 is known as a time-based assessment, where the specified time frame depends on the needs of decision makers (e.g., one year, 50 years, etc.) [3], and the probabilities are converted from annual rates of exceedance, based on an assumption of earthquake occurrence in time [3] [32]. The process of determining these exceedance rates, or seismic demand hazard curves (SDHCs), is known as a risk-based assessment [31], or a probabilistic seismic demand analysis (PSDA) [33].

In this study, we develop a framework for evaluating GMSM procedures in the context of PSDA. This choice is motivated by the fact that for a given structure at a given site, distributions 1-3 above are not "unique"; for example, different versions of distribution 3 exist for different definitions of the IM and for different intensity levels under consideration [34]. In contrast, the SDHC from PSDA is unique for a given structure at a given site [35].

In the proposed framework, all estimates of the SDHC from GMSM procedures are compared against a benchmark SDHC, under a common set of ground motion information. The benchmark SDHC is determined by incorporating an EDP prediction model that is developed from unmodified ground motions into the probabilistic seismic hazard analysis (PSHA) calculations. Currently, a GMSM procedure is evaluated in the context of PSDA by comparing several resulting estimates of the SDHC, each derived from a different definition of the conditioning IM. To illustrate an important but subtle limitation of this approach, PSDA is critically examined next and a simple structural model at a realistic site is chosen as the case study.

2.3 Probabilistic Seismic Demand Analysis

The objective of performing RHAs in PSDA is to develop a SDHC for a given structure at a given site. Denoted by the symbol $\lambda_{EDP}(z)$, a SDHC is a plot of the annual rate of exceedance, λ, against the seismic demand; it is similar to a traditional hazard curve in PSHA, except that the IM on the horizontal axis has been replaced by the EDP. Once developed, SDHCs are used to: (1) determine the annual rate of seismic demand exceeding

[3] In this study, all conversions are made with the Poisson assumption.

a particular structural capacity, or (2) determine the seismic demand associated with a specified annual rate of exceedance.

The SDHC is governed by (see e.g., [15, 36, 35]):

$$\lambda_{EDP}(z) = \int \Pr(EDP > z \mid IM = x) \cdot |\mathrm{d}\lambda_{IM}(x)| \tag{2.1}$$

where $\Pr(EDP > z \mid IM = x)$ is the probability of EDP exceeding demand level z given intensity level x and $\lambda_{IM}(x)$ is the intensity measure hazard curve (IMHC). In Eq 2.1, the IM is often defined as the spectral acceleration at a conditioning period of vibration, T^*, while the EDP is commonly defined as the maximum story drift ratio over all stories of a multistory building [37]. However, the IM may be defined in many different ways. For example, it may be defined as peak ground acceleration (PGA), peak ground velocity (PGV), or significant duration [35]. Alternatively, it may be defined as a vector of IMs (e.g., $\{A(T_1), M\}$, or $\{A(T_1), \epsilon(T_1)\}$, where $\epsilon(T_1)$ is the number of standard deviations between the observed and the predicted value of $A(T_1)$); if it is defined as a vector, then Eq 2.1 needs to be modified appropriately [36]. Note that Eq 2.1 has been extended to consider a vector of EDPs (e.g., drift ratios for individual stories, etc.) [35] and to account for the possibility of structural collapses (see e.g., [33, 36, 37]); however, these extensions are beyond the scope of this study.

The SDHC is typically computed from the following equation:

$$\widehat{\lambda}_{EDP}(z) = \sum_{i=1}^{N_{IM}} \widehat{\Pr}(EDP > z \mid IM = x_i) \cdot |\Delta\widetilde{\lambda}_{IM}(x_i)| \tag{2.2}$$

where N_{IM} is the number of intensity levels considered and x_i is the i^{th} intensity level; $\Delta\widetilde{\lambda}_{IM}(x_i)$ is the discrete form of $|\mathrm{d}\lambda_{IM}(x)|$, which is obtained from PSHA, while $\widehat{\Pr}(EDP > z \mid IM = x_i)$ is the discrete form of $\Pr(EDP > z \mid IM = x)$, which is computed from RHAs of the structure. The hat symbols in Eq 2.2 serve to emphasize the fact that the quantities computed are *estimates* (of the corresponding exact quantities in Eq 2.1) that depend primarily on the particular choice of ground motions selected for RHAs of the structure. This implies that different GMSM procedures lead to different estimates of the SDHC. The meaning of the tilde symbol in $\widetilde{\lambda}_{IM}(x_i)$ will become evident in Section 2.4.

The steps to compute a SDHC in PSDA, when $IM \equiv A(T^*)$, are schematically illustrated in Fig 2.1. The IMHC for $A(T^*)$ is shown in Fig 2.1a. The number of intensity levels, N_{IM}, is chosen to satisfactorily approximate the integral and $|\mathrm{d}\lambda_{IM}(x)|$ in Eq 2.1. For illustration only, Fig 2.1a shows three intensity levels and the discrete form of $|\mathrm{d}\lambda_{IM}(x)|$ at intensity level x_o.

For each i^{th} intensity level, an intensity-based assessment of seismic demand is conducted to determine $\widehat{\Pr}(EDP > z \mid IM = x_i)$. First, an ensemble of scaled ground motions is selected as excitations for RHAs of the system. Recorded ground motions are often scaled because the record-to-record variability of interest is conditioned so that the IM is exactly equal to x_i. Consequently, all candidate ground motions are first scaled, so that $IM = x_i$,

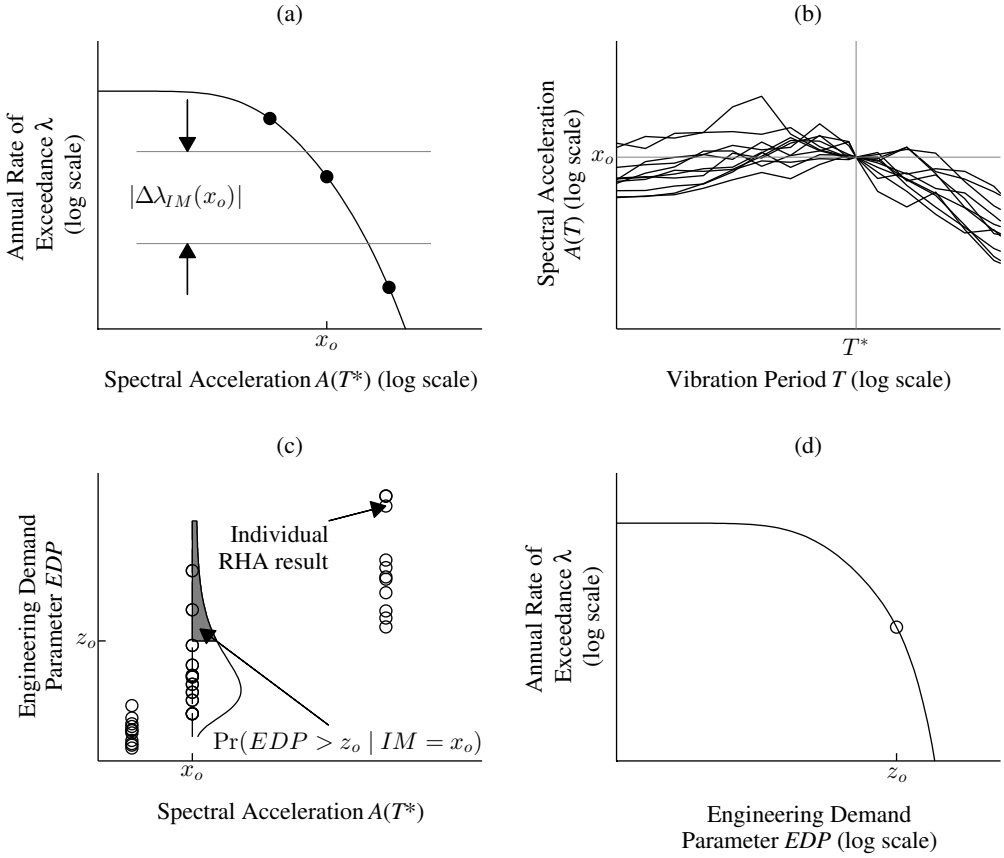

Figure 2.1: The elements of PSDA when $IM \equiv A(T^*)$: (a) discretization of the IMHC, $\lambda_{IM}(x)$; (b) ground motions selected and scaled such that $IM = x_o$; (c) estimation of $\Pr(EDP > z \mid IM = x)$ from RHAs of the structure; (d) resulting SDHC, $\lambda_{EDP}(z)$.

before a subset of them are selected as excitations for RHAs of the structure. For example, the response spectra of one such ensemble, with each ground motion scaled to satisfy $A(T^*) = x_o$, are shown in Fig 2.1b.

Next, RHAs of the structure are performed for the selected ensemble and the computed values of EDPs are processed by statistical inference methods. The list of EDPs corresponding to the ensemble in Fig 2.1b is depicted as circles above $A(T^*) = x_o$ in Fig 2.1c. A lognormal distribution is used to model $\Pr(EDP > z \mid IM = x_i)$ and the two parameters of this distribution are estimated by the mean, $\widehat{\mu}_{\ln EDP}$, and standard deviation, $\widehat{\sigma}_{\ln EDP}$, of the list of logarithmic EDPs [38, 39]:

$$\widehat{\Pr}(EDP > z \mid IM = x_i) = 1 - \Phi\left(\frac{\ln z - \widehat{\mu}_{\ln EDP}}{\widehat{\sigma}_{\ln EDP}}\right) \tag{2.3}$$

where $\Phi(\cdot)$ denotes the cumulative distribution function of the standard normal distribution. For illustration, the probability of EDP exceeding z_o given intensity x_o is shown as the

shaded area in Fig 2.1c. Although a lognormal distribution is commonly employed, an alternative is to apply nonparametric inference to the results from RHAs [40, 38]:

$$\widehat{\Pr}(EDP > z \mid IM = x_i) = \frac{1}{n}\sum_{l=1}^{n} I(z_l > z) \tag{2.4}$$

where n is the number of records selected for intensity level x_i, z_l is the value of EDP for the l^{th} record, and $I(\cdot)$ denotes the indicator function (i.e., $I(z_l > z) = 1$ only if $z_l > z$; otherwise, it is equal to zero); we will revisit Eq 2.4 in Section 2.7.

To illustrate how a GMSM procedure is utilized to estimate a SDHC in PSDA, let us first consider how to estimate the annual rate of the EDP exceeding some demand level, say z_o. Substituting $\widehat{\Pr}(EDP > z_o \mid IM = x_i)$, computed from either Eqs 2.3 or 2.4, in Eq 2.2 leads to $\widehat{\lambda}_{EDP}(z_o)$, which is identified by the circle in Fig 2.1d. Repeating such calculations for all demand levels leads to the SDHC shown in Fig 2.1d.

How can we evaluate a GMSM procedure in its ability to provide 'unbiased' estimates of the SDHC? We define a SDHC estimate to be *unbiased* or *accurate* if it is practically equal to the SDHC from Eq 2.1 (i.e., $\widehat{\lambda}_{EDP}(z) \approx \lambda_{EDP}(z)$); otherwise, it is *biased* or *inaccurate* (i.e., $\widehat{\lambda}_{EDP}(z) \neq \lambda_{EDP}(z)$). Two approaches have been proposed to assess whether the resulting SDHC estimates from a given GMSM procedure are biased or not:

1. Compare the SDHC estimate from Eq 2.2, which is based on a scalar IM, against another estimate from a version of Eq 2.2 where the IM is vector-valued. If the two estimates are appreciably different, then they are biased; if they are practically equal to each other, then they are unbiased [9].

2. Compare the SDHC estimate from Eq 2.2, based on one definition of the scalar IM, against another estimate from Eq 2.2, based on a different definition of the scalar IM. If the two estimates are practically equal to each other, then they are unbiased [35, 37].

As will be demonstrated later, the two approaches above are not always adequate for definitively evaluating a GMSM procedure in its ability to provide unbiased estimates of the SDHC. Since Eq 2.1 is valid for any definition of the IM, $\lambda_{EDP}(z)$ determined from Eq 2.1 for one definition must be identical to $\lambda_{EDP}(z)$ determined from Eq 2.1 for another definition. Therefore, if SDHC estimates from a GMSM procedure are unbiased, then $\widehat{\lambda}_{EDP}(z)$ computed from Eq 2.2 for one definition of the IM must be practically equal to another estimate from Eq 2.2 for a different definition of the IM. However, the converse of this statement is not true: the fact that the two SDHC estimates (corresponding to two different IMs) are practically equal to each other does not *necessarily* imply that SDHC estimates from the GMSM procedure are unbiased. This subtle but important limitation is illustrated next with a simple case study.

2.4 Case study

Site, Structural Model, and Engineering Demand Parameter

UC Berkeley is selected as the example site. Its latitude and longitude coordinates are 37.876 °N and 122.251 °W respectively. The shear wave velocity, V_{s30}, is specified as 600 m/s, and the basin depths, $Z_{1.0}$ and $Z_{2.5}$, are specified as 0.1 and 1 km respectively. OpenSHA [41] is used to perform PSHA; the "USGS/CGS 2002 Adj. Cal. ERF" model is chosen for the earthquake rupture forecast, 5 km is specified for the rupture offset, and background seismicity is excluded.

The selected system is a 5% damped bilinear SDF model with 5% post-yield hardening. Its natural period of small-amplitude vibration, T_1, is 1s and its yield displacement, u_y, is $0.2g \times (T_1/2\pi)^2$. The EDP of interest is its peak deformation, u_m, and we wish to estimate the SDHC for this particular response quantity using RHAs of the system due to ground motions determined by a GMSM procedure.

Intensity Measure Hazard Curve

The IMHC shown schematically in Fig 2.1a is obtained from PSHA for a given site. It is governed by the standard equation (see e.g., [32]):

$$\lambda_{IM}(x) = \sum_{i=1}^{N_{src}} \nu_i \cdot \left\{ \int\int \Pr(IM > x \mid M = m, R = r) f_{R|M}(r \mid m) f_M(m)\, \mathrm{d}r\, \mathrm{d}m \right\}_i \tag{2.5}$$

where N_{src} is the number of earthquake sources, ν_i is the activity rate for the i^{th} earthquake source, $\Pr(IM > x \mid M = m, R = r)$ is the probability of IM exceeding level x for a given earthquake scenario, $f_{R|M}(r \mid m)$ is the probability density function (PDF) of distance for a given magnitude, and $f_M(m)$ is the PDF of magnitude. The activity rate, magnitude PDF, and distance PDF for each of the N_{src} earthquake sources are supplied by an *earthquake rupture forecast* whereas the probability distribution of IM for a given earthquake scenario is obtained from a ground motion prediction model (GMPM) [4].

In practice, $\lambda_{IM}(x)$ in Eq 2.5 is computed from the following equation:

$$\widetilde{\lambda}_{IM}(x) = \sum_{i=1}^{N_{src}} \nu_i \cdot \left\{ \sum_m \sum_r \widetilde{\Pr}(IM > x \mid M = m, R = r) \Pr(M = m, R = r) \right\}_i \tag{2.6}$$

Comparing Eq 2.5 against Eq 2.6, we see that the integrals have been replaced with summations, the PDFs have been replaced with a joint probability mass function, and two

[4] GMPMs are also known as "ground motion prediction equations" (GMPEs) and were formerly referred to as "attenuation relationships". In the context of GMPMs, the phrase "ground motion" refers to an IM whereas in the rest of this study, the phrase refers to ground acceleration as a function of time; the two different uses of "ground motion" should be clear from the context.

expressions have been annotated with tilde symbols. Similar to Eq 2.2, the tilde symbols in Eq 2.6 serve to emphasize the fact that the quantities computed are *estimates* (of the corresponding exact quantities in Eq 2.5) that depend primarily on the particular set of ground motions selected in developing the GMPM. Consequently, different GMPMs lead to different estimates of the IMHC, $\widetilde{\lambda}_{IM}(x)$.

Four estimates of an IMHC at the selected site, for two definitions of the conditioning IM, are presented in Fig 2.2. They correspond to four GMPMs: (1) Campbell & Bozorgnia 2008 (CB08) [42], (2) Boore & Atkinson 2008 (BA08) [43], (3) Abrahamson & Silva 2008 (AS08) [44], and (4) Chiou & Youngs 2008 (CY08) [45]; the differences among the four IMHC estimates are apparent. Which IMHC should one choose to proceed? We will answer this question in Section 2.6 but for now, the CB08 model is chosen and the resulting IMHC is discretized to compute $\Delta\widetilde{\lambda}_{IM}(x_i)$ in Eq 2.2. For each conditioning IM, the IMHC is discretized with $N_{IM} = 11$ intensity levels corresponding to 11 hazard levels: 99%, 80%, 50%, 20%, 10%, 5%, 2%, 1%, 0.5%, 0.2%, and 0.1% probability of exceedance in 50 years, which are identical to those in [35]. For each intensity level, $\widehat{\Pr}(EDP > z \mid A(T^*) = x_i)$ is obtained from an intensity-based assessment (Fig 2.1c).

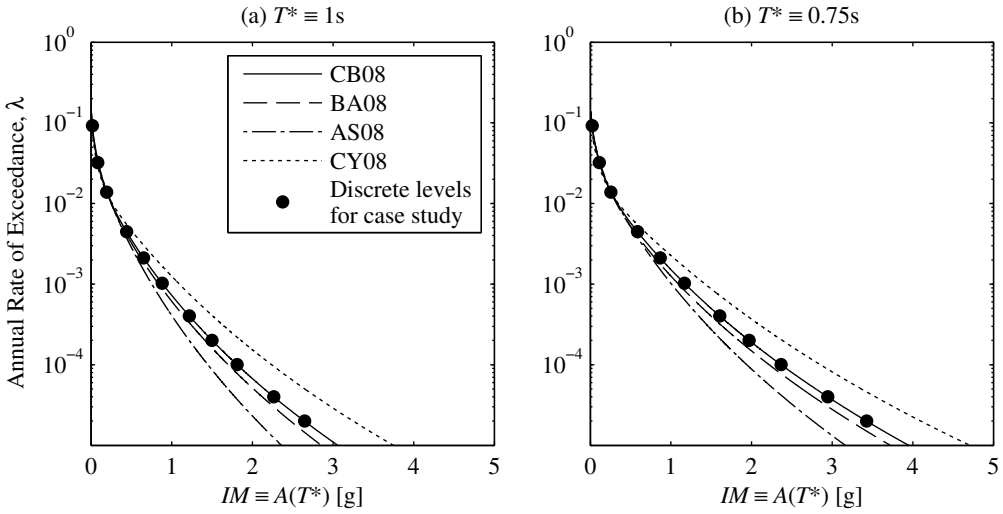

Figure 2.2: Four estimates of the IMHC for the conditioning IM in Eq 2.2: (a) $IM \equiv A(1s)$; (b) $IM \equiv A(0.75s)$.

Intensity-Based Assessment

As shown in Fig 2.1, a single intensity-based assessment involves (1) ground motion selection (Fig 2.1b), (2) RHAs of the structural system due to the selected ensemble (Fig 2.1c), and (3) statistical inference (Fig 2.1c), at a specified intensity level. In this case study, each intensity-

based assessment computes $\widehat{\Pr}(EDP > z \mid A(T^*) = x_i)$ from Eq 2.3 using the results from RHAs of the structure for $n = 44$ ground motions. To illustrate the limitation of the two approaches for evaluating GMSM procedures (mentioned at the end of Section 2.3), we select two GMSM procedures: (1) Incremental Dynamic Analysis (IDA) [46], and (2) a special case of the Generalized Conditional Intensity Measure approach (GCIM) [47, 48, 35]. In IDA, a single 'seed' ensemble of ground motions is scaled to multiple intensity levels; here, the Far-Field record set from FEMA P695 [49], which contains $n = 44$ records from the PEER Next-Generation Attenuation database [50], is selected as the seed ensemble. Since some readers may not be familiar with GCIM, which is a generalization of the Conditional Spectrum approach (CS) [1], we will first briefly review CS and then identify the generalizations that led to GCIM.

Fig 2.3 schematically illustrates the steps involved in CS-based ground motion selection at some particular intensity level, say x_o from Fig 2.1. First, the seismic hazard at $A(T^*) \approx x_o$ is deaggregated [51] to obtain the percent contribution to the hazard from an earthquake with magnitude M at distance R; it is summarized by a mean M and a mean R (Fig 2.3a). The US Geological Survey online hazard tool provides deaggregation for $A(T^*) > x_o$ [52], thus requiring an additional step to convert the results to obtain deaggregation for $A(T^*) \approx x_o$ [36].

Next, the probability distribution of response spectrum, for a given earthquake scenario with mean M at mean R, is determined (Fig 2.3b). For a given vibration period, T, the probability distribution is modeled with a lognormal distribution and its two parameters are obtained from a selected GMPM. The mean values of M and R from deaggregation (Fig 2.3a) are used as inputs to this GMPM; other inputs (e.g., style of faulting, dip, etc.) are inferred [25]. For example, a GMPM provides the median and one-sigma response spectra, which are shown in Fig 2.3b as solid and chain lines, respectively. In practice, the distribution of response spectrum is determined for a specific range of vibration periods, which are denoted as $\mathbf{T}_{IM}$ in Fig 2.3b; typically, T^* is equal to T_1, and $\mathbf{T}_{IM}$ consists of 50 logarithmically spaced periods between $0.2T_1$ to $2T_1$ [25].

For a given rupture scenario, the collection of spectral acceleration values at vibration periods $\mathbf{T}_{IM}$ is viewed as a random vector. Due to lognormality, the logarithm of the response spectrum follows a multivariate normal distribution [53]. In order to specify the covariance matrix for this distribution, the correlations between spectral ordinates at different vibration periods are needed and are available in the literature [54, 55]. An example of this multivariate normal distribution is schematically shown in Fig 2.3b. When $A(T^*)$ is conditioned to be equal to x_o, the logarithm of the response spectrum still follows a multivariate normal distribution but with different parameters [1]; this is illustrated in Fig 2.3c.

Suppose n records are desired to estimate $\Pr(EDP > z \mid A(T^*) = x_o)$. To select these records, all candidate motions are first scaled so that $A(T^*) = x_o$. Then, n response spectra are randomly generated (Fig 2.3d) from the multivariate normal distribution in Fig 2.3c. For each simulated spectrum, a record whose scaled response spectrum most closely matches the simulated one is selected (Fig 2.3d). Such matching is quantified by the sum-of-squared-

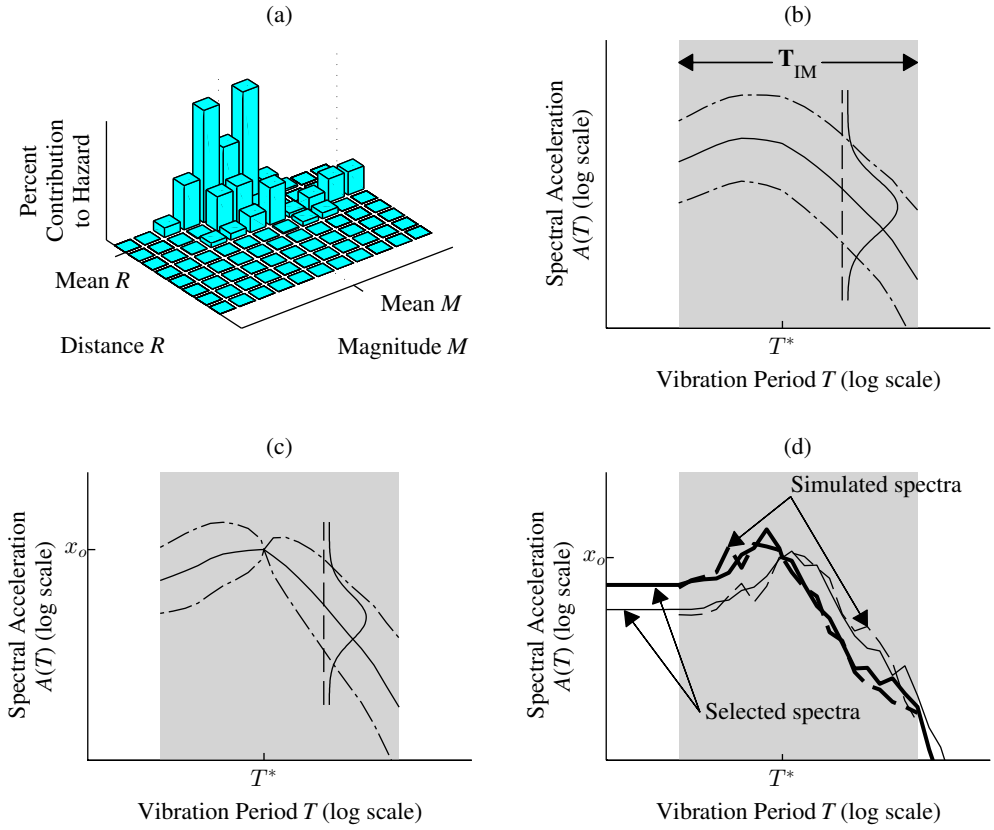

Figure 2.3: Schematic illustration of the Conditional Spectra approach [1] to ground motion selection at some particular intensity level, say x_o, of $IM \equiv A(T^*)$: (a) deaggregation to determine mean M and mean R; (b) definition of $\mathbf{T}_{IM}$ and marginal distributions of $A(T)$ from a single GMPM for a given earthquake scenario with mean M at mean R; (c) Conditional Spectrum; (d) ground motion selection based on comparing recorded against simulated response spectra.

errors metric in CS [1]. Because ground motions are matched to randomly generated response spectra, the ensemble obtained from a single implementation of CS is *not* unique.

GCIM generalizes CS in four main aspects. First, GCIM considers IMs in addition to spectral accelerations for record selection. Consistent with the notation employed in [47], the complete vector of IMs for selection is denoted as **IM**, the conditioning scalar IM used for record scaling is denoted as IM_j, and all IMs that are not used for record scaling but are used for selection are denoted as $\mathbf{IM}_i$; that is, $\mathbf{IM} = \{IM_j, \mathbf{IM}_i\}$. Thus, PGA, PGV, or significant duration, are all valid options for specifying IM_j or any element of $\mathbf{IM}_i$. Second, GCIM offers the option of weighting IMs. Third, a more sophisticated version of the target spectrum than that shown in Fig 2.3c is derived in GCIM. Instead of the mean M-R, the

conditional distribution in Fig 2.3c is computed for *each and every* scenario in Fig 2.3a, and the percent contributions are used to combine all such distributions [47]; this feature avoids the need to inflate standard deviations in CS [37]. Fourth, the variability of IM_i, for a given value of IM_j, is incorporated into the sum-of-squared-errors metric for the selection of records.

In the special case of GCIM chosen herein, denoted by GCIM-SA, **IM** comprises spectral accelerations with all periods equally weighted (i.e., $\mathbf{IM} \equiv \{A(T^*), A(\mathbf{T}_{IM_i})\}$). As a result, GCIM-SA differs from CS only in (1) the construction of the target spectrum, and (2) the metric utilized for record selection. For each intensity level, the GCIM-SA target spectrum and the n corresponding simulated response spectra (Fig 2.3d) are obtained from Bradley's GCIM application in OpenSHA [48]; the model by Baker & Jayaram 2008 (BJ08) [55] is used to determine the correlations between spectral ordinates at different vibration periods. For each of the n simulated spectra, the record whose response spectrum most closely matches the simulated one, which is quantified by the generalized metric in GCIM (Eq 10 in [48]), is selected from the PEER Next-Generation Attenuation database (Fig 2.3d) [5]. As in CS, the selected ensemble obtained from a single implementation of GCIM-SA is not unique.

As an example of the GCIM-SA target spectrum, the one for $IM_j \equiv A(1s)$ at 2% probability of exceedance in 50 years, computed with the CB08 model, is shown in Fig 2.4 as dark solid lines. As illustrated in the figure, it is computed at 11 vibration periods: $\mathbf{T}_{IM} = \{0.05, 0.1, 0.2, 0.3, 0.5, 0.75, 1, 2, 3, 5, 10\}$. Unlike the target spectrum from CS, the one from GCIM-SA does not follow a multivariate normal distribution. Hence, the median (Fig 2.4a) and the interquartile range (Fig 2.4b) are employed to summarize the probability distribution of response spectrum; the median $A(T)$ corresponds to a probability of 0.50, whereas the interquartile range of $A(T)$ refers to the difference between the values of $A(T)$ at two probabilities: (1) 0.75 and (2) 0.25.

Fig 2.4 also depicts the GCIM-SA target spectrum computed from three other GMPMs: (1) BA08, (2) AS08, and (3) CY08. Although each of the four targets corresponds to the same probability of exceedance, the conditioning value of $A(1s)$ is different, as seen in Fig 2.4a and in Fig 2.2a. Furthermore, the differences among the four interquartile ranges are apparent, which is especially noticeable at short vibration periods in Fig 2.4b. Since the CB08 model was already chosen for determining $|\Delta\widetilde{\lambda}_{IM}(x_i)|$ in Eq 2.2 (Fig 2.2a) and conducting deaggregation (Fig 2.3a), it is also chosen for the construction of the target spectrum in this case study; hence, GCIM-SA also differs from the "exact CS", where the target spectra is determined from multiple GMPMs [57, 58].

Seismic Demand Hazard Curve

Fig 2.5 presents estimates of the SDHC from IDA and from GCIM-SA, for three different definitions of the conditioning IM. For each scalar IM and each GMSM procedure, the SDHC

[5] Instead of selecting scaled ground motions, note that ground motions from the PEER database may be spectrum matched to each of these simulated spectra [56].

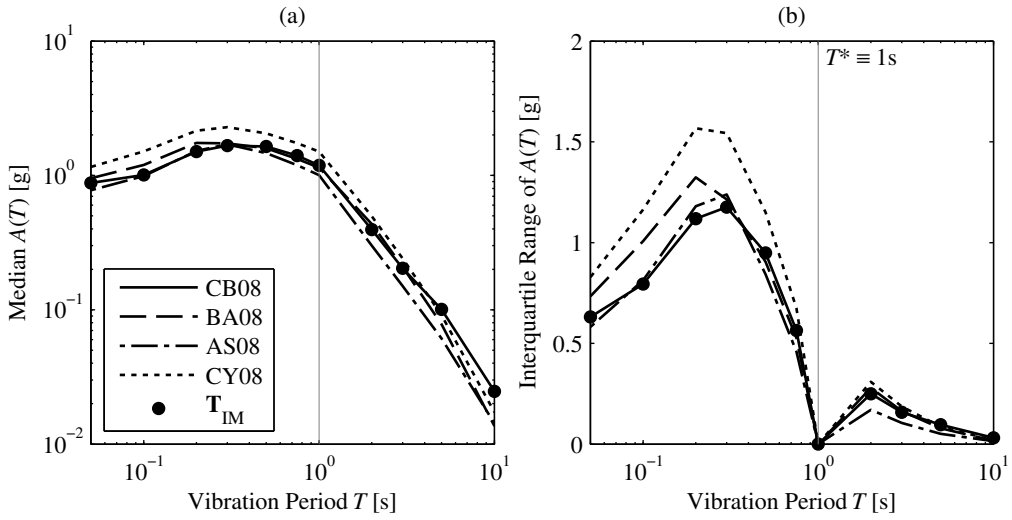

Figure 2.4: Target conditional response spectra from GCIM-SA for $IM_j \equiv A(1s)$ at 2% probability of exceedance in 50 years: (a) median $A(T)$; (b) interquartile range of $A(T)$.

estimate was computed from Eq 2.2 (Fig 2.1); in total, $N_{IM_j} \times 2 = 22$ deaggegrations were conducted and $N_{IM_j} \times n \times 2 \times 2 = 1936$ RHAs were performed. For the vector-valued IM, the SDHC estimates are obtained by the approach outlined in [36]. Note that the results correspond to highly inelastic behavior and are meaningful only at exceedance rates above around 2×10^{-5}, because the lowest probability of exceedance considered in the discretization is 0.1% in 50 years. To facilitate interpretation of these curves, the guidelines corresponding to the design basis earthquake (DBE) and maximum considered earthquake (MCE) levels are also provided [6].

According to approach 2 at the end of Section 2.3, Fig 2.5 suggests that the IDA estimates are more accurate [7] than the GCIM-SA estimates. For both GMSM procedures, the SDHC estimate from $A(1s)$ is noticeably different than that from $A(0.75s)$ at exceedance rates below the MCE level. However, the difference between these two SDHC estimates, which correspond to two different definitions of T^*, is smaller for IDA than for GCIM-SA. Based on this observation alone, the IDA estimates appear to be more accurate than those from GCIM-SA.

Approach 1 at the end of Section 2.3 leads to a different conclusion. For each GMSM procedure, the SDHC estimate from $A(1s)$ is practically equal to that from $\{A(1s), M\}$. Based on this observation alone, *both* GMSM procedures seem to produce unbiased estimates of the SDHC. However, the IDA estimate for $A(1s)$ is significantly different than the GCIM-

[6] The DBE level corresponds to a rate of 2×10^{-3} and a return period of 475 years; the MCE level corresponds to a rate of 4×10^{-4} and a return period of 2475 years.

[7] Recall that the concepts of 'accuracy' and 'bias' were defined at the end of Section 2.3.

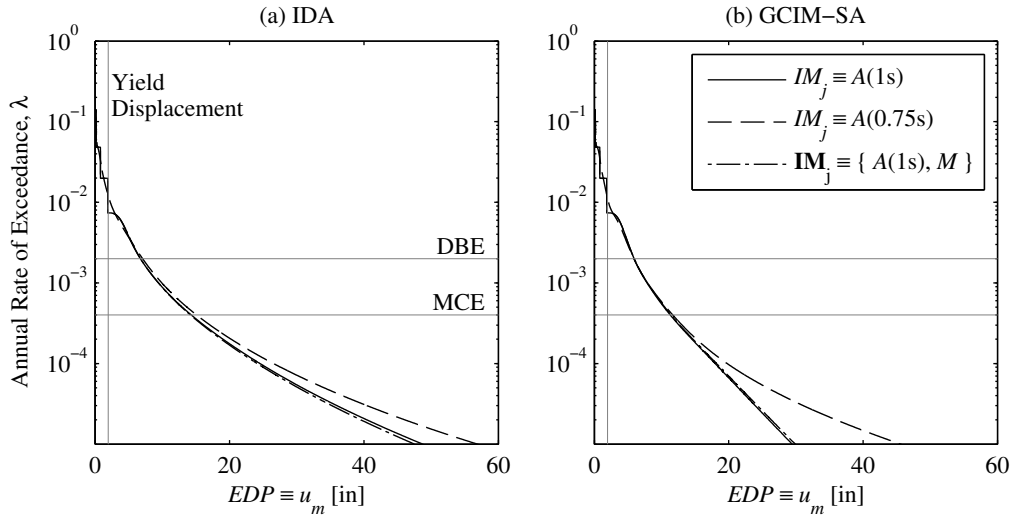

Figure 2.5: Estimates of the SDHC from PSDA, for three different conditioning IMs: (a) IDA; (b) GCIM-SA.

SA estimate for $A(1s)$, contradicting the claim that both SDHC estimates are unbiased.

Since the ground motions from GCIM-SA are scaled much more severely than those from IDA in Fig 2.5, it is not immediately obvious as to which of the two GMSM procedures provides more accurate estimates of the SDHC. For example, let us focus on the scale factors that were employed to compute the SDHCs in Fig 2.5 corresponding to $IM_j \equiv A(1s)$. These scale factors are shown in Fig 2.6, where we observe that at each intensity level, the median scale factor from GCIM-SA is larger than that from IDA. If one started with the preconceived notion that small scale factors are desirable, then one would conclude that IDA is the more preferable procedure. As will be demonstrated later in Section 2.7 however, the results from GCIM-SA are more accurate than those from IDA despite the fact that larger scale factors were employed.

In the preceding discussion, only two definitions of the conditioning IM were considered when implementing each of the two approaches at the end of Section 2.3. This was done solely to emphasize a subtle point: the practical equality between two SDHCs from different conditioning IMs does not *necessarily* indicate that an unbiased SDHC has been obtained. In practical implementation of these two approaches, many more definitions of the conditioning IM than those shown in Fig 2.5 are considered before conclusions are drawn. For example, several significantly different scalar IMs were considered when implementing approach 2 in [35] and in [37]. It is important to note however, that as more definitions of IM_j are considered, more RHAs are necessary in the evaluation because for one definition of IM_j and one GMSM procedure, a total of $N_{IM_j} \times n$ RHAs are required to compute the SDHC. To supplement the two approaches at the end of Section 2.3 when evaluating GMSM procedures

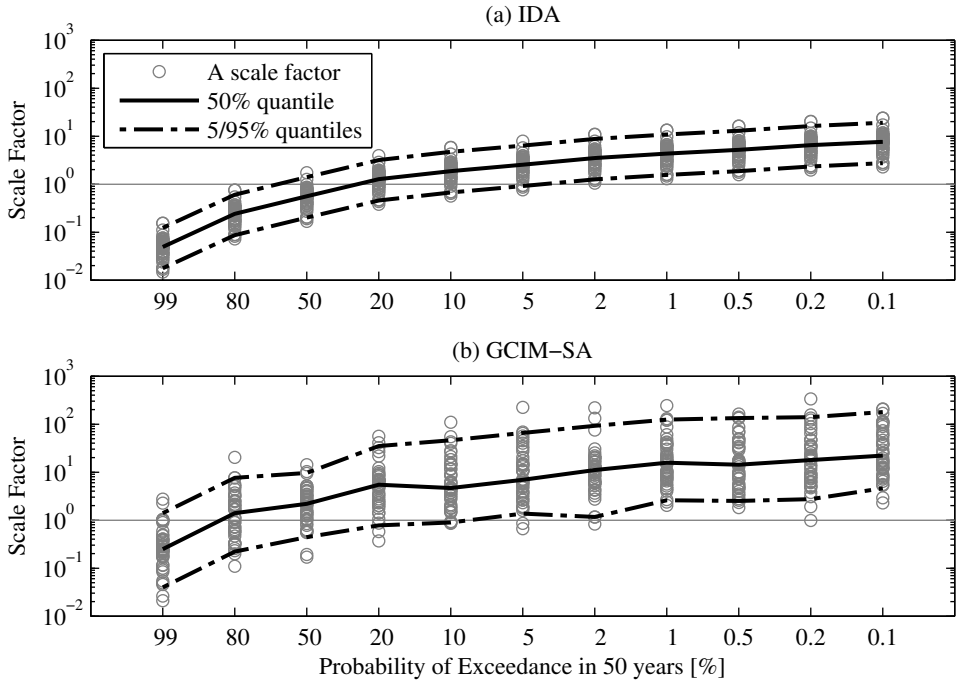

Figure 2.6: Scale factors employed in PSDA when $IM_j \equiv A(1s)$; in each panel, $n = 44$ scale factors are shown for each of the $N_{IM_j} = 11$ intensity levels: (a) IDA; (b) GCIM-SA.

and to quantify bias in any estimate of the SDHC, we propose an alternative approach that involves the notion of a benchmark SDHC.

2.5 The benchmark seismic demand hazard curve

Instead of choosing definitions for the conditioning IM in order to evaluate the accuracy of SDHC estimates from GMSM procedures (Fig 2.5), we propose to compare such estimates against a benchmark SDHC that is developed from unmodified ground motions. The benchmark SDHC is determined by accounting for all plausible rupture scenarios near the site, as is done in PSHA. Comparing the SDHCs in Fig 2.5 against the IMHCs in Fig 2.2, we see that EDP in PSDA plays the same role as IM in PSHA. Thus, if we replace the IM in Eq 2.6 by the EDP, then the benchmark SDHC may be computed from the following equation:

$$\widetilde{\lambda}_{EDP}(z) = \sum_{i=1}^{N_{src}} \nu_i \cdot \left\{ \sum_m \sum_r \widetilde{\Pr}(EDP > z \mid M = m, R = r) \Pr(M = m, R = r) \right\}_i \qquad (2.7)$$

where $\widetilde{\Pr}(EDP > z \mid M = m, R = r)$ is determined from unmodified ground motions by a process similar to the development of a GMPM in PSHA.

The elements of computing a benchmark SDHC, for a given structure at a given site, are schematically illustrated in Fig 2.7. The specification of an activity rate, a PDF for magnitude (Fig 2.7b), and a PDF for distance (Fig 2.7c) for each of the N_{src} earthquake sources (Fig 2.7a), is identical to that in the PSHA for the site. For the case study described earlier, the benchmark SDHC is computed with the same earthquake rupture forecast introduced in Section 2.4.

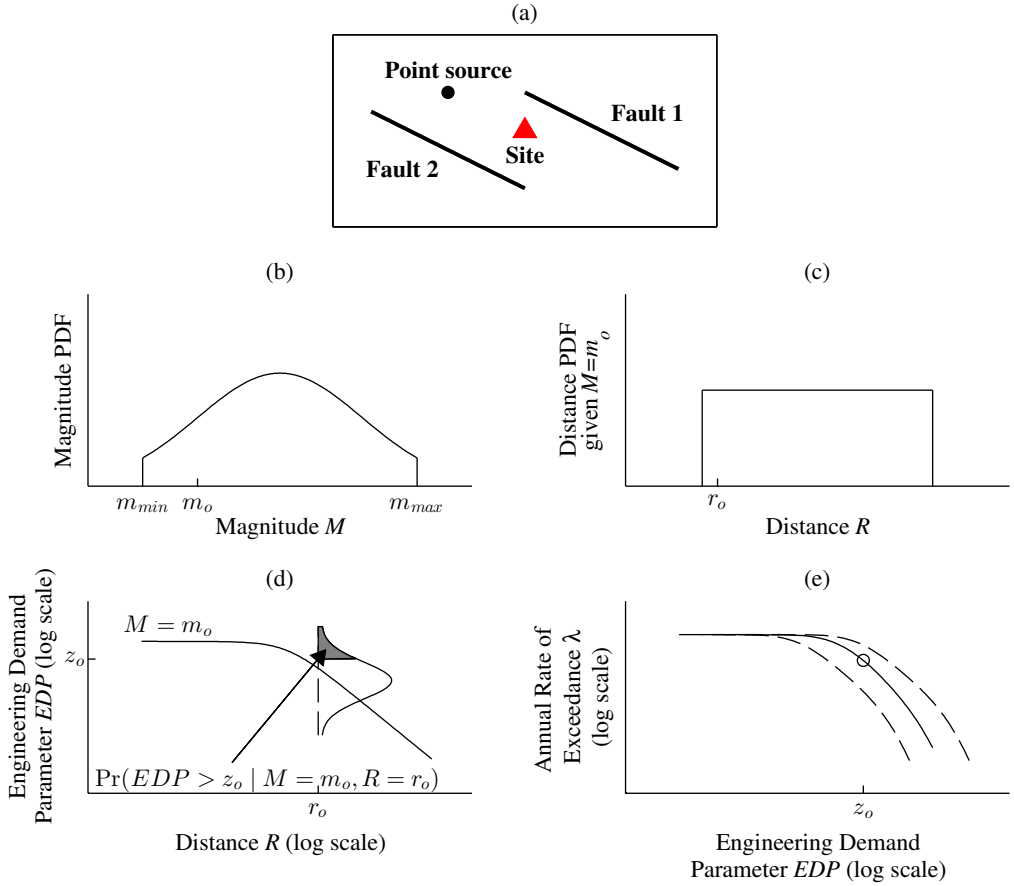

Figure 2.7: The elements of computing a benchmark SDHC: (a) specification of N_{src} earthquake sources and corresponding activity rates, ν_i; for the i^{th} source, a (b) PDF for magnitude, $f_M(m)$; (c) PDF for distance given magnitude, $f_{R|M}(r \mid m_o)$; and (d) probability distribution of demand for a given earthquake scenario, $\Pr(EDP > z \mid M = m_o, R = r_o)$, are shown; (e) benchmark SDHCs from various prediction models.

Like PSHA, a prediction model is needed to estimate the probability of EDP exceeding level z for a given rupture scenario (Fig 2.7d). For example, Heo et al developed such a prediction model for the maximum inter-story drift of a 4- and 12-story building by (1)

performing 200 nonlinear RHAs of each building, (2) exploring many different models to predict each EDP as a function of IMs, and (3) choosing the optimal model on the basis of regression diagnostics; to predict an EDP for a given rupture scenario, the optimal model is combined with a GMPM [28]. As another example, Hancock et al developed a prediction model for several EDPs of an 8-story building by (1) performing 1656 nonlinear RHAs of the building, (2) exploring many different functional forms to predict each EDP directly as a function of the rupture scenario, and (3) again choosing the final model on the basis of regression diagnostics [29]. Such an onerous undertaking is generally difficult to justify since the resulting prediction model is limited to the one structure considered. However, we note that a prediction model is readily available for two special cases: (1) EDP is the normalized base shear, $A(T)/g$ of 5% damped linear elastic SDF systems [23], and (2) EDP is the peak deformation, u_m, of 5% damped bilinear SDF systems with 5% post-yield hardening [59].

The distribution of u_m for a given rupture scenario is obtained herein from the Tothong & Cornell 2006 (TC06) model [59]. However, the TC06 model requires the peak deformation of the corresponding linear system, u_o, as an input. Because u_o is not known a priori for a given rupture scenario [59], the TC06 model must be combined with a GMPM to determine the desired distribution of u_m. Consequently, different GMPMs lead to different benchmark SDHCs, which is schematically shown in Fig 2.7e. Which benchmark SDHC should one choose? This question is answered in the next section.

2.6 Proposed framework to evaluate GMSM procedures in PSDA

The proposed framework is schematically presented in Fig 3.1. We propose to compare estimates of the SDHC from GMSM procedures, $\widehat{\lambda}_{EDP}(z)$ from Eq 2.2, against a benchmark SDHC, $\widetilde{\lambda}_{EDP}(z)$ from Eq 2.7, under a *single set* of ground motion information for the site. This single set includes an earthquake rupture forecast, a database of many plausible records, and prediction models derived from these records (i.e., a single GMPM for one IM, a single GMPM for another IM, a single model for the correlation among two IMs, etc.). It is important that the same ground motion information be chosen when computing $\widetilde{\lambda}_{IM}(x)$ and $\widetilde{\lambda}_{EDP}(z)$, because the purpose of the comparison between $\widehat{\lambda}_{EDP}(z)$ from Eq 2.2 and $\widetilde{\lambda}_{EDP}(z)$ from Eq 2.7 is to isolate the effects of a particular GMSM procedure on the resulting SDHC estimate, which is emphasized by the hat symbols in Eq 2.2.

As shown in Fig 3.1, the proposed framework does *not* compare $\widehat{\lambda}_{EDP}(z)$ against the SDHC from Eq 2.1, $\lambda_{EDP}(z)$, because the latter cannot be calculated for realistic problems, which is why the PEER GMSM working group refers to their benchmark as a "Point-Of-Comparison", or a "High-End-Prediction" [26]. However, we note that this inability to calculate $\lambda_{EDP}(z)$ is just an example of *epistemic uncertainty*, because it arises from the fact that our data and knowledge are always incomplete. For example, $\Pr(IM > x \mid M = m, R = r)$ in Eq 2.5 is not known with absolute certainty since it is estimated with a

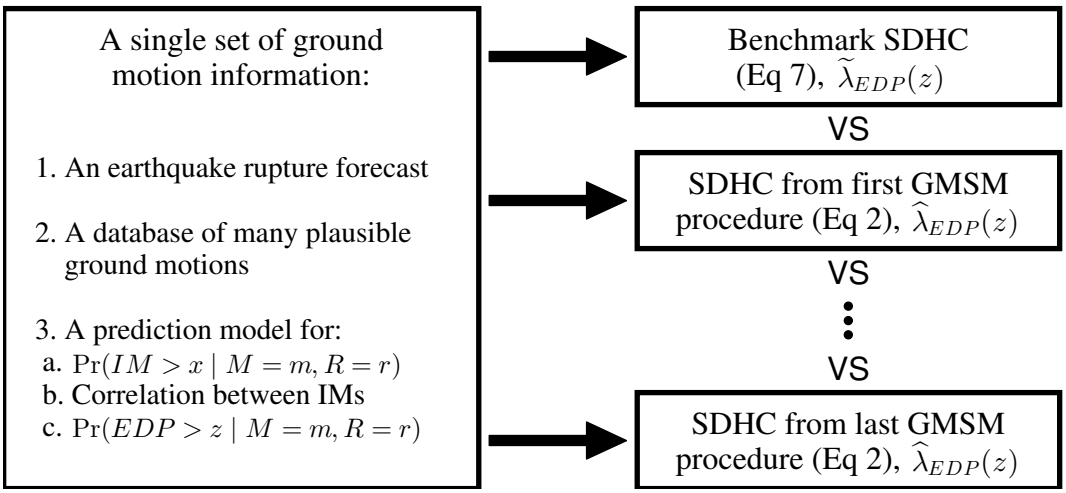

Figure 2.8: Schematic illustration of the proposed framework for evaluating GMSM procedures in their ability to accurately estimate the SDHC.

limited collection of ground motions and an *assumed* functional form. Consequently, several GMPMs have been developed to estimate this term, leading to multiple IMHCs in Fig 2.2 and multiple target spectra in Fig 2.4. Another example of epistemic uncertainty is portrayed in Fig 2.7e, where different EDP prediction models lead to different SDHCs. With these variety of models, it might seem difficult to claim a single model as the benchmark.

We overcome this apparent difficulty by recognizing that the purpose of comparing $\widehat{\lambda}_{EDP}(z)$ against a benchmark is to establish the causal relationship between a particular GMSM procedure and the potential bias in its resulting estimate of the SDHC. Therefore, we propose that any EDP prediction model may be chosen, as long as all variables other than the GMSM procedure are controlled as much as possible. For example, any GMPM may be chosen to obtain the final EDP prediction model (see e.g., [59, 28]) when computing the benchmark SDHC (Eq 2.7), as long as $\widetilde{\lambda}_{IM}(x)$ in Eq 2.2 is given by the IMHC resulting from the *same* GMPM. As another example, if a particular functional form was chosen to develop the prediction model for an EDP, then the *same* functional form should be employed to predict the IM as a function of a rupture scenario (e.g., [29]). Unlike the Point-Of-Comparison in [26], we recommend that the EDP prediction model be developed from *unmodified* ground motions because otherwise, it is impossible to establish the causal relationship between the modification of ground motions and the potential bias in its resulting SDHC; for some structures however, this recommendation will result in a small number of inelastic responses (see end of Section 2.8).

2.7 Bias, hazard consistency, and IM sufficiency

The results from implementing the proposed framework (Fig 3.1), using the CB08 model, are presented in Fig 2.9. The benchmark SDHC is obtained from Eq 2.7 with $\widetilde{\Pr}(EDP > z \mid M = m, R = r)$ given by the TC06-CB08 model and the PSDA-based estimates of the SDHC are repeated from Fig 2.5. Comparing the PSDA-based estimates against the benchmark, we see that both GMSM procedures, IDA and GCIM-SA, lead to essentially unbiased results at exceedance rates above the DBE level and biased results at rates below the MCE level. Furthermore, the curves from GCIM-SA are more accurate than those from IDA, and those corresponding to $T^* \equiv 1s$ are more accurate than those corresponding to $T^* \equiv 0.75s$. The latter observation suggests that the choice of the conditioning period is important in PSDA, which confirms the conclusion by Lin et al [37]. We also observe that the bias increases with decreasing exceedance rates; using the GCIM-SA curve corresponding to $T^* \equiv 1s$ as an example, the estimated demand differs from the benchmark by 1% at the DBE level, and by 12% at the MCE level. Without a benchmark, it would be impossible to make such statements with regard to the accuracy of any SDHC estimate from a GMSM procedure.

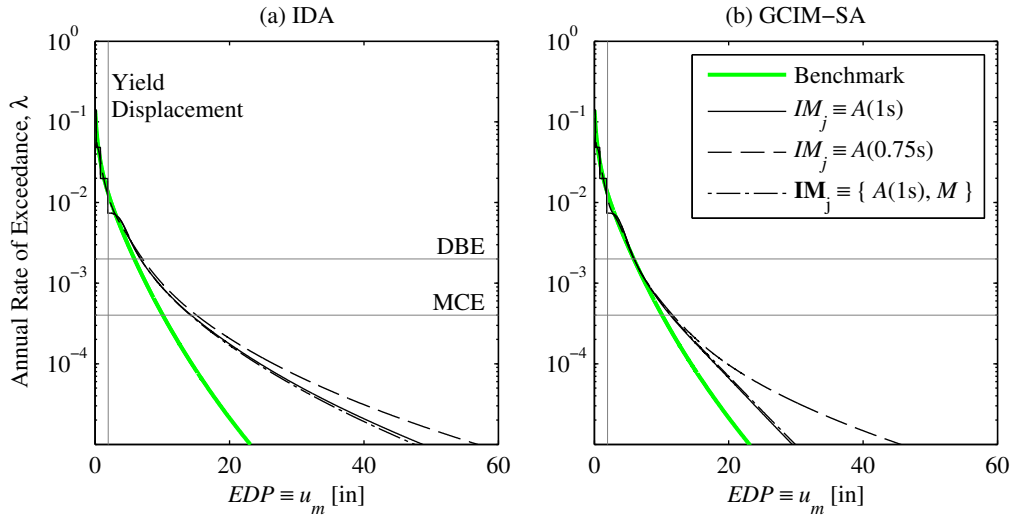

Figure 2.9: Comparison of various estimates of the SDHC from PSDA against the benchmark SDHC: (a) IDA; (b) GCIM-SA.

The IDA and GCIM-SA estimates of the SDHC, corresponding to $A(1s)$ in Fig 2.9, are compared directly against each other and against the benchmark SDHC in Fig 2.10a. This direct comparison confirms that the results from both procedures are unbiased above the DBE level; at rates below this level, the GCIM-SA estimate is more accurate than that from IDA. Such a comparison between the two GMSM procedures does not require that the CB08 model be chosen as the GMPM for spectral acceleration at various vibration

periods. As previously mentioned in Section 2.6, any single GMPM may be chosen as long as it is utilized in *all* estimates of the SDHC. The comparison in Fig 2.10a is repeated for three other GMPMs in Fig 2.10b-d, implying that a total of $N_{IM_j} \times n \times 2 \times 4 = 3872$ RHAs were performed. As expected from earlier discussion, the benchmark SDHC changes for each GMPM and the SDHC estimate from each GMSM procedure also changes with GMPMs. However, the SDHC estimate from GCIM-SA remains consistently more accurate than that from IDA below the DBE level. Fig 2.10 also shows that the GCIM-SA estimate is essentially unbiased for AS08 and CY08 but is somewhat biased for the other two GMPMs. The discrepancy between the benchmark SDHC and the GCIM-SA estimate varies for each GMPM because the GCIM-SA estimate, for each of the four separate implementations, is not unique (Section 2.4). For example, when another estimate of the SDHC from GCIM-SA is computed using the AS08 model, a different selection of ground motions (Fig 2.3d) and hence a different SDHC estimate would be obtained; this new SDHC would not be equal to the benchmark SDHC determined by the AS08 model, unlike the GCIM-SA curve shown in Fig 2.10c.

Why are the estimates from GCIM-SA more accurate than those from IDA even though larger scale factors were employed in GCIM-SA (Fig 2.6)? We can answer this question by introducing the concept of "hazard consistency". Originally defined by Lin et al [37], an ensemble [8] of ground motions is *hazard consistent for some IM*, if the estimated IMHC from the ensemble, $\widehat{\lambda}_{IM}(y)$, is practically equal to the IMHC determined by PSHA, $\widetilde{\lambda}_{IM}(x)$ from Eq 2.6. Once $N_{IM_j} \times n$ records have been selected to determine a SDHC, estimating an IMHC from such an ensemble is just a matter of (1) replacing EDP with IM in Eqs 2.2 and 2.4, and (2) applying these equations to the selected ground motions. Specifically, the estimated IMHC from the ensemble is computed from:

$$\widehat{\lambda}_{IM}(y) = \sum_{k=1}^{N_{IM_j}} \widehat{\Pr}(IM > y \mid IM_j = x_k) \cdot |\Delta\widetilde{\lambda}_{IM_j}(x_k)| \tag{2.8}$$

where IM_j was previously defined near the end of Section 2.4 and $\widehat{\Pr}(IM > y \mid IM_j = x_k)$ is determined from:

$$\widehat{\Pr}(IM > y \mid IM_j = x_k) = \frac{1}{n}\sum_{l=1}^{n} I(y_l > y) \tag{2.9}$$

where y_l is the value of IM for record l that has been scaled to intensity x_k.

For the choice of GMPM $\equiv$ CB08 and $IM_j \equiv A(1s)$, Fig 2.11 examines the hazard consistency of the ground motions selected from IDA and GCIM-SA for IM defined as spectral acceleration at various vibration periods. The PSHA curves are obtained from Eq 2.6 with $\widetilde{\Pr}(IM > x \mid M = m, R = r)$ given by the CB08 model. For each GMSM procedure, the estimated IMHCs are obtained by applying Eqs 3.16 and 2.9 to the 484 motions that were used to construct the corresponding SDHC estimate in Fig 2.10a.

[8] In the context of hazard consistency, the word 'ensemble' refers to all $N_{IM_j} \times n$ ground motions utilized for a single estimate of the SDHC.

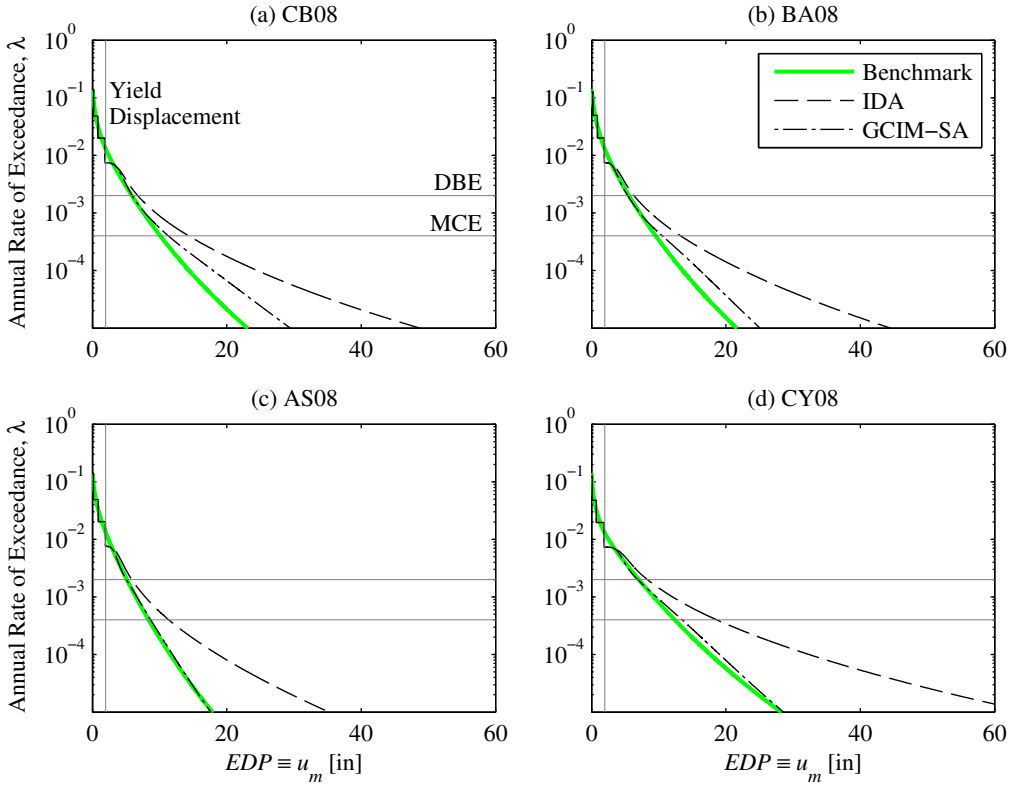

Figure 2.10: Comparison of SDHC estimates from IDA and from GCIM-SA, when $IM_j \equiv A(1s)$, against the benchmark SDHC, for four different GMPMs: (a) CB08; (b) BA08; (c) AS08; and (d) CY08.

In Fig 2.10a, the SDHC estimate from GCIM-SA is more accurate than that from IDA because the ground motions selected from GCIM-SA are hazard consistent for *more* IMs than those selected from IDA. Fig 2.11 demonstrates that the ground motions from GCIM-SA are hazard consistent for spectral acceleration at nearly all the vibration periods shown (except for 0.1s and 10s). This is so because records were selected to deliberately match the distribution of $A(T)$, for a given value of $A(T^*)$, at these periods (see Fig 2.4 and Fig 2.3d in Section 2.4). In contrast, one does not have control over the hazard consistency of the ground motions from IDA for such IMs. Although (1) the ground motions from GCIM-SA are hazard consistent for $A(T)$ between T_1 to $3T_1$ (Fig 2.11c-e), and (2) the GCIM-SA estimate is more accurate than that from IDA (Fig 2.10a), it is nevertheless biased at rates below the MCE level.

This bias below the MCE level is due to the fact that the vector-valued IM, defined as $A(T)$ at T_1, $2T_1$, and $3T_1$, is *not* a 'sufficient' IM for $EDP \equiv u_m$. An IM, which may be scalar or vector-valued, is defined to be *sufficient* for an EDP when, given a fixed value of this

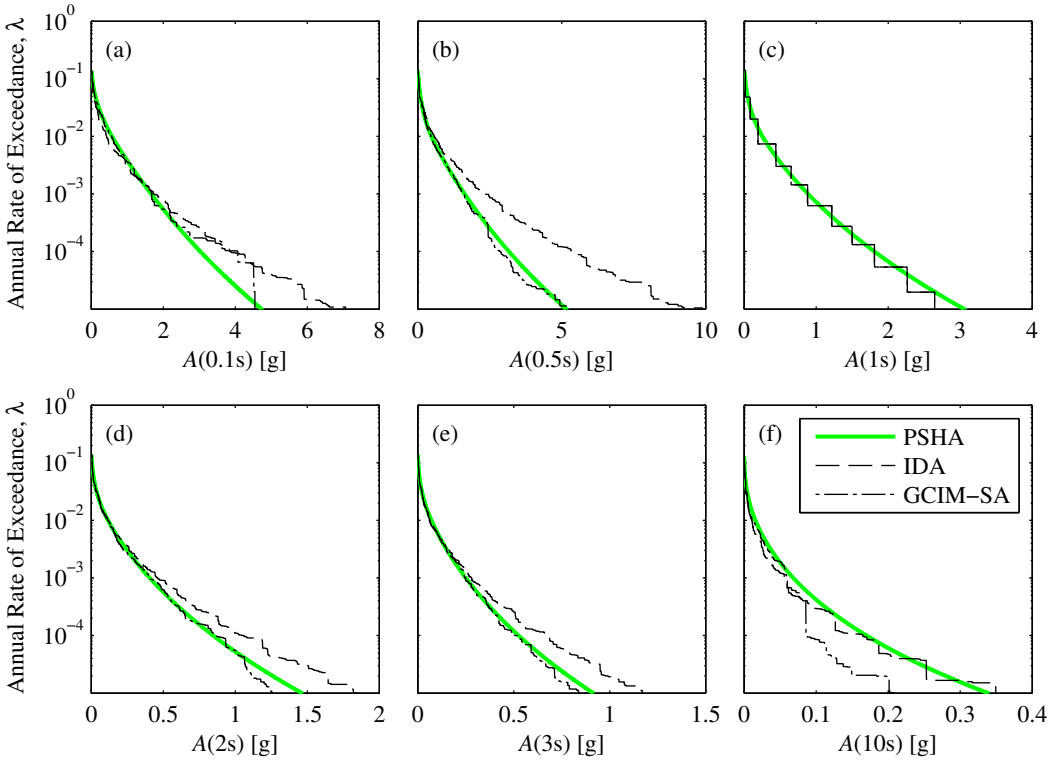

Figure 2.11: Hazard consistency of the ground motions selected from $IM_j \equiv A(1s)$ for spectral acceleration at: (a) 0.1s; (b) 0.5s; (c) 1s; (d) 2s; (e) 3s; (f) 10s.

IM, the record-to-record variability of the EDP does not depend on any other aspects of the record [15, 12]. If a vector-valued IM (e.g., $A(T)$ at T between T_1 and $3T_1$) is indeed sufficient for u_m, then the fact that ground motions are hazard consistent for this IM must imply that the corresponding SDHC estimate is unbiased; as a corollary, if the ground motions are hazard consistent for a vector-valued IM, then the fact that the corresponding estimate of the SDHC is biased must imply that the vector-valued IM is insufficient for the EDP of interest. To motivate this assertion, we next consider two definitions of a scalar IM.

First, let us define IM as EDP [12]. This implies that IM is sufficient for EDP, because once a fixed value of EDP is given, the variability of EDP does not depend on any other aspects of the ground motion. If ground motions were selected to be hazard consistent *for this particular definition* of the IM, then by definition of hazard consistency, $\widehat{\lambda}_{IM}(y)$ from Eq 3.16 will be practically equal to $\widetilde{\lambda}_{IM}(x)$ from Eq 2.6. This is equivalent to stating that the SDHC estimate is unbiased, since $IM \equiv EDP$.

Second, let us define IM as IM_j. Since ground motions are scaled to IM_j in PSDA (Fig 2.1b), they are *always* hazard consistent *for this particular definition* of the IM. For example, Fig 2.11c shows that the selected motions from both GMSM procedures are hazard

consistent for $IM_j \equiv A(1s)$; in fact, the estimated IMHCs from both procedures are identical, because the term $\widehat{\Pr}(IM > y \mid IM_j = x_k)$ in Eq 3.16 becomes a step function when $IM \equiv IM_j$. The fact that the ground motions from both procedures are hazard consistent for $A(1s)$ implies that the corresponding SDHC estimates are unbiased at exceedance rates above the DBE level (Fig 2.10a), because (1) $A(1s)$ is a sufficient IM for the peak deformation of the corresponding linear system, u_o, and (2) $EDP \equiv u_m$ is approximately equal to u_o at rates above the DBE level. On the other hand, the SDHC estimates are biased at rates below the MCE level, even though the selected motions from both procedures are hazard consistent for $A(1s)$, because $A(1s)$ alone is not a sufficient IM for $EDP \equiv u_m$.

Since $A(1s)$ is not a sufficient IM for u_m, then u_m must depend on other aspects of the ground motion. Fig 2.12 examines the hazard consistency of the same records from Fig 2.11, for six miscellaneous IMs. Specifically, these IMs include PGA, PGV, acceleration spectrum intensity (ASI), cumulative absolute velocity (CAV), and two measures of significant duration: (1) D_{5-75}, and (2) D_{5-95}. The CB08 model was used to develop the PSHA curves for PGA and PGV, the Bradley 2010 model [60] for ASI, the Campbell & Bozorgnia 2010 model [61] for CAV, and the Bommer et al 2009 model [62] for duration. As in Fig 2.11, the estimated IMHCs were obtained from Eqs 3.16 and 2.9.

Fig 2.12a-c and Fig 2.12e-f demonstrate that the ground motions from GCIM-SA are hazard consistent for PGA, PGV, ASI, D_{5-75}, and D_{5-95}. Since the corresponding SDHC estimate is biased at exceedance rates below the MCE level (Fig 2.10a), we conclude that the vector-valued IM, defined as a collection of PGA, PGV, ASI, D_{5-75}, and D_{5-95}, *must not be sufficient* for u_m. In other words, the bias in the SDHC estimate is influenced by the hazard consistency of the ground motions for *other* IMs. However, such a vector-valued IM appears to be less insufficient than $A(1s)$ alone, since the GCIM-SA estimate of the SDHC is more accurate than that from IDA (Fig 2.10a). In summary, we conclude that severely scaled ground motions (Fig 2.6) may still lead to an accurate estimate of the SDHC, as long as they are hazard consistent *for an IM that is sufficient*.

In general, an IM – scalar or vector-valued – will almost never be truly sufficient for an EDP that is related to the inelastic response of realistic models of structures. As a result, even if ground motions are deliberately forced to be hazard consistent for a vector-valued IM (as in procedures like CS or GCIM), the modification of ground motions in PSDA (e.g., Fig 2.1b) will likely lead to some degree of bias in the subsequent SDHC estimates. Without a benchmark to compare against, such bias cannot be quantified. Fortunately, the framework and benchmark proposed in this study enable a direct determination of the bias.

2.8 Avoid a potential pitfall

If we want to establish the causal relationship between a particular GMSM procedure and the potential bias in its resulting estimate of the SDHC, then we must specify the *same* GMPM in both the benchmark SDHC and the estimate from the GMSM procedure, which is illustrated in Fig 3.1. This was done for the results shown in Fig 2.10 since for each of

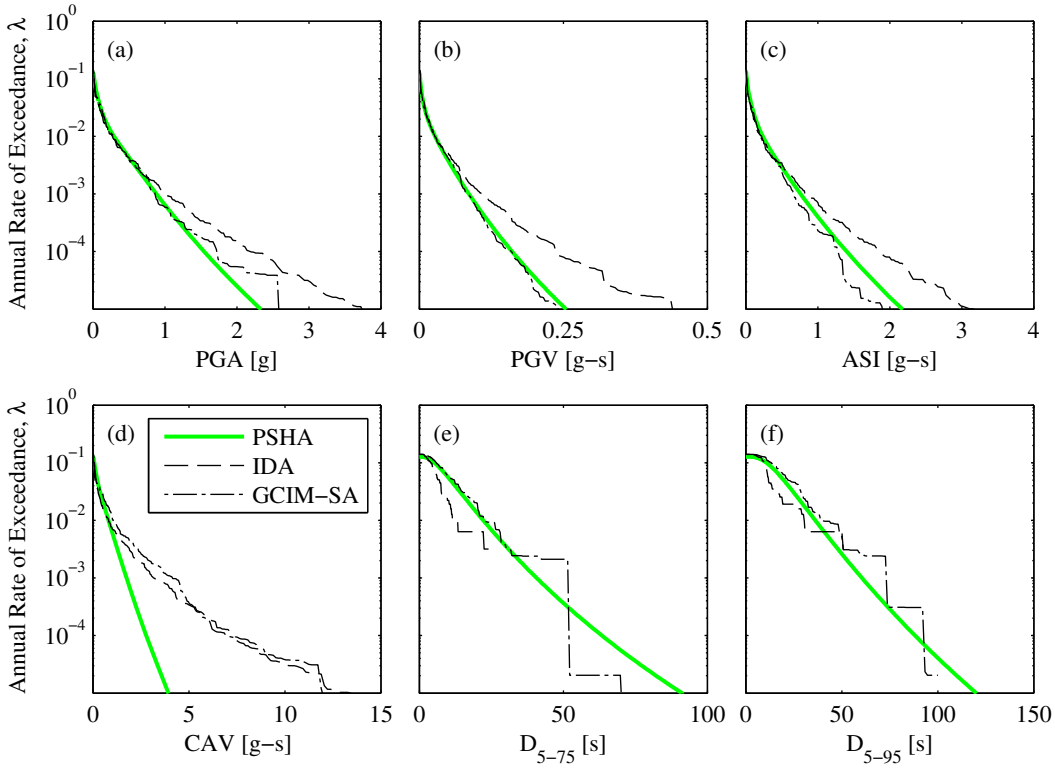

Figure 2.12: Hazard consistency of the ground motions selected from $IM_j \equiv A(1s)$ for several miscellaneous IMs: (a) PGA; (b) PGV; (c) ASI; (d) CAV; (e) D_{5-75}; (f) D_{5-95}.

the four cases, the same GMPM was chosen for both the benchmark SDHC and the GMSM-based estimates. By controlling the GMPM in this manner, the discrepancies between a PSDA-based estimate of the SDHC and the benchmark SDHC are due primarily to the GMSM procedure.

If we do not specify a common GMPM for both the benchmark and the GMSM-based estimate, then the resulting observations are misleading. For example, consider Fig 2.13a, where the GCIM-SA curve in Fig 2.11c is compared against two different PSHA-based IMHCs: (1) that from Fig 2.11c, and (2) that from a weighted average of the four IMHCs in Fig 2.2a. The weighted IMHC might be of interest because one might consider it to be a 'best estimate' of the target IMHC for comparison (see e.g., the US Geological Survey online hazard tool); however, it is erroneous to use this curve for examining hazard consistency of the ground motions from the GCIM-SA procedure that employs the CB08 model (Fig 2.4). Another example is illustrated in Fig 2.13b, where the GCIM-SA curve in Fig 2.10a is compared against two benchmark SDHCs: (1) that in Fig 2.10a, and (2) that from a weighted average of the four benchmark SDHCs in Fig 2.10. It is erroneous to use the weighted benchmark SDHC for evaluating the accuracy of the SDHC that is determined from the CB08 model. If

one insists on specifying the weighted SDHC as the benchmark, then (1) the *same* weights should be employed in determining $\widetilde{\lambda}_{IM}(x_i)$ in Eq 2.2, and (2) ground motions should be selected via the "exact CS" [57] for a fair comparison.

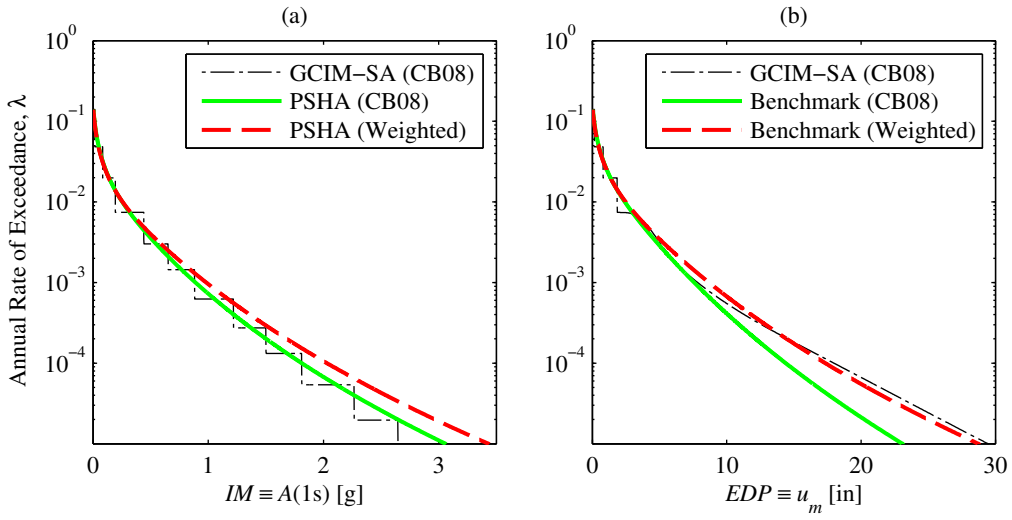

Figure 2.13: Two examples for illustrating the importance of specifying a common GMPM when implementing the proposed framework: (a) 'hazard consistency' of the ground motions from GCIM-SA when $IM \equiv A(1s)$; (b) GCIM-SA estimate of the SDHC versus 'the benchmark'.

There are two limitations of the proposed framework in this study (Fig 3.1). First, the framework can only be applied when an EDP prediction model is readily available for the structure (e.g., bilinear SDF systems in [59], the 4-story building in [28], the 8-story building in [29], etc.). In general, it is a major computational task to develop an EDP prediction model for a realistic structure because the number of necessary RHAs is typically large (e.g., 200 RHAs of a 12-story building were performed in [28]) and the selection of an optimal functional form requires an iterative approach. Second, the range of applicability of the proposed framework is limited by the availability of recorded ground motions. As shown in Fig 3.1, the prediction model for EDP is to be developed from a database of *unmodified* ground motions, because the purpose of the comparison between the resulting benchmark SDHC and an estimate from a GMSM procedure is to reveal potential biases from the modification of ground motions. However, such a recommendation will result in a small number of inelastic responses when the number of intense (relative to the strength of the structure) ground motions in the database is small.

2.9 Conclusions

This investigation of developing a framework for the evaluation of GMSM procedures has led to the following conclusions:

1. Meaningful evaluation of GMSM procedures requires clearly stating the objective of the RHAs of the structure. In this study, four objectives are identified and the evaluation of GMSM procedures is investigated when the objective of the RHAs is to estimate a SDHC for a given structure at a given site.

2. Using a simple case study, we highlight an important but subtle limitation of the existing approaches for evaluating GMSM procedures in PSDA: the practical equality between two SDHCs from different conditioning IMs does not *necessarily* indicate that an unbiased SDHC has been obtained. Consequently, an alternative approach for evaluating GMSM procedures in PSDA is desirable.

3. To quantify bias in any estimate of the SDHC, we introduce the notion of a benchmark; the benchmark SDHC is determined by incorporating an EDP prediction model that is developed from unmodified ground motions into the PSHA calculations. Consequently, this study is limited by the availability of EDP prediction models and the availability of recorded ground motions.

4. With the variety of benchmarks in past studies, it might seem difficult to claim a single choice as the benchmark. We overcome this apparent difficulty by recognizing that (1) different choices correspond to different instances of epistemic uncertainty, (2) the purpose of a benchmark is to isolate the effects of GMSM procedures on the resulting SDHC estimates, and (3) the same ground motion information should be utilized in obtaining the benchmark SDHC and all estimates of the SDHC from GMSM procedures.

5. To develop an understanding of why one GMSM procedure may provide more accurate estimates of the SDHC than another, we identify the role of IM sufficiency in the relationship between (1) bias in the SDHC, and (2) hazard consistency of the corresponding selected ground motions. If the IM, scalar or vector-valued, used for record selection is sufficient, then ensuring hazard consistency of the selected ground motions for this IM must imply that the corresponding estimate of the SDHC is unbiased, even when the ground motions are scaled by large scale factors; as a corollary, if the ground motions are hazard consistent for a vector-valued IM, then the fact that the corresponding estimate of the SDHC is observed to be biased must imply that the IM is *not* sufficient for the EDP of interest. Therefore, accurate estimates of the SDHC may be obtained from severely scaled ground motions, as long as the selected motions are hazard consistent *for an IM that is sufficient*.

6. We do not know, a priori, which IM is sufficient for an arbitrary EDP associated with the inelastic response of a realistic structure; in fact, rarely will an IM that is sufficient exist. Consequently, the modification of ground motions in PSDA will likely cause some amount of bias in the SDHC estimate, despite the fact that ground motions may be hazard consistent for some vector-valued IM. Without a benchmark to compare against, such bias cannot be quantified.

7. When implementing the proposed framework for the evaluation of GMSM procedures, one may draw misleading conclusions if the benchmark SDHC and a PSDA-based estimate are not derived from a common set of ground motion information.

Chapter 3

Evaluation of GMSM procedures using synthetic ground motions

3.1 Abstract

This study presents a novel approach for evaluating ground motion selection and modification (GMSM) procedures in the context of probabilistic seismic demand analysis (PSDA). In essence, synthetic ground motions are employed to derive the benchmark seismic demand hazard curve (SDHC), for any structure and response quantity of interest, and to establish the causal relationship between a GMSM procedure and the bias in its resulting estimate of the SDHC. An example is presented to illustrate how GMSM procedures may be evaluated using synthetic motions. To demonstrate the robustness of the proposed approach, two significantly different stochastic models for simulating ground motions are considered. By quantifying the bias in any estimate of the SDHC, the proposed approach enables the analyst to rank GMSM procedures in their ability to accurately estimate the SDHC, examine the sufficiency of intensity measures (IMs) employed in ground motion selection, and assess the significance of the conditioning IM in PSDA.

3.2 Introduction

Ground motions [1] required to conduct nonlinear response history analysis (RHA) of structures may either be recorded or synthetic; recorded ground motions are obtained from strong motion instruments whereas synthetic ground motions are simulated from models [63]. Such models may be purely physics-based, purely stochastic, or a combination of the two. Recorded ground motions are usually modified because *intense* records, typically of interest in earthquake engineering, are scarce.

[1] In this paper, "ground motion" refers to ground acceleration as a function of time (i.e., an accelerogram). Although the same term also refers occasionally to an intensity measure (as in "ground motion prediction models"), its meaning should be clear from the context.

Many ground motion selection and modification (GMSM) procedures have been developed. For example, several records may be selected on the basis of magnitude and distance [15, 5], or spectral shape [9, 25]. Selected records are sometimes amplitude scaled [15, 36] and other times adjusted with wavelets such that the response spectrum of the modified record is compatible with a target spectrum (see e.g., [29]). A review of many GMSM procedures may be found in Appendix A of [26] and in [27]. How should one choose among the variety of GMSM procedures available? This question will be answered in this paper.

Among the variety of contexts where RHAs are conducted [64], we choose probabilistic seismic demand analysis (PSDA) [15], which is also known as a risk-based assessment [31]. For a given structure at a given site, a PSDA couples probabilistic seismic hazard analysis (PSHA) of the site with RHA of the structure in order to determine the seismic demand hazard curve (SDHC) of an engineering demand parameter (EDP). The exact SDHC, $\lambda_{EDP}(z)$, is governed by

$$\lambda_{EDP}(z) = \int \Pr(EDP > z \mid IM^* = x) \cdot |\mathrm{d}\lambda_{IM^*}(x)| \tag{3.1}$$

where IM^* denotes the conditioning intensity measure (IM), $\lambda_{IM^*}(x)$ denotes its corresponding exact hazard curve, and $\Pr(EDP > z \mid IM^* = x)$ denotes the exact complementary cumulative distribution function (CCDF) of EDP when the intensity level is equal to x [2]. In practical application, $\lambda_{EDP}(z)$ is estimated from

$$\widehat{\lambda}_{EDP}(z) = \sum_{i=1}^{N_{IM^*}} \widehat{\Pr}(EDP > z \mid IM^* = x_i) \cdot |\Delta\widetilde{\lambda}_{IM^*}(x_i)| \tag{3.2}$$

where $\widetilde{\lambda}_{IM^*}(x_i)$ denotes the intensity measure hazard curve (IMHC) that is computed from a particular ground motion prediction model (GMPM) in PSHA, N_{IM^*} denotes the number of intensity levels chosen to approximate the integral in Eq 3.1, and $\widehat{\Pr}(EDP > z \mid IM^* = x_i)$ denotes the CCDF of EDP that is determined by performing RHAs of the structure for an ensemble of ground motions from a GMSM procedure. To include the possibility of structural collapse, $\widehat{\Pr}(EDP > z \mid IM^* = x_i)$ in Eq 3.2 may be expanded to obtain

$$\widehat{\Pr}(EDP > z \mid IM^* = x_i) = \widehat{\Pr}(EDP > z \mid \mathrm{NC}, IM^* = x_i)\,[1 - \widehat{p}_C(x_i)] + \widehat{p}_C(x_i) \tag{3.3}$$

where NC denotes the event corresponding to "No Collapse" and $\widehat{p}_C(\cdot)$ refers to the fragility function that is determined from multiple ensembles of ground motions that have been scaled to different intensity levels [65]. At each intensity level x_i, an ensemble of ground motions is obtained from a GMSM procedure (e.g., Incremental Dynamic Analysis (IDA) [40], Conditional Spectrum [1], etc.). A SDHC estimate from Eq 3.2, corresponding to a particular GMSM procedure, is defined to be *unbiased* when it is essentially equal to $\lambda_{EDP}(z)$; it is defined to be *biased* when it differs significantly from $\lambda_{EDP}(z)$.

It is currently difficult to definitively evaluate the accuracy of any estimate of the SDHC because the exact SDHC, $\lambda_{EDP}(z)$, is unknown. To circumvent this limitation, the accuracy

[2] In this study, an asterisk is included to the symbol IM when denoting a conditioning intensity measure.

of a SDHC estimate is often judged by comparing it against several other estimates of the SDHC, each determined from the same GMSM procedure but selecting different definitions of the conditioning IM in Eq 3.2 [35, 37]. With enough definitions of the conditioning IM, close agreement between the corresponding SDHCs suggests that the associated GMSM procedure provides unbiased estimates of the SDHC. However, the SDHCs from different definitions of the conditioning IM are almost always different from each other and without a "benchmark" for comparison, it is difficult to judge the accuracy of any SDHC estimate. Alternatively, the potential bias may be approximated using the Generalized Conditional Intensity Measure approach [47]; however, the quality of such approximations is also difficult to ascertain for lack of a benchmark. To supplement the conclusions from the previous approaches, SDHC estimates were compared against a benchmark SDHC that is computed from a prediction model for the EDP [64]. With this approach, the bias of any SDHC estimate may be quantified; however, it is limited by the availability of prediction models for the EDP and structure of interest and such prediction models are in turn limited by the availability of recorded ground motions.

In this paper, we establish *the causal relationship* between a GMSM procedure and the bias in its resulting SDHC estimate by using a large database of synthetic ground motions to determine the "benchmark" SDHC and to control as many variables as possible. By comparing Eq 3.2 against Eq 3.1, three major sources of bias may be identified: (1) approximation of the integral in Eq 3.1 with a summation in Eq 3.2, (2) approximation of $\lambda_{IM^*}(x)$ with $\widetilde{\lambda}_{IM^*}(x)$, and (3) approximation of $\Pr(EDP > z \mid IM^* = x)$ with $\widehat{\Pr}(EDP > z \mid IM^* = x)$, which is obtained from RHAs of the structure for an ensemble of ground motions determined by a GMSM procedure. The first source can be essentially eliminated if N_{IM^*} is adequately large. The second source can be essentially eliminated with the aid of synthetic ground motions (Section 3.6). With these two contributions eliminated, potential biases from a particular GMSM procedure can be identified (third source). This approach with synthetic ground motions is developed in the next section.

3.3 Proposed approach to evaluate GMSM procedures

The proposed approach is schematically illustrated in Fig 3.1 [3]. The SDHC estimate from each GMSM procedure, $\widehat{\lambda}_{EDP}(z)$, is compared against the benchmark SDHC, $\lambda_{EDP}(z)$, under a controlled setting; the benchmark SDHC is computed from a large database of synthetic ground motions and each GMSM-based SDHC is computed from a subset of this database. It is important to derive all SDHCs from a common set of ground motion information (i.e., earthquake rupture forecast, GMPMs, etc.) because the purpose of each comparison in Fig 3.1 is to isolate the effect of the GMSM procedure on its resulting SDHC estimate.

[3] Unlike the approach in [64], the approach herein employs synthetic ground motions and as a result, the benchmark SDHC and prediction models significantly differ from those described in [64].

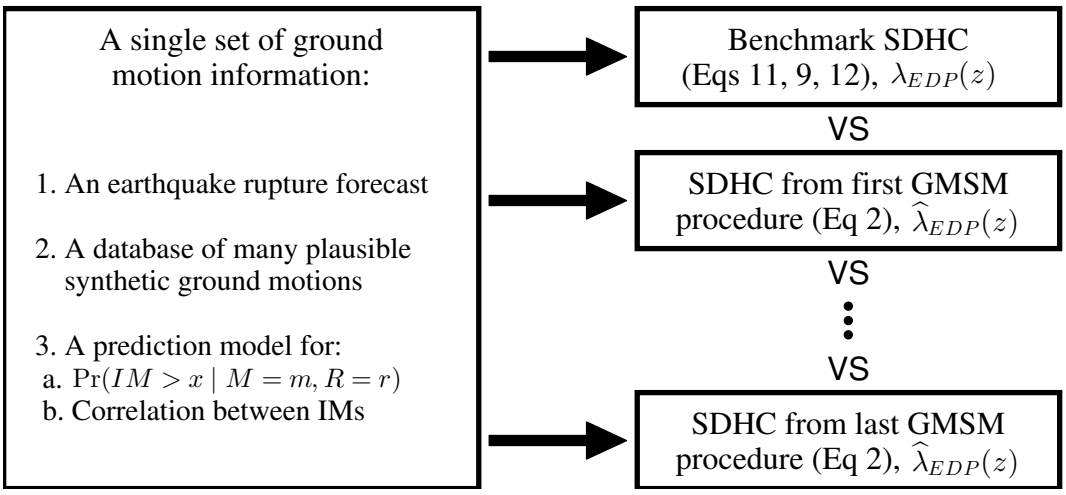

Figure 3.1: Schematic illustration of the framework for evaluating GMSM procedures using synthetic ground motions.

To develop this common set of ground motion information for a given site, an earthquake rupture forecast and a database of ground motions are needed. Each of the N_{src} earthquake sources is characterized by an activity rate, ν, and a probability density function (PDF) for earthquake magnitude and distance, $f_{M,R}(m,r)$. Next, a model for simulating synthetic ground motions is chosen for the given site; although only two stochastic models are illustrated herein – Rezaeian-Der Kiureghian [66] and Yamamoto-Baker [67] – other well-vetted models (e.g., physics-based, hybrid, etc.) may be considered. A large number of intense synthetic ground motions is then simulated from the chosen model, for the specified earthquake rupture forecast (Section 3.4).

This large database of intense ground motions enables computation of the exact hazard curves, $\lambda_{IM^*}(x)$ and $\lambda_{EDP}(z)$ in Eq 3.1, which are unique for a given ground motion simulation model (Section 3.5); however, the number of synthetic ground motions in such databases is nevertheless finite. Furthermore, different ground motion simulation models lead to different $\lambda_{IM^*}(x)$ and $\lambda_{EDP}(z)$. For this reason, the hazard curves that correspond to a particular database of synthetic ground motions are referred to as the *benchmark* (as opposed to "exact") hazard curves. Note that such a benchmark could not have been determined from recorded ground motions for lack of an adequate number of intense records.

Several contemporary GMSM procedures (e.g., [9], [1], [47], etc.) require GMPMs to select ground motions. Therefore, we will develop new GMPMs from the previously simulated database of ground motions, as shown in the left part of Fig 3.1. These GMPMs may then be used to construct IMHCs, $\widetilde{\lambda}_{IM}(x)$, or perform deaggregation [32]. Since our objective is to isolate the effect of a GMSM procedure on the resulting SDHC estimate, it is mandatory that the GMPM-based IMHC, $\widetilde{\lambda}_{IM^*}(x)$ in Eq 3.2, be essentially equal to the benchmark

IMHC, $\lambda_{IM^*}(x)$ in Eq 3.1. For this reason, the GMPMs developed in this paper are referred to as *benchmark-consistent* GMPMs (Section 3.6).

For each GMSM procedure of interest, a corresponding SDHC estimate is determined from the ground motion information depicted in the left part of Fig 3.1 (Section 3.7). Specifically, all GMSM procedures select and modify a subset of the previously simulated database of ground motions. If prediction models are needed as input to the GMSM procedure, then the benchmark-consistent prediction models that are developed in Section 3.6 are employed. For each GMSM procedure, the corresponding estimate of the SDHC is obtained from Eq 3.2 and compared against the benchmark SDHC, $\lambda_{EDP}(z)$. Since (1) $\lambda_{EDP}(z)$ may now be determined from synthetic ground motions (Section 3.5), and (2) $\widetilde{\lambda}_{IM^*}(x)$ is essentially equal to $\lambda_{IM^*}(x)$ (Section 3.6), a comparison of $\widehat{\lambda}_{EDP}(z)$ against $\lambda_{EDP}(z)$ indicates the bias caused by the corresponding GMSM procedure (Section 3.7). To illustrate this approach for evaluating GMSM procedures, an example is presented; the details of this example are described next.

3.4 Case study

Site, stochastic models, and databases of synthetic ground motions

We select the simple site illustrated in Fig 3.2a, which is appropriate for this study [4]. The site is situated on soil with a shear-wave velocity, V_{s30}, of 400 m/s and a basin depth, $Z_{2.5}$, of 1 km. A single strike-slip fault with an activity rate of $\nu = 0.02$ earthquakes per year is located 10 km away from the site. All earthquakes are assumed to occur at a fixed distance, $R = 10$ km; in contrast, the magnitude of each earthquake, M, is random and follows the PDF that is given by the Youngs & Coppersmith model [68] (Fig 3.2b). This completes the specification of an earthquake rupture forecast in Fig 3.1.

There are several advantages to selecting a simple site. For the selected site, the general equation governing any IMHC in PSHA (see e.g., [32]) is greatly simplified:

$$\begin{aligned}\lambda_{IM}(x) &= \sum_{i=1}^{N_{src}} \nu_i \cdot \left\{ \int\int \Pr(IM > x \mid M = m, R = r) f_{R|M}(r \mid m) f_M(m)\, \mathrm{d}r\, \mathrm{d}m \right\}_i \\ &= \nu \cdot \left\{ \int \Pr(IM > x \mid M = m) f_M(m)\, \mathrm{d}m \right\} \end{aligned} \tag{3.4}$$

where $\Pr(IM > x \mid M = m)$ refers to the CCDF of the IM for a given earthquake magnitude. This simplification facilitates the computation of benchmark hazard curves (Section 3.5) and the development of benchmark-consistent GMPMs (Section 3.6). Furthermore, such a simple site is sufficient to illustrate the approach described in Section 3.3.

[4] Except for the activity rate, this site is identical to that considered in Section 5.4 of Yamamoto's Ph.D. dissertation [67].

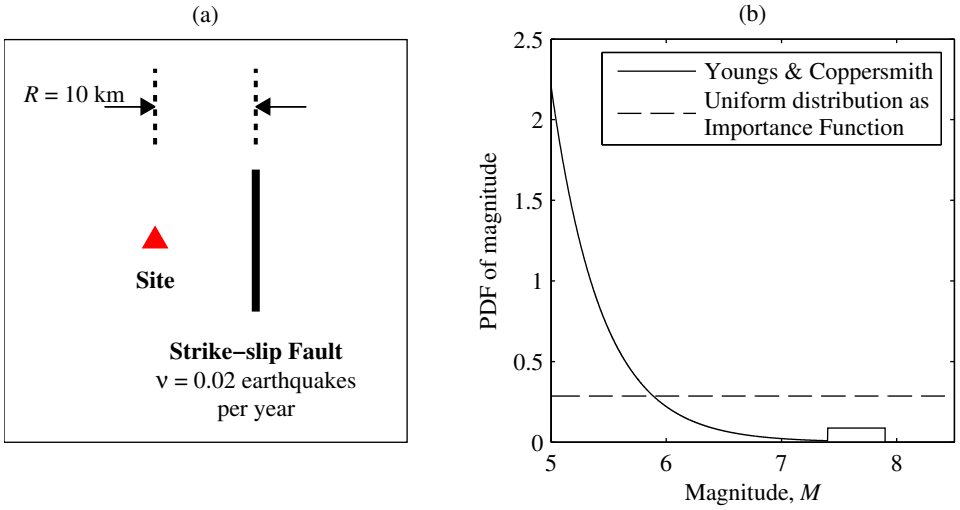

Figure 3.2: Source characterization for case study site: (a) specification of earthquake source; (b) PDF of magnitude for the strike-slip fault.

Two stochastic models, referred to as Rezaeian [69, 66] and Yamamoto [67, 70], are employed to simulate synthetic ground motions. Two models are chosen in order to test the robustness of the proposed approach for evaluating GMSM procedures. Given magnitude, distance, style-of-faulting, and V_{s30} as inputs, Rezaeian's model simulates a ground motion by time-modulating a filtered white-noise stochastic process. The resulting ground motion is fully nonstationary because the parameters of both (1) the time-modulating function and (2) the filter vary with time. In contrast, Yamamoto's model simulates a fully nonstationary ground motion via the Wavelet Packet Transform. Example waveforms from Rezaeian's model can be seen in Figs 7-8 of [66]; example waveforms from Yamamoto's model can be seen in Figs 4-5 of [70].

For each stochastic model, a database of 10^4 synthetic ground motions is randomly simulated. The Youngs & Coppersmith PDF of magnitude in Fig 3.2b, $f_M(m)$, indicates that a wide range of magnitudes is possible for the given site. Therefore, a natural approach to simulate a database that adequately covers the range of possible magnitudes is to first generate 10^4 random values of magnitude from $f_M(m)$, and then simulate a ground motion for each of the 10^4 magnitudes. However, the number of *intense* ground motions in such a database would be small, as suggested by $f_M(m)$ in Fig 3.2b. To overcome this limitation, Yamamoto and Baker proposed to employ the concept of Importance Sampling [67], a standard procedure in statistics (see e.g., Section 24.3 of [39]). Using the uniform distribution in Fig 3.2b as the Importance Function, $g_M(m)$, 10^4 values of magnitude are randomly generated and the corresponding value of Importance Sampling weights, $w(m) = f_M(m) \div g_M(m)$, are saved. Corresponding to each of the 10^4 values of magnitude, a synthetic ground motion

is randomly simulated from the two stochastic models.

Structural models and engineering demand parameters

To highlight the generality of the proposed approach, two nonlinear SDF systems and two EDPs are considered. Although SDF systems are chosen to facilitate reproducibility of the results in this study, any structural model and EDP may be chosen (see end of Section 3.8). The first SDF structure is a 5% damped bilinear system with a linear vibration period, T_1, of 1 s, a yield displacement of $0.2\text{g} \times (T_1/2\pi)^2$, and a post-yield hardening ratio of 5%. The second SDF structure is a 3.4% damped degrading system with a linear vibration period, T_1, of 1.1 s, a yield displacement of $0.18\text{g} \times (T_1/2\pi)^2$, and a post-yield softening ratio of 2%; it is the first-mode inelastic SDF system of the 4-story building considered in [71]. For each SDF structure, the SDHCs corresponding to two EDPs are of interest: (1) peak deformation, u_m, and (2) peak total acceleration, $\ddot{u}_o^t$.

The force-deformation relationships for the two selected SDF structures are presented in Fig 3.3. The relationship for the degrading system is represented by the Modified Ibarra-Medina-Krawinkler (IMK) model [72] with peak-oriented hysteretic response; the specific parameters for this model may be found in Tables 4.2 and 4.3 of [71]. The post-yield hardening portrayed in Fig 3.3a indicates that collapse is impossible for the bilinear system. In contrast, collapse is possible for the degrading system because the Modified IMK model captures both stiffness and strength deterioration (Fig 3.3b). Strictly speaking, collapse occurs when the deformation of the system increases without bounds. Practically however, collapse is defined herein as the event where the peak deformation exceeds 29 inches (see e.g., Section 3.2.2 of [26]), which corresponds to the ultimate rotation capacity that is specified in the Modified IMK model.

GMSM procedures

To emphasize the flexibility of the proposed approach, two significantly different GMSM procedures are considered in this study: (1) IDA [40], and (2) a special case of the Generalized Conditional Intensity Measure approach (GCIM) [47, 48, 35], where only spectral accelerations, $A(T)$, are considered as IMs for ground motion selection; this special case is denoted by GCIM-SA. IDA represents a simple and well known technique for estimating SDHCs in PSDA (see e.g., [49]), whereas GCIM-SA is a more sophisticated GMSM procedure. The latter permits examination of the premise that spectral shape is a sufficient IM [12] for EDPs of nonlinear SDF systems.

3.5 Benchmark hazard curves

For a specified ground motion simulation model, a unique set of hazard curves, $\lambda_{IM}(x)$ and $\lambda_{EDP}(z)$ in Eq 3.1, exist. We will see that these hazard curves may be approximated from a

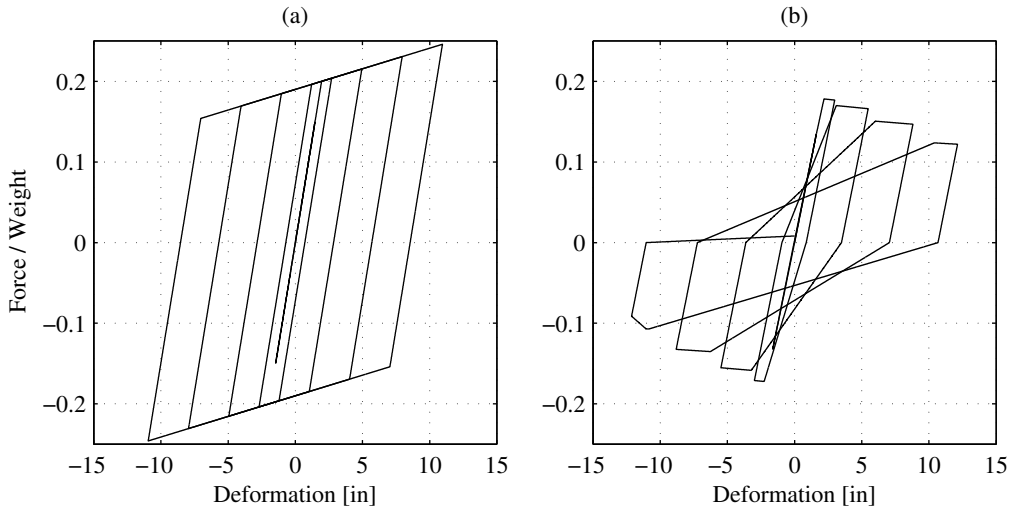

Figure 3.3: Force-deformation relationships from cyclic pushover analysis: (a) bilinear; (b) Modified IMK model with peak-oriented response.

database of synthetic ground motions. The theory for such calculations is presented in this section.

Intensity measure hazard curve

The exact hazard curve for any IM at the site described in Section 3.4 is governed by Eq 3.4. In this equation, $f_M(m)$ is given by the PDF shown in Fig 3.2b and $\Pr(IM > x \mid M = m)$ is given by the stochastic model for randomly simulating ground motions. If magnitudes were randomly generated from $f_M(m)$ and used as input to the selected stochastic model, then $\lambda_{IM}(x)$ may be computed from the usual Monte Carlo estimator (see e.g., Section 4.5 of [73]):

$$\lambda_{IM}^{(\mathrm{MC})}(x) = \frac{\nu}{N} \sum_{i=1}^{N} I(x_i > x) \tag{3.5}$$

where the superscript MC refers to "Monte Carlo", N is the total number of synthetic ground motions in a database, x_i is the value of IM for the i^{th} ground motion, and $I(\cdot)$ denotes the indicator function, which is equal to unity when the event inside the parenthesis occurs and zero otherwise. When N is very large, $\lambda_{IM}^{(\mathrm{MC})}(x)$ is essentially equal to $\lambda_{IM}(x)$.

As mentioned earlier in Section 3.4, each database of synthetic ground motions was obtained using magnitudes that are randomly generated from the uniform distribution in Fig 3.2b, $g_M(m)$, instead of $f_M(m)$. Replacing $f_M(m)$ in Eq 3.4 with $f_M(m) \times g_M(m) \div g_M(m)$

leads to

$$\lambda_{IM}(x) = \nu \cdot \left\{ \int \left[\Pr(IM > x \mid M = m) \frac{f_M(m)}{g_M(m)} \right] g_M(m)\, \mathrm{d}m \right\} \tag{3.6}$$

Defining the ratio of $f_M(m)$ over $g_M(m)$ as the Importance Sampling weight, $w(m)$, the benchmark IMHC may therefore be computed from

$$\lambda_{IM}(x) \simeq \frac{\nu}{N} \sum_{i=1}^{N} [I(x_i > x) \cdot w(m_i)] \tag{3.7}$$

where m_i is randomly generated from $g_M(m)$ instead of $f_M(m)$, and x_i now refers to the value of IM for the corresponding i^{th} ground motion. For example, application of Eq 3.7 to the database of $N = 10^4$ synthetic ground motions from Rezaeian's model leads to the results shown by thick solid curves in Fig 3.4. As demonstrated in this figure, Eq 3.7 may be used to compute benchmark IMHCs for a wide variety of IMs.

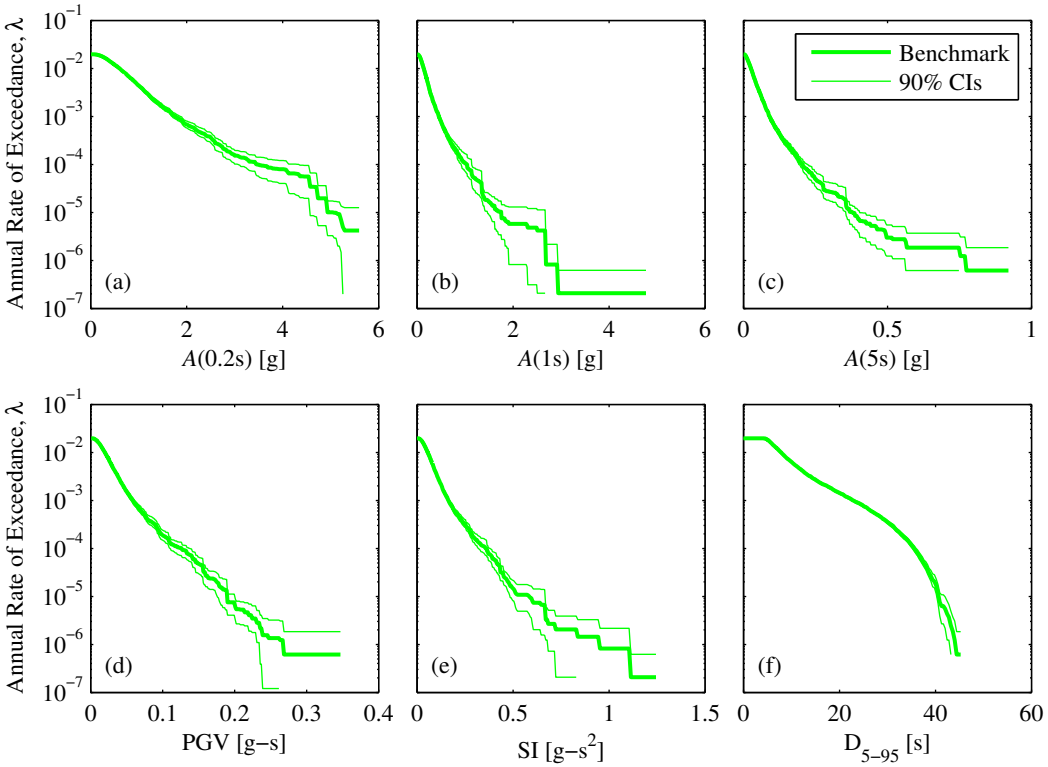

Figure 3.4: Benchmark IMHCs determined from 10^4 ground motions simulated by Rezaeian's stochastic model, for several IMs: (a) $A(0.2s)$; (b) $A(1s)$; (c) $A(5s)$; (d) peak ground velocity (PGV); (e) spectrum intensity (SI); (f) 5-95% significant duration, D_{5-95}.

There is epistemic uncertainty in the benchmark IMHCs because they are developed from a finite number of ground motions. For example, the value of the benchmark hazard curve

in Fig 3.4b is zero at intensity levels greater than 4.77g because the largest value of $A(1s)$ observed in the database is 4.77g. For another database of 10^4 ground motions simulated by Rezaeian's model, the largest observed value of $A(1s)$ will be different and hence the corresponding value of the benchmark IMHC will be different. To assess the quality of results achieved by using $N = 10^4$, a 90% confidence interval was determined for each IMHC by the bootstrap procedure [74] with 100 bootstrap samples. With these confidence intervals, we see in Fig 3.4 that at high exceedance rates (i.e., rates above 10^{-3} or return periods less than 1000 years), the approximation expressed in Eq 3.7 is nearly perfect. As the exceedance rate decreases, the quality of the approximation deteriorates, which should be recognized when interpreting subsequent results.

Seismic demand hazard curve when collapse is impossible

For structural models where collapse is impossible, the steps to develop a benchmark SDHC for any EDP are nearly identical to that just presented for the benchmark IMHC. By replacing IM in Eq 3.4 with EDP, the equation that governs the exact SDHC at this site becomes

$$\lambda_{EDP}(z) = \nu \cdot \left\{ \int \Pr(EDP > z \mid M = m) f_M(m)\, \mathrm{d}m \right\} \tag{3.8}$$

By replacing $f_M(m)$ in Eq 3.8 with $f_M(m) \times g_M(m) \div g_M(m)$ and applying the concept of Importance Sampling as before, the benchmark SDHC for structures where collapse is impossible may be computed from

$$\lambda_{EDP}(z \mid \mathrm{NC}) \simeq \frac{\nu}{N'} \sum_{i=1}^{N'} [I(z_i > z) \cdot w(m_i)] \tag{3.9}$$

where NC stands for "No Collapse", N' is the total number of ground motions where collapse did not occur, and z_i is the value of the EDP corresponding to the i^{th} ground motion. Observe that we can compute the benchmark SDHC from Eq 3.9, without a prediction model for the EDP [64]. However, depending on the exceedance rates of interest, a large number of RHAs may be necessary to implement the calculations in Eq 3.9.

With ground motions simulated by Rezaian's stochastic model, the benchmark SDHCs for the bilinear system are presented in the top row of Fig 3.5. For each EDP, the thick solid curve is computed by Eq 3.9 from the $N' = N = 10^4$ values of the EDP corresponding to the database of synthetic motions. As in Section 3.5, the 90% confidence intervals for these benchmark SDHCs are again obtained from the bootstrap procedure with 100 bootstrap samples.

To facilitate interpretation of these curves, exceedance rates of 2×10^{-3} (return period of 500 years) and 4×10^{-4} (return period of 2500 years), that correspond roughly to the design basis earthquake (DBE) and maximum considered earthquake (MCE) levels specified in [6], are noted in Fig 3.5. At exceedance rates above the MCE level, the 90% confidence intervals indicate that the approximation in Eq 3.9 is nearly perfect. Although the quality

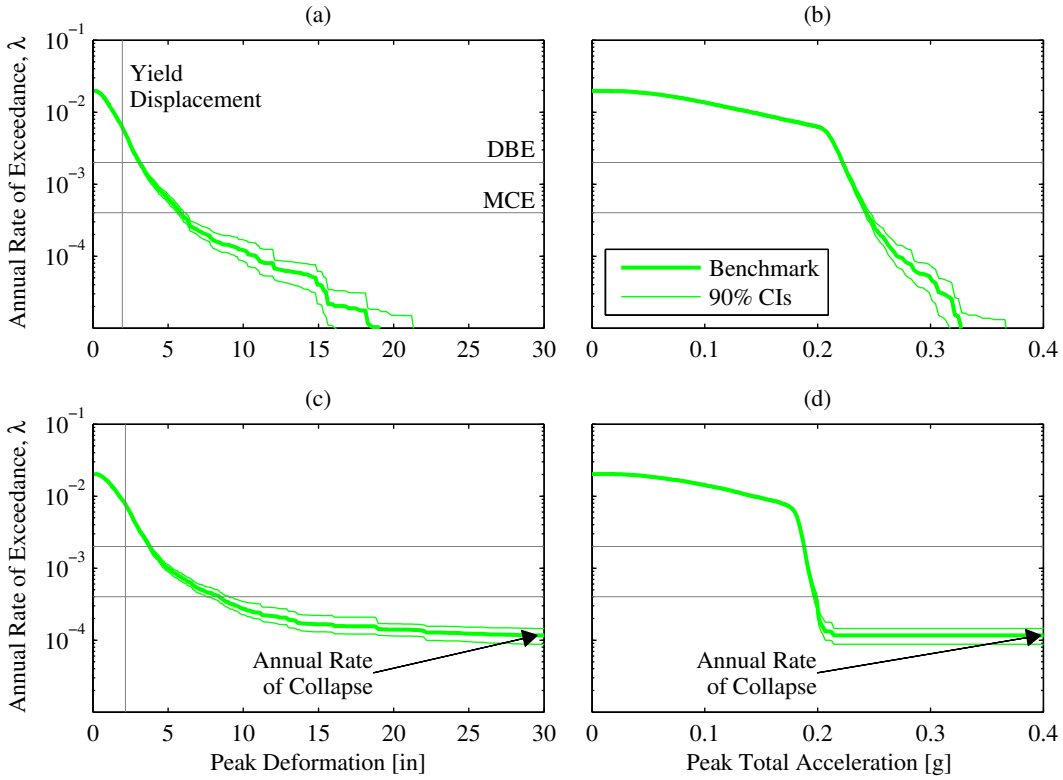

Figure 3.5: Benchmark SDHCs determined from 10^4 ground motions simulated by Rezaeian's stochastic model: (a-b) u_m and $\ddot{u}_o^t$ of bilinear system, respectively; (c-d) u_m and $\ddot{u}_o^t$ of degrading system, respectively.

of this approximation deteriorates for decreasing exceedance rates, the thick solid curves are still referred to as "benchmark" for purposes of revealing potential biases in SDHC estimates from a GMSM procedure. In passing, we observe that the system responds nonlinearly at exceedance rates below around 6×10^{-3}, as indicated by the yield displacement identified in Fig 3.5a and the sudden change in slope in Fig 3.5b.

Seismic demand hazard curve when collapse is possible

Using the total probability theorem and assuming that the probability of EDP exceeding z is equal to unity when the structure collapses [36] [5], the term $\Pr(EDP > z \mid M = m)$ in

[5] If a different assumption is desired (e.g., assuming $\Pr(PFA > z \mid \mathrm{C}, M = m) = \Pr(PGA > z \mid \mathrm{C}, M = m)$ instead of $\Pr(PFA > z \mid \mathrm{C}, M = m) = 1$, where PFA and PGA denote, respectively, peak floor acceleration of a multistory building and peak ground acceleration [37]), then Eqs 3.10-3.11 should be modified appropriately.

Eq 3.8 is expanded:

$$\Pr(EDP > z \mid M = m) = \Pr(EDP > z, \text{NC} \mid M = m) + \Pr(\text{C} \mid M = m) \tag{3.10}$$

where NC and C denote events corresponding to "No Collapse" and "Collapse", respectively. Substituting Eq 3.10 into Eq 3.8 and rearranging terms leads to

$$\lambda_{EDP}(z) = \lambda_{EDP}(z \mid \text{NC}) \left[1 - \frac{\lambda_C}{\nu}\right] + \lambda_C \tag{3.11}$$

where $\lambda_{EDP}(z \mid \text{NC})$ is the benchmark SDHC given that collapse is impossible, and λ_C is the annual rate of collapse.

Computation of the benchmark SDHC for any structural model, with the possibility of collapse, can be organized in five steps. First, RHA of the structure is performed for all N ground motions in the database. Second, the N results from RHA are subdivided into EDP values for the N' non-collapsed cases and $N - N'$ collapsed cases. Third, $\lambda_{EDP}(z \mid \text{NC})$ is determined by applying Eq 3.9 to only the N' values of EDP. Fourth, all N RHA results are employed to compute the annual rate of collapse, λ_C, from

$$\lambda_C \simeq \frac{\nu}{N} \sum_{i=1}^{N} [I(\text{C}_i) \cdot w(m_i)] \tag{3.12}$$

where $I(\text{C}_i)$ is equal to 1 if collapse is observed for the i^{th} ground motion and equal to zero otherwise. Fifth, $\lambda_{EDP}(z \mid \text{NC})$ and λ_C from the latter two steps are substituted in Eq 3.11 to obtain the final benchmark SDHC, $\lambda_{EDP}(z)$. With ground motions simulated by Rezaeian's stochastic model, the benchmark SDHCs of the degrading system are presented in the bottom row of Fig 3.5. As the value of the EDP increases, the benchmark SDHC approaches the annual rate of collapse (Fig 3.5c-d), and the quality of the approximations in Eqs 3.9 and 3.12 decreases, as indicated by wider confidence intervals.

3.6 Benchmark-consistent prediction models

Prediction models, which provide the probability distribution of an IM for a given rupture scenario, are needed to select ground motions in contemporary GMSM procedures (e.g., [1, 47]). In order to isolate the effect of a GMSM procedure on its resulting SDHC estimate, prediction models must be consistent with the particular database of synthetic ground motions (Fig 3.1); otherwise, an additional source of bias would be introduced. For example, if the GMPM-based IMHC in Eq 3.2, $\widetilde{\lambda}_{IM^*}(x)$, is significantly different than the benchmark IMHC in Eq 3.1, $\lambda_{IM^*}(x)$, then any difference between $\widehat{\lambda}_{EDP}(z)$ in Eq 3.2 and $\lambda_{EDP}(z)$ in Eq 3.1 cannot be solely attributed to the GMSM procedure under consideration. This section describes how such benchmark-consistent prediction models are developed.

Ground motion prediction model

Fig 3.6 illustrates how the median value of $IM \equiv A(1s)$ is estimated for a given magnitude. For each database of 10^4 ground motions (Section 3.4), the logarithmic values of $A(1s)$ are plotted against magnitude. Ordinary least squares (OLS) regression is then performed to determine the predicted median as a polynomial function of magnitude, which is shown in solid black. The degree of the polynomial function is chosen such that its corresponding regression results do not differ appreciably from those corresponding to the next higher degree. Based on this criterion, the functional forms for Rezaeian's and Yamamoto's stochastic models were determined as:

$$\ln IM = b_0 + b_1 M + \epsilon \qquad \ln IM = c_0 + c_1 M + c_2 M^2 + \epsilon \tag{3.13}$$

respectively, where for a given value of magnitude, ϵ is a zero mean normally distributed random variable with standard deviation σ; the b's and c's are coefficients to be estimated from regression analysis.

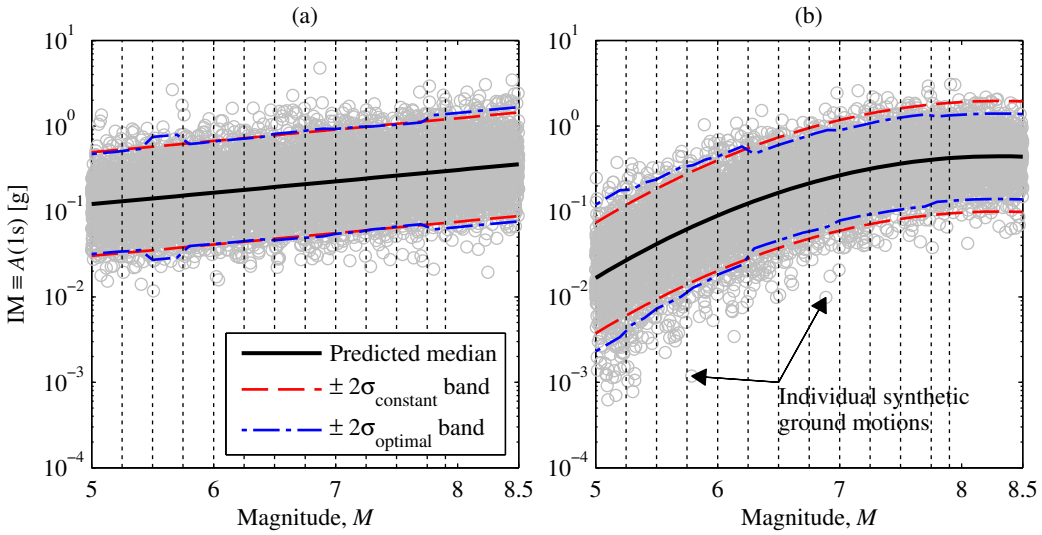

Figure 3.6: Example of GMPM development using synthetic ground motions: (a) Rezaeian's stochastic model; (b) Yamamoto's stochastic model.

Synthetic ground motions for the simple site (Fig 3.2) makes the development of GMPMs herein more manageable than that performed in practice with recorded ground motions. For example, there is no need to apply the random effects model or the two-stage regression technique, since each synthetic ground motion corresponds to an earthquake with a unique magnitude. Therefore, the terms associated with seismological parameters other than magnitude (e.g., distance, style-of-faulting, etc.) that appear in practical GMPMs [75] are not relevant for this particular site (see Section 3.4). Consequently, the development of GMPMs

reduces to estimating the CCDF of IM for a given magnitude, $\Pr(IM > x \mid M = m)$ in Eq 3.4, assumed to be lognormal.

Fig 3.6 permits three additional observations about the development of GMPMs from synthetic ground motions. First, the estimate of the median IM at large magnitudes is robust because the magnitudes in the ground motion database were randomly generated from the uniform PDF instead of the Youngs & Coppersmith PDF (Fig 3.2b). Second, the relationship between IM and M is unaffected by Importance Sampling since it is specified by the ground motion simulation model. Third, the standard deviation of the IM, σ, depends on magnitude for Yamamoto's model because the $\pm 2\sigma_{constant}$ band in Fig 3.6b covers fewer ground motions at large M than at small M; in contrast, σ is essentially independent of magnitude in Rezaeian's model because the $\pm 2\sigma_{constant}$ band in Fig 3.6a covers a similar amount of data at all M. For generality, σ is modeled as a function of magnitude in both stochastic models.

A natural way to model σ as a function of magnitude is to divide the magnitude domain into discrete bins and determine a value of σ at each bin. We chose the 12 bins shown in Fig 3.6. For each magnitude interval, the value of σ may be obtained by applying OLS to the binned ground motions; such values are denoted by σ_{binned}. At magnitudes beyond the domain of $f_M(m)$ in Fig 3.2b, σ is given by that from the closest magnitude bin.

Once a GMPM is finalized, $\widetilde{\Pr}(IM > x \mid M = m)$ is known and the corresponding IMHC may be computed from a discrete form of Eq 3.4:

$$\widetilde{\lambda}_{IM}(x) = \nu \cdot \left\{ \sum_{m} \widetilde{\Pr}(IM > x \mid M = m) \Pr(M = m) \right\} \tag{3.14}$$

For example, suppose $\widetilde{\Pr}(IM > x \mid M = m)$ is a lognormal CCDF with the median obtained from the solid black curve in Fig 3.6b and the standard deviation obtained from σ_{binned}. Applying Eq 3.14 to this model leads to the dashed curve in Fig 3.7a.

GMPMs based on σ_{binned} may not be benchmark-consistent. For example, the model for $A(1s)$ mentioned in the preceding paragraph is not benchmark-consistent because its corresponding IMHC differs from the associated benchmark IMHC at intensity levels greater than 1g (Fig 3.7a). By comparing Eq 3.14 against Eq 3.4, we see that the discrepancy between $\widetilde{\lambda}_{IM}(x)$ and $\lambda_{IM}(x)$ is due primarily to the discrepancy between $\widetilde{\Pr}(IM > x \mid M = m)$ and $\Pr(IM > x \mid M = m)$ at small exceedance probabilities (Fig 3.7b). For other IMs and other ground motion simulation models, this issue will introduce an additional source of bias to the GMSM-based estimate of the SDHC.

Since we wish to isolate the effects of a GMSM procedure on its resulting SDHC estimate, $\widetilde{\lambda}_{IM^*}(x)$ in Eq 3.2 must agree as closely as possible with $\lambda_{IM^*}(x)$ in Eq 3.1. To achieve this goal, σ is determined for each magnitude bin such that its resulting lognormal CCDF agrees most closely with the empirical CCDF at the 'tails'; this standard deviation is denoted as $\sigma_{optimal}$. An example of the tail region is presented as the shaded area in Fig 3.7b. The right boundary of this region corresponds to the largest value of the observed IM within the magnitude bin whereas the left boundary corresponds to the intensity level at which the

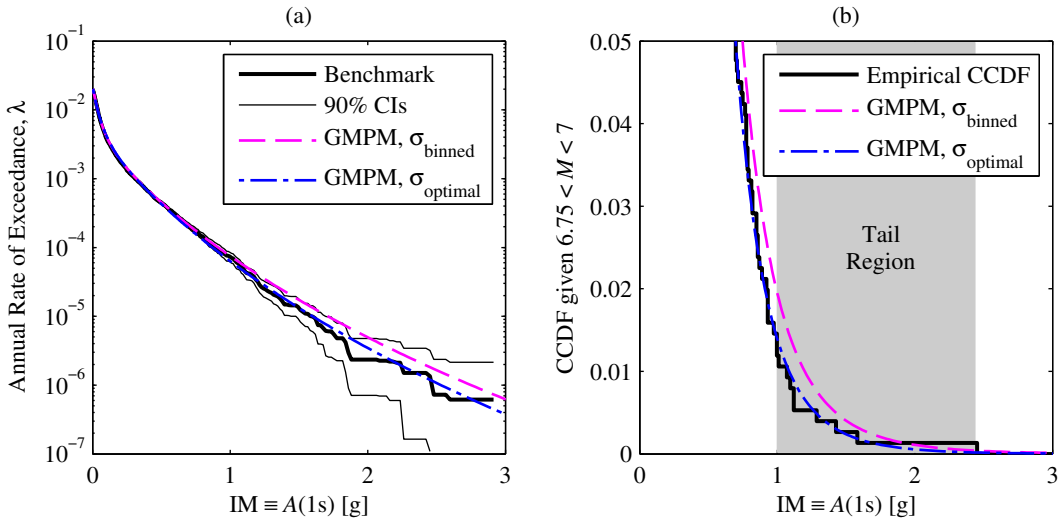

Figure 3.7: Example of enforcing benchmark-consistency on GMPMs developed from ground motions simulated by Yamamoto's stochastic model; comparison of: (a) IMHCs; (b) CCDFs at small probabilities.

IMHC from σ_{binned} begins to differ from the benchmark IMHC (Fig 3.7a) [6]; if the latter is larger than the former (or if there is only one ground motion within this tail region), then the tail region is undefined and $\sigma_{optimal}$ is specified as σ_{binned}. To quantify the discrepancy between $\widetilde{\Pr}(IM > x \mid M = m)$ and $\Pr(IM > x \mid M = m)$ at small exceedance probabilities, we introduce the following metric:

$$\Delta = \sum_{x \in \Omega} \left[\frac{\widetilde{G}(x, \sigma) - G(x)}{G(x)} \right]^2 \tag{3.15}$$

where Ω denotes the tail region, $G(x)$ is a shorthand notation for the empirical CCDF, and $\widetilde{G}(x, \sigma)$ is a shorthand notation for the lognormal CCDF corresponding to a trial value of σ. The value of σ that minimizes Δ is the desired $\sigma_{optimal}$. Determined using $\sigma_{optimal}$, the IMHC for $A(1s)$ agrees closely with the benchmark IMHC, confirming that the corresponding GMPM is benchmark-consistent (Fig 3.7a). Such benchmark-consistent GMPMs were developed for 21 periods of vibration that are logarithmically spaced between 0.05s and 10s; for other vibration periods, linear interpolation on the logarithmic scale was employed. This process of determining $\sigma_{optimal}$ may also be employed when developing benchmark-consistent GMPMs for other IMs.

[6] In this study, the left boundaries of the tail regions for all IMs were determined from visual comparison of the IMHCs. Alternatively, the left boundary of the tail region for an IM may be determined from its benchmark IMHC as the intensity level that corresponds to a single user-defined exceedance rate (e.g., 4×10^{-4}).

Correlation between intensity measures

Correlations between IMs are needed to specify the joint distribution of a vector IM (see e.g., [47, 1]). Derived subsequently are new correlations that are consistent with the database of synthetic ground motions.

For a given stochastic model, the correlation between two IMs is determined from the correlation between the residuals of each IM, defined as the differences between the observed and predicted values of each synthetic ground motion; e.g., the residuals for $A(1s)$, under Rezaeian's model, are the vertical deviations between each circle and the black solid curve in Fig 3.6a. For both stochastic models, the correlations between spectral accelerations at vibration periods from 0.05s to 10s are presented in Fig 3.8. The significant differences between the correlations from the two stochastic models indicate the need for benchmark-consistent correlations.

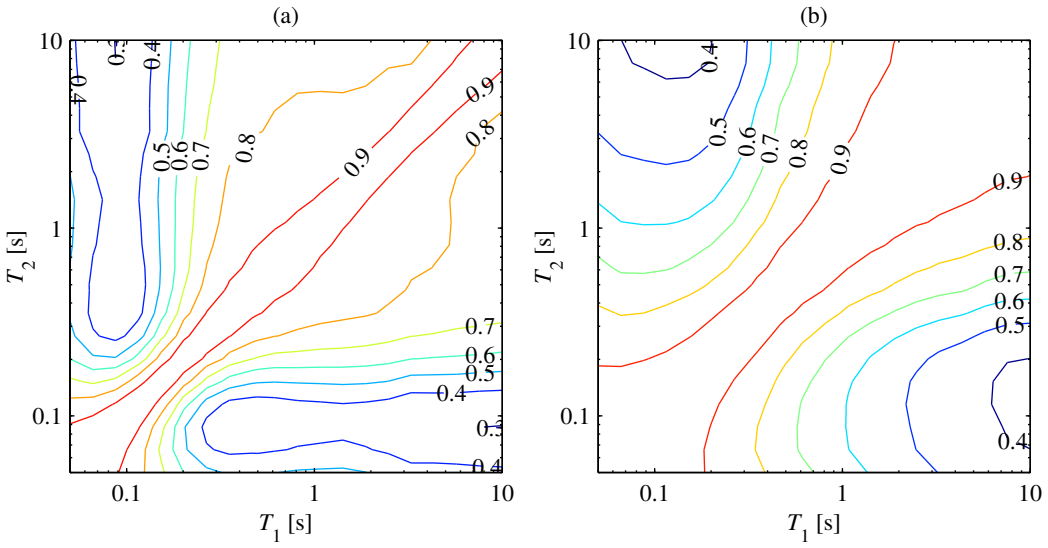

Figure 3.8: Correlations between spectral accelerations at periods from 0.05 to 10 s observed in 10^4 ground motions simulated by: (a) Rezaeian's stochastic model; and (b) Yamamoto's stochastic model.

For both stochastic models, the correlation between two IMs appears to be magnitude-dependent. To examine this magnitude dependence, we used the approach outlined in Appendix B of [76]. For each IM, the associated 10^4 residuals are partitioned into the 12 magnitude bins shown in Fig 3.6. A correlation is then computed for each magnitude bin and compared against the correlation from all bins. From such comparisons, we observed magnitude dependence for many pairs of IMs. For generality, the correlation between two IMs is modeled herein as a function of magnitude by providing a correlation value for each of the 12 magnitude bins.

3.7 Illustrative evaluation of GMSM procedures

With a large database of synthetic ground motions obtained for the given site (Section 3.4), benchmark SDHCs determined for the given structures (Section 3.5), and benchmark-consistent prediction models developed (Section 3.6), we are now ready to illustrate the evaluation of GMSM procedures in their ability to accurately estimate the SDHC (Fig 3.1). For each of the two GMSM procedures mentioned in Section 3.4, an estimate of the SDHC is computed from Eq 3.2. The conditioning IM is defined as spectral acceleration at 1 s and $N_{IM^*} = 12$ intensity levels are chosen, which correspond to: 50%, 20%, 10%, 5%, 2%, 1%, 0.5%, 0.2%, 0.1%, 0.05%, 0.02%, and 0.01% probability of exceedance in 50 years. At each intensity level, a subset of $n = 44$ synthetic ground motions are selected by the GMSM procedure, as excitations for RHAs of the structure, and the lognormal distribution is employed to determine $\widehat{\Pr}(EDP > z \mid IM^* = x_i)$; in total, $N_{IM^*} \times n = 528$ RHAs are performed to compute a single estimate of the SDHC.

In this study, the seed ensemble for IDA is selected in a manner that is inspired by the approach taken to develop the Far-Field record set in [49]. As described in Appendix A.7 of [49], the Far-Field record set for use in IDA was determined by preferentially selecting intense ground motions that were likely to induce structural collapse. To mimic this practical approach, we first filtered the database of 10^4 synthetic ground motions according to the following criteria: (1) $6.5 < M < 7.5$, (2) peak ground acceleration greater than 0.2g, and (3) peak ground velocity greater than 15 cm/s. Among the remaining ground motions, the 44 motions with the largest values of peak ground velocity are chosen as the seed ensemble. Unlike Appendix A.7 of [49], an upper limit for magnitude is provided in the first selection criterion because records from earthquakes with $M > 7.5$ are rare whereas over 2000 synthetic ground motions satisfied the three criteria above.

The selection of ground motions in GCIM-SA is significantly more sophisticated than that in IDA. In this case, 44 ground motions are re-selected at each of the 12 intensity levels. For a particular intensity level, deaggregation is performed and the target GCIM-SA spectrum is constructed using the prediction models developed in Section 3.6. For example, the target spectrum for the MCE level is presented in Fig 3.9a, which is defined at 11 vibration periods: $\mathbf{T}_{IM} = \{0.05, 0.1, 0.2, 0.3, 0.5, 0.75, 1, 2, 3, 5, 10\}$. From such a target spectrum, n response spectra may be simulated by methods presented in [47, 48]; for example, two simulated spectra are illustrated by markers in Fig 3.9b. For each of the n simulated spectra, the synthetic ground motion whose response spectrum agrees most closely with the simulated one is selected (see solid and dashed curves in Fig 3.9b).

RHAs of each system, subjected to the same selection of ground motions from a GMSM procedure, are performed to compute the corresponding SDHCs. For example, the results from RHAs of the degrading system due to ground motions selected by both GMSM procedures are presented in Fig 3.10. At each intensity level, the 44 results are classified either as non-collapsed or collapsed. The non-collapsed results, which are shown in the top row of Fig 3.10, are used in conjunction with the lognormal distribution to estimate $\widehat{\Pr}(EDP > z \mid \text{NC}, IM^* = x_i)$ in Eq 3.3. On the other hand, the fragility function, $\widehat{p}_C(x_i)$

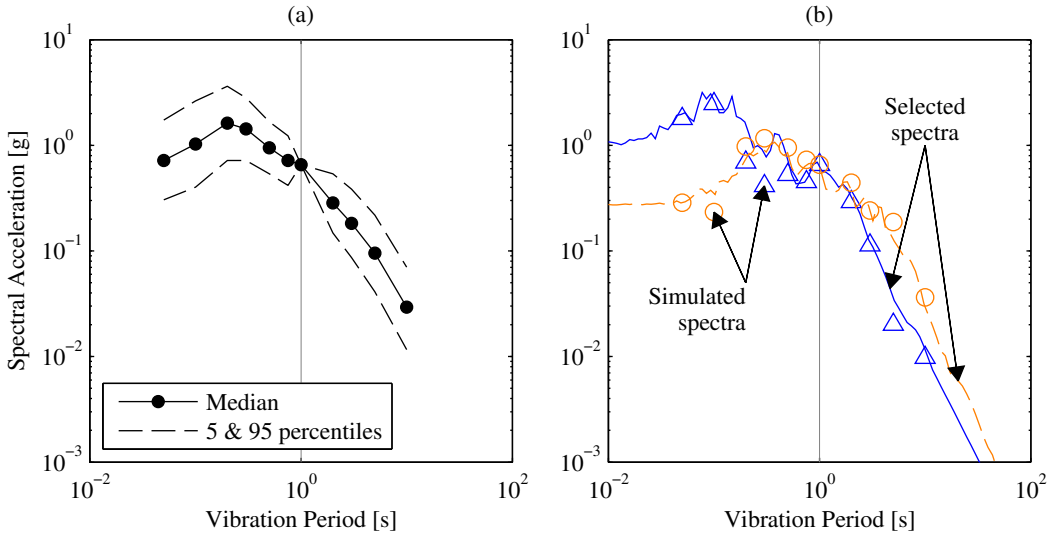

Figure 3.9: Illustration of ground motion selection via GCIM-SA for $A(1s)$ at the MCE level using Rezaeian's stochastic model: (a) target spectrum; and (b) simulated spectra from the target spectrum versus selected spectra from the database of synthetic ground motions.

in Eq 3.3, is determined from all 44 results, using the maximum likelihood fitting procedure described by Baker in [65]. For each GMSM procedure, $\widehat{\Pr}(EDP > z \mid \text{NC}, IM^* = x_i)$ and $\widehat{p}_C(x_i)$ are combined via Eq 3.3 and the resulting estimate of the SDHC is computed from Eq 3.2.

The GMSM-based SDHCs for the two EDPs – peak deformation, u_m, and peak total acceleration, $\ddot{u}_o^t$ – are presented in Fig 3.11. For a particular EDP, the SDHCs from both GMSM procedures are essentially identical at exceedance rates above the DBE level but become increasingly different below the MCE level. Since N_{IM^*} and $\widetilde{\lambda}_{IM^*}(x_i)$ in Eq 3.2 are identical in both GMSM procedures, the two resulting SDHCs differ because the ground motions selected in the two cases are not the same. Thus the natural question is: which of the two SDHCs is more accurate and by how much?

To answer this question, we compare both GMSM-based SDHCs against the benchmark SDHCs from Fig 3.5; these comparisons reveal two important observations. First, the bias in an estimate of the SDHC depends on the exceedance rate. Using the two EDPs of the degrading system as an example (Fig 3.11c-d), the SDHCs from both GMSM procedures are unbiased at exceedance rates above the DBE level; at exceedance rates below the MCE level however, the SDHC from GCIM-SA remains unbiased whereas that from IDA overestimates the demand. Second, the accuracy of a SDHC from a GMSM procedure depends on the structure of interest. For example, the SDHCs from GCIM-SA are unbiased for the degrading system (Fig 3.11c-d) but they underestimate the demand for the bilinear system at exceedance rates below 10^{-4} (Fig 3.11a-b). These observations may be explained using

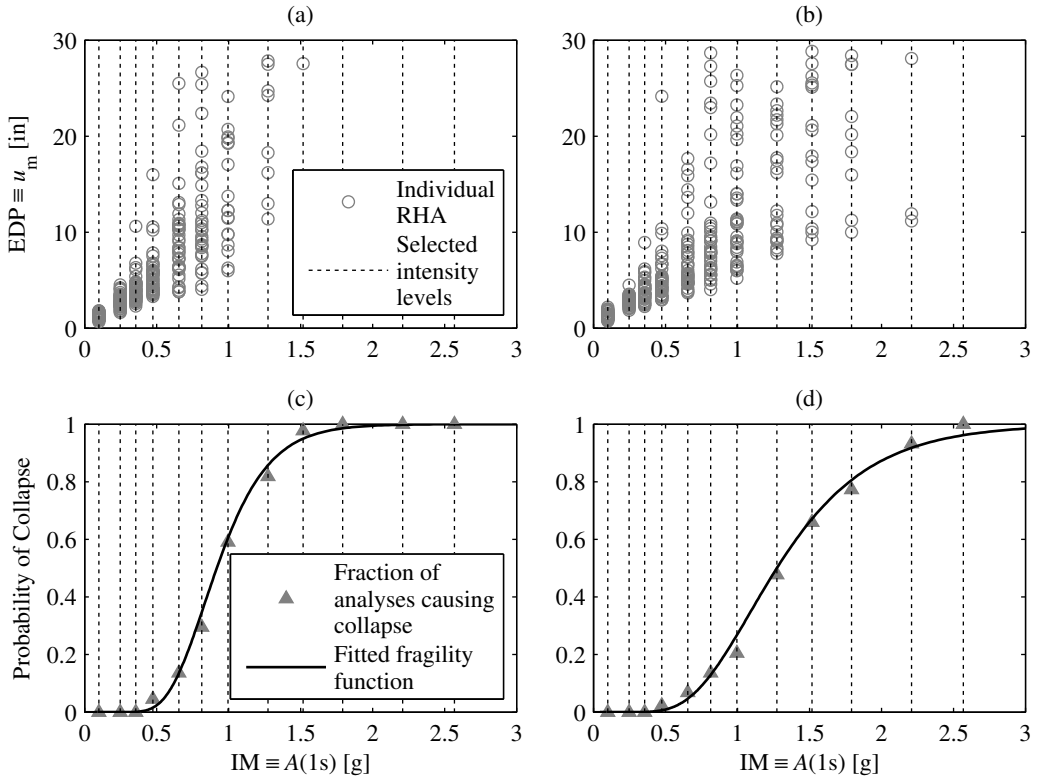

Figure 3.10: RHA results of the degrading system subjected to ground motions selected from Rezaeian's database for PSDA: (a-b) non-collapse data from IDA and GCIM-SA, respectively; (c-d) collapse data from IDA and GCIM-SA, respectively.

the concepts of "hazard consistency" and "IM sufficiency" [64], which are introduced next.

We define an ensemble of ground motions to be *hazard consistent for some IM* if its resulting estimate of the IMHC, denoted by $\widehat{\lambda}_{IM}(x)$, is essentially equal to the benchmark IMHC, $\lambda_{IM}(x)$ (Eq 3.7). The former hazard curve is estimated from

$$\widehat{\lambda}_{IM}(y) = \sum_{i=1}^{N_{IM^*}} \widehat{\Pr}(IM > y \mid IM^* = x_i) \cdot |\Delta\widetilde{\lambda}_{IM^*}(x_i)| \tag{3.16}$$

where $\widehat{\Pr}(IM > y \mid IM^* = x_i)$ is the empirical CCDF of IM corresponding to all ground motions scaled to intensity x_i; for example, applying Eq 3.16 to the ground motions from IDA leads to the IMHC estimates shown as dashed curves in Fig 3.12. In previous research, hazard consistency was defined relative to the IMHC computed from a GMPM in PSHA, $\widetilde{\lambda}_{IM}(x)$ in Eq 3.14, because the benchmark IMHC, $\lambda_{IM}(x)$, could not be obtained from recorded ground motions [37, 64]. Since the latter may now be determined from synthetic

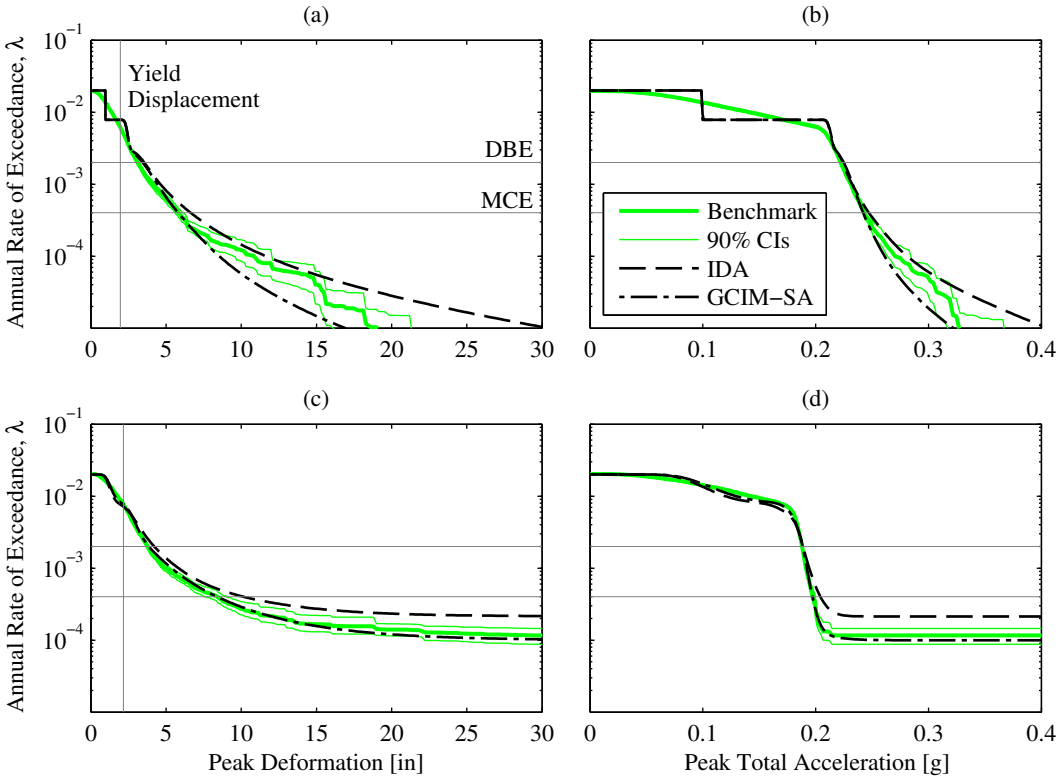

Figure 3.11: Comparison of GMSM-based SDHCs against the benchmark SDHC using Rezaeian's stochastic model: (a-b) u_m and $\ddot{u}_o^t$ of bilinear system, respectively; (c-d) u_m and $\ddot{u}_o^t$ of degrading system, respectively.

motions, (1) hazard consistency is defined herein relative to the benchmark IMHC, and (2) the issue of benchmark-consistency arises for the first time (Section 3.6).

Conceptually, hazard consistency is a property of the selected ground motions: it indicates whether or not the 'intensity' of a particular ensemble is representative of that assumed in PSHA (i.e., assumed via GMPMs, stochastic models of ground motions, etc.). For example, suppose the intensity is measured by $IM^* \equiv A(1s)$. The ground motions from both GMSM procedures are hazard consistent for this IM because each GMSM-based estimate of the hazard curve agrees closely to the benchmark (Fig 3.12c). This is to be expected since for each GMSM procedure, all ground motions were deliberately scaled such that the estimated hazard curve for IM^*, $\widehat{\lambda}_{IM^*}(x)$, is essentially identical to that computed from a GMPM, $\widetilde{\lambda}_{IM^*}(x)$ (see Eq 3.16), and the latter is in turn practically equal to the associated benchmark, $\lambda_{IM^*}(x)$ (see Section 3.6). However, such scaling distorts other aspects of the ground motion, potentially leading to hazard inconsistencies with respect to other IMs. For instance, Fig 3.12e demonstrates that the ground motions from IDA are hazard *inconsistent*

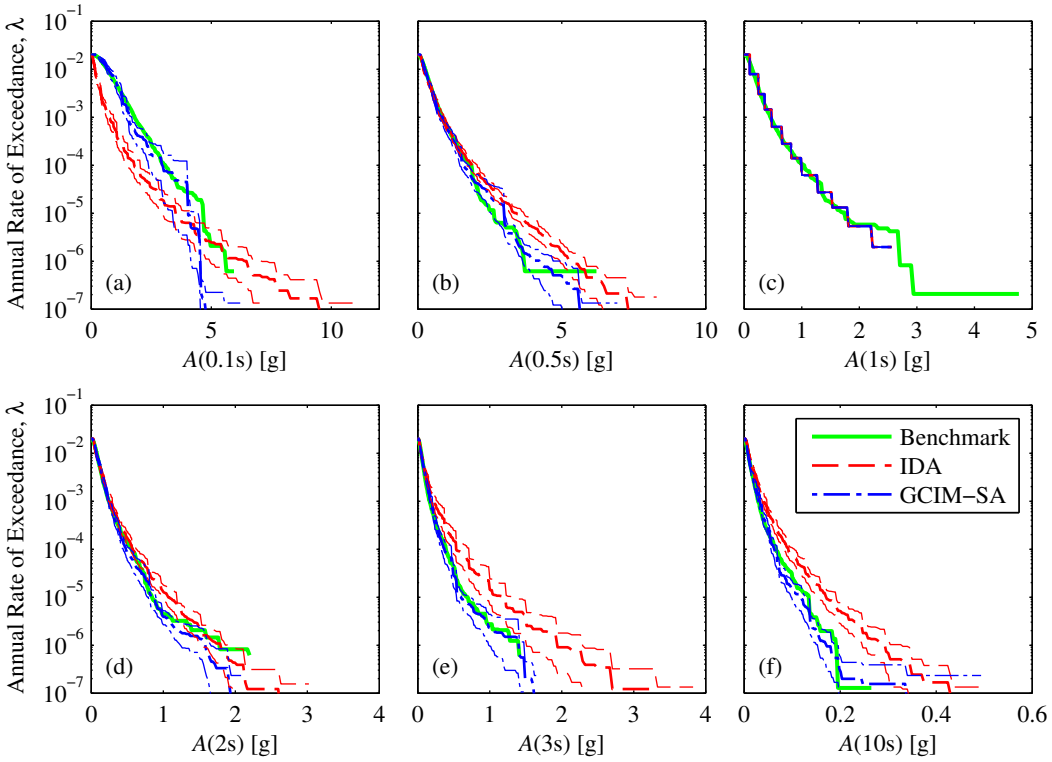

Figure 3.12: Hazard consistency of ground motions selected by both GMSM procedures in PSDA, for spectral accelerations at six periods of vibration: (a) 0.1s; (b) 0.5s; (c) 1s; (d) 2s; (e) 3s; (f) 10s.

with respect to $IM \equiv A(3s)$ whereas those from GCIM-SA are indeed hazard consistent for this IM. It is to be expected that ground motions from GCIM-SA are hazard consistent for spectral accelerations at many vibration periods, because they have been selected to deliberately match the target spectra (see Fig 3.9). However, they are potentially hazard inconsistent with respect to IMs that are not included in the selection process (e.g., cumulative absolute velocity, significant duration, etc.).

An IM, which may be scalar or vector-valued, is defined to be *sufficient* with respect to an EDP when, given a fixed value of this IM, the EDP does not depend on any other aspects of the ground motion [15, 12]. Put differently, a sufficient IM completely controls the response of the system. For example, the peak response of a linear-elastic MDF structure is essentially controlled by spectral acceleration at its modal periods of vibration; therefore, this vector IM is expected to be sufficient with respect to such EDPs.

The concepts of sufficiency and hazard consistency may be used to explain why the bias in an estimate of the SDHC depends on the exceedance rate. For instance, consider the SDHCs for the degrading system in Fig 3.11c-d. At exceedance rates above the DBE level, the system

responds linearly and hence $A(1s)$ is sufficient. Because ground motions from both GMSM procedures are hazard consistent for this IM (Fig 3.12c), the resulting SDHCs are unbiased at this range of linear elastic behavior. At exceedance rates below the MCE level however, the system deforms in the inelastic range and we know from structural dynamics that $A(1s)$ alone no longer controls the peak deformation. Consequently, the hazard consistency of the selected ground motions, with respect to IMs other than $A(1s)$, determines the accuracy of the resulting SDHCs. Because the ground motions from IDA are hazard inconsistent with respect to spectral accelerations at vibration periods longer than 2 s (Fig 3.12e-f), the resulting SDHCs overestimate the demand.

The accuracy of a SDHC from a GMSM procedure depends on the structure and EDP of interest because an IM that is insufficient for one structure or EDP may turn out to be sufficient for another. For example, consider the ground motions from GCIM-SA that were deliberately selected to be hazard consistent with respect to the vector IM, comprising spectral accelerations at vibration periods from 0.05 to 10 s. This vector IM, or spectral shape, is insufficient for the two EDPs of the bilinear system at exceedance rates below 10^{-4}. This conclusion may be deduced as follows: if the vector IM is indeed sufficient for the EDP at exceedance rates below 10^{-4}, then the fact that the ground motions are hazard consistent with respect to this IM (Fig 3.12) should have resulted in an unbiased estimate of the SDHC at such exceedance rates [64]; since this is not the case however (Fig 3.11a-b), the IM must not be sufficient. At such extreme levels of nonlinearity, the EDPs of the bilinear system are controlled by aspects of the ground motion other than spectral shape; in particular, the duration of the ground motion seems to affect the system's peak response because the system is able to experience many cycles of vibration, as its strength is unlimited. In contrast, the degrading system would have collapsed for exceedance rates below 10^{-4}. As a result, spectral shape appears to be sufficient for the degrading system at all exceedance rates of interest whereas it is only sufficient for the bilinear system at exceedance rates above 10^{-4}.

In general, estimates of the SDHC will be unbiased as long as the corresponding ground motions are hazard consistent with respect to an IM that is sufficient [64]. However, sufficient IMs may not exist for EDPs of a complex, realistic structure as its response is sensitive to many details of the ground motion. Therefore, any modification of ground motions may result in biased SDHCs for such systems. The approach proposed in Fig 3.1 makes it possible to quantify potential biases and assess the sufficiency of IMs employed for ground motion selection.

To further test the proposed approach for evaluating GMSM procedures, it was reimplemented for the database of 10^4 ground motions from Yamamoto's stochastic model. Using this new database, new benchmark hazard curves were computed (Section 3.5), new benchmark-consistent prediction models were developed (Section 3.6), and new GMSM-based estimates of the SDHC were obtained; in total, this effort required an additional 11056 more RHAs of each structure. The results from utilizing Yamamoto's stochastic model are summarized in Fig 3.13.

We expect similar observations regarding bias in the SDHCs resulting from Yamamoto's stochastic model because the proposed approach aims to isolate the effects of a GMSM

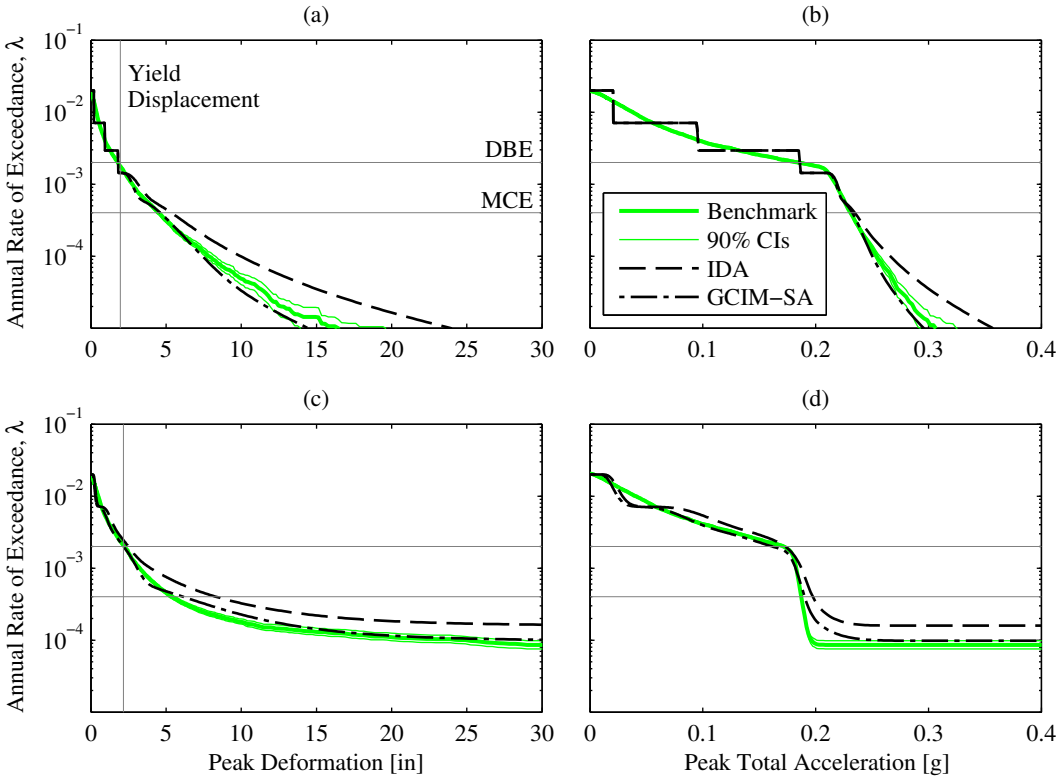

Figure 3.13: Comparison of GMSM-based SDHCs against the benchmark SDHC using Yamamoto's stochastic model: (a-b) u_m and $\ddot{u}_o^t$ of bilinear system, respectively; (c-d) u_m and $\ddot{u}_o^t$ of degrading system, respectively.

procedure on its resulting estimates of the SDHC. This expectation is confirmed in Fig 3.13; observe that although the benchmark SDHCs in this figure differ from those in Fig 3.11, the GMSM-based SDHCs are *also different* between the two figures. The SDHCs from GCIM-SA again underestimate the demand of the bilinear system at exceedance rates below 10^{-4}; this confirms that the response of the bilinear system is controlled by aspects of the ground motion other than spectral shape at such extreme levels of nonlinearity. For the degrading system, the SDHCs from GCIM-SA are again unbiased and those from IDA again overestimate the demand at exceedance rates below the MCE level. The fact that the SDHCs from GCIM-SA are unbiased for the degrading system in both stochastic models strongly suggests that spectral shape is indeed a sufficient IM for this system.

However, we observe a few minor differences between the results from the two stochastic models. First, both structures yield at different rates of exceedance (e.g., the bilinear system yields at 6×10^{-3} in Rezaeian's model but yields at the DBE level in Yamamoto's model); this is expected since the benchmark SDHC differs in each stochastic model (Section 3.3).

Second, the SDHCs from IDA are unbiased for the bilinear system at exceedance rates between 2×10^{-4} and 5×10^{-5} in Rezaeian's model (Fig 3.11a-b) but overestimate the demand at this range of exceedance rates in Yamamoto's model (Fig 3.13a-b). The latter difference regarding IDA arises because ground motions from this procedure are hazard consistent with respect to $A(2s)$ in Rezaeian's model (Fig 3.12d) but are hazard *inconsistent* with respect to $A(2s)$ in Yamamoto's model (not shown). Aside from such differences, the overall similarity between the relationships depicted in Figs 3.11 and 3.13 indicates that the proposed approach for evaluating GMSM procedures is robust.

3.8 Comparison with previous research

In previous research, a GMSM-based estimate of the SDHC was considered unbiased if different choices of the conditioning IM led to essentially the same estimate [35, 37]. This approach is illustrated in Fig 3.14 where estimates of the SDHC for the peak deformation of the degrading system, computed from Eq 3.2 for four choices of the conditioning period, T^*, are presented. The fact that the four SDHCs are closer to each other for GCIM-SA than for IDA suggests that SDHC estimates from GCIM-SA are less biased – or more accurate – than those from IDA.

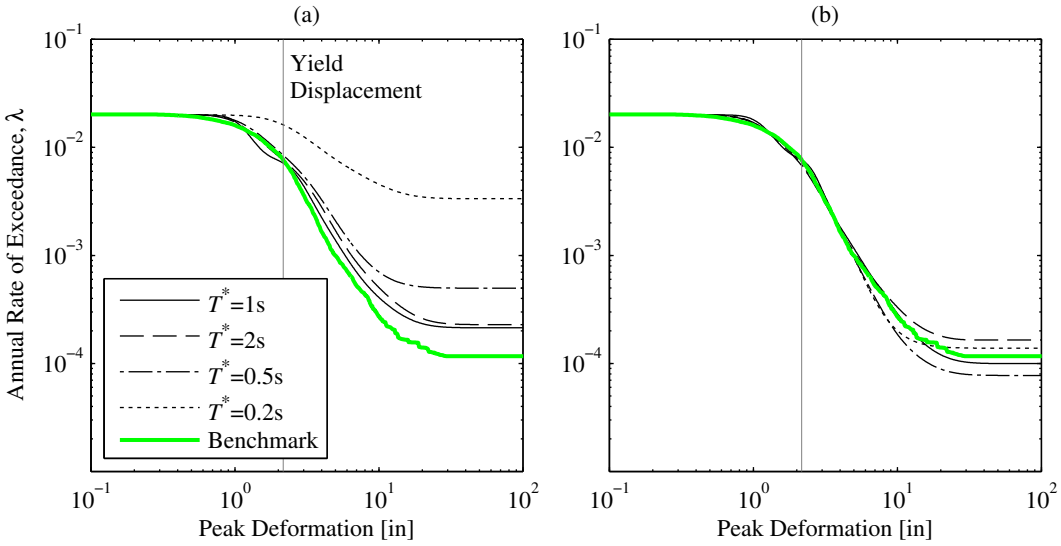

Figure 3.14: Comparison of GMSM-based SDHCs from different definitions of the conditioning IM for $EDP \equiv u_m$ of the degrading system, using ground motions simulated by Rezaeian's stochastic model: (a) IDA; (b) GCIM-SA.

This existing approach has two limitations. First, it is not possible to quantify the bias in any GMSM-based SDHC for lack of a benchmark. Second, several significantly different

definitions of the conditioning IM are typically needed to draw definitive conclusions from the existing approach. For example, if only 1 s and 2 s were considered as definitions for T^*, then Fig 3.14 may erroneously suggest that the SDHCs from IDA are less biased than those from GCIM-SA.

These two limitations are overcome by the approach presented in this work. First, the bias in any SDHC estimate can be quantified by comparing the estimate against the benchmark SDHC in a controlled setting (Fig 3.1). For example, the benchmark SDHC in Fig 3.14 verifies that the SDHCs from GCIM-SA are more accurate than those from IDA. For each GMSM procedure, the SDHC corresponding to 1 s is most accurate among the four conditioning periods considered; this confirms the conclusion by Lin et al [37] that the choice of the conditioning period is important for accurate estimation of SDHCs in PSDA. Moreover, the ability to quantify bias enables the analyst to assess the sufficiency of IMs for an EDP of interest (Section 3.7). Second, the need to choose several definitions of the conditioning IM is avoided in the proposed approach since the benchmark SDHC is developed only once, regardless of the number of GMSM procedures considered (see Sections 3.5 and 3.5). For a more comprehensive comparison of hazard curves in Figs 3.11-3.14, a bootstrap confidence interval may also be provided for each GMSM-based hazard curve, which is useful when the total number of ground motions used for each hazard curve is less than that in this study ($N_{IM^*} \times n = 528$).

These two limitations were also overcome in [64], where benchmark SDHCs for the peak deformation of a bilinear SDF system were developed from prediction models based on recorded ground motions. However, the benchmark SDHC in the current study may be computed for *any* EDP of interest and the bias in a SDHC estimated from a particular GMSM procedure may be isolated more completely with the aid of synthetic ground motions. Note that the models for simulating ground motions should be appropriate for the site considered.

Applying the proposed approach for other structures and other sites can be much more complicated and computationally demanding. For example, computation of the benchmark SDHC (Section 3.5) for complex, realistic structures would require enormous effort because a large number of RHAs is necessary. For sites with multiple earthquake sources and earthquakes occurring at random locations, the methods for developing a database of ground motions and benchmark-consistent prediction models will be slightly different than those presented in this study. When developing the database of ground motions (Section 3.4), the ground motion simulation models will require randomly generated rupture scenarios from all earthquake sources as input for simulating ground motions. When developing benchmark-consistent GMPMs (Section 3.6), the probability distribution of IMs will depend on seismological parameters (e.g., distance, style-of-faulting, etc.) in addition to magnitude, increasing the complexity of the functional forms (Eq 3.13).

3.9 Conclusions

This investigation of employing synthetic ground motions to evaluate GMSM procedures has led to the following conclusions:

1. A novel approach for evaluating GMSM procedures, in the context of PSDA, is presented. In essence, synthetic ground motions are employed to: (1) derive the benchmark SDHC, for the structure and response quantity of interest, and (2) establish the causal relationship between a GMSM procedure and the bias in its resulting estimate of the SDHC. To achieve the latter goal, new benchmark-consistent prediction models are developed.

2. A case study is presented to illustrate the proposed approach. For two simple systems at a simple site, two GMSM procedures – IDA and GCIM-SA – are evaluated, leading to the following observations:

   a) The bias in an estimate of the SDHC depends on the exceedance rate. At exceedance rates above (or greater than) the DBE level, SDHCs from both procedures are unbiased for both systems and both EDPs; below the MCE level however, SDHCs from GCIM-SA are generally more accurate than those from IDA.

   b) The accuracy of a SDHC from a GMSM procedure depends on the structure and EDP of interest. At exceedance rates below the MCE level, SDHCs from GCIM-SA are unbiased for the degrading system but not for the bilinear system.

   c) Spectral shape appears to be sufficient for the degrading system at all exceedance rates of interest; however, it is insufficient for the bilinear system at exceedance rates below 10^{-4}. Below this exceedance rate, the response of the bilinear system is influenced by aspects of the ground motion other than spectral shape because the system is able to experience many cycles of vibration, as its strength is unlimited; in contrast, the degrading system would have already collapsed.

   d) For the degrading system and for both GMSM procedures, the peak deformation hazard curve that corresponds to the system's fundamental period is most accurate among the four conditioning periods considered.

3. The proposed approach is demonstrated to be robust, as similar conclusions are obtained from two significantly different stochastic models for simulating ground motions.

4. Unlike previous research, the current approach offers the ability to quantify bias in SDHCs for *any* structure and EDP of interest, avoids the need to choose several different conditioning IMs, and isolates the bias in the SDHC estimate from a GMSM procedure more completely with synthetic ground motions.

5. In general, estimates of the SDHC will be unbiased as long as the corresponding ground motions are hazard consistent with respect to an IM that is sufficient. However, sufficient IMs may not exist for EDPs of a complex, realistic structure. Therefore, any modification of ground motions may result in biased SDHCs for such systems. The proposed approach makes it possible to quantify potential biases and assess the sufficiency of IMs employed for ground motion selection.

Chapter 4

Importance Sampling based procedure for estimating seismic demand hazard curves

4.1 Abstract

This paper develops a procedure to select unscaled ground motions for estimating seismic demand hazard curves (SDHCs) in performance-based earthquake engineering (PBEE). Currently, SDHCs are estimated from a probabilistic seismic demand analysis (PSDA), where several ensembles of ground motions are selected and scaled to a user-specified conditioning intensity measure (IM). In contrast, the procedure developed herein provides a way to select a *single* ensemble of *unscaled* ground motions for estimating the SDHC. In the context of unscaled motions, the proposed procedure requires three inputs: (i) database of unscaled ground motions, (ii) **IM**, the vector of IMs for selecting ground motions, and (iii) sample size, n; in the context of scaled motions, two additional inputs are needed: (i) a maximum acceptable scale factor, SF_{max}, and (ii) a target fraction of scaled ground motions, γ. Using a recently developed approach for evaluating ground motion selection and modification procedures, the proposed procedure is evaluated for a variety of inputs and is demonstrated to provide accurate estimates of the SDHC when ground motions are unscaled, or when the vector of IMs chosen to select ground motions is sufficient for the response quantity of interest.

4.2 Introduction

In performance-based earthquake engineering (PBEE), response history analyses (RHAs) of structural models are typically performed for three different contexts: (i) intensity-based assessment, (ii) scenario-based assessment, and (iii) risk-based assessment [3, 31]. This paper focuses on a risk-based assessment, or a probabilistic seismic demand analysis (PSDA), which

is the most comprehensive context among the three. The primary output of a PSDA is a plot of the annual rate of exceedance, λ, as a function of the seismic demand, or engineering demand parameter (EDP); such a plot is referred to as a seismic demand hazard curve (SDHC), which is unique for a given structure at a given site [35]. In essence, a SDHC is computed from a PSDA by selecting several ensembles [1] of ground motions and scaling each ensemble to a user-specified conditioning intensity measure (IM); a detailed explanation of this approach may be found elsewhere (e.g., Section 2 of [64], among others).

The objective of performing RHAs in this study is to estimate the SDHCs of a given structure at a particular site. Once constructed, the SDHC may be used to determine the seismic demand for a given annual rate of exceedance, or conversely, the exceedance rate for a given structural capacity. Furthermore, the SDHC may be integrated with fragility and consequence functions to estimate damage and loss, respectively (Chapter 9 of [77]).

There are three limitations to the existing approach for computing SDHCs from a PSDA. First, the choice of the conditioning IM may not be obvious for some structures and yet it determines the influence from other IMs on the EDP [37]. Second, ground motions selected from a PSDA are almost always amplitude scaled to various levels of the conditioning IM, potentially causing bias in the resulting demands. Third, several ensembles of scaled ground motions are typically needed to determine the SDHC for a wide range of exceedance rates.

The choice of the conditioning IM and the effects of amplitude scaling are relatively unimportant when ground motions are carefully selected to be consistent with the hazard [35, 37]. Specifically, the SDHCs are unbiased – irrespective of the extent of record scaling – when the corresponding ground motions are hazard-consistent with respect to IMs that are sufficient for the EDP in question [64, 78]. An IM, which may be scalar or vector-valued, is defined to be *sufficient with respect to an EDP* when the EDP is essentially controlled only by this IM and no other features of the ground motion [15, 12]. Since sufficient IMs may not exist for EDPs of a complex, realistic structure, a method that permits selection of unscaled ground motions is desirable.

The procedure developed herein permits selection of a single ensemble of unscaled ground motions, without the need to choose a conditioning IM. First, a vector of IMs is selected on the basis of the structure and EDPs considered. Next, the theoretical probability distribution of this vector, derived from probabilistic seismic hazard analysis (PSHA), is employed as the target for ground motion selection. By selecting a single ensemble of unscaled ground motions to be consistent with this target, hazard consistency at high exceedance rates (or short return periods) is directly enforced. To enforce hazard consistency of ground motions at low exceedance rates (or long return periods), the concept of Importance Sampling is utilized. Finally, a case study is chosen to illustrate the proposed procedure, evaluate its ability in providing accurate estimates of the SDHC, and develop recommendations for user-defined inputs to the procedure.

[1] In this study, an "ensemble" refers to a collection of single horizontal components of ground motion.

4.3 Theoretical background

Target for ground motion selection

The target is defined by **IM**, a vector of IMs, and its probability distribution from PSHA of the particular site; although a scalar IM may also be considered, this paper focuses on a vector of IMs for generality. Examples of such IMs include peak ground acceleration (PGA), spectral accelerations at various vibration periods, $A(T)$, and significant duration, D_{5-75}, which are explicit measures of the ground motion [48]. The number of IMs in the vector, denoted by N_{IM}, is referred to as its *dimension*. The IMs should be specified based on structural dynamics and on the analyst's experience with structures that are similar to the one in question. For example, spectral acceleration at vibration periods between the system's fundamental period, T_1, and twice the fundamental period, $2T_1$, might control inter-story drift ratios [79] whereas PGA might control floor accelerations [37].

The proposed procedure aims to select an ensemble of ground motions that is consistent with respect to the hazard curves of the IMs specified in the preceding paragraph. An ensemble of ground motions is said to be *hazard-consistent with respect to an IM* when its resulting estimate of the intensity measure hazard curve (IMHC), $\widehat{\lambda}_{IM}(x)$, is practically the same as [2] the target IMHC, $\lambda_{IM}(x)$ (see Section 4.4). The latter IMHC is given by PSHA of the site:

$$\lambda_{IM}(x) = \sum_{i=1}^{N_{Rup}} \nu(rup_i) \cdot \Pr(IM > x \mid rup_i) \tag{4.1}$$

where N_{Rup} refers to the total number of rupture scenarios considered in the PSHA [3], $\nu(rup_i)$ refers to the rate of the ith scenario, and $\Pr(IM > x \mid rup_i)$ refers to the complementary cumulative distribution function (CCDF) of the IM for a given rupture scenario. An estimate of the IMHC from an ensemble of ground motions will be defined later in this section.

In addition to hazard curves, a PSHA also provides the ingredients to determine the multivariate probability distribution of a vector of IMs. The marginal CCDF of each IM for a given earthquake (with unknown magnitude and location) near the site, $\Pr(IM > x)$, may be obtained by normalizing its corresponding hazard curve:

$$\Pr(IM > x) = \frac{\lambda_{IM}(x)}{\nu_0} = \sum_{i=1}^{N_{Rup}} \frac{\nu(rup_i)}{\nu_0} \cdot \Pr(IM > x \mid rup_i) \tag{4.2}$$

where $\nu_0 = \sum_{i=1}^{N_{Rup}} \nu(rup_i)$ refers to the annual rate of earthquake occurrence; by definition of ν_0, the sum of all normalized activity rates in the first term of the summation in Eq 4.2 is unity. The marginal probability density function (PDF) of each IM, $f_{IM}(x)$, may be derived from such CCDFs. For example, Fig 4.1a shows an example IMHC from PSHA;

[2] Due to the presence of epistemic uncertainty, the comparison of hazard curves requires judgment.

[3] A rupture scenario is defined by the magnitude and location of rupture at the earthquake source.

its corresponding PDF is depicted in Fig 4.1b. Assuming the distribution of ln(**IM**) for a given rupture scenario is multivariate normal [47], where marginal means and standard deviations are given by ground motion prediction models (e.g., [42], [62]), and correlations among the IMs are given by correlation models (e.g., [55], [80]), Eq 4.2 indicates that the target distribution of **IM** is a *finite mixture of multivariate lognormals*:

$$f_{\mathbf{IM}}(\mathbf{x}) = \sum_{i=1}^{N_{Rup}} \frac{\nu(rup_i)}{\nu_0} \cdot f_{\mathbf{IM}|Rup}(\mathbf{x} \mid rup_i) \tag{4.3}$$

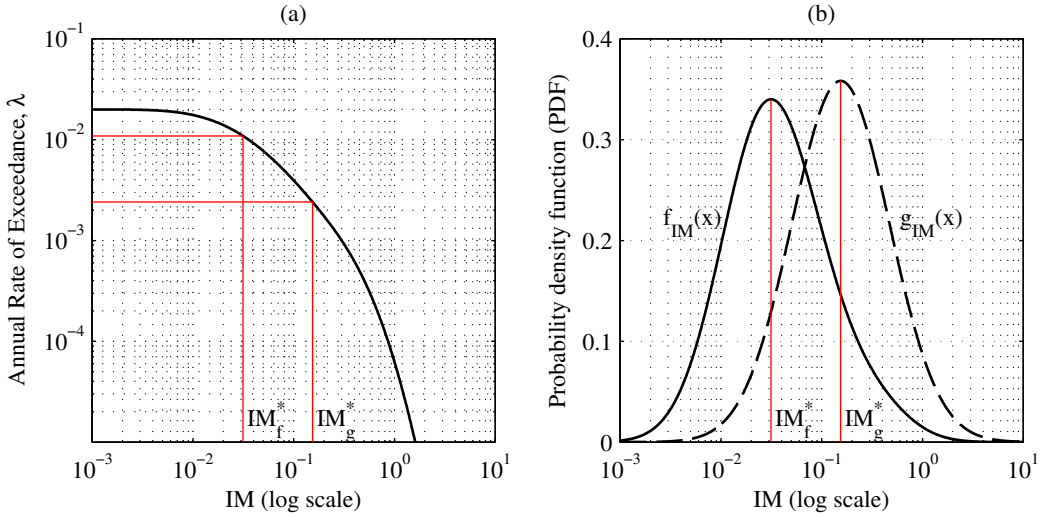

Figure 4.1: Output from PSHA: (a) example hazard curve; (b) target PDF, $f_{IM}(x)$, that corresponds to the example hazard curve (an example of an Importance Function, $g_{IM}(x)$, is also shown). The modes of the two PDFs are denoted by IM_f^* and IM_g^*.

Assuming the N_{Rup} rupture scenarios are mutually exclusive and collectively exhaustive, Eqs 4.2-4.3 may be derived from the total probability theorem [81]. First, we note that all events associated with Eq 4.2 are conditioned on the fact that an earthquake, with unknown magnitude and location, has occurred near the site. Second, the normalized activity rate, $\nu(rup_i) \div \nu_0$, may be interpreted as the probability of the ith rupture occurring near the site, given occurrence of an earthquake. The probabilities expressed in Eq 4.2 are unconventional because they are *not* based on a specified assumption of earthquake occurrence in time (e.g., Poisson assumption, etc.).

The simple relationship between an IMHC and its CCDF, as stated by the equality in the left part of Eq 4.2, permits the estimation of hazard curves using a *single* ensemble of unscaled ground motions [4]. Fig 4.2 illustrates one such ensemble of n ground motions,

[4]Eq 4.2 is also applicable to the EDPs of a given structure under the assumption of ergodicity in time, which is implicitly assumed in many applications of PBEE [82].

where each data point corresponds to a unique, unscaled ground motion; the values of IM and EDP from the ensemble are quantified on the horizontal and vertical axes, respectively. Combining the empirical CCDF of each variable – IM or EDP – with the annual rate of earthquake occurrence leads to the following estimates of the hazard curves:

$$\widehat{\lambda}_{IM}^{(\mathrm{MC})}(x) = \frac{\nu_0}{n}\sum_{i=1}^{n} I(x_i > x) \qquad \widehat{\lambda}_{EDP}^{(\mathrm{MC})}(z) = \frac{\nu_0}{n}\sum_{i=1}^{n} I(z_i > z) \tag{4.4}$$

where the superscript MC denotes "Monte Carlo", and $I(\cdot)$ refers to the indicator function, which is equal to unity when the event inside the parenthesis occurs and zero otherwise. The observed values of IM and EDP from the ith ground motion are denoted respectively by x_i and z_i. When an IMHC estimate from, say Eq 4.4a, is practically the same as the theoretical one in Eq 4.1, the corresponding ground motions are said to be hazard-consistent with respect to that particular IM; otherwise, the ground motions are hazard-inconsistent. Similarly, an SDHC estimate from, say Eq 4.4b, is said to be *unbiased*, or *accurate*, when it is essentially equal to the theoretical SDHC from PSHA, denoted by $\lambda_{EDP}(z)$.

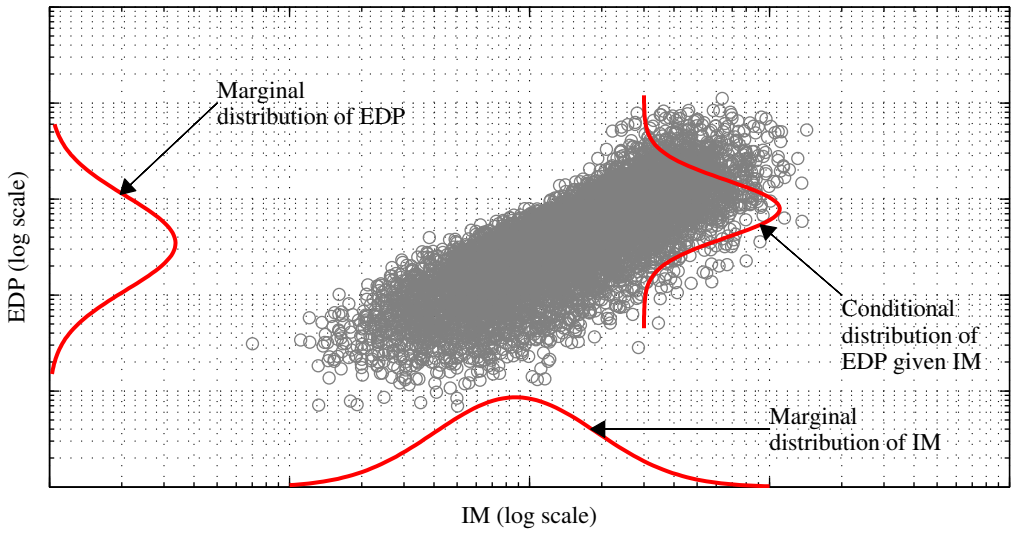

Figure 4.2: Schematic illustration of PDFs related to scattergrams of results from RHAs.

In order to enforce hazard consistency and obtain unbiased SDHCs, ground motions should be selected such that their empirical joint distribution of IM and EDP is essentially the same as the theoretical joint distribution, which is depicted in Fig 4.2 by its corresponding marginal distributions and conditional distribution of $EDP \mid IM$. The agreement between the two joint distributions can be achieved by randomly sampling IM-EDP pairs directly from the theoretical joint distribution; that is, randomly sampling first from the marginal distribution of IM and then from the conditional distribution of $EDP \mid IM$. In practice,

this two-step approach is equivalent to (i) randomly generating vectors of IMs from Eq 4.3, and then (ii) selecting ground motions whose IMs agree well with those generated from Eq 4.3. However, direct sampling from Eq 4.3 leads to ground motions that are relatively weak, as suggested by the exceedance rate in Fig 4.1a corresponding to the modal value of the target PDF in Fig 4.1b. Consequently, such motions will be hazard-consistent at high exceedance rates (i.e., frequent events) and are useful for computing linear response. In order to obtain ground motions that are hazard-consistent at small exceedance rates (i.e., rare events) and are useful for computing nonlinear response, the concept of Importance Sampling is introduced next.

Importance Sampling

Importance Sampling is a standard technique from statistics that is commonly used to estimate probabilities of rare events, among other applications (e.g., see [73]); in this study, we employ Importance Sampling to estimate hazard curves at small exceedance rates. First, the theoretical PDF given by Eq 4.3 is replaced by another PDF that samples the tail region more frequently; this new PDF is called an *Importance Function* (IF) and denoted by $g_{IM}(\cdot)$. An example of an IF is illustrated in Fig 4.1b, where its mode corresponds to an exceedance rate that is smaller than that corresponding to the mode of the theoretical PDF. Then, the IF is used to randomly generate vectors of IMs that are ultimately used to estimate hazard curves. When computing hazard curves from such data, the data are weighted in order to account for the bias introduced by replacing the target PDF with the IF.

After vectors of IMs have been randomly generated from the IF, there are three deterministic steps in computing hazard curves. First, the vectors are used to identify ground motions whose corresponding vector-valued IMs agree most closely to those from the IF (Section 4.4). Second, the selected ground motions are analyzed to determine any feature of interest, including IMs excluded from **IM** and EDPs of any structural model (through RHA). Third, the features from the selected motions are employed to compute hazard curves:

$$\widehat{\lambda}_{IM}(x) = \frac{\nu_0}{n}\sum_{i=1}^{n}\left[I(x_i > x)\cdot w_i\right] \qquad \widehat{\lambda}_{EDP}(z) = \frac{\nu_0}{n}\sum_{i=1}^{n}\left[I(z_i > z)\cdot w_i\right] \tag{4.5}$$

where x_i and z_i refer, respectively, to the observed values of IM and EDP from the ith ground motion. The *Importance Sampling weight* for the ith ground motion, w_i, is defined as the ratio between the values of the two PDFs:

$$w_i = f(\mathbf{x}_i) \div g(\mathbf{x}_i) \tag{4.6}$$

where $\mathbf{x}_i$ refers to the computed value of **IM** from the ith ground motion, $f(\cdot)$ refers to the PDF given by Eq 4.3, $g(\cdot)$ refers to the IF, and the subscript "IM" has been dropped henceforth for brevity. Note that implementing Eq 4.6 involves the rates for all rupture scenarios considered in the PSHA, along with the target probability distribution of **IM** | *Rup* from ground motion prediction models (see Eq 4.3). When the ith ground motion leads to

collapse, the resulting value of the EDP can be modified before Eq 4.5b is implemented; for example, the displacement may be set to infinity and the acceleration may be set to PGA after collapse has been observed [67, 37].

There is epistemic uncertainty in the estimates of hazard curves in Eq 4.5, implying that two estimates from independent executions of the proposed procedure will not be perfectly identical. The expected values of the estimates in Eq 4.5 are (see derivations in Sections A.1 and A.2)

$$\mathbb{E}\left[\widehat{\lambda}_{IM}(x)\right] = \lambda_{IM}(x) \qquad \mathbb{E}\left[\widehat{\lambda}_{EDP}(z)\right] = \lambda_{EDP}(z) \tag{4.7}$$

where $\mathbb{E}[\cdot]$ denotes expectation [5]. These expectations imply that the estimates from the proposed procedure with unscaled ground motions are, on average, hazard-consistent and unbiased; however, this might not be the case when ground motions are scaled (see Section 4.7). The epistemic uncertainty of the estimates in Eq 4.5 is quantified by their variances (see derivations in Sections A.3 and A.4):

$$\mathbb{V}\left[\widehat{\lambda}_{IM}(x)\right] = \frac{1}{n}\left\{\nu_0^2\left[\int_{\mathbf{s}:s>x} \frac{f^2(\mathbf{s})}{g(\mathbf{s})}\,\mathrm{d}\mathbf{s}\right] - \lambda_{IM}^2(x)\right\} \tag{4.8}$$

and

$$\mathbb{V}\left[\widehat{\lambda}_{EDP}(z)\right] = \frac{1}{n}\left\{\nu_0^2\left[\int_{\mathbf{s}} \Pr(EDP > z \mid \mathbf{IM} = \mathbf{s}) \cdot \frac{f^2(\mathbf{s})}{g(\mathbf{s})}\,\mathrm{d}\mathbf{s}\right] - \lambda_{EDP}^2(z)\right\} \tag{4.9}$$

where $\mathbb{V}[\cdot]$ denotes variance, $\Pr(EDP > z \mid \mathbf{IM} = \mathbf{s})$ refers to the CCDF of EDP for a given test value of $\mathbf{IM}$, and the integrals in both variances are multidimensional. Eqs 4.7-4.9 suggest theoretically that as the number of unscaled ground motions increases, the hazard curve estimates become increasingly repeatable, converging to the theoretical values.

Eq 4.9 permits several observations regarding the epistemic uncertainty of the SDHC estimate from the proposed procedure. First, the epistemic uncertainty is influenced by two user-specified inputs: (i) sample size, n; and (ii) the IF, $g(\cdot)$, which appears only in the integrand; the rest of the expression is fixed for a given structure at a given site. Second, both $\Pr(EDP > z \mid \mathbf{IM} = \mathbf{s})$ and $\lambda_{EDP}(z)$ are unknown; therefore, one cannot analytically determine the IF by minimizing the variance in Eq 4.9. Third, the variance increases as the dimension of $\mathbf{IM}$ increases because the integrand is always nonnegative. Fourth, the SDHC estimate can become meaningless when $g(\cdot) = 0$. Fifth, $\Pr(EDP > z \mid \mathbf{IM} = \mathbf{s})$ is close to zero when $\mathbf{s}$ is small and close to unity when $\mathbf{s}$ is large, under two assumptions that are commonly satisfied in earthquake engineering: (i) large demand levels, z, are of interest, and (ii) the EDP is positively correlated with $\mathbf{IM}$.

[5] In the case of $\mathbf{IM}$, the expectation is with respect to $g(\mathbf{x})$, and in the case of EDP, the expectation is with respect to $f_{EDP|\mathbf{IM}}(z \mid \mathbf{x}) \cdot g(\mathbf{x})$, where $f_{EDP|\mathbf{IM}}(z \mid \mathbf{x})$ refers to the theoretical conditional distribution of $EDP \mid \mathbf{IM}$.

The observations from the preceding paragraph provide insight for choosing an Importance Function. In theory, many different IFs may be chosen but the desirable ones are those that minimize the first summand of the variance in Eq 4.9. In particular, the dimension of **IM** (Section 4.3) should not be too large and hence, IMs for ground motion selection should be judiciously chosen. To avoid the possibility of infinite variance, the value of the IF must not be zero within the domain of Eq 4.3. Furthermore, the ratio $f^2(\cdot) \div g(\cdot)$ should be less than unity at the tails of the target distribution (see e.g., Fig 4.1b). The theory in this section facilitates the preceding discussion of desirable IFs in a general, qualitative manner; specific recommendations, which are derived from practical considerations, are provided in Section 4.4.

4.4 Ground motion selection procedure

Overview

Fig 4.3 presents a block diagram of the proposed ground motion selection procedure. First, the analyst specifies inputs to the procedure and then performs PSHA of the given site to determine the target for ground motion selection (Eq 4.3). Based on the inputs, an IF is constructed (Section 4.4) and is then employed to select an ensemble of ground motions (Section 4.4). Next, the Importance Sampling weights, computed from the selected ground motions, are used to confirm hazard consistency; if hazard consistency is judged to be unsatisfactory, then new ground motions may be reselected from the proposed procedure (Section 4.4). Finally, nonlinear RHAs of the structural model, subjected to the selected ground motions, are performed and the results are combined with the Importance Sampling weights to compute the SDHC.

There are five inputs to the proposed procedure: (i) a database of prospective ground motions, (ii) **IM**, a vector of IMs, (iii) a maximum acceptable scale factor, SF_{max}, (iv) a target fraction of scaled ground motions, γ, and (v) a sample size, n. The database of prospective ground motions should contain unscaled motions that originate from tectonic environments and soil conditions that are similar to those for the site under consideration [16]. In this paper, the proposed procedure is applied to synthetic ground motions in order to preliminarily evaluate its ability to estimate SDHCs (Sections 4.5-4.8); a more comprehensive explanation of the procedure's application to recorded motions is in preparation by the authors. The vector of IMs should be chosen based on our understanding of the dynamics of the structure; to reflect higher-mode, inelastic, and duration-sensitive response, we recommend the vector $\mathbf{IM} = \{A(T_k), A(T_1), A(2T_1), D_{5-75}\}$, where T_1 and T_k refer, respectively, to the first and kth mode of the structure (Section 4.6). One possibility for identifying the kth mode is through the concept of modal contribution factors [22]. The parameters SF_{max} and γ should be chosen based on the sufficiency of **IM**: if **IM** is deemed sufficient, then large scale factors may be employed; otherwise, the degree of scaling should be minimized (Section 4.7). Finally, the parameter n should be chosen based on a tolerable level of epistemic uncertainty in the

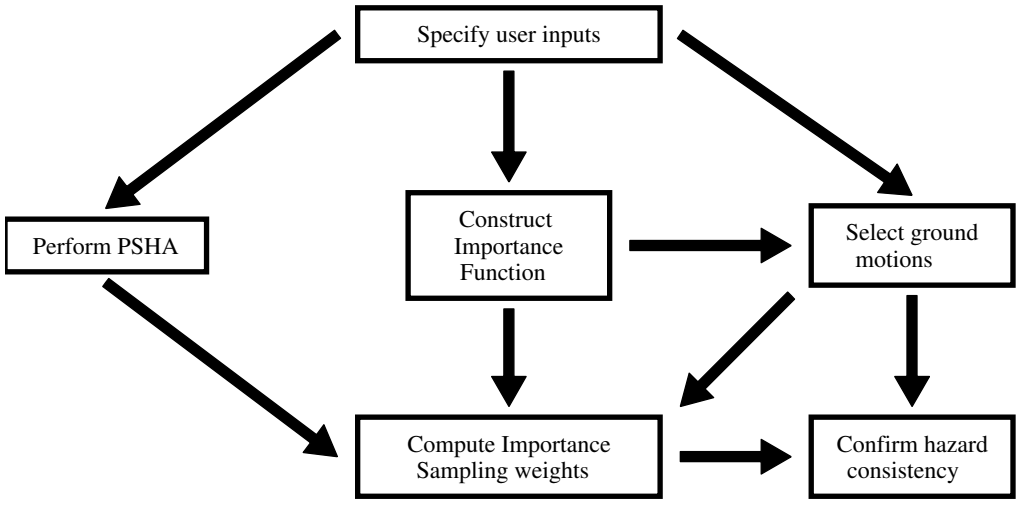

Figure 4.3: Block diagram of proposed ground motion selection procedure.

SDHC estimates (Section 4.8).

Database-driven Importance Function

The purpose of the IF in Fig 4.3 is to select ground motions that are intense while simultaneously consistent with the target defined by Eq 4.3. The proposed procedure achieves this goal in two steps: (i) randomly generate a vector of IMs from the IF, and (ii) select the ground motion whose corresponding vector of IMs agrees most closely to the one from the IF. Since ground motions are selected from a user-specified database of prospective motions, this database plays a major role in fulfilling the purpose of the IF. For example, when the largest observed value of $A(1s)$ in the database is, say $1g$, there would be no point in specifying an IF whose probability density is nonzero at intensities greater than $1g$. Because the database of prospective motions may be effectively enlarged by allowing ground motions to be scaled, we recommend an IF that is controlled by three inputs: (i) the specified database of unscaled ground motions, (ii) SF_{max}, and (iii) γ.

If ground motions are restricted to be unscaled, the proposed IF is a multivariate lognormal distribution whose parameters are determined from the database of unscaled ground motions; this IF is denoted by $g_u(\mathbf{x})$. To determine the parameters of this multivariate distribution – μ_{IF} and $\mathbf{\Sigma}_{IF}$ – we first consider the corresponding marginal distributions. The marginal distribution of the jth IM within **IM** is lognormal; its two parameters – μ_j and σ_j – are computed from the mean and standard deviation of the observed values of $\ln(IM_j)$ in the database. An example of this lognormal distribution is shown in Fig 4.4a, where the fitted CCDF is compared to the empirical CCDF from the database of ground motions.

Repeating such calculations for all IMs gives the mean vector of $g_u(\mathbf{x})$:

$$\mu_{IF} = [\mu_1 \quad \mu_2 \quad \dots \quad \mu_{N_{IM}}] \tag{4.10}$$

Next, the correlation between the jth and kth IM, denoted by $\rho_{j,k}$, is computed from the correlation between the observed values of $\ln(IM_j)$ and $\ln(IM_k)$ in the database. Combining such correlations with all σ_j provides the covariance matrix of $g_u(\mathbf{x})$:

$$\mathbf{\Sigma}_{IF} = \begin{bmatrix} \sigma_1^2 & \rho_{1,2}\sigma_1\sigma_2 & \dots & \rho_{1,N_{IM}}\sigma_1\sigma_{N_{IM}} \\ \rho_{2,1}\sigma_2\sigma_1 & \sigma_2^2 & \dots & \rho_{2,N_{IM}}\sigma_2\sigma_{N_{IM}} \\ \vdots & \vdots & \ddots & \vdots \\ \rho_{N_{IM},1}\sigma_{N_{IM}}\sigma_1 & \rho_{N_{IM},2}\sigma_{N_{IM}}\sigma_2 & \dots & \sigma_{N_{IM}}^2 \end{bmatrix} \tag{4.11}$$

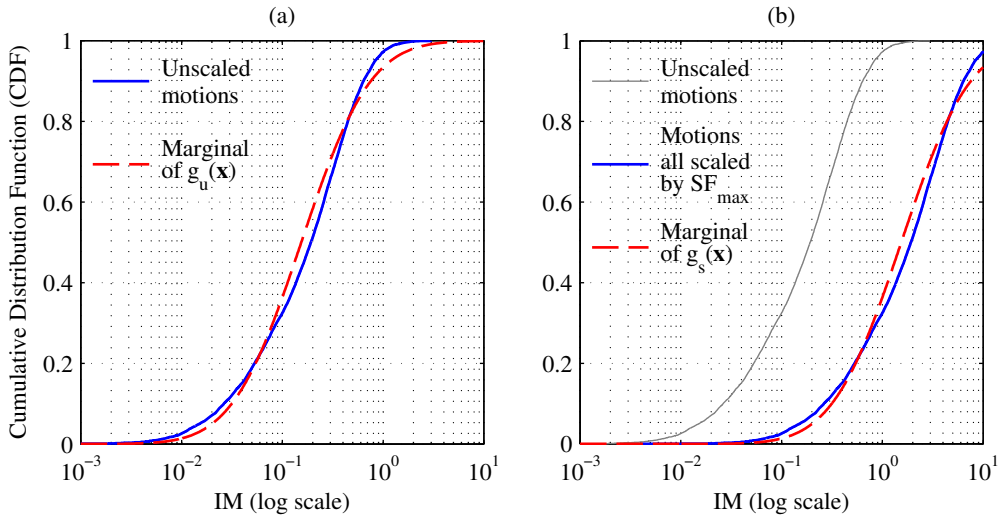

Figure 4.4: Illustration of Importance Functions derived from a database of prospective ground motions that are all: (a) unscaled, $g_u(\mathbf{x})$; or (b) scaled by SF_{max}, $g_s(\mathbf{x})$.

The approach described in the preceding paragraph may also be applied to determine an IF when ground motions are all scaled by the same scale factor. When the given database of ground motions is deemed to lack an adequate number of strong ground motions, judged by comparing $g_u(\cdot)$ against $f(\cdot)$ (Fig 4.1b), it is natural to consider scaling the motions upwards. For example, suppose it is desired to scale all the motions in the database by a factor of SF_{max} in order to create a new database of prospective motions. The IMs computed from scaled ground motions may be different, depending on the type of IM (e.g., spectral acceleration increases linearly with scale factor whereas many common measures of duration are unaffected by scaling) [48]. Applying the approach in the preceding paragraph to the new database of scaled ground motions leads to the IF denoted by $g_s(\mathbf{x})$, which is illustrated

in Fig 4.4b. Observe that $g_s(\mathbf{x})$ differs from $g_u(\mathbf{x})$ only in its mean vector; the covariance matrices (and σ_j) are the same in both cases.

In general, the recommended IF is a two-component mixture of multivariate lognormals:

$$g(\mathbf{x}) = [1-\gamma] \cdot g_u(\mathbf{x}) + \gamma \cdot g_s(\mathbf{x}) \tag{4.12}$$

where $0 \leq \gamma \leq 1$ may be interpreted as the fraction of scaled ground motions in the ensemble of n selected motions. An example of this IF is shown by the solid curve in Fig 4.5a; for comparison, the target PDF (Eq 4.3) and its two individual components – $g_u(x)$ and $g_s(x)$ – are also shown. This two-component mixture distribution permits the selection of ground motions that are scaled by factors between unity and SF_{max}, where the fraction of scaled motions is roughly controlled by γ (Fig 4.5b). For instance, when $\gamma = 0$, the general two-component IF reduces to $g_u(\cdot)$ whereas when $\gamma = 1$, it reduces to $g_s(\cdot)$. Note that when $SF_{max} = 1$, the general two-component IF also reduces to $g_u(\cdot)$, irrespective of γ.

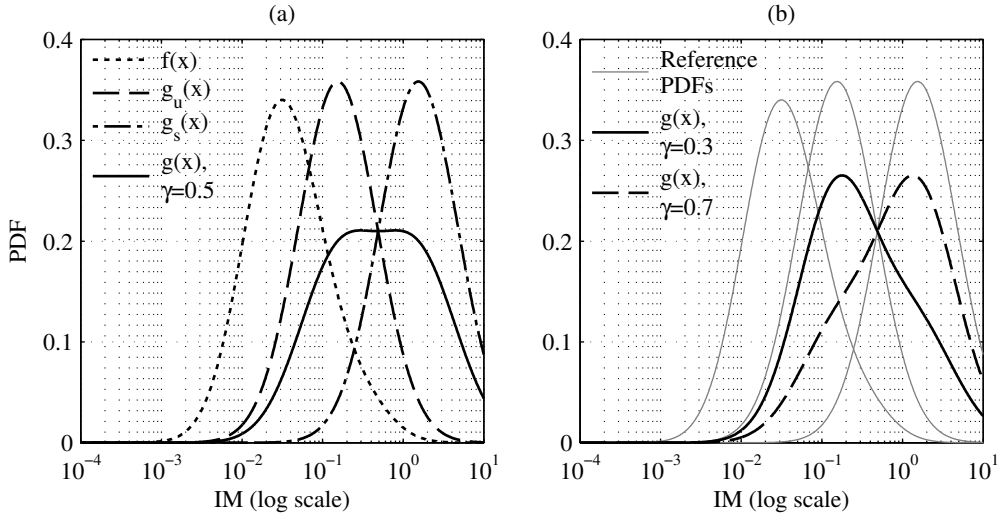

Figure 4.5: Illustration of the recommended two-component Importance Function, $g(x) = [1-\gamma] \cdot g_u(x) + \gamma \cdot g_s(x)$: (a) comparison of $g(x)$, with $\gamma = 0.5$, against its two individual components and the target PDF; (b) the effect of γ on $g(x)$.

Selection and scaling of ground motions from randomly generated intensity measures

The IF is used to randomly generate n vectors of IMs, which are in turn used to select a corresponding ensemble of n ground motions. Consequently, the ability to randomly generate a vector of IMs is an important consideration in choosing the IF. When the IF is specified

as either $g_u(\mathbf{x})$ or $g_s(\mathbf{x})$, a vector of IMs can be readily generated from the multivariate lognormal distribution. When the IF is the two-component IF given by Eq 4.12, a vector of IMs can be obtained in two steps: (i) identify one of the two components by randomly sampling from the Bernoulli distribution with probability γ, and (ii) randomly generate a vector of IMs from the component identified.

After a collection of n vectors is randomly generated from the IF, denoted by $\mathbf{IM}_{IF}$, a corresponding ensemble of ground motions is selected. For each successive $\mathbf{IM}_{IF}$, the database of prospective ground motions is searched for the optimal match while ensuring that no motion is duplicated. The optimal ground motion is defined as the one whose computed vector of (potentially scaled) IMs, denoted by $\mathbf{IM}_P$, agrees most closely with the current $\mathbf{IM}_{IF}$. The misfit between $\mathbf{IM}_{IF}$ and $\mathbf{IM}_P$ is quantified by Δ [6]:

$$\Delta = \sum_{j=1}^{N_{IM}} \left[\frac{\ln(IM_{IF,j}) - \ln(IM_{P,j})}{\sigma_j} \right]^2 \tag{4.13}$$

where N_{IM} refers to the dimension of $\mathbf{IM}$ (Section 4.3) and σ_j refers to the standard deviation of $\ln(IM_j)$ from the IF (Section 4.4). Thus, for a given $\mathbf{IM}_{IF}$, the selected ground motion (and corresponding scale factor) is the one whose value of Δ is the smallest among all prospective motions. To avoid selection of duplicate motions, the selected motion is removed from the database before proceeding to the next $\mathbf{IM}_{IF}$.

When scaled ground motions are of interest, the optimal scale factor for each prospective ground motion must be determined before computing Δ. To determine the optimal scale factor for a given $\mathbf{IM}_{IF}$, we first note the relationship between the scaled and unscaled values of the jth IM:

$$IM_{P,j} = IM_{U,j} \times SF^{\alpha_j} \tag{4.14}$$

where $IM_{P,j}$ and $IM_{U,j}$ refer, respectively, to the scaled and unscaled values of the jth IM, SF refers to a scale factor, and α_j denotes how the jth IM changes with record scaling (e.g., $\alpha_j = 1$ for spectral acceleration, $\alpha_j = 0$ for significant duration, etc.). Substituting Eq 4.14 into Eq 4.13 shows that, for a given $\mathbf{IM}_{IF}$, Δ is a quadratic function of the scale factor. By minimizing Δ with respect to SF, the optimal scale factor may be derived for each prospective ground motion:

$$SF_{optimal} = \exp\left\{ \frac{\sum_{j=1}^{N_{IM}} \left(\frac{\alpha_j}{\sigma_j^2}\right) \ln\left(\frac{IM_{IF,j}}{IM_{U,j}}\right)}{\sum_{j=1}^{N_{IM}} \left(\frac{\alpha_j}{\sigma_j}\right)^2} \right\} \tag{4.15}$$

where $IM_{IF,j}$ refers to the jth IM within the current $\mathbf{IM}_{IF}$ under consideration. When $SF_{optimal}$ is greater than SF_{max} (or less than SF_{max}^{-1}), its value is replaced by SF_{max} (or SF_{max}^{-1}), before Δ is computed.

[6] Each IM in the vector may be weighted based on its importance relative to the other IMs; however, this is omitted herein for the sake of simplicity.

Estimating hazard curves

The ground motions selected from the proposed procedure should be examined for hazard consistency with respect to **IM** before proceeding with RHAs. In other words, the 95% confidence interval (CI) of an IMHC estimate (Eq 4.5a) should cover the target IMHC (Eq 4.1). Such CIs may be readily computed by applying the bootstrap procedure [74] to the selected ground motions, generating a different IMHC estimate from Eq 4.5a per bootstrap sample. The concept of hazard consistency is illustrated in Fig 4.6. The ground motions in Fig 4.6a are hazard-consistent with respect to $A(1s)$, at exceedance rates greater than 10^{-6}, because the 95% bootstrap CI covers the target IMHC in this range. In contrast, the bootstrap CIs in Fig 4.6b do not cover the target IMHC at exceedance rates less than 10^{-5} and therefore, the corresponding ground motions are hazard-*inconsistent* with respect to PGA in this range of exceedance rates.

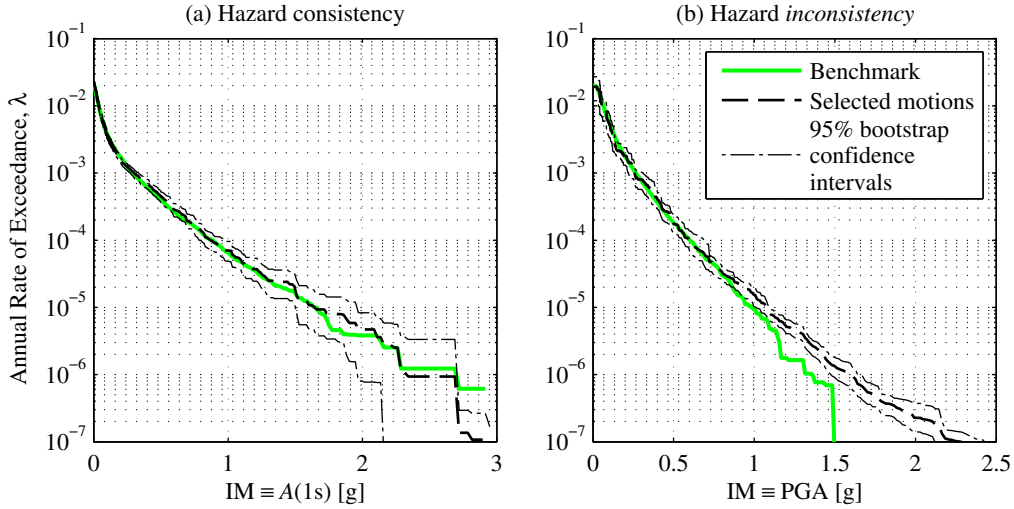

Figure 4.6: The concept of hazard consistency. An example of ground motions that are: (a) hazard-consistent with respect to $A(1s)$ at exceedance rates greater than 10^{-6}; (b) hazard-*inconsistent* with respect to PGA at exceedance rates less than 10^{-5}.

When hazard consistency is judged to be unsatisfactory at a particular range of exceedance rates, there are two options to explore for improving hazard consistency. First, ground motions may be re-selected by randomly generating another collection of n vector-valued IMs from the IF. If the re-selected motions remain hazard-inconsistent, then the next option is to vary the sample size, n. By decreasing n, the CI of the IMHC estimate widens and the likelihood of satisfying hazard consistency increases; however, the epistemic uncertainty in the SDHC estimate also increases. By increasing n, the CI of the IMHC estimate shrinks, converging to the target IMHC (Section 4.3); however, the maximum value of n

may be limited by the number of prospective motions in the database or by time constraints associated with performing RHAs.

When the preceding two options are inadequate to satisfy hazard consistency, the next option to consider is modifying the IF. First, we recommend changing SF_{max} and γ to experiment with different IFs (Fig 4.5). With each IF, new ground motions may be selected and checked for hazard consistency with respect to **IM**. When changing SF_{max} and γ is inadequate, then the database of prospective ground motions can be enlarged (e.g., adding synthetic ground motions to a database of recorded motions).

There are four steps to estimate SDHCs from an ensemble of hazard-consistent ground motions. First, RHA of the structural model is performed for all n ground motions. Second, the results from RHAs are partitioned into collapse and noncollapse cases. Third, the EDPs corresponding to the collapsed cases are replaced by appropriate values (e.g., drifts may be replaced by infinity and floor accelerations by PGA). Applying Eq 4.5b to the latter values of EDP – where the Importance Sampling weights are identical to those for the IMHC estimates (Eq 4.5a) – leads to the desired estimate of the SDHC.

4.5 An illustrative example

A 4-story reinforced concrete frame is chosen to demonstrate the applicability of the proposed procedure to realistic buildings. This well-vetted frame has been studied by past researchers in various contexts (e.g., [67], [26], [83]) and consequently, details regarding its geometry and material properties may be found in such references. In essence, the frame satisfies the strong column-weak beam philosophy and is modeled in OpenSEES [84], where the inelasticity is captured by plastic hinges at the ends of beam-column elements; its four modal periods of vibration are: $T_1 = 0.94$ sec, $T_2 = 0.30$ sec, $T_3 = 0.17$ sec, $T_4 = 0.12$ sec. The frame is classified as collapsed when its displacement increases without bounds. We consider two EDPs: (i) maximum inter-story drift ratio (MIDR), defined as the largest peak inter-story drift ratio among the four stories, and (ii) maximum floor acceleration (MFA), defined as the largest peak floor acceleration among the four stories and the ground.

The selected site and earthquake rupture forecast are identical to those shown in Fig 2 of [78]. A single strike-slip fault, with an activity rate of $\nu_0 = \nu = 0.02$ earthquakes per year, is located 10 km away from the site. Each earthquake is assumed to occur at a fixed distance of 10 km but with different magnitudes that are characterized by the Youngs & Coppersmith PDF shown in Fig 2b of [78]; the database of prospective ground motions is specified as 10^4 synthetic motions that are simulated from the stochastic model by Yamamoto and Baker [70, 67], with input magnitudes from the uniform distribution shown in Fig 2b of [78]. This example is chosen because benchmark SDHCs may be readily computed from synthetic ground motions to evaluate the proposed ground motion selection procedure [78].

Assuming in this section that no **IM** is perfectly sufficient for the response of this complex, realistic frame, the proposed selection procedure is applied to only unscaled ground motions; that is, $SF_{max} = 1$ and $\gamma = 0$. Since the first and fourth mode periods of the 4-story

frame are $T_1 = 0.94$ sec and $T_4 = 0.12$ sec, respectively, the vector of IMs is specified as $\mathbf{IM} = \{A(0.1s), A(1s), A(2s), D_{5-75}\}$; thus, $N_{IM} = 4$. In order to minimize the effects of epistemic uncertainty on the accuracy of the SDHC estimate (Section 4.3), n is specified as 1000.

For our example site, the target probability distribution of **IM** from PSHA (Eq 4.3) reduces to

$$f_{\mathbf{IM}}(\mathbf{x}) = \sum_{m} \Pr(M = m) \cdot f_{\mathbf{IM}|M}(\mathbf{x} \mid m) \tag{4.16}$$

where the summation is over the number of magnitude bins chosen to discretize the Youngs & Coppersmith magnitude PDF, $\Pr(M = m)$ refers to the probability of an earthquake with magnitude m occurring, and $f_{\mathbf{IM}|M}(\mathbf{x} \mid m)$ denotes the multivariate lognormal distribution of $\mathbf{IM} \mid M$ whose parameters are given by the benchmark-consistent prediction models. Since $SF_{max} = 1$ in this example, the general two-component IF in Eq 4.12 reduces to $g_u(\mathbf{x})$; its parameters are derived from the 10^4 unscaled ground motions (Fig 4.4a). With the IF constructed, a subset of n motions is selected from the specified database (Section 4.4).

Before proceeding with RHAs, the selected motions are checked for hazard consistency with respect to **IM**. First, the Importance Sampling weights are determined by applying Eq 4.6 to all IMs computed from the selected motions, where $f(\cdot)$ is given by Eq 4.16 and $g(\cdot)$ is given by $g_u(\mathbf{x})$ as mentioned in the preceding paragraph. Then, a hazard curve is estimate for each IM, using Eq 4.5a, and compared against the corresponding benchmark. In this example, ground motions were re-selected a few times in order to achieve hazard consistency for a wide range of exceedance rates. This consistency is confirmed in Fig 4.7, where each benchmark hazard curve falls within the 95% bootstrap CIs, for a wide range of exceedance rates.

After hazard consistency is confirmed, SDHCs are estimated for both EDPs of the 4-story frame. Since the selected motions are unscaled in this example, each motion corresponds to a unique value of the EDP that was already computed when determining the benchmark SDHC. As a result, selecting ground motions becomes equivalent to selecting a subset of EDPs from the specified database. The SDHC estimates, obtained by applying Eq 4.5b to the selected values of EDP, are shown by dashed black curves in Fig 4.8. In order to convey the epistemic uncertainty of the SDHCs, 95% bootstrap CIs are also shown in this figure, which were obtained by applying the bootstrap procedure to the selected motions.

Fig 4.8 demonstrates that the SDHC estimates from the proposed procedure, using a large number of unscaled ground motions, are accurate because the benchmark SDHCs are approximately covered by the 95% CIs. The agreement between the proposed estimate and the associated benchmark is excellent for both EDPs, at a wide range of exceedance rates. Such excellent agreement is likely due to the fact that the selected motions are hazard-consistent with respect to many different features of the ground motion, even though only four IMs were chosen to select ground motions. The selected motions in this example are consistent with the hazard for a wide range of IMs because (i) the motions are unscaled, and (ii) the chosen **IM** is strongly correlated with many other IMs. Alternatively, the excellent

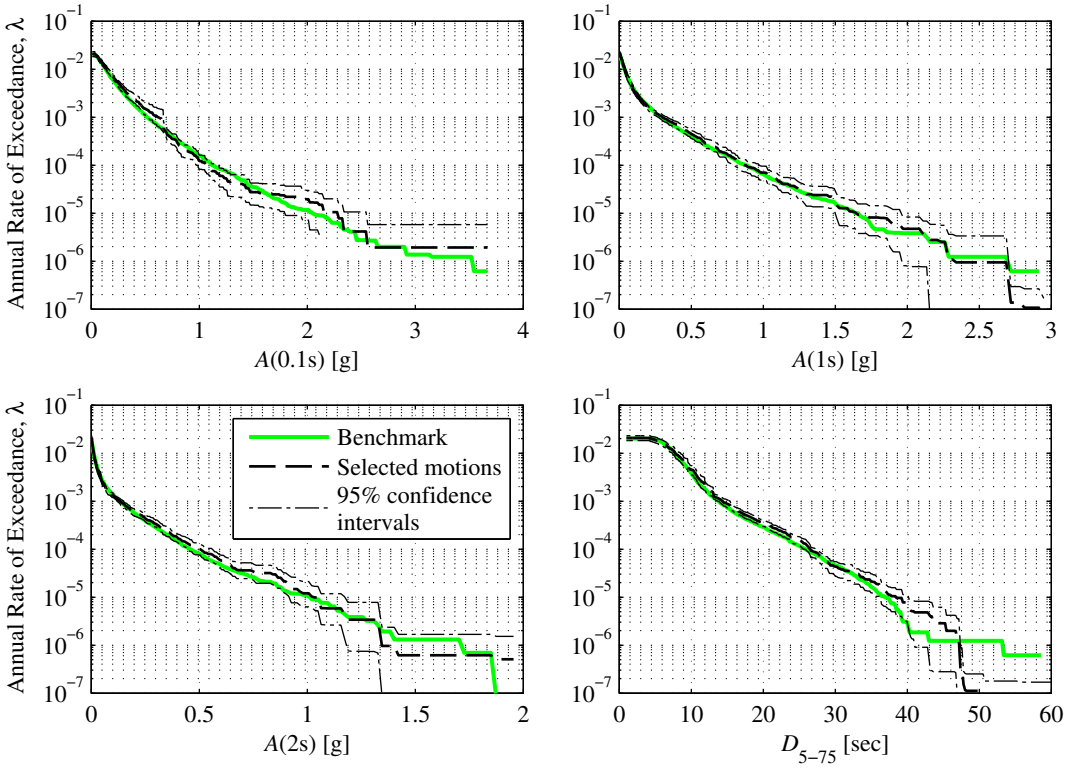

Figure 4.7: Hazard consistency of 1000 unscaled ground motions selected from $g(\mathbf{x}) = g_u(\mathbf{x})$; Confidence intervals (CIs) from 100 bootstrap samples of the selected motions.

agreement in the SDHCs may also be due to the fact that the chosen **IM** is sufficient; this possibility is investigated in the next two sections of this paper.

4.6 Minimum number of intensity measures to be considered

The results from the preceding section demonstrate that accurate SDHC estimates may be obtained from the proposed procedure when a large number of unscaled motions are selected using four IMs: (i) $A(T_1)$, (ii) $A(2T_1)$, (iii) $A(T_k)$, and (iv) D_{5-75}. At the same time, Eq 4.9 suggests that as the dimension of **IM** decreases, the epistemic uncertainty in the SDHC estimate also decreases because the integrand within the multidimensional integral is nonnegative. Consequently, the natural question is: can accurate SDHC estimates be obtained with fewer than four IMs?

To answer this question, four different choices of **IM** are considered: (i) "bestIM", (ii) "SAonly", (iii) "T1plus2T1", and (iv) "T1only"; these denote, respectively, (i) vector com-

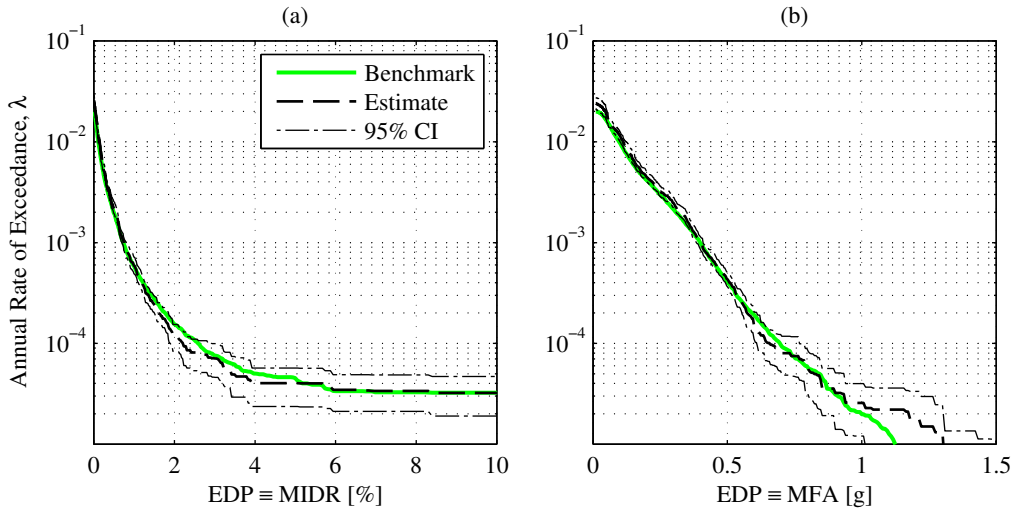

Figure 4.8: SDHC estimates from proposed procedure with $n = 1000$ unscaled ground motions selected using $\mathbf{IM} = \{A(0.1s), A(1s), A(2s), D_{5-75}\}$: (a) MIDR; (b) MFA. CIs from 100 bootstrap samples.

prising $A(0.1s)$, $A(1s)$, $A(2s)$, and D_{5-75}, (ii) vector comprising $A(0.1s)$, $A(1s)$, and $A(2s)$, (iii) vector comprising $A(1s)$ and $A(2s)$, and (iv) $A(1s)$ alone. To investigate the effects of **IM** on the resulting SDHC estimate, other inputs to the procedure are fixed and SDHC estimates from different choices of **IM** are compared against the benchmark. The SDHC estimate for a given choice of **IM** is obtained by selecting a subset of $n = 1000$, unscaled motions from the database of synthetic motions described in Section 4.5. This estimate varies with each execution of the procedure because each execution produces a different selection of ground motions from the IF (Section 4.4); thus, it's desirable to consider the epistemic uncertainty of the SDHC estimate when comparing results from different choices of **IM**. Since ground motions are unscaled, no additional RHAs are required in each execution of the procedure and therefore, the epistemic uncertainty for a given choice of **IM** may be rigorously quantified through many executions of the procedure.

The MIDR hazard curves from different choices of **IM** are presented in Fig 4.9. For each choice of **IM**, 100 SDHCs were obtained from 100 independent executions of the procedure; these SDHCs are summarized by the mean and 95% CI. This figure shows that the epistemic uncertainty is similar across the four choices of **IM**, since the width of CIs are similar. Comparing the CIs against the benchmark indicates that the SDHC from "bestIM" is unbiased at all exceedance rates whereas those from the other three choices of **IM** are unbiased only at exceedance rates greater than 10^{-4}; this implies that D_{5-75}, or duration, should not be excluded when estimating MIDR hazard curves, especially near collapse. Note that the differences between the results from "T1only" and "SAonly" are small because the

corresponding ground motions are unscaled and any inconsistencies in the hazard with respect to IMs beyond **IM** are typically less pronounced for unscaled motions than for scaled motions.

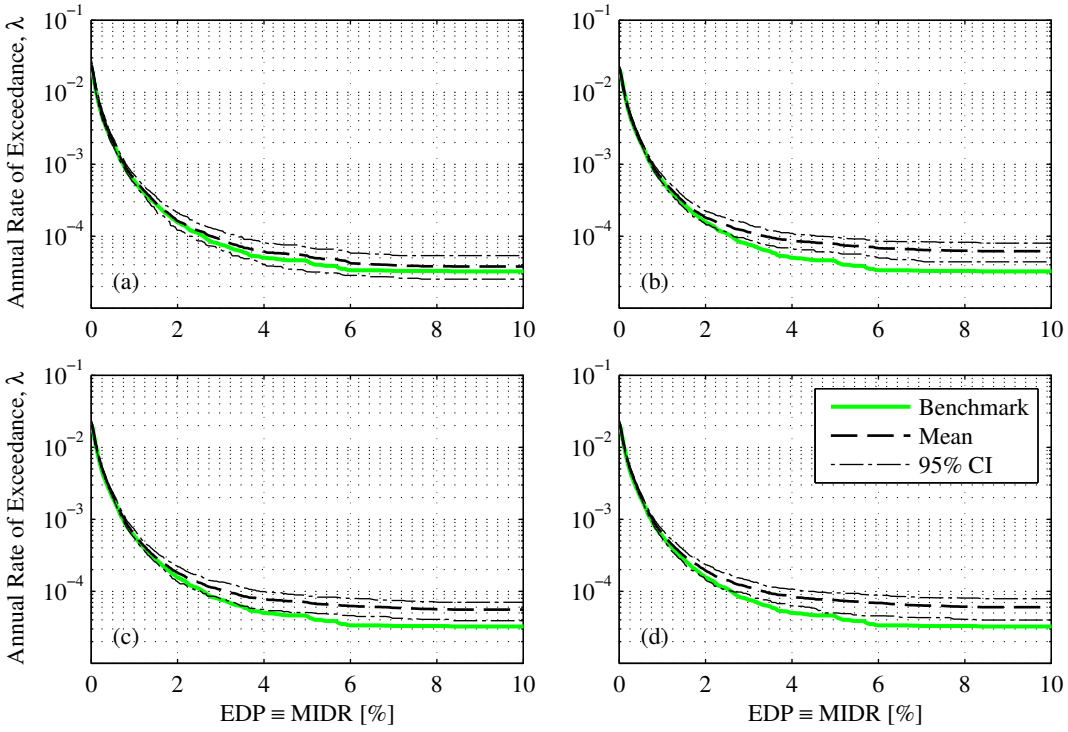

Figure 4.9: MIDR hazard curves from proposed procedure with four different choices for **IM**: (a) "bestIM" $\equiv \{A(0.1s), A(1s), A(2s), D_{5-75}\}$; (b) "SAonly" $\equiv \{A(0.1s), A(1s), A(2s)\}$; (c) "T1plus2T1" $\equiv \{A(1s), A(2s)\}$; and (d) "T1only" $\equiv A(1s)$. CIs from 100 independent executions of the proposed procedure with 1000 unscaled motions per execution.

Fig 4.10 shows the MFA hazard curves from different choices of **IM**. Like the results for MIDR, the epistemic uncertainty is again similar across the four choices of **IM**; this suggests that, as long as ground motions are unscaled, more than four IMs may be specified in the proposed procedure without significantly increasing the epistemic uncertainty in the resulting SDHC estimates. Unlike the results for MIDR, the SDHCs from *both* "bestIM" and "SAonly" are unbiased at a wide range of exceedance rates, implying that duration may be excluded when estimating MFA hazard curves. On the other hand, spectral accelerations at short vibration periods are important for the accurate prediction of MFA, because slight biases at rates between $5 \cdot 10^{-4}$ to 10^{-2} are observed for choices of **IM** that exclude $A(0.1s)$; this conclusion is consistent with the findings from Lin et al [37]. The results from Figs 4.9-4.10 suggest collectively that, as long as ground motions are unscaled, the sufficiency of **IM**

plays a lesser role in determining the accuracy of the SDHC estimate than when ground motions are scaled.

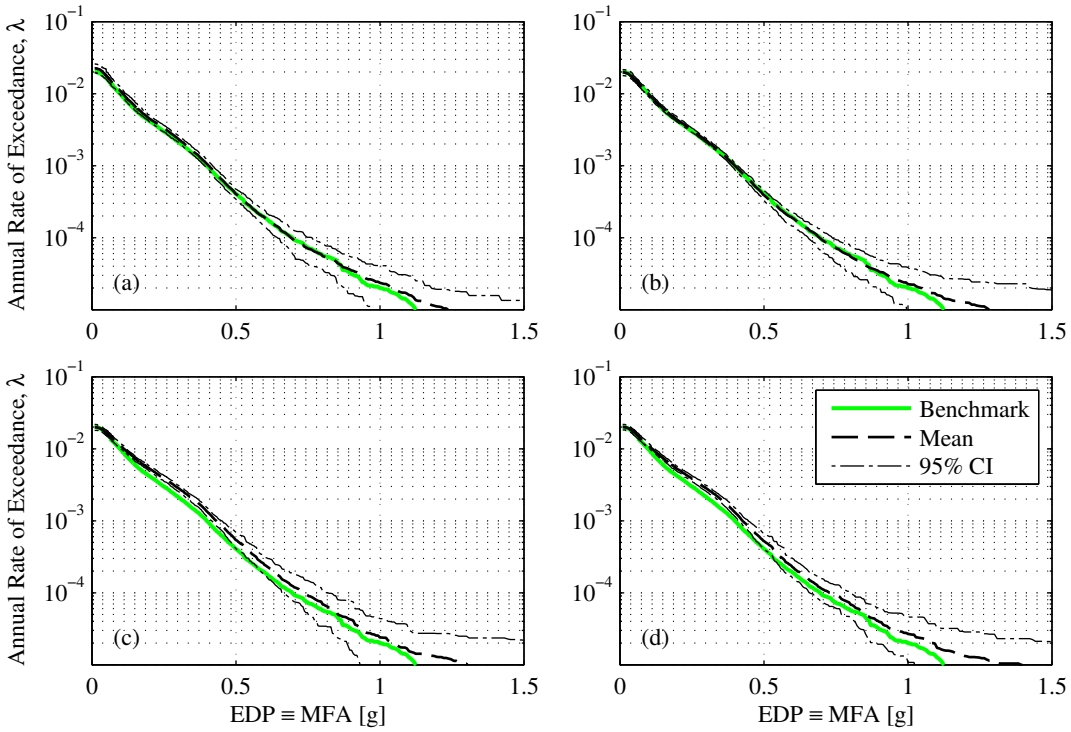

Figure 4.10: MFA hazard curves from proposed procedure with four different choices for **IM**: (a) "bestIM" $\equiv \{A(0.1s), A(1s), A(2s), D_{5-75}\}$; (b) "SAonly" $\equiv \{A(0.1s), A(1s), A(2s)\}$; (c) "T1plus2T1" $\equiv \{A(1s), A(2s)\}$; and (d) "T1only" $\equiv A(1s)$. CIs from 100 independent executions of the proposed procedure with 1000 unscaled motions per execution.

4.7 Maximum scaling of ground motions

In general, scaling distorts ground motions and causes inconsistencies with respect to the hazard. However, such hazard inconsistencies may be deliberately avoided for some IMs through sophisticated ground motion selection procedures [37, 35]. For example, by using the probability distribution of **IM** from PSHA (Eq 4.3) as the target to select scaled ground motions, the resulting motions will be, not surprisingly, consistent with the hazard for this particular vector of IMs. Nevertheless, inconsistencies with respect to features of the ground motion beyond **IM** will become increasingly pronounced as the level of record scaling increases.

Are hazard inconsistencies with respect to IMs excluded from **IM** practically significant? The answer to this question depends strongly on the sufficiency of **IM** with respect to the EDP at hand. If **IM** is insufficient (i.e., the EDP depends appreciably on other features of the ground motion besides **IM**), then such inconsistencies are significant, leading to biased SDHCs. On the other hand, if **IM** is sufficient (i.e., the EDP depends primarily on **IM** only), then by definition, such inconsistencies are immaterial and do not cause bias.

Comparing the complexity of the ground motion time series against the simplicity of IMs, it seems unlikely for an IM to be simultaneously sufficient with respect to several EDPs of a realistic structural model [35]. As a result, ground motions selected for RHAs should, ideally speaking, not be scaled, which can be achieved using the selection procedure developed herein. When ground motions must be scaled, the vector of IMs for selecting ground motions should be chosen judiciously. Based on the results presented in Sections 4.5 and 4.6, the vector $\mathbf{IM} = \{A(0.1s), A(1s), A(2s), D_{5-75}\}$, denoted by "bestIM", appears to be sufficient for both EDPs of the 4-story frame; however, how sufficient is this vector and what degree of scaling can be combined with it?

To answer these questions, n is again fixed as 1000, and four different combinations of SF_{max} and γ, which represent increasing levels of scaling (see Fig 4.5), are considered: (i) 5 and 0.5; (ii) 5 and 0.9; (iii) 10 and 0.5; and (iv) 10 and 0.9. For each combination, an estimate of the SDHC is determined and compared against the benchmark. Unlike Section 4.6, each implementation of the procedure with a different combination of scaling requires additional RHAs because EDPs corresponding to scaled ground motions have *not* been computed previously; in total, 4000 RHAs of the 4-story frame were performed to obtain the results presented in this section. Since additional RHAs are needed for each implementation of the procedure, the epistemic uncertainty in the SDHC estimate is approximately quantified by a bootstrap CI. To make meaningful comparisons among the four cases of scaling, each of the four ensemble of ground motions was carefully checked for hazard consistency with respect to **IM**; this is demonstrated in Fig 4.11, where the CIs of each IMHC estimate have been omitted for clarity. With hazard consistency satisfied for all four cases of scaling, the degree of bias in the resulting SDHCs indicates the degree to which "bestIM" is insufficient for this 4-story frame.

The SDHCs from the four combinations of scaling are presented in Figs 4.12-4.13. Taking into account the epistemic uncertainty depicted in Fig 4.12, the MIDR hazard curve from $SF_{max} = 5$ and $\gamma = 0.5$ is least biased and that from $SF_{max} = 10$ and $\gamma = 0.9$ is most biased, among the four combinations considered. With the exception of Fig 4.12d at exceedance rates less than $4 \cdot 10^{-5}$, the biases are generally conservative in the sense that for a given level of exceedance rate, the demand is overestimated. For fixed γ, the bias in the MIDR hazard curve increases with increasing SF_{max}. Similarly, for fixed SF_{max}, the bias in the MIDR hazard curve increases with increasing γ. In contrast, the MFA hazard curves from all four combinations are practically unbiased.

Since ground motions are hazard-consistent with respect to **IM** (Fig 4.11), the bias observed in Fig 4.12b suggests that "bestIM" is insufficient for MIDR. Relative to MIDR, "bestIM" appears to be less insufficient with respect to MFA, as suggested by the excellent

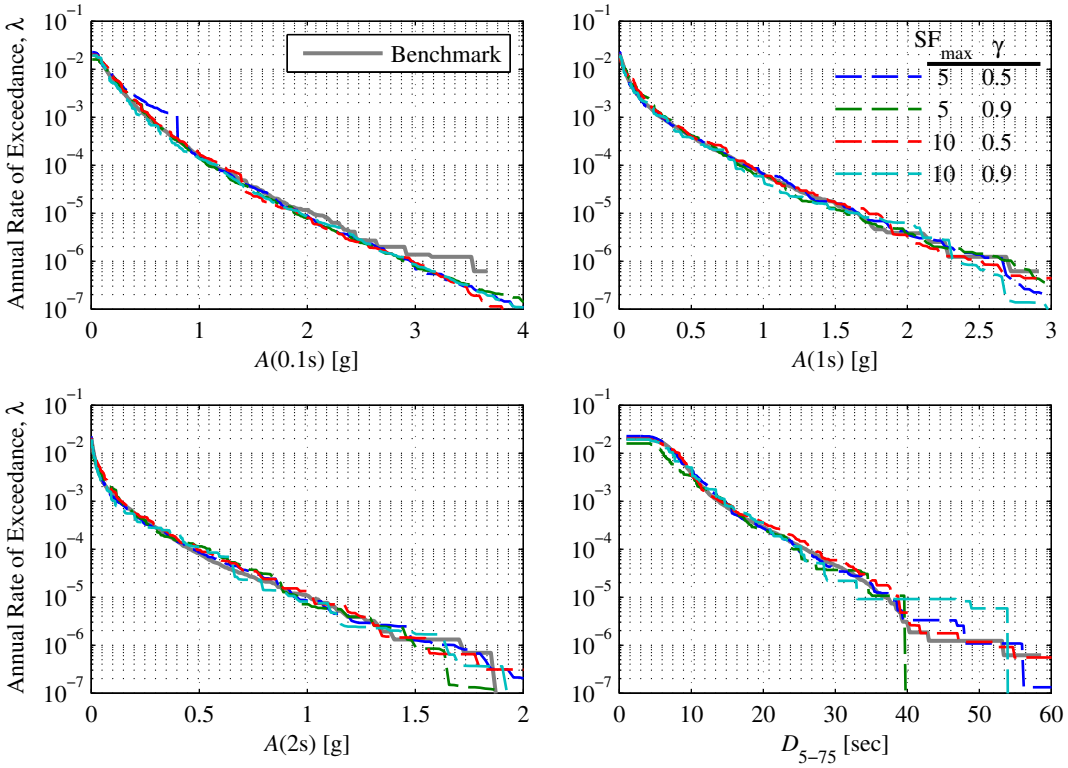

Figure 4.11: Hazard consistency of ground motions, scaled to various degrees, with respect to IMs employed for ground motion selection: (a) $A(0.1s)$; (b) $A(1s)$; (c) $A(2s)$; and (d) D_{5-75}.

agreement among the four cases shown in Fig 4.13. This can be explained partially by the fact that unlike drifts or displacements, accelerations are limited by the strength of the system and thus, MFA is less sensitive to scaling than MIDR. Considering the epistemic uncertainty and the extent of scaling, the biases shown in Figs 4.12-4.13 suggest that "bestIM" is still a useful, practical vector for selecting ground motions with the proposed procedure.

When **IM** is sufficient with respect to EDP, the conditional probability distribution of $EDP \mid \mathbf{IM}$ is essentially independent of record scaling; that is, the conditional distribution from scaled ground motions, $f(EDP \mid \mathbf{IM}, \text{scaled})$, is nearly the same as that from unscaled motions, $f(EDP \mid \mathbf{IM}, \text{unscaled})$. In contrast, an insufficient **IM** implies that the two conditional distributions are different, with the difference increasingly significant as the degree of scaling increases; in this case, the expectation in Eq 4.7b no longer holds, which can be seen in Fig 4.12. Given the relationship between scaling and bias, ground motions should not be scaled (i.e., $SF_{max} = 1$ or $\gamma = 0$) but if scaling is necessary, then some bias in the SDHC should be anticipated, depending on the sufficiency of the vector-valued IM chosen to select ground motions. Based on the results shown in Figs 4.12-4.13, the optimal values

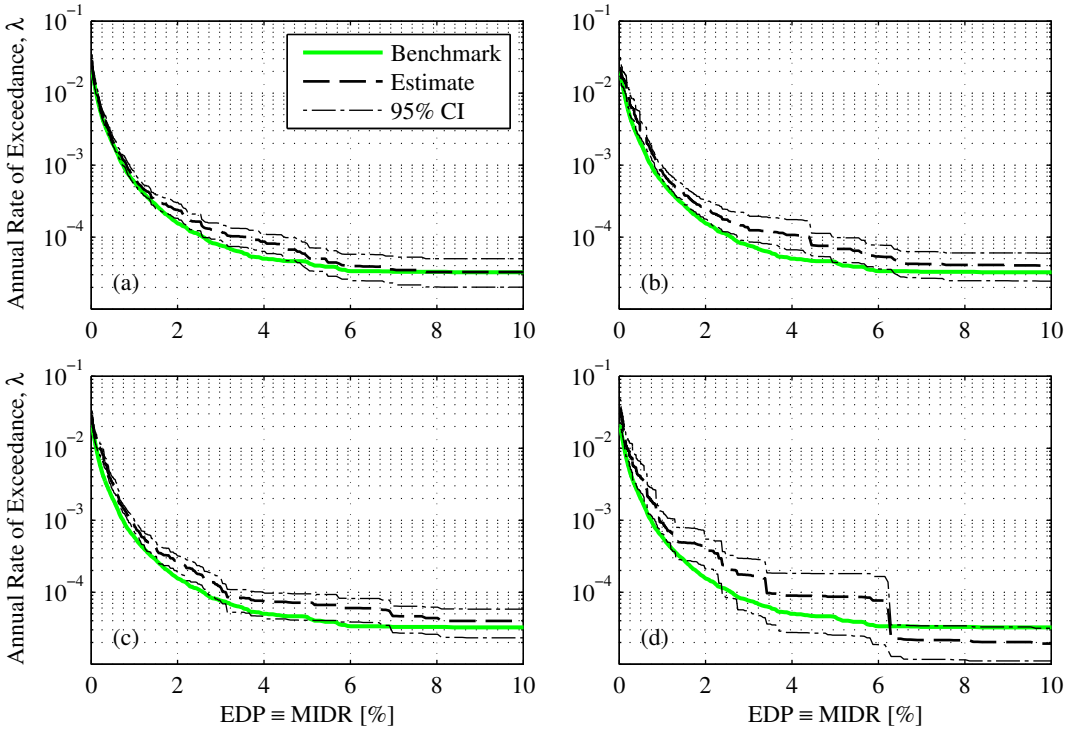

Figure 4.12: MIDR hazard curves from proposed procedure with four different combinations of SF_{max} and γ: (a) 5 and 0.5; (b) 5 and 0.9; (c) 10 and 0.5; and (d) 10 and 0.9. CIs from 100 bootstrap samples with "bestIM" and $n = 1000$ per bootstrap sample.

of SF_{max} and γ depend on the EDP of interest and on the specified **IM**; when **IM** consists of $A(T_1)$, $A(2T_1)$, $A(T_k)$, and D_{5-75}, we recommend $SF_{max} \leq 5$ and $\gamma \leq 0.5$.

The lack of sufficiency in "bestIM" with respect to MIDR implies that hazard inconsistencies with respect to other features of the ground motion cause bias in MIDR hazard curves. In Fig 4.14, the ground motions from the four combinations of scaling are examined for hazard consistency with respect to four IMs that are excluded from "bestIM": (i) peak ground acceleration (PGA), (ii) peak ground velocity (PGV), (iii) peak ground displacement (PGD), and (iv) cumulative absolute velocity (CAV). These IMs are chosen to represent the frequency content (at short, moderate, and long periods) and duration of the ground motion. The differences between the four ensembles are most pronounced for PGD; in fact, many other IMs were also examined and the differences are most pronounced for spectral accelerations at periods longer than 2 sec. Therefore, the MIDR of the 4-story frame appears to be sensitive to the long period content of the ground motion.

The motions from the four combinations of scaling are similar to each other in that they are hazard-consistent with respect to PGA, PGV, and CAV (Fig 4.14). This is the case because such IMs are strongly correlated with "bestIM": PGA and PGV are correlated with

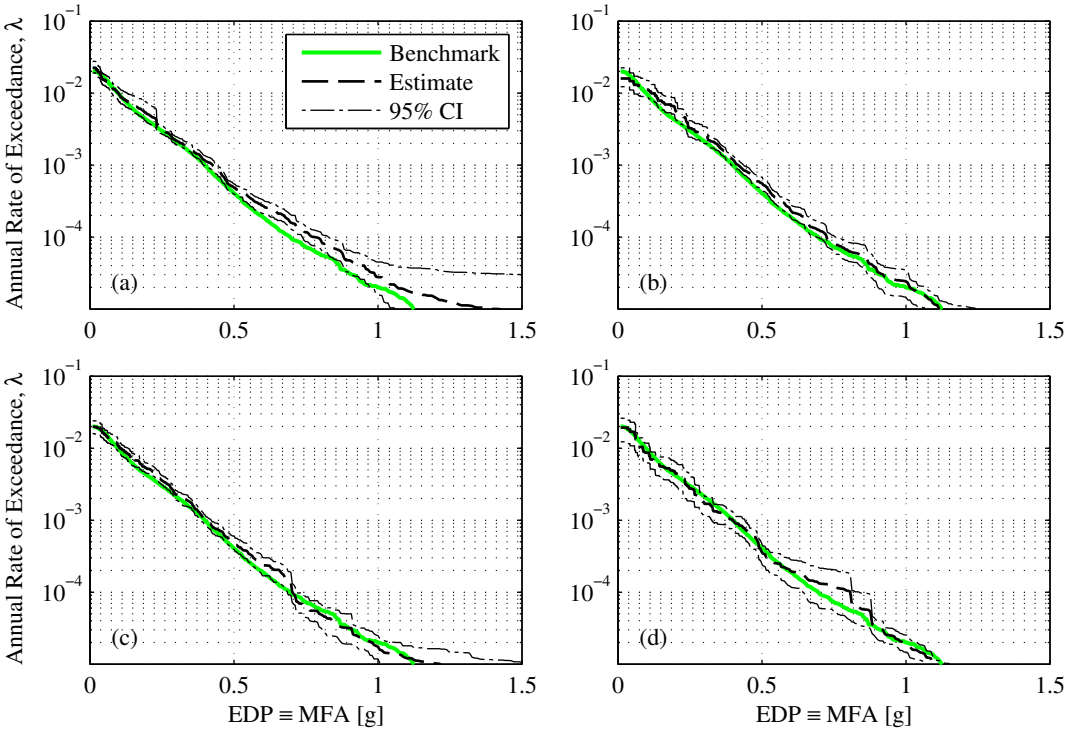

Figure 4.13: MFA hazard curves from proposed procedure with four different combinations of SF_{max} and γ: (a) 5 and 0.5; (b) 5 and 0.9; (c) 10 and 0.5; and (d) 10 and 0.9. CIs from 100 bootstrap samples with "bestIM" and $n = 1000$ per bootstrap sample.

spectral accelerations at vibration periods between 0.1 and 2 sec while CAV is correlated with D_{5-75}. On the other hand, PGD is correlated with spectral accelerations at periods longer than 2 sec, which were excluded from "bestIM". At the same time, we know from Fig 4.10 that the MFA is sensitive to spectral accelerations at short periods. Therefore, the excellent agreement in Fig 4.13, despite extensive scaling, is likely due to the fact that all four ensembles are hazard-consistent with respect to spectral accelerations at short periods of vibration.

The degree of scaling also affects the epistemic uncertainty of the SDHC estimates because different values of SF_{max} and γ lead to different IFs (Fig 4.5). For $EDP \equiv MIDR$, the widths of the CIs from Figs 4.12a-c are similar to each other and differ with those from Fig 4.12d. For $EDP \equiv MFA$ however, the widths of the CIs from all four cases shown in Fig 4.13 are similar to each other. These observations imply that the effect of scaling on the epistemic uncertainty varies with the type of EDP. From Eq 4.9, we see that the epistemic uncertainty is affected by two quantities that depend on the EDP and are unknown a-priori: (i) $\Pr(EDP > z \mid \mathbf{IM} = \mathbf{s})$ and (ii) $\lambda_{EDP}(z)$. In order to approximately quantify the epistemic uncertainty contained in any particular SDHC estimate from the proposed

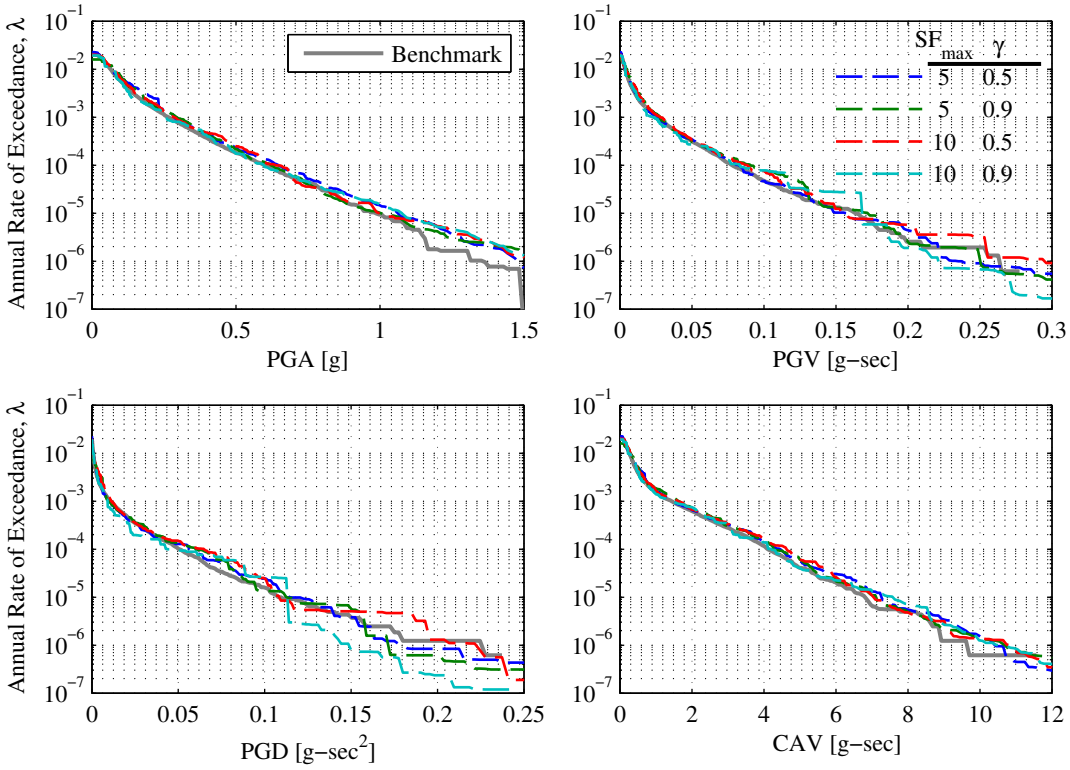

Figure 4.14: Hazard consistency of ground motions, scaled to various degrees, with respect to four miscellaneous IMs: (a) PGA; (b) PGV; (c) PGD; and (d) CAV.

procedure, we recommend supplying the estimate with a bootstrap CI (e.g., Fig 4.8). In addition to varying the IF (through SF_{max}, γ, and the database of prospective motions), the epistemic uncertainty may also be reduced by increasing the sample size, which is discussed next.

4.8 Minimum number of selected motions

How many ground motions should be specified for the proposed procedure (Fig 4.3)? In general, a large sample size is desirable because as the value of n increases, the epistemic uncertainty in the SDHC decreases (Eq 4.9) and consequently, the estimate becomes more repeatable. Furthermore, when scaling is not permitted and **IM** is sufficient, the SDHC estimate converges to the theoretical value (Eq 4.7b) with increasing values of n. However, the maximum value of n that can be specified is limited by the total number of prospective ground motions in the specified database. Hence, small values of n are also of interest and for a given site, EDP, and IF, the desirable value of n depends on the tolerable level of

epistemic uncertainty.

We investigate the effects of different sample sizes for $SF_{max} = 1$ and "bestIM" (Section 4.6). Unscaled ground motions are considered in this section because when ground motions are scaled significantly and **IM** is insufficient, the resulting SDHC estimate is biased, regardless of the sample size (Section 4.7). Four different values of n are considered: (i) 100, (ii) 250, (iii) 500, and (iv) 1000. For each value of n, the procedure is executed 100 times, yielding 100 independent estimates of the SDHC; these SDHCs, summarized by the mean and 95% CI, are compared against the benchmark.

The MIDR hazard curves from different sample sizes are presented in Fig 4.15. As indicated by the mean, the estimate from the proposed procedure is, on average, unbiased regardless of the sample size, which is consistent with Eq 4.7b. For a given value of n, the epistemic uncertainty in the SDHC estimate increases for decreasing exceedance rates and is largest at collapse. As n decreases from 1000 to 100, the epistemic uncertainty increases. In particular, the relatively wide CIs near collapse in Fig 4.15a indicate that the SDHC estimate from a single execution with $n = 100$ is not very repeatable; that is, another execution with $n = 100$ will likely produce a different estimate of the SDHC. The repeatability of an SDHC estimate is measured by the standard deviation of the logarithm of the collapse rate, denoted by σ_C, since exceedance rates may be considered to be approximately lognormally distributed [85]; the values of σ_C for each choice of sample size are displayed in Fig 4.15.

Assuming a σ_C value of 0.4 is tolerable, values of n between 250 to 500 are recommended for the proposed procedure with $SF_{max} = 1$ and "bestIM"; this recommended range appears to be also applicable to scaled ground motions, but more research is needed to confirm this tentative conclusion. If smaller values of σ_C are desired, then n should be increased. To provide some context for such values of σ_C, note that the epistemic uncertainty in seismic hazard and in seismic response is on the order of 0.5-1.5 and 0.4, respectively [35, 85]. The recommended range of $250 \leq n \leq 500$ is tantamount to performing 25 to 50 RHAs at 10 intensity levels in a PSDA, except that a non-parametric approach is employed in the proposed procedure (Eq 4.5) whereas a parametric approach is typically employed in PSDA. Consequently, the required sample size for the proposed procedure may be reduced if the estimates from Eq 4.5 are fitted with a parametric probability distribution.

4.9 Conclusions

A novel ground motion selection procedure is developed in this paper. For a given structure at a given site, the procedure provides a single ensemble of ground motions and a corresponding collection of Importance Sampling weights for estimating SDHCs. The procedure requires five inputs: (i) database of prospective ground motions, (ii) **IM**, a vector of IMs for selecting ground motions, (iii) maximum acceptable scale factor, SF_{max}, (iv) a target fraction of scaled ground motions, γ, and (v) sample size, n. This procedure provides the following advantages:

1. The ability to estimate SDHCs from a *single* ensemble of ground motions;

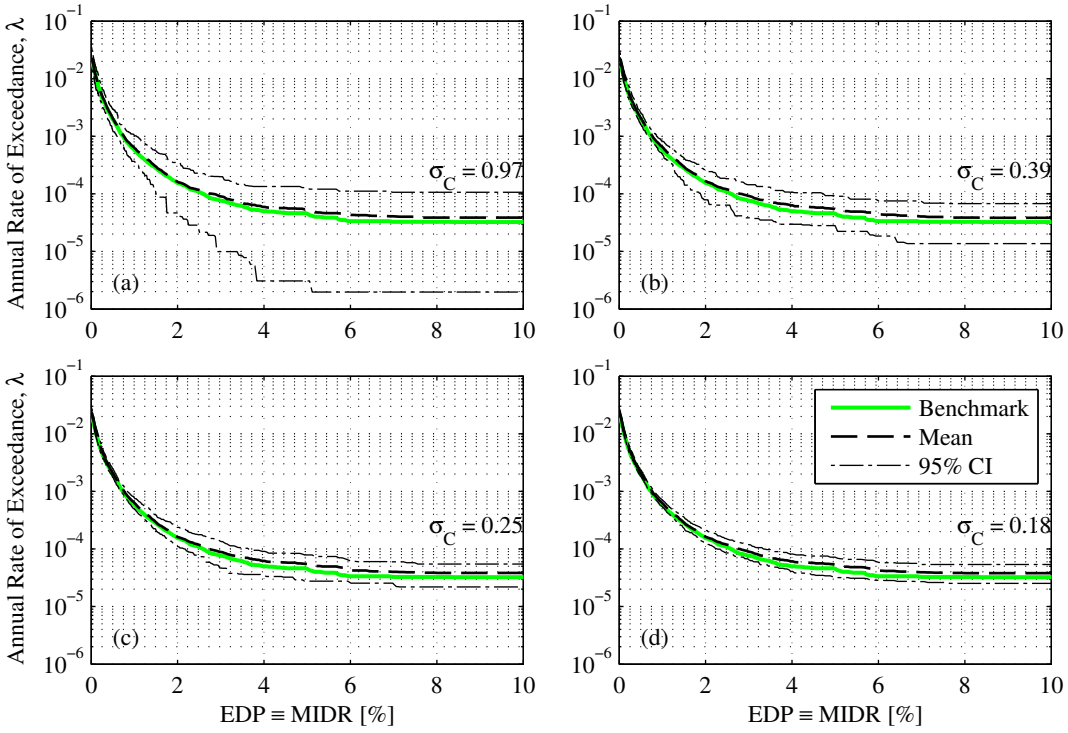

Figure 4.15: MIDR hazard curves from proposed procedure with four different choices for n: (a) 100; (b) 250; (c) 500; and (d) 1000. CIs from 100 independent executions of the procedure with unscaled motions selected using "bestIM" per execution.

2. The option to select ground motions that are scaled to varying degrees, including the important case of selecting *only* unscaled ground motions;

3. The means to achieve hazard consistency with respect to a specified vector of IMs.

Using a recently developed method for evaluating ground motion selection procedures, the proposed procedure is evaluated in its ability to estimate SDHCs of a 4-story reinforced concrete frame, leading to the following conclusions:

1. The proposed procedure provides accurate estimates of the SDHC when ground motions are unscaled, or when the vector of IMs chosen to select ground motions is sufficient for the response quantity of interest.

2. If ground motions are restricted to be unscaled, then the sufficiency of the vector-valued IM comprising $A(0.1s)$, $A(1s)$, $A(2s)$, and D_{5-75}, denoted by "bestIM", plays a lesser role in determining the accuracy of the SDHC estimate than when ground motions are scaled. When ground motions are unscaled, "bestIM" is sufficient for both MIDR and

MFA of the 4-story frame; in fact, D_{5-75} may be excluded for estimating MFA hazard curves.

3. If scaling of ground motions is permitted, the sufficiency of "bestIM" plays a major role in determining the accuracy of the SDHC estimate. When ground motions are scaled by factors as large as 10, "bestIM" remains sufficient for MFA but not for MIDR; the latter EDP seems to be influenced also by spectral acceleration at vibration periods longer than $2T_1$. The bias in MIDR hazard curves caused by amplitude scaling is generally conservative.

4. The epistemic uncertainty of the SDHC estimate, which increases for decreasing exceedance rates, is influenced by both the IF and the sample size n. For a given IF, the desired sample size depends on the level of epistemic uncertainty that can be tolerated.

5. Based on the exploratory analyses in this paper, inputs for the proposed procedure are recommended as:

   - $\mathbf{IM} = \{A(T_k), A(T_1), A(2T_1), D_{5-75}\}$, where T_1 and T_k refer, respectively, to the first and kth mode of the structure;
   - $SF_{max} \leq 5$ and $\gamma \leq 0.5$ when $\mathbf{IM} = \{A(T_k), A(T_1), A(2T_1), D_{5-75}\}$;
   - $250 \leq n \leq 500$ when $\mathbf{IM} = \{A(T_k), A(T_1), A(2T_1), D_{5-75}\}$, $SF_{max} \leq 5$, and $\gamma \leq 0.5$.

   The application of these recommendations, which are based on analyses of a 4-story frame, should be tested for taller buildings.

Chapter 5

Evaluation of existing, contemporary GMSM procedures

5.1 Abstract

Two existing, contemporary GMSM procedures – CSexact and GCIM – are evaluated in their ability to accurately estimate seismic demand hazard curves (SDHCs) of a given structure at a specified site. The amount of effort involved in implementing these procedures to compute a single SDHC is summarized and a case study is chosen where rigorous benchmark SDHCs can be determined for evaluation purposes. By comparing estimates from GMSM procedures against the benchmark, we conclude that whether or not the estimate from a particular GMSM procedure is biased depends on the particular problem, because the underlying cause of SDHC bias involves two important aspects of the specific selection of ground motions: (i) hazard consistency, and (ii) IM sufficiency. A GMSM procedure is only a tool for achieving hazard consistency with respect to a user-specified collection of IMs; whether or not the resulting SDHC is biased depends on how sufficient the vector of IMs is, relative to the EDP of interest. We find that it is possible to obtain biased SDHCs from GCIM, even after implementing the bias-checking procedure, because in many situations, it is difficult to identify IMs that are sufficient for the response of a complex, MDF system.

5.2 Introduction

Several ground motion selection and modification (GMSM) procedures have been proposed in the past to select ground motions for conducting intensity-based assessments. The goal of an intensity-based assessment is to estimate the probability distribution of a response quantity, or engineering demand parameter (EDP), given the fact that an intensity measure (IM) is known to be of a certain intensity level [31, 3]. A common example of this type of assessment is when the IM is defined as the spectral acceleration at the fundamental period of the structure, $A(T_1)$, and the intensity level is determined from a specified return period

(e.g., 475 years, 2475 years, etc.).

In the context of intensity-based assessments, Baker and Cornell [9] investigated four different approaches to select ground motions and concluded that when matching parameters to select ground motions, spectral shape is a more important parameter to match than causal parameters such as earthquake magnitude, M, and source-to-site distance, R. Based on this finding, the Conditional Mean Spectrum (CMS) was proposed as the target spectrum for selecting ground motions [51, 9, 25]. However, the CMS, by definition, does not provide the proper aleatory variability in the response spectrum and as a result, extensions of the CMS have been developed by Jayaram *et al.* [1] and Lin *et al.* [57]; these new spectra are known respectively as the Conditional Spectrum (CS), and the "exact" CS. Moreover, the CMS (again by definition) does not account for IMs that are unrelated to spectral accelerations and consequently, the Generalized Conditional Intensity Measure (GCIM) method was developed by Bradley [47], which may be interpreted as a generalization of the CMS approach.

The previously mentioned methods for selecting ground motions are highly sophisticated in the sense that explicit measures of the ground motion (e.g., spectral acceleration, significant duration, etc.) are carefully accounted for in the selection process through knowledge from probabilistic seismic hazard analysis (PSHA) of the site. Despite this sophistication, the accuracy of the results from such procedures is unclear because ground motions are almost always scaled and record scaling remains a subject of debate [86]. For example, Grigoriu [21] argues (on the basis of analyzing stochastic processes) that scaled ground motions provide "limited if any information on the seismic performance of structural systems". On the other hand, Bradley [35] argues that scaling will not cause bias in the EDP (due to an IM), as long as either (i) the EDP is not dependent on the IM, or (ii) the probability distribution of the IM from the selected ground motions is consistent with the theoretical distribution.

In this study, we evaluate the accuracy of the results from sophisticated, contemporary GMSM procedures. More precisely, we evaluate the "exact" CS (henceforth denoted as CSexact for brevity) and GCIM approaches in their ability to accurately estimate seismic demand hazard curves (SDHCs) of a given structure at a specified site. This context is chosen in order to draw definitive conclusions, since the SDHC of a given structure at a given site is unique [34]. In order to evaluate these procedures, we introduce the notion of a benchmark (Section 2.5) and apply the methodology described in Section 3.3.

We will see later that whether or not SDHC bias exists depends on the particular problem under consideration. Specifically, the bias in the SDHC depends on the "hazard consistency" of the selected ground motions with respect to an IM that is "sufficient" (for that particular EDP) [64] and *not* on the specific GMSM procedure. An IM, which is considered vector-valued for generality, is formally defined to be *sufficient with respect to EDP*, and denoted as $\mathbf{IM}_s$, when it satisfies the following equation:

$$\Pr(EDP > z \mid \mathbf{IM}_s, IM_1, IM_2, \ldots, IM_\infty) = \Pr(EDP > z \mid \mathbf{IM}_s) \tag{5.1}$$

where "$IM_1, IM_2, \ldots, IM_\infty$" denotes any other features of the ground motion time series such as duration, M, R, etc. (see Appendix A of [12]); otherwise, it is insufficient with respect to this particular EDP.

We will see that GMSM procedures, such as CSexact and GCIM, are tools for obtaining ground motions that are hazard-consistent with respect to a collection of IMs specified by the user: in CSexact, ground motions are selected to be consistent with the hazard in terms of spectral accelerations at various vibration periods whereas in GCIM, ground motions are selected to be consistent with the hazard in terms of any IM specified by the user. When ground motions are hazard-consistent with respect to a vector of IMs, whether or not the resulting estimate of the SDHC is biased depends on how sufficient the vector-valued IM is relative to the particular EDP at hand. For complex nonlinear MDF systems, identifying sufficient IMs is difficult but with a benchmark (Section 5.4), one can definitively identify IMs that are *insufficient* for a given EDP. A case study is chosen to illustrate these ideas; the details of this case study are described next.

5.3 Case study site, structural models, and EDPs considered

The site chosen is identical to that depicted in Fig 3.2a and described in Section 3.4. In essence, the seismicity of the site is controlled by a single strike-slip fault that is located 10 km away. Earthquakes occur randomly with magnitudes following the Youngs & Coppersmith PDF shown by the solid curve in Fig 3.2b, at an activity rate of $\nu = 0.02$ earthquakes per year.

Nine SDF systems are considered in order to explore a range of vibration periods and strengths. All SDF systems are variations of the degrading SDF system discussed in Section 3.4, whose force-deformation relationship is portrayed in Fig 3.3b; the systems share a common damping of 5% and differ only in two aspects: (i) their natural period of vibration, T_1, and (ii) yield strength, f_y. The nine SDF systems represent combinations of three vibration periods, T_1, – 0.25, 1, and 4 sec – and three yield strength reduction factors, $R_y(T_1)$, – 1, 4, and 8 – where $R_y(T_1) = f_o(T_1) \div f_y(T_1)$ and $f_o(T_1)$ is defined as the minimum strength required for the system to remain elastic for an event with a return period of 2475 years. From PSHA of the site with Yamamoto's stochastic model (see Section 5.4), the values of f_o, normalized by the weight of the system, are determined respectively as 0.93, 0.50, and 0.10g, for vibration periods 0.25, 1, and 4 sec.

Two reinforced concrete frames – 4-story and 20-story – are also considered. These well-vetted frames have been studied by past researchers in various contexts (e.g., [67], [26], [83]) and consequently, details regarding geometry and material properties may be found in such references. In essence, both frames satisfy the strong-column, weak-beam philosophy and are modeled in OpenSEES [84], where the inelasticity is captured by plastic hinges at the ends of beam-column elements; each frame is classified as collapsed when its displacement increases without bounds. The four modal periods of vibration for the 4-story frame are: $T_1 = 0.94$ sec, $T_2 = 0.30$ sec, $T_3 = 0.17$ sec, $T_4 = 0.12$ sec; for the 20-story frame, the four modal periods are: $T_1 = 2.6$ sec, $T_2 = 0.85$ sec, $T_3 = 0.46$ sec, $T_4 = 0.32$ sec.

Peak displacement is the only EDP considered for all SDF systems. In contrast, many more EDPs are considered for the multistory frames. For each frame, the EDPs considered are: (i) peak (over time) floor displacements (PFD), (ii) peak story drift ratios (PSDR), (iii) peak floor accelerations (PFA), (iv) maximum story drift ratio over all stories (MSDR), and (v) maximum floor acceleration over all floors (MFA). Thus, a total of 14 EDPs are considered for the 4-story frame and a total of 62 EDPs are considered for the 20-story frame.

5.4 Methodology for evaluating GMSM procedures

In this study, we are interested in evaluating CSexact and GCIM in their ability to accurately estimate SDHCs. Both GMSM procedures scale ground motions but differ primarily in the IMs considered for selecting ground motions. If the IMs considered are indeed sufficient for all EDPs of interest and the selected ground motions are also hazard-consistent with respect to such IMs, then scaling should not cause any bias in the final SDHCs [64]. In many cases however, the degree of sufficiency for any IM is unknown and as a result, potential EDP biases may occur. Therefore, it is important that when comparing SDHC estimates from GMSM procedures against a benchmark SDHC, the benchmark should involve neither record scaling nor IMs.

Such benchmark SDHCs can be determined from the approach described in Section 3.3 and schematically illustrated in Fig 3.1. In essence, this approach involves three main steps. First, a universe of synthetic ground motions is generated such that they are consistent with the earthquake rupture forecast of the site, either by matching the specified PDFs or utilizing Importance Sampling (see Fig 3.2 and Section 3.5). Second, benchmark hazard curves are computed using Eqs 3.6, 3.9, and 3.12; note that the Importance Sampling weights, $w(m_i)$ are used only in these equations and nowhere else in the approach. Third, all GMSM procedures are applied to a subset of this universe of synthetic ground motions when estimating SDHCs; this is important for isolating the biases caused by a GMSM procedure on its resulting SDHC estimates.

For the subsequent results, the two stochastic models described in Section 3.4, referred to as Rezaeian and Yamamoto, are utilized to generate two universes of 10^4 ground motions. With two stochastic models and two multistory frames, at least 4×10^4 response history analyses (RHAs) of multistory frames were performed for this study. Examples of benchmark hazard curves from the two stochastic models are shown in Fig 5.1, where the differences between the two models highlight the purpose of a benchmark SDHC: to isolate the effects of GMSM procedures on the resulting SDHC estimates and *not* to estimate the absolute 'true' SDHC. Observe that at an exceedance rate of 10^{-3}, the corresponding value of the hazard curve is greater from Rezaeian's model than from Yamamoto's model; this implies that the response of a given structure is generally more nonlinear in Rezaeian's model than in Yamamoto's model.

In order to apply CSexact and GCIM to a database of synthetic ground motions, ground

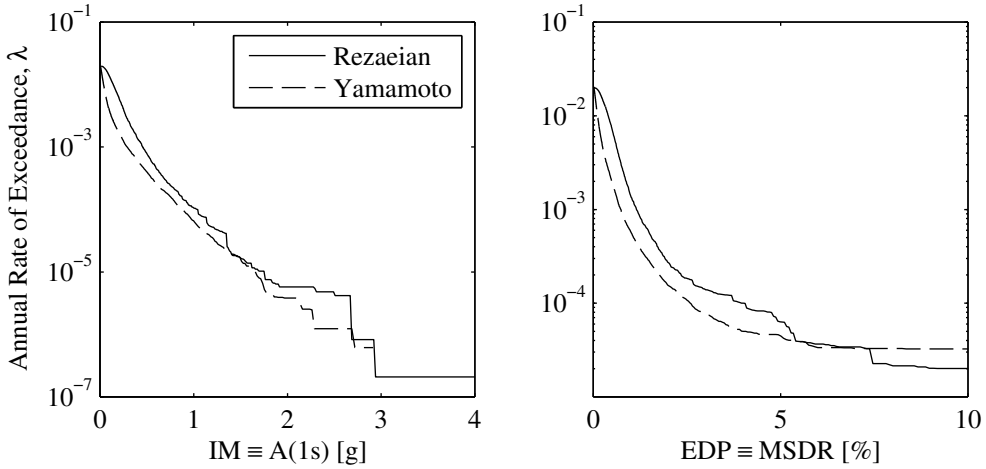

Figure 5.1: Examples of benchmark hazard curves for an: (a) IM; (b) EDP.

motion prediction models (GMPMs) that are "consistent with the benchmark" (Section 3.3) must be available. Such benchmark-consistent GMPMs were developed for 120 IMs and for each stochastic model, following the approach outlined in Section 3.6. The selection of functional forms, determination of optimal standard deviations, and consideration of correlations, are documented in Appendix B. With these benchmark-consistent prediction models developed, CSexact is evaluated first before GCIM; for each procedure, a step-by-step summary is presented, followed by results from implementation.

5.5 Step-by-step summary of CSexact

The CSexact approach for estimating a SDHC is summarized as follows:

1. Specify the conditioning period, T^*.
2. Determine the hazard curve for $A(T^*)$ from PSHA of the site and select N_{IM^*} intensity levels for conducting intensity-based assessments (see Fig 2.1a).
3. For the ith intensity level of $A(T^*)$, denoted by x_i, select n ground motions from a master database using the "exact" CS [57] as the target:
   a) Perform deaggregation to determine the percent contribution of each rupture scenario to $A(T^*) = x_i$ (see Fig 2.3a).
   b) Scale all ground motions from the master database so that $A(T^*) = x_i$; optionally reduce the size of this database of scaled, prospective ground motions with a user-specified maximum scale factor, SF_{max}.

c) Specify vibration periods for computing the target spectrum (see shaded region in Fig 2.3b).

d) Compute the "exact" Conditional Spectrum, using either Method 4 in [57] (specialized for a single GMPM), or equivalently, Eqs 1-5 in [48] (specialized for the case where all IMs are spectral accelerations).

e) Randomly simulate n response spectra from the target spectrum in Step 3d, using the approach discussed in Section 3.2 of [48] (specialized for the case where all IMs are spectral accelerations).

f) Select n ground motions (from the database developed in Step 3b) whose response spectra most closely agree with those simulated from Step 3e, using the approach discussed in Section 3.3 of [48] (specialized for the case where all IMs are equally weighted spectral accelerations).

g) Confirm that the selected ground motions are consistent with the target spectrum: apply Kolmogorov-Smirnov (KS) tests on the selected motions for spectral acceleration at each of the vibration periods specified in Step 3c. If the selected motions pass the KS tests for all vibration periods, then proceed; otherwise, repeat Steps 3e-3f to reselect another set of n ground motions. If the KS tests cannot be satisfied for all vibration periods after N_{Iter} attempts, then reselect another set of n ground motions by applying the greedy optimization procedure (as described on Pages 800-801 in [1]) to the latest set with the target spectrum from Step 3d (i.e., the target means and standard deviations at each period are given by Eqs 14-15 in [57], specialized for a single GMPM).

4. Repeat the ground motion selection process, as described in Step 3, for all N_{IM^*} levels.

5. Check hazard consistency of all $N_{IM^*} \times n$ ground motions with respect to spectral accelerations at T_1, T_2, T_3, and $2T_1$ of the structure, using Eq 3.16 and following the approach discussed in Section 2 of [87]. If the motions are deemed hazard-inconsistent, then repeat Steps 3-4.

6. Perform RHAs of the structure due to all $N_{IM^*} \times n$ ground motions.

7. Estimate the SDHC using the approach outlined in Section 3.2; when the EDP is a measure of total acceleration (i.e., the acceleration at a specific floor or over all floors), replace the values of the EDP corresponding to collapse by peak ground acceleration (PGA) and apply Eq 3.2 (see also Section 5 in [37]).

Step 3 of the summary above differs from the well known CS method described by Jayaram *et al.* [1] in two ways: (i) the target spectrum (Step 3d), and (ii) the selection process (Steps 3e-3g). In [1], the target spectrum is a multivariate lognormal distribution whereas in this study, the target spectrum is *not* multivariate lognormal (see Fig 5 in [37]).

Consequently, ground motions are selected in [1] by matching the target mean vector and covariance matrix with a greedy optimization technique whereas in this study, ground motions are selected so that they pass the KS tests at all vibration periods (see Fig 4a in [47]). These choices are motivated by the desire to select ground motions that are hazard-consistent with respect to spectral accelerations at T_1, T_2, T_3, and $2T_1$ of the structure while simultaneously avoiding the need to inflate standard deviations [37]; the investigation of the CS method described by Jayaram *et al.* [1], which is less rigorous than CSexact, is left for future research.

5.6 Evaluation of CSexact

Specific implementation of CSexact

The step-by-step summary listed in Section 5.5 represents an implementation of probabilistic seismic demand analysis (PSDA), which is schematically illustrated in Fig 2.1 and elaborated in Section 2.3, where ground motions at each intensity level are selected using Steps 3-5. In this study, the conditioning period, T^*, is defined as the fundamental period of the structure, T_1. In order to minimize the majority of the six sources of error when computing SDHCs, identified by Bradley on page 1430 of [35], $N_{IM^*} = 12$ intensity levels were chosen to discretize the hazard curve for $A(T_1)$, $n = 25$ ground motions are selected at each intensity level, and Eq 2.4 is utilized to estimate the probability distribution of EDP at a given intensity level (i.e., a non-parametric approach); the $N_{IM^*} = 12$ intensity levels correspond to: 50%, 20%, 10%, 5%, 2%, 1%, 0.5%, 0.2%, 0.1%, 0.05%, 0.02%, and 0.01% probability of exceedance in 50 years [1]. Moreover, 95% confidence intervals (CIs) are provided for each PSDA-based estimate of the SDHC using the bootstrap technique [74] with 100 bootstrap samples.

In order to be as faithful as possible to the original intentions behind the CSexact method, the following parameters were chosen for implementation. First, the scale factors for all ground motions are limited by $SF_{max} = 4$ (Step 3b). Second, 25 vibration periods, logarithmically spaced between 0.05 to 10 sec, are chosen to compute the target spectrum. Third, each KS test is conducted at the 10% significance level, and ground motions may be reselected up to $N_{Iter} = 10$ times per intensity level, before resorting to the greedy optimization technique (the greedy technique is treated as a last resort here because given the "exact" CS, the technique matches only the first two statistical moments and not the complete probability distribution). In the author's experience, the greedy technique was primarily needed at the intensity levels corresponding to 0.02% and 0.01% probability of exceedance in 50 years.

[1] The Poisson assumption is used here.

SDF systems

Fig 5.2 examines hazard consistency [2] of the ground motions selected for the SDF system with $T_1 = 1$ sec and $R_y = 1$, with respect to spectral accelerations at four vibration periods: (i) $0.2T_1$, (ii) $0.3T_1$, (iii) T_1, and (iv) $2T_1$. To facilitate comparison between the benchmark hazard curve and that estimated from PSDA, we provide bootstrap CIs to the latter, as discussed in Section 2 of [87]. As expected, the selected motions are hazard-consistent with respect to these four vibration periods because the ground motions were deliberately selected in CSexact to be consistent with the target spectra at all intensity levels of $A(T^*)$, over a period range of 0.05 to 10 sec. However, some discrepancy between the benchmark hazard curve and the PSDA-based estimate can be seen for $A(0.2T_1)$ and $A(0.3T_1)$, at exceedance rates between 10^{-5} and 10^{-6}, despite the fact that the selected motions passed the KS tests for all intensity levels and for these two vibration periods. This discrepancy arises from the fact that the KS test does not examine the 'tail' of the probability distribution of $IM \mid A(T^*)$ (see Eq 3.16 and Section 2 in [87]). Whether or not such discrepancies are important for this particular SDF system remains unclear.

Fig 5.3b presents the peak displacement hazard curve of the SDF system with $T_1 = 1$ sec and $R_y = 1$, subjected to the ground motions depicted in Fig 5.2. As expected, this SDHC is unbiased at exceedance rates greater than 4×10^{-4} (or return periods less than 2475 years) because the system responds linearly (see definition of f_o in Section 5.3), and ground motions are scaled to $A(T_1)$ over a wide range of exceedance rates (Fig 5.2c). However, the SDHC is biased at exceedance rates less than 5×10^{-5}. Since the ground motions are hazard-consistent with respect to $A(T_1)$ and $A(2T_1)$, this bias implies that the vector-valued IM, consisting of $A(T_1)$ and $A(2T_1)$, is insufficient for the peak displacement of this system; i.e., the response depends also on other aspects of the ground motion (see Eq 5.1).

The selection of ground motions, via CSexact, was repeated for eight other SDF systems. In each case, the motions are selected to be consistent with the target spectra at all intensity levels of $A(T_1)$, over a vibration period range of 0.05 to 10 sec. The SDHCs resulting from these motions are presented in Fig 5.3; in total, $9 \times (10^4 + 12 \times 25) = 92,700$ RHAs of SDF systems were performed to generate the results for this figure.

These results demonstrate that, for most cases, the peak displacement hazard curves from CSexact are unbiased, from linear-elastic behavior to collapse. Such good agreement is expected because a wide range of vibration periods are chosen to compute the target spectrum and scale factors are limited to within $SF_{max} = 4$ and 1/4. With 25 vibration periods between 0.05 to 10 sec, the vector of IMs for selecting ground motions, **IM**, contains 25 elements and consequently, it is likely to satisfy Eq 5.1 (since a vector that contains an infinite number of IMs satisfies Eq 5.1). This should be intuitive: as **IM** includes more and more aspects of the time series, the description of the time series through **IM** becomes increasingly complete. Even if such a vector of spectral accelerations is insufficient, the specification of $SF_{max} = 4$ reduces potential hazard inconsistencies with respect to other aspects of the ground motion.

[2] All results in this section are generated from Yamamoto's stochastic model

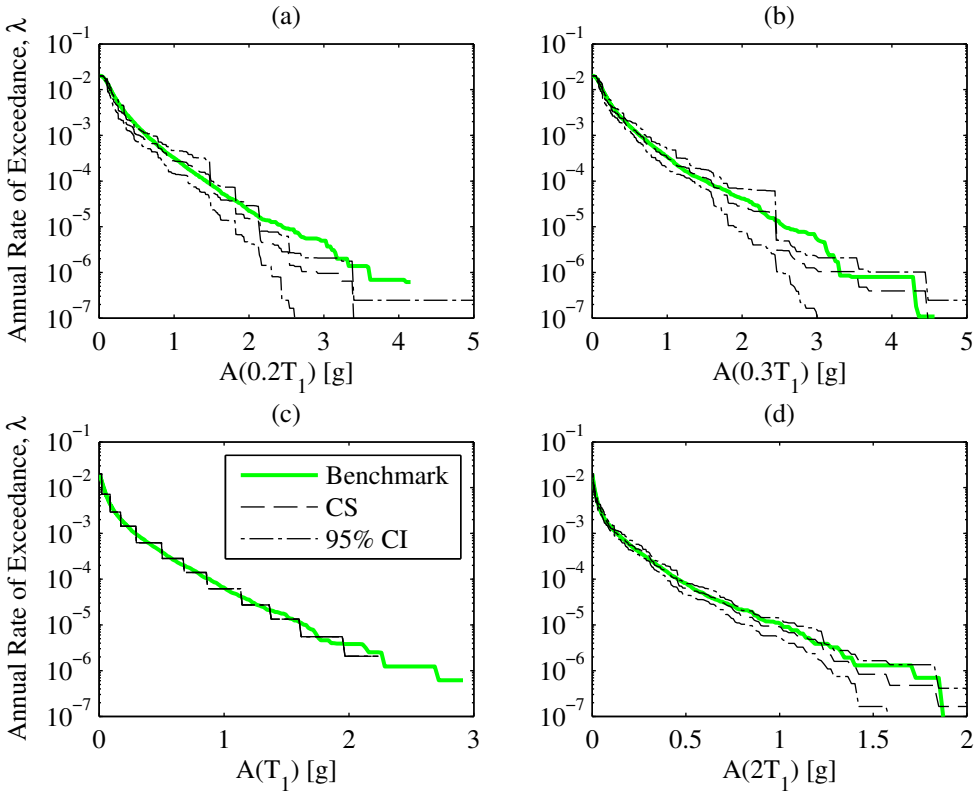

Figure 5.2: Hazard consistency of ground motions, selected by CSexact for the SDF system with $T_1 = 1$ sec and $R_y = 1$, with respect to spectral accelerations at four vibration periods.

Although most SDHCs in Fig 5.3 are unbiased, the estimated annual rates of collapse in Figs 5.3a-b are biased. Compared to other SDF systems in this figure, the collapse rate for these two systems is close to or less than 10^{-5}. The bias in Fig 5.3a at an exceedance rate of about 10^{-6} (not shown) is not very meaningful because even the benchmark contains a high degree of epistemic uncertainty; to draw more definitive conclusions for this case, more than 10^4 ground motions should be generated from the stochastic model. On the other hand, the bias in Fig 5.3b is more meaningful and suggests that the vector-valued IM, consisting of spectral accelerations at 25 vibration periods from 0.05 to 10 sec, is insufficient for this particular case. In summary, whether or not the SDHC estimates from CSexact are biased depends on the particular system because an IM that is insufficient for one case may turn out to be sufficient for another.

To further understand this notion of sufficiency in relation to bias in the SDHC, let us re-examine the selected ground motions that were utilized for Figs 5.3a-c. Fig 5.4 examines the hazard consistency of these ground motions with respect to four IMs: (i) peak ground acceleration (PGA), (ii) peak ground velocity (PGV), (iii) peak ground displacement (PGD), and (iv) 5-75% significant duration, D_{5-75}. Recall that these IMs are not utilized in the

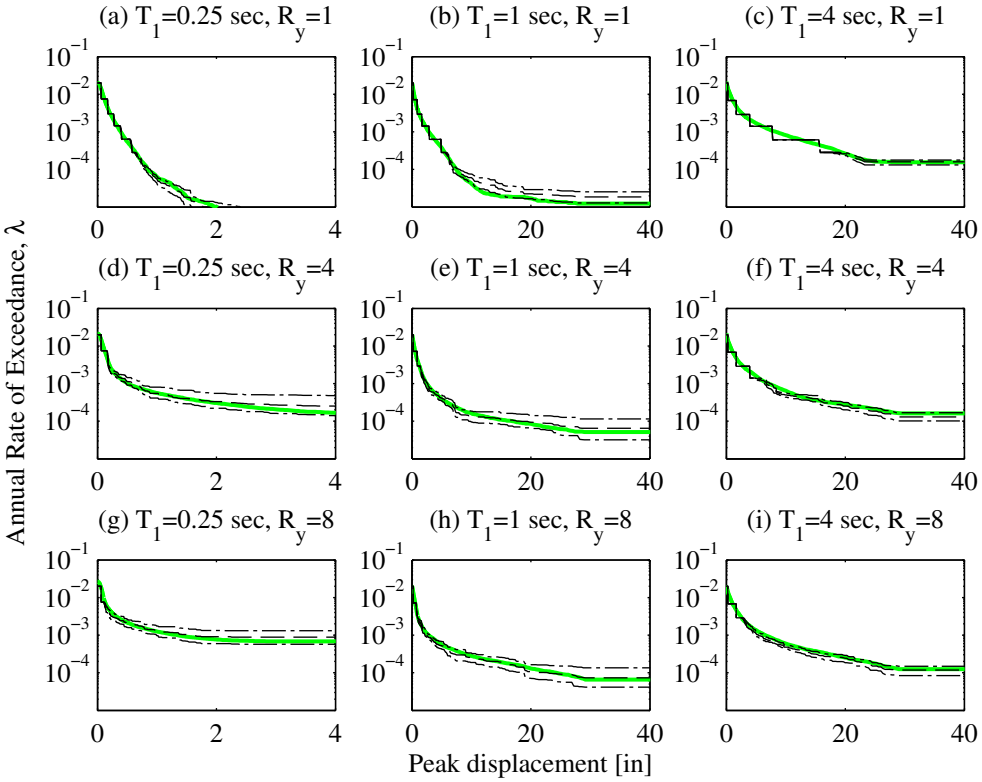

Figure 5.3: Comparison of SDHC estimates for all SDF systems from CSexact (dashed black) against benchmark (solid green).

selection process in CSexact (Section 5.5). Therefore, whether or not the selected motions are hazard-consistent with respect to these IMs is beyond the analyst's control. For example, the selected motions for $T_1 = 1$ sec, $R_y = 1$, are hazard-*inconsistent* with respect to D_{5-75} (Fig 5.4d) but hazard-consistent with respect to PGV (Fig 5.4b). Whether or not hazard inconsistencies, such as those shown in Fig 5.4d, are important to estimating the response, depends on the particular system (and EDP) considered. In this work, D_{5-75} appears to be important for estimating the collapse rate of the system in Fig 5.3b but unimportant for estimating the collapse rate of the system in Fig 5.3c.

4-story frame

Fig 5.5 summarizes the ground motions selected for the 4-story frame, by applying the procedure outlined in Section 5.5 to the universe of synthetic ground motions generated by Yamamoto's stochastic model. As expected, the selected motions are hazard-consistent with respect to spectral accelerations at the first three modal periods and twice the fundamental period of the 4-story frame, because CSexact aims to develop ground motions that are

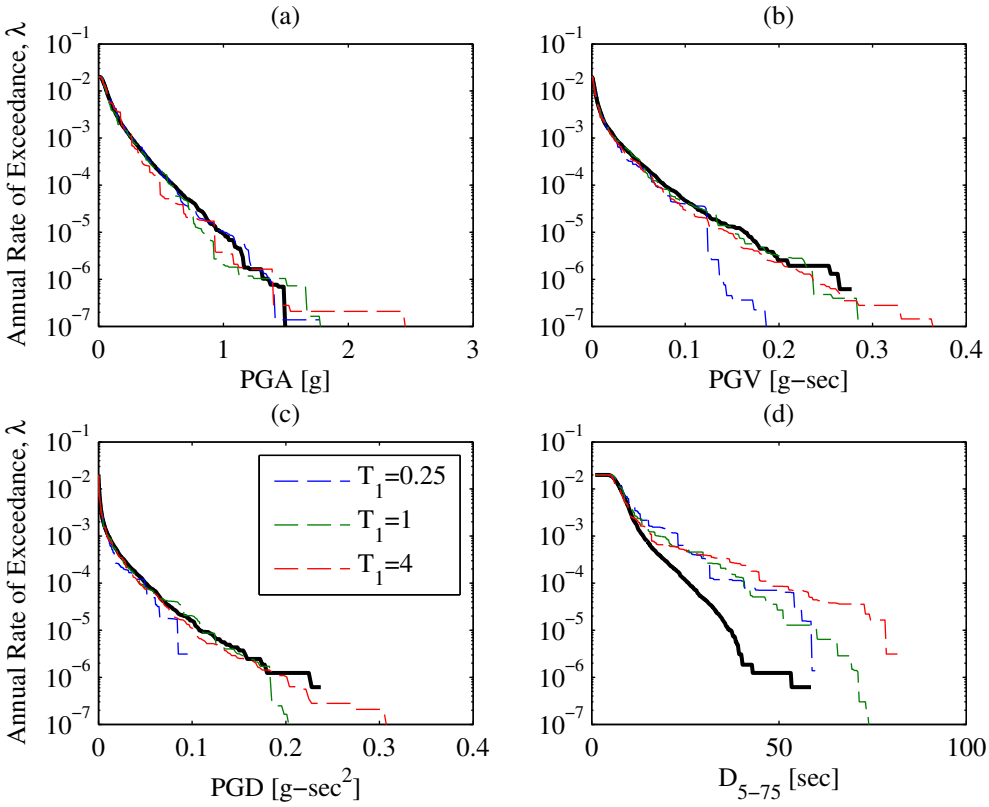

Figure 5.4: Hazard consistency of ground motions, selected by CSexact for three SDF systems with $R_y = 1$, with respect to PGA, PGV, PGD, and D_{5-75}.

consistent with the target spectra at a wide range of vibration periods. However, some discrepancies between the benchmark hazard curve and estimate from CSexact for $A(2T_1)$ at exceedance rates less than 10^{-5}; as discussed in Section 2 of [87], these discrepancies arise from the fact that the selection of ground motions at a particular intensity level (Step 3 in Section 5.5) does not account for the 'tail' of the probability distribution of $IM \mid A(T^*)$.

Fig 5.6 presents the SDHCs of the 4-story frame, resulting from the ground motions summarized in Fig 5.5. The EDPs considered in this figure, a subset of all EDPs examined in this study, include: (i) roof displacement, PFD_4, (ii) first-story drift ratio, $PSDR_1$, (iii) roof acceleration, PFA_4, and (iv) maximum story drift ratio over all stories, $MSDR$. For PFD_4, $PSDR_1$, and $MSDR$, the SDHC estimate from CS is unbiased at exceedance rates greater than about 5×10^{-5} but biased near collapse. For PFA_4, the SDHC estimate from CS is unbiased at exceedance rates greater than about 5×10^{-4} but underestimates the benchmark otherwise. Without the benchmark SDHCs, a concept developed in [64] and in [78], such biases may not have been detected; specifically, it would be difficult to identify such biases by varying conditioning periods as in Figs A.17d and A.17f of [88], where a very similar

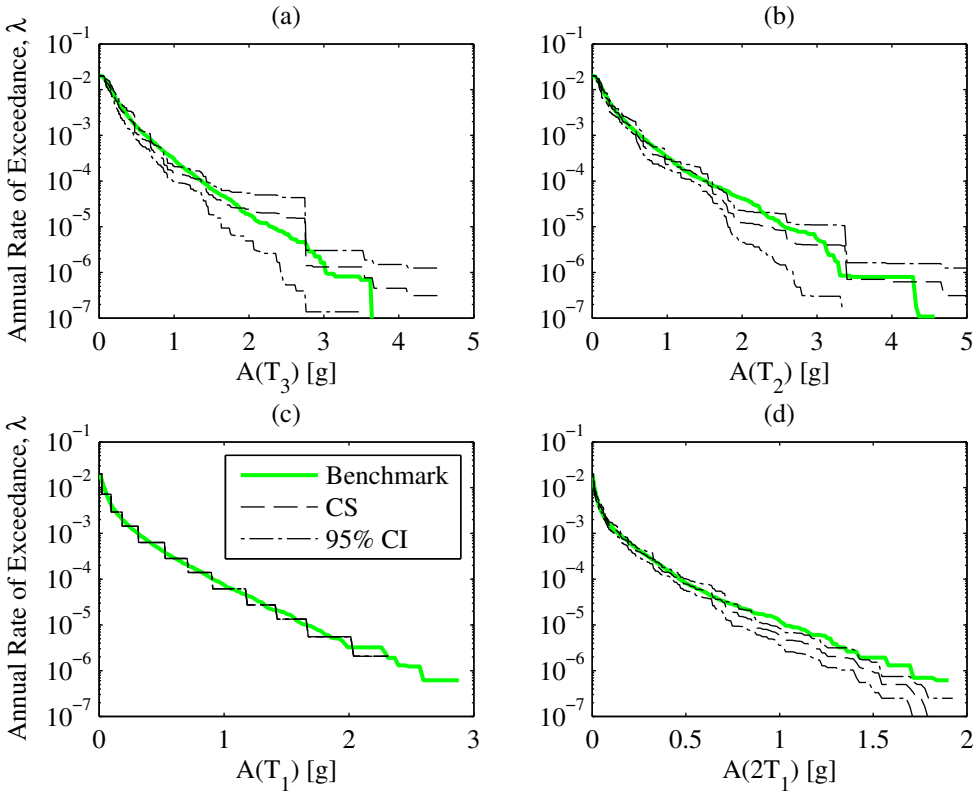

Figure 5.5: Hazard consistency of ground motions, selected by CSexact for the 4-story frame, with respect to spectral accelerations at four vibration periods (Yamamoto's model).

4-story frame was studied. Since the corresponding selected motions are hazard-consistent with respect to spectral accelerations at a wide range of vibration periods (Fig 5.5), the biases observed in Fig 5.6 suggest spectral accelerations, at periods from 0.05 to 10 sec, are insufficient for the response of this 4-story frame at such low exceedance rates.

The selection of $N_{IM^*} \times n = 300$ ground motions via CSexact for the 4-story frame, and computation of benchmark SDHCs (10^4 RHAs), were repeated for Rezaeian's stochastic model. Fig 5.7 confirms that the motions selected under Rezaeian's model are again hazard-consistent with respect to spectral accelerations over a wide range of vibration periods, just like those under Yamamoto's model (Fig 5.5). However, the SDHCs resulting from such motions (Fig 5.8) differ from in Yamamoto's model (Fig 5.6). Specifically, the annual rate of collapse from CSexact is now unbiased. This observation does *not* imply that spectral accelerations, from 0.05 to 10 sec, are *sufficient*. Why? Because one does not have control over the hazard consistency of the selected motions with respect to other IMs.

Figs 5.9 and 5.10 examine hazard consistency of the motions, from Yamamoto's and Rezaeian's models, with respect to four IMs: (i) PGA, (ii) PGV, (iii) PGD, and (iv) D_{5-75}. In both stochastic models, the selected motions are essentially hazard-consistent with respect

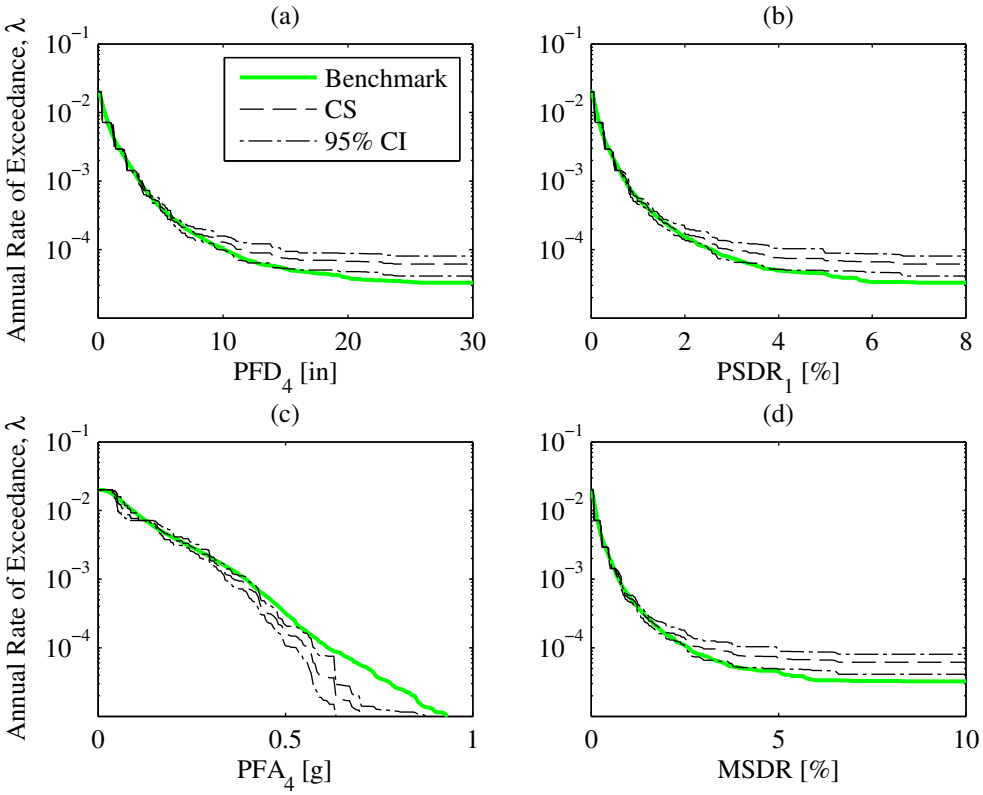

Figure 5.6: Comparison of SDHC estimates for several EDPs of the 4-story frame from CSexact against benchmark (Yamamoto's model).

to PGA, PGV, and PGD, despite the fact that these IMs are not utilized in the selection of ground motions (see Step 3c in Section 5.5). This is the case because in the current implementation of CSexact, the response spectrum from 0.05 to 10 sec, is carefully accounted for in the selection process and at the same time, the three peak ground parameters correlate strongly with the short, moderate, and long period content of the response spectrum. It can be seen from Figs 5.9d and 5.10d that the ground motions from the two stochastic models differ significantly in terms of hazard consistency with respect to D_{5-75}. This occurs because in Rezaeian's model, D_{5-75} happens to be somewhat correlated with PGV ($\rho = -0.34$) whereas in Yamamoto's model, D_{5-75} is weakly correlated with PGV ($\rho = -0.06$). Based on these results and Fig 4.9, D_{5-75} appears to be important for estimating the collapse rate of this 4-story frame. Before leaving this section, it should be noted that the bias observed in the roof acceleration hazard curve (Figs 5.6c and 5.8c) is a surprising finding because the selected motions are hazard-consistent with respect to PGA (Figs 5.9a and 5.10a) and one might expect roof accelerations to be sensitive to the response spectrum at short vibration periods (see e.g., Appendix A.1 of [88]). This finding implies that roof acceleration depends on a feature of the ground motion time series that has not been considered in the analysis

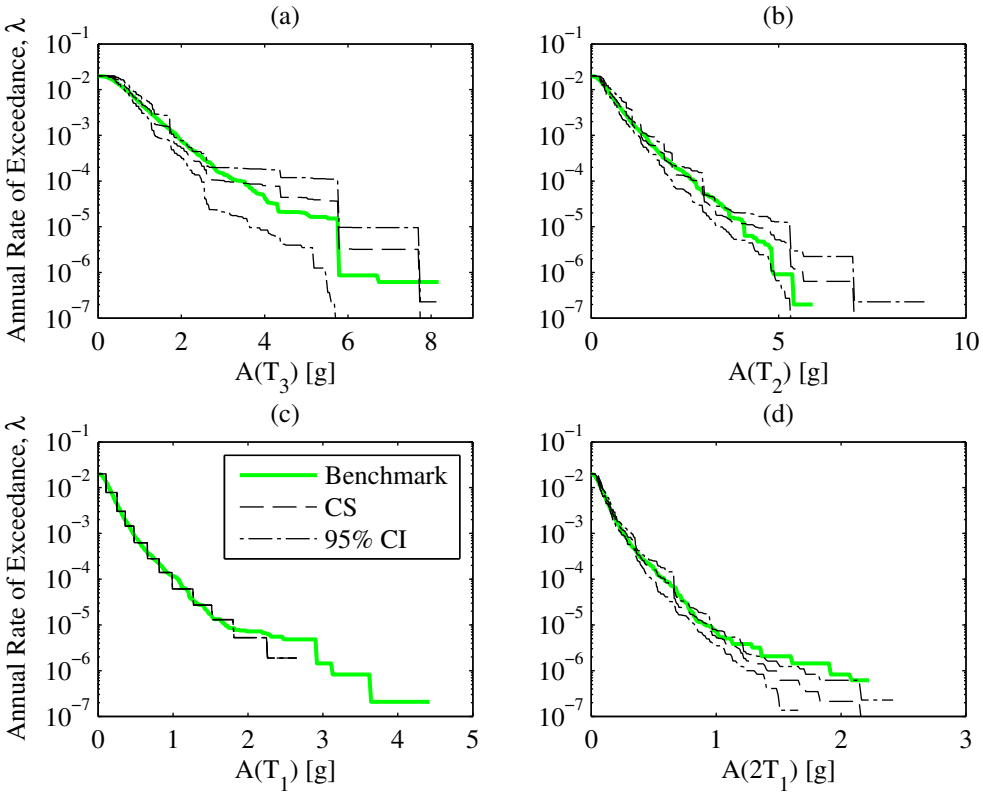

Figure 5.7: Hazard consistency of ground motions, selected by CSexact for the 4-story frame, with respect to spectral accelerations at four vibration periods (Rezaeian's model).

thus far, pointing out the importance of developing a rigorous benchmark when evaluating results from GMSM procedures.

20-story frame

The CSexact procedure (Section 5.5) is also implemented for the 20-story frame (Section 5.3). In each of the two stochastic models, the ground motions are again carefully selected to be hazard-consistent with respect to spectral accelerations at vibration periods between 0.05 to 10 sec (not shown). The SDHCs of the 20-story frame for Yamamoto's model are presented in Fig 5.11 whereas those for Rezaeian's model are presented in Fig 5.12. The four EDPs – (i) roof displacement, PFD_{20}, (ii) first-story drift ratio, $PSDR_1$, (iii) roof acceleration, PFA_{20}, and (iv) maximum story drift ratio over all stories, $MSDR$ – are again chosen to summarize the 62 EDPs considered for this frame (Section 5.3).

Unlike the CSexact-based SDHCs for the 4-story frame (Figs 5.6 and 5.8), the CSexact-based SDHCs for the 20-story frame are less biased for all EDPs. Specifically, (i) the roof acceleration is now unbiased for both stochastic models, and (ii) in Yamamoto's model,

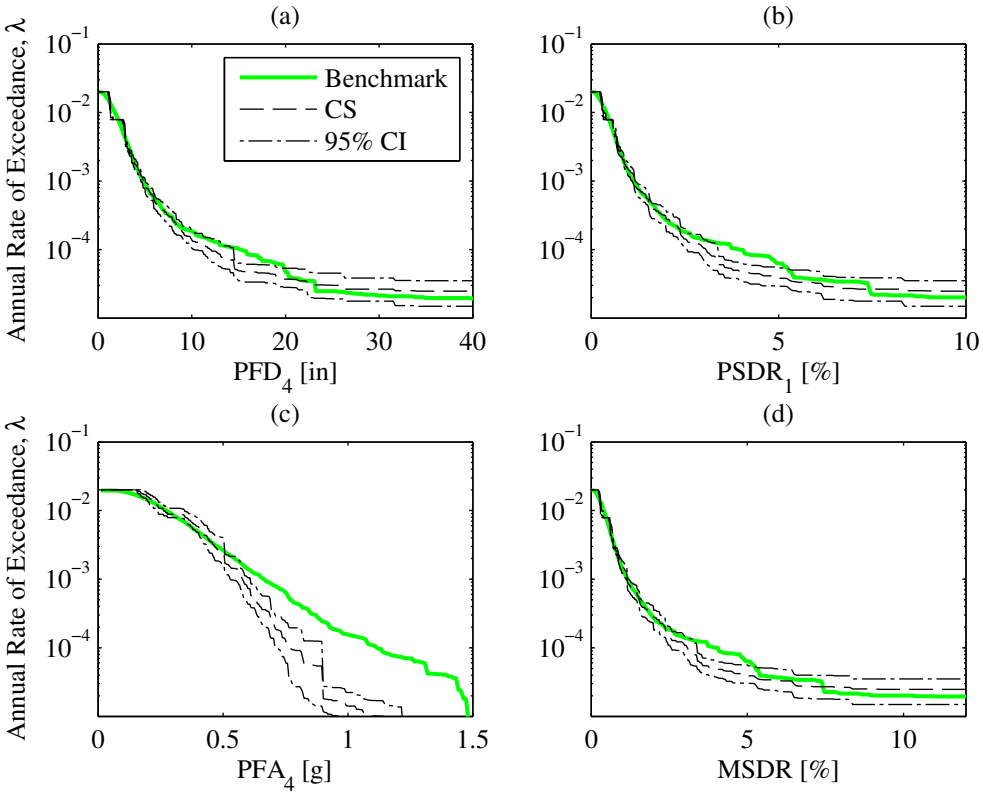

Figure 5.8: Comparison of SDHC estimates for several EDPs of the 4-story frame from CSexact against benchmark (Rezaeian's model).

the overestimation in the collapse rate is smaller than that for the 4-story frame. These differences between the two multistory frames imply that the underlying cause of bias is not directly related to the particular GMSM procedure. Instead, the SDHC bias appears to be directly related to the particular set of ground motions in terms of (i) hazard consistency, and (ii) IM sufficiency [64].

Recall that the selected motions for both frames are hazard-consistent with respect to spectral accelerations over a wide range of vibration periods. Since less bias is observed for the 20-story frame (Figs 5.11-5.12) than for the 4-story frame (Figs 5.6 and 5.8), we conclude that this collection of spectral accelerations appears to be less insufficient for the 20-story frame than for the 4-story frame. Similarly, this collection of spectral accelerations appears to be less insufficient for displacements and drift ratios of the 4-story frame than for floor accelerations (see Figs 5.6 and 5.8). The phrase "less insufficient" is utilized because it is difficult to prove that an IM is sufficient; i.e., the good agreement in SDHCs does *not* imply that an IM is sufficient because hazard consistencies (i.e., good agreement) with respect to other IMs may occur by chance (Fig 5.4). In order to control IMs in addition to spectral accelerations, the GCIM approach was developed, which is studied next.

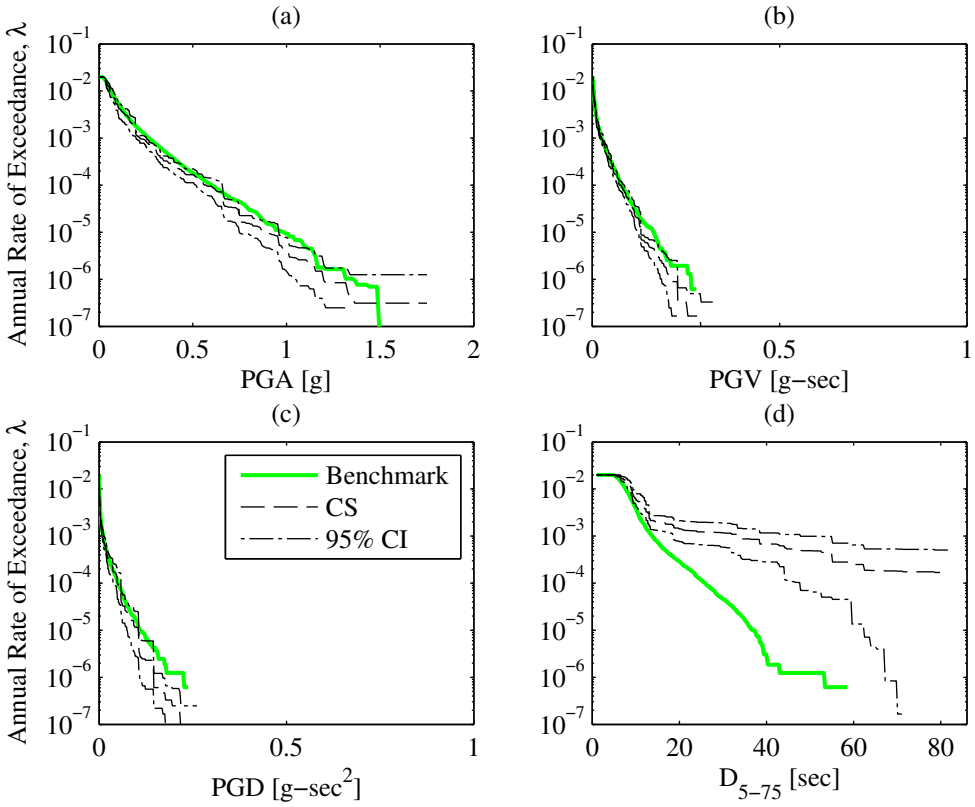

Figure 5.9: Hazard consistency of ground motions, selected by CSexact for the 4-story frame, with respect to four IMs unrelated to spectral accelerations (Yamamoto's model).

5.7 Step-by-step summary of GCIM

The GCIM approach for estimating a SDHC is summarized as follows:

1. Specify a large number of IMs to be potentially utilized for selecting ground motions (e.g., PGD, D_{5-75}, etc.).

2. Specify the conditioning IM, IM^*.

3. Determine the hazard curve for IM^* from PSHA of the site and select N_{IM^*} intensity levels for conducting intensity-based assessments (see Fig 2.1a).

4. For the ith intensity level of IM^*, denoted by x_i, select n ground motions from a master database using the GCIM approach:

   a) Perform deaggregation to determine the percent contribution of each rupture scenario to $IM^* = x_i$ (see Fig 2.3a).

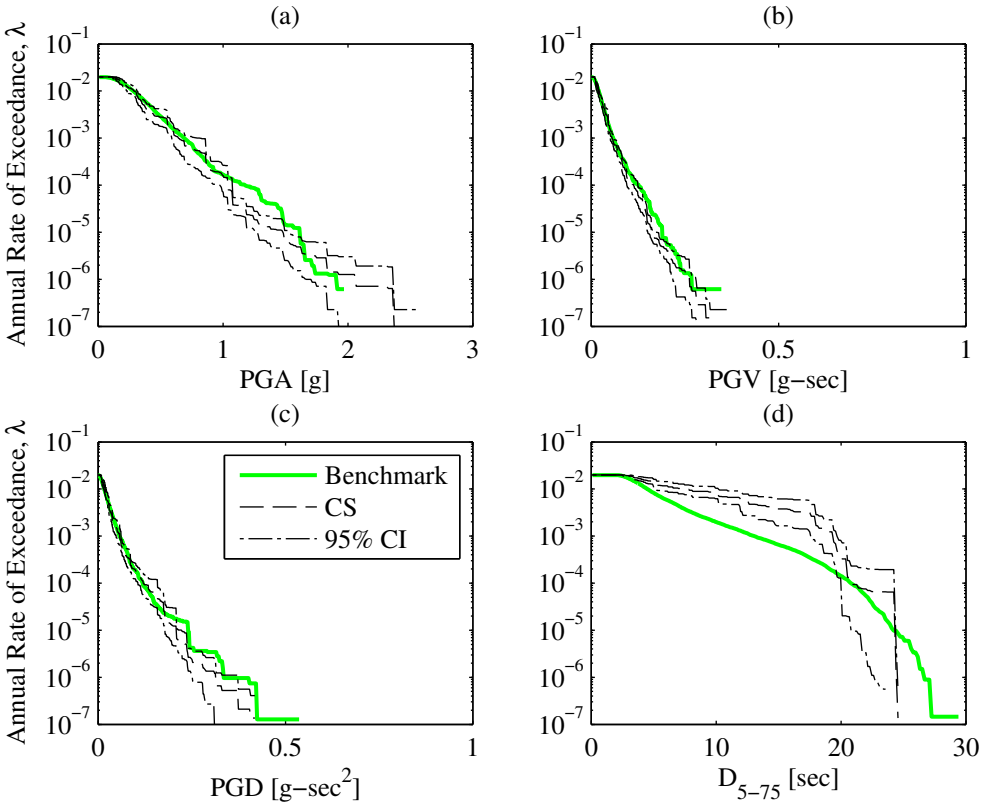

Figure 5.10: Hazard consistency of ground motions, selected by CSexact for the 4-story frame, with respect to four IMs unrelated to spectral accelerations (Rezaeian's model).

b) Scale [3] all ground motions from the master database so that $IM^* = x_i$.

c) Specify a subset of the IMs identified in Step 1, **IM**, to be utilized for ground motion selection using a weight vector as discussed in Section 5.2 of [35].

d) Compute the multivariate GCIM distribution of **IM** | IM^*, using the vector version of Eqs 8-12 in [47].

e) Randomly simulate n vectors of **IM** from the multivariate GCIM distribution in Step 4d, using the approach discussed in Section 3.2 of [48].

f) Select n ground motions (from the database developed in Step 4b) whose computed values of **IM** most closely agree with those simulated from Step 4e, using the approach discussed in Section 3.3 of [48].

g) Confirm that the selected ground motions are consistent with the target from GCIM: apply Kolmogorov-Smirnov (KS) tests on the selected motions for each of

[3] This eliminates IMs that do not change with amplitude scaling as candidates for IM^* (e.g., significant duration).

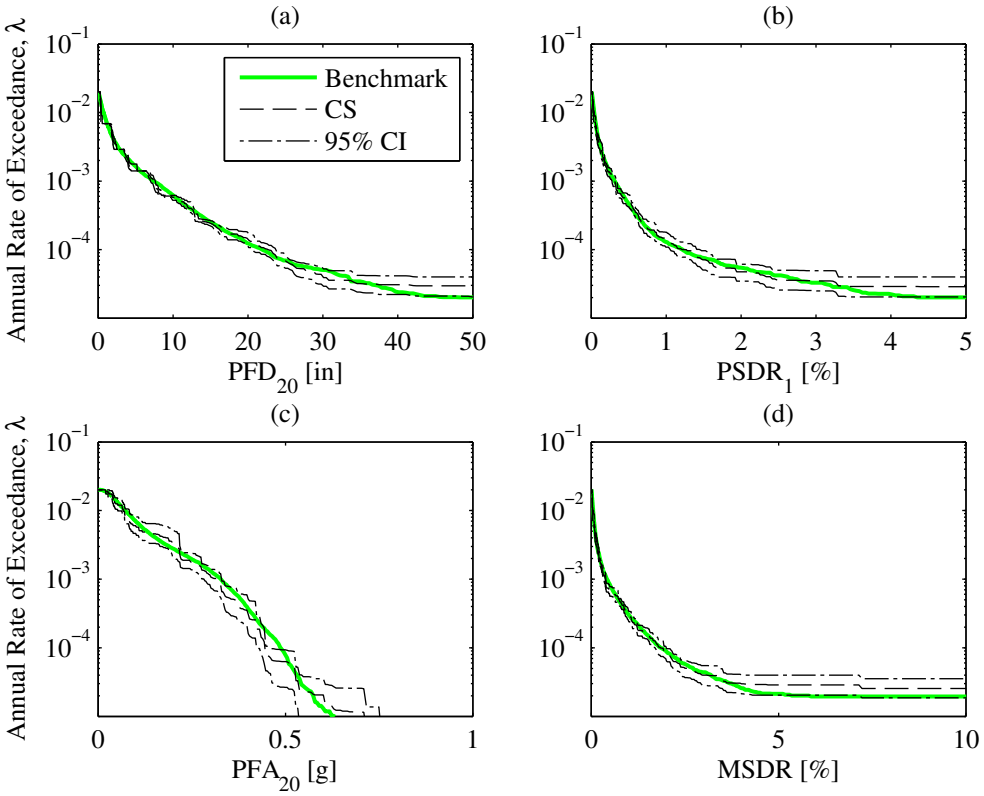

Figure 5.11: Comparison of SDHC estimates for several EDPs of the 20-story frame from CSexact against benchmark (Yamamoto's model).

the IMs specified in Step 4c. If the selected motions pass the KS tests for all IMs, then proceed; otherwise, reselect another set of n ground motions until either the selected motions pass all KS tests or a maximum number of reselections has been reached. For the latter case, both the IMs that failed the KS test and the current intensity level of IM^* are noted before proceeding.

5. Repeat the ground motion selection process, as described in Step 4, for all N_{IM^*} levels.

6. Perform RHAs of the structure due to all $N_{IM^*} \times n$ ground motions.

7. Check for potential biases in EDPs caused by improper ground motion selection noted from Step 4g:

   a) For each of the intensity levels of IM^* where improper ground motion selection was observed:

      i. Specify an EDP (e.g., floor displacement, story drift ratio, etc.) for checking.

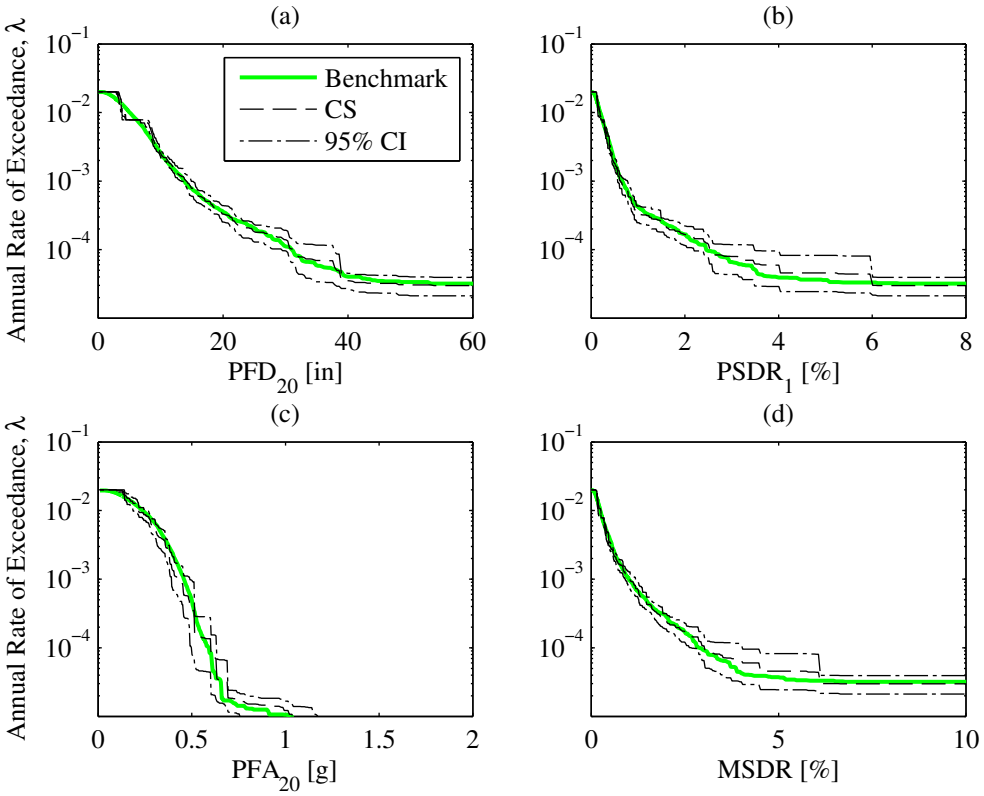

Figure 5.12: Comparison of SDHC estimates for several EDPs of the 20-story frame from CSexact against benchmark (Rezaeian's model).

ii. Check whether or not the troublesome IMs noted in Step 4g are important for the current EDP considered by applying the approach shown schematically in Fig 7a of [47].

iii. If the IM is indeed important to the current EDP considered, then estimate the potential bias in the EDP due to the particular IM, following the approach outlined on pages 1337-1340 of [47].

iv. Repeat Steps 7(a)ii-7(a)iii for all EDPs in order to determine whether or not a new set of n ground motions should be reselected at this particular intensity level and with what new weight vector for selection (see Step 4c). If ground motions are indeed reselected at this particular intensity level, then perform RHAs of the structure subjected to the new motions.

8. Estimate the SDHC using the approach outlined in Section 3.2; when the EDP is a measure of total acceleration (i.e., the acceleration at a specific floor or over all floors), replace the values of the EDP corresponding to collapse by PGA and apply Eq 3.2 (see also Section 5 in [37]).

The GCIM approach summarized above differs from the CSexact approach (Section 5.5) in two major aspects: (i) any IM (not just spectral acceleration) can be considered for selecting ground motions (Step 4c), and (ii) any potential biases in the EDP due to improper ground motion selection can be examined relatively quickly (Step 7). Note that unlike CSexact (Step 3b), scale factors are not limited in GCIM because GCIM aims to capture many more IMs than in CSexact when selecting ground motions. Hence, this approach is holistic but can be quite involved. For example, the bias-checking procedure (Step 7) requires RHAs of the structure to be performed first, before scattergrams of EDP vs IM can be developed (see e.g., Fig 7a of [47], Fig 3 of [87]). In addition, as the number of EDPs of interest increases (e.g., 62 EDPs are considered herein for the 20-story frame), the number of checks and ground motion re-selections (Step 7) can become onerous.

5.8 Evaluation of GCIM

Specific implementation of GCIM

As in CSexact, the step-by-step summary listed in Section 5.7 represents an implementation of PSDA, which is schematically illustrated in Fig 2.1 and elaborated in Section 2.3, where ground motions at each intensity level are selected using the GCIM approach. In this study, the conditioning IM, IM^*, is defined as spectral acceleration at the fundamental period of the structure, $A(T_1)$. In order to minimize error in computing SDHCs and facilitate understanding of results relative to CSexact, the same parameters for PSDA that were mentioned in Section 5.6 are employed here to compute SDHCs from GCIM (i.e., choices for N_{IM^*}, n, etc.).

In order to be as faithful as possible to the original intentions behind the GCIM method, the following parameters were chosen for implementation. First, 24 IMs are considered for selecting ground motions: PGA, PGV, PGD, acceleration spectrum intensity (ASI), spectrum intensity (SI), displacement spectrum intensity (DSI), cumulative absolute velocity (CAV), 5-95% significant duration (D_{5-95}), 5-75% significant duration (D_{5-75}), and 5%-damped spectral accelerations at 15 vibration periods: 0.05, 0.1, 0.2, 0.25, 0.3, 0.5, 0.75, 0.95, 1, 2, 2.6, 3, 4, 5, and 10 sec. Second, following the implementation by the author of GCIM [35], weights for each IM are assigned by giving 85% to amplitude-based IMs and 15% to the cumulative-based IMs (see Table I in [35]). Third, all KS tests (and t-tests from Step 7(a)ii) are conducted at the 10% significance level, and ground motions may be reselected up to $N_{Iter} = 10$ times per intensity level, before proceeding with RHAs and resorting to the bias-checking procedure. In the author's experience, the bias-checking procedure was primarily needed at large intensity levels (i.e., those corresponding to 0.02% and 0.01% probability of exceedance in 50 years). More details on the bias-checking procedure will come when we present results for the 4-story frame from GCIM.

SDF systems

The GCIM approach, as outlined in Section 5.7, was implemented for all nine SDF systems, using Yamamoto's stochastic model. Fig 5.13 examines hazard consistency of the ground motions selected for the three SDF systems with $R_y = 1$; specifically, with respect to PGA, PGV, PGD, and D_{5-75}. Unlike the ground motions selected from CSexact for the same systems (Fig 5.4), those selected from GCIM are hazard-consistent for all of these IMs because they were explicitly "matched" (i.e., between the empirical and target GCIM distributions) in the selection process (Step 4c). However, some discrepancy between the benchmark hazard curve and the PSDA-based estimate can be seen for the curve corresponding to $T_1 = 0.25$ sec in Fig 5.13c, at exceedance rates less than 10^{-4}, despite the fact that the selected motions passed the KS tests for PGD at all $N_{IM^*} = 12$ intensity levels. As mentioned earlier, this discrepancy arises from the fact that the KS test does not examine the 'tail' of the probability distribution of $IM \mid A(T^*)$ (see Section 2 in [87]). As a side note, such inconsistencies can be minimized by directly focusing on this range of exceedance rates with an Importance Function in the Importance Sampling procedure (Section 4.4).

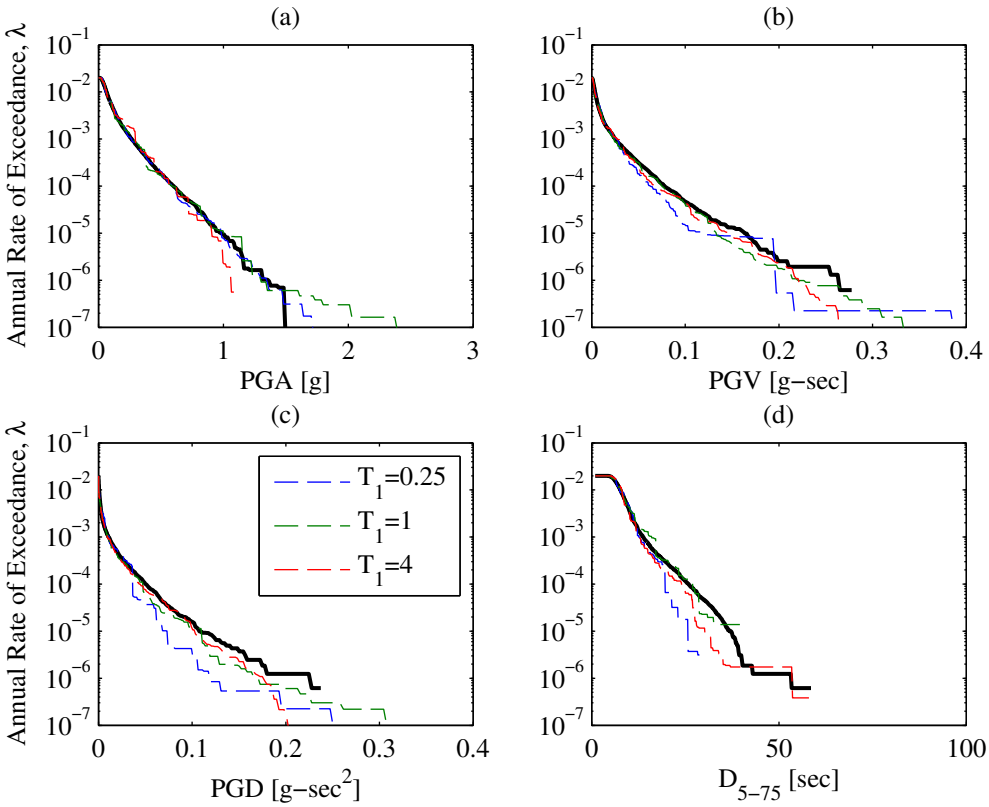

Figure 5.13: Hazard consistency of ground motions, selected by GCIM for three SDF systems with $R_y = 1$, with respect to PGA, PGV, PGD, and D_{5-75}.

Fig 5.14 presents the SDHCs of all SDF systems, resulting from ground motions selected by the GCIM method. The SDHCs from GCIM are essentially unbiased for all SDF systems, from linear-elastic behavior to collapse. This is to be expected since the GCIM approach considered several *more* IMs in addition to 5%-damped spectral accelerations, and good agreement was already observed for many cases in CSexact (Fig 5.3), where only spectral accelerations were employed for ground motion selection. Furthermore, the unbiased collapse rate in Fig 5.14b suggests that D_{5-75} is important for estimating the collapse rate of this particular SDF system; strictly speaking, the response spectrum from 0.05 to 10 sec is insufficient for the response of this system at such low exceedance rates (Fig 5.3b).

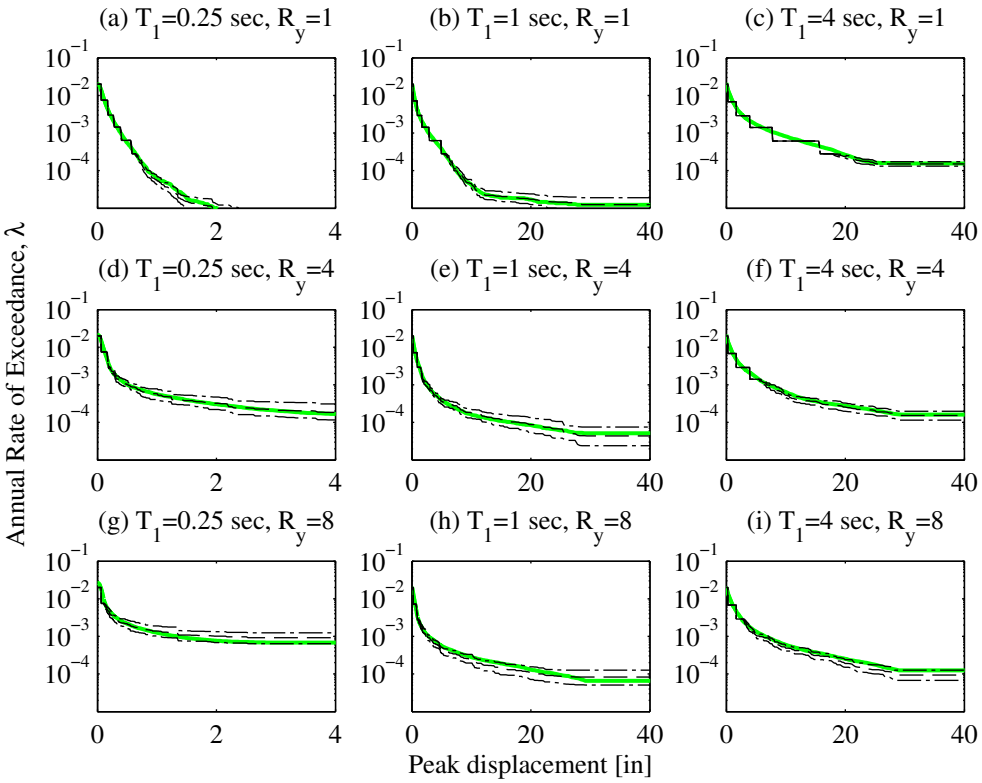

Figure 5.14: Comparison of SDHC estimates for all SDF systems from GCIM (dashed black) against benchmark (solid green).

4-story frame

The GCIM method was implemented for the 4-story frame and for both stochastic models. Fig 5.15 examines hazard consistency of the ground motions from Yamamoto's model, with respect to PGA, PGV, PGD, and D_{5-75}. As expected, the motions are essentially hazard-consistent with respect to these four IMs, because they were iteratively selected so that they

satisfy the KS tests for these IMs (and others) at all intensity levels of $A(T^*)$ (Step 4g in Section 5.7). Limiting the number of ground motion re-selections at each intensity level to $N_{Iter} = 10$, the selected motions passed all KS tests except for the largest intensity level of $A(T^*)$. As a result, the bias-checking procedure (Step 7) was implemented for this intensity level (implying that RHAs of the 4-story frame were conducted) and ground motions are reselected until whatever remaining KS test failures are demonstrated to be unimportant for all EDPs of the 4-story frame (Step 7(a)ii). This process will be described more fully in Section 5.8, but for now, it suffices to recognize that the ground motions summarized in Fig 5.15 actually correspond to the new selection of motions after RHAs of the frame was already performed for the largest intensity level of $A(T^*)$.

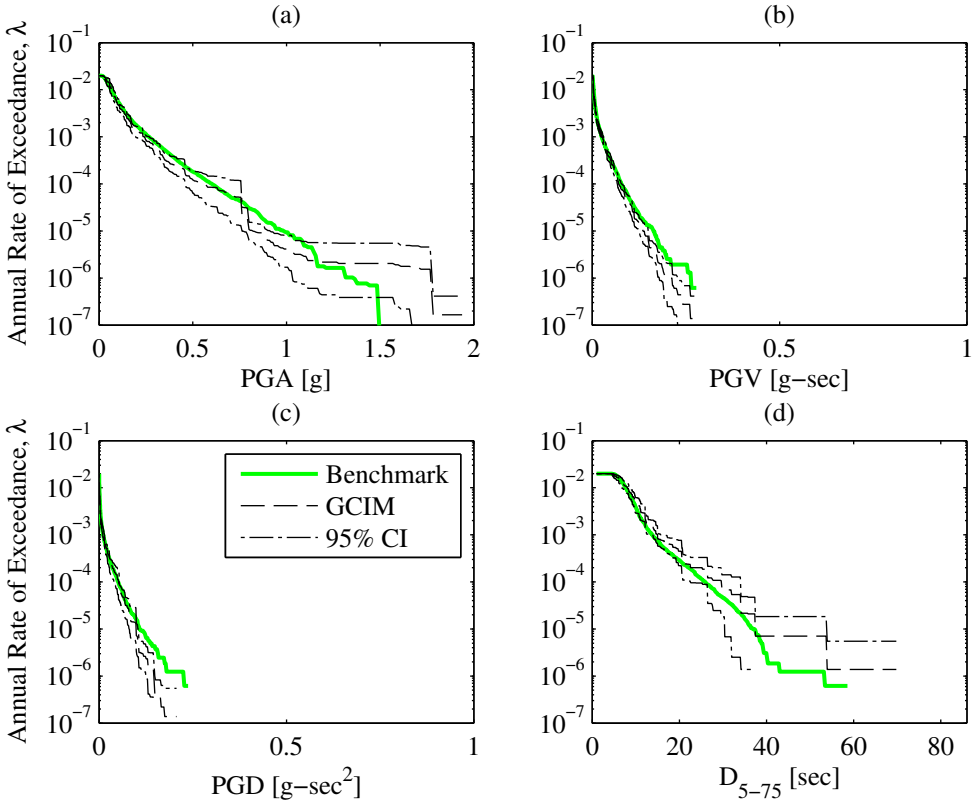

Figure 5.15: Hazard consistency of ground motions, selected by GCIM for the 4-story frame, with respect to four IMs unrelated to spectral accelerations (Yamamoto's model).

The SDHCs of the 4-story frame resulting from the preceding ground motions are presented in Fig 5.16. This figure demonstrates that the SDHCs from GCIM are unbiased for many of the EDPs, from linear-elastic behavior to collapse. However, the SDHCs from GCIM are biased for some of the floor accelerations, including roof acceleration as shown in Fig 5.16c. Since GCIM accounts for cumulative effects of the ground motion (e.g., CAV,

D_{5-75}, etc.) in addition to spectral accelerations over a wide range of vibration periods, the good agreement near the annual rate of collapse suggests that such cumulative effects are important for estimating the collapse rate of this structure (compare Fig 5.16a against Fig 5.6a). However, even the inclusion of such cumulative effects does not improve the estimate of the roof acceleration hazard curve, as demonstrated by comparing Fig 5.16c against Fig 5.6c. This bias in floor accelerations indicates that there is no guarantee that the resulting SDHC estimates from GCIM are unbiased, even after enforcing hazard consistency of the selected motions with respect to a very broad range of IMs (i.e., spectral accelerations, spectrum intensities, significant duration, etc.).

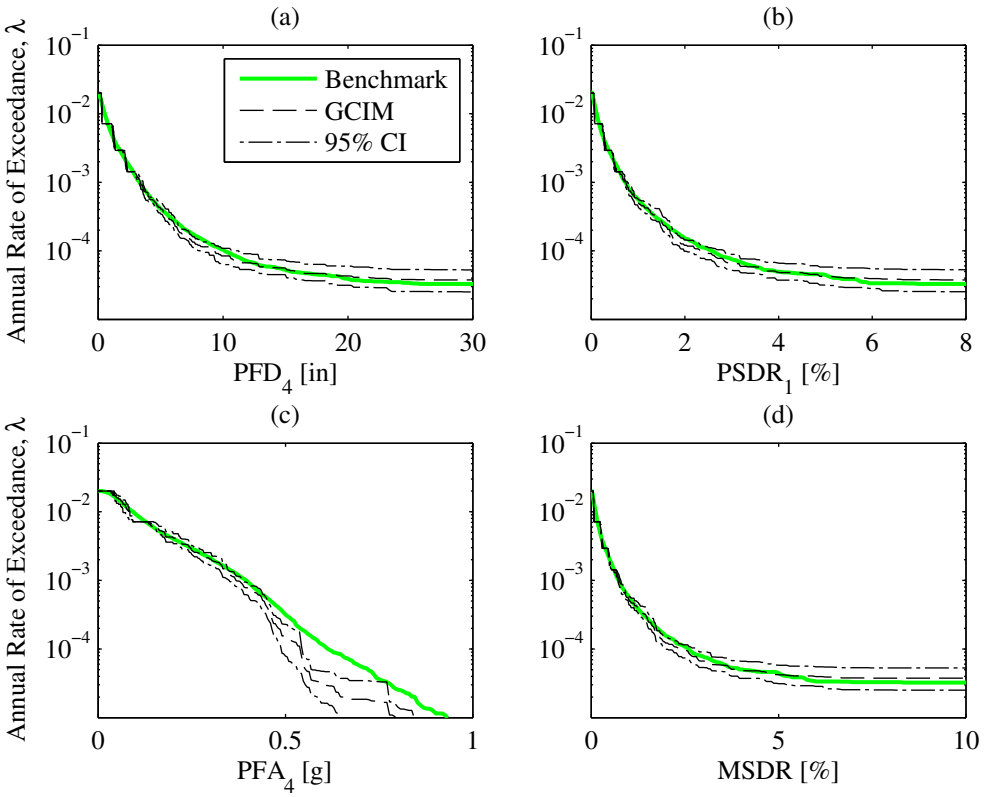

Figure 5.16: Comparison of SDHC estimates for several EDPs of the 4-story frame from GCIM against benchmark (Yamamoto's model).

The GCIM procedure was also applied to the 4-story frame using the stochastic model from Rezaeian; i.e., $25 \times 12 = 300$ RHAs of the frame was conducted in addition to those done for the results shown in Fig 5.16. As in the case for Yamamoto's model, ground motions were again iteratively selected until all inconsistencies from KS tests are demonstrated to be statistically insignificant for all EDPs considered. As verified in Fig 5.17, these ground motions are essentially hazard-consistent with respect to PGA, PGV, PGD, and D_{5-75}.

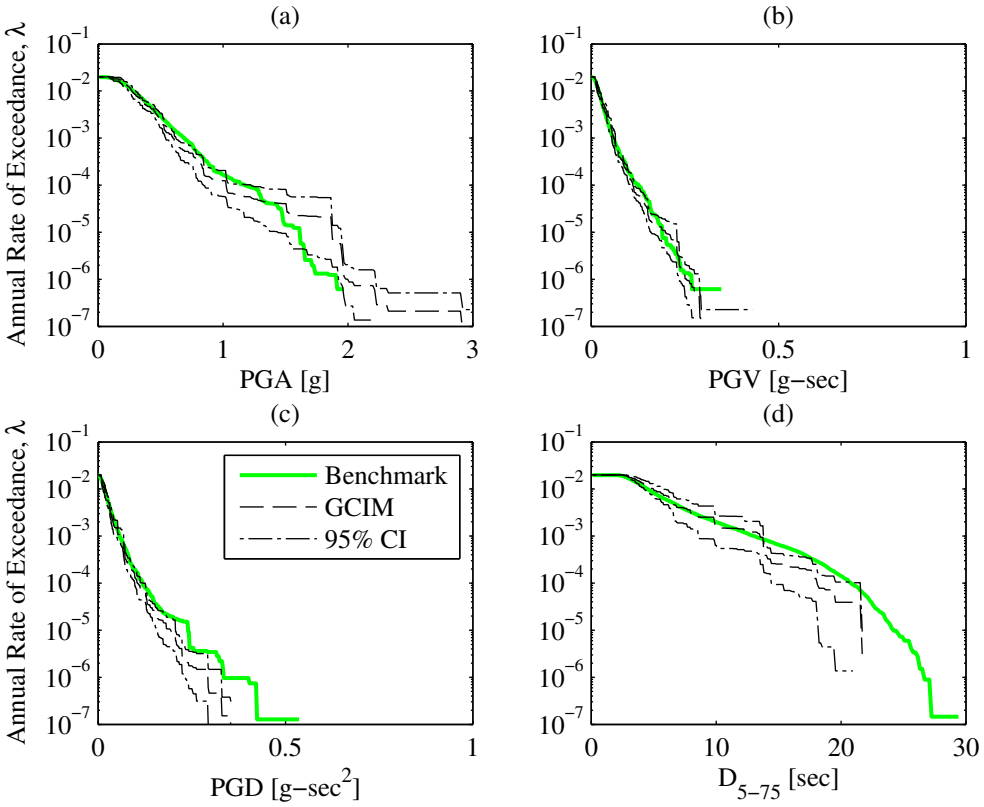

Figure 5.17: Hazard consistency of ground motions, selected by GCIM for the 4-story frame, with respect to four IMs unrelated to spectral accelerations (Rezaeian's model).

The SDHCs of the 4-story frame, subjected to the preceding ground motions from Rezaeian's model, are presented in Fig 5.18. As in the case of Yamamoto's model, the SDHCs from GCIM are again unbiased for the majority of EDPs considered (i.e., floor displacements, story drift ratios, etc.) but biased for roof acceleration. The larger underestimation in Fig 5.18c, relative to that in Fig 5.16c, arises from differences in correlation of IMs between the two stochastic models. Because ground motions were carefully selected to be hazard-consistent with respect to a collection of 24 IMs (see Section 5.8) in both stochastic models, the biases in Figs 5.18c and 5.16c reveal that such a collection of IMs is *insufficient with respect to roof acceleration*. In other words, this EDP depends on a feature of the ground motion time series that has not been considered thus far in the analysis.

The bias-checking procedure in GCIM

Would the biases in roof acceleration have been detected by implementing the bias-checking procedure in GCIM (Step 7 in Section 5.7)? In order to answer this question, let us revisit the selection of ground motions for the 4-story frame under the stochastic model by Rezaeian.

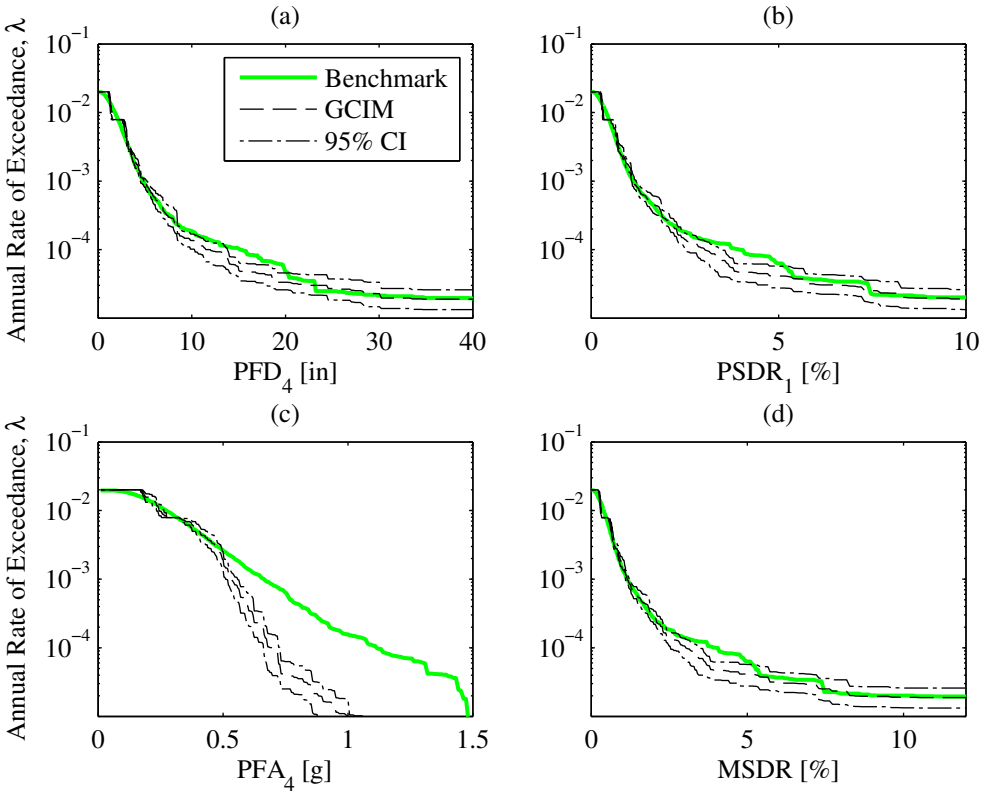

Figure 5.18: Comparison of SDHC estimates for several EDPs of the 4-story frame from GCIM against benchmark (Rezaeian's model).

Specifically, let us carefully examine how ground motions were selected (Step 4g) and how the bias-checking procedure (Step 7) was implemented for this case.

Fig 5.19a presents an example of applying the KS test to a selection of ground motions at an intensity level of $A(T^*)$, with respect to a particular choice of IM. The empirical CDF of the IM from the selected motions is shown in dashed black and the target GCIM probability distribution for this IM is shown in solid green. The KS test indicates whether or not the difference between the two CDFs – empirical and GCIM – is statistically significant. At the 10% significance level, both the KS bounds (chained green) and p-value in Fig 5.19a indicate that the selected motions are *inconsistent* with respect to spectral acceleration at 0.1 sec, because the empirical CDF falls outside of the KS bounds and the p-value is smaller than a probability of 0.10 (i.e., the significance level). Such an inconsistency prompted several more reselections of ground motions (via Steps 4e-4f of Section 5.7), until the selected motions pass the KS tests for all 24 IMs; an example of passing the KS test with respect to an IM is portrayed in Fig 5.19b.

If one is unable to pass the KS tests for all 24 IMs after $N_{Iter} = 10$ ground motion reselections, as was the case for the intensity level of $A(T^*)$ corresponding to 0.02% probability

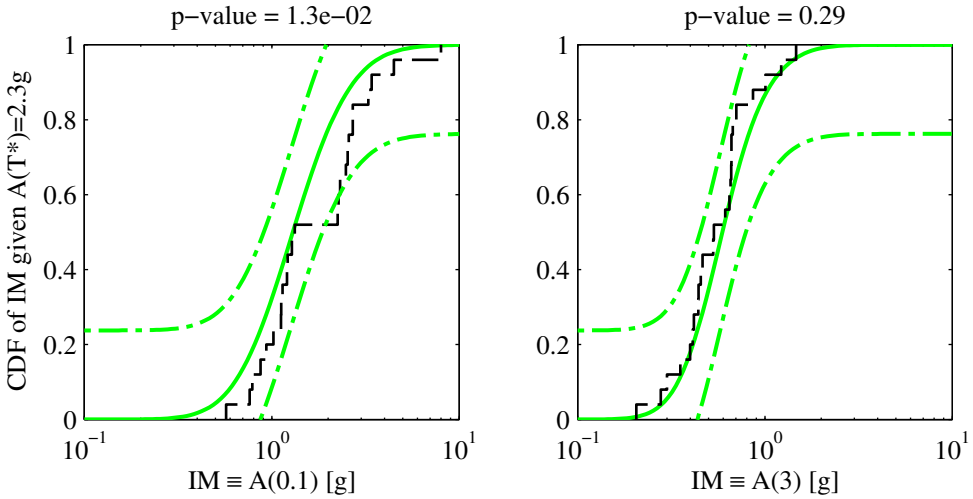

Figure 5.19: Results from applying KS tests (GCIM target in solid green, 10% KS bounds in chained green, and empirical CDF in dashed black) to ground motions selected for $A(T^*)$ at 0.02% probability of exceedance in 50 years: (a) $IM \equiv A(0.1)$; and (b) $IM \equiv A(3)$ (Rezaeian's model).

of exceedance in 50 years, then the next step is to examine the potential significance of such inconsistencies relative to an EDP of interest. This is done in GCIM by (i) creating a scattergram of the EDP vs the IM in log-log space, (ii) determining the regression line, and (iii) applying the t-test to determine whether or not the slope of the regression line is statistically significant (Step 7(a)ii). For example, the potential significance of the inconsistency shown in Fig 5.19a, relative to roof acceleration of the 4-story frame, is examined in Fig 5.20a. In this figure, only 8 out of the $n = 25$ RHA results are shown (blue circles) because the rest of the ground motions led to collapse. From this subset of the RHA results, the regression line is determined (solid red) and its slope is tested for statistical significance via the t-test. Because the p-value from the t-test (shown in title of Fig 5.20a) is less than the significance level, the inconsistency of the selected motions with respect to $A(0.1)$ is deemed to be statistically significant for PFA_4 and hence the potential bias in PFA_4 due to $A(0.1)$ should be estimated next in order to decide whether or not ground motions should be reselected. If the slope had turned out to be statistically insignificant, which suggests that PFA_4 is not sensitive to $A(0.1)$, then the inconsistency in Fig 5.19a would have been deemed unimportant and hence reselection of ground motions would not be necessary.

Before proceeding with the rest of the bias-checking procedure in GCIM, we make several important observations about the procedure as presented thus far. First, RHAs of the 4-story frame must be performed before the scattergram in Fig 5.20a can be constructed. Second, the treatment of collapses in the bias-checking procedure is unclear. One option to proceed with is to exclude the collapses, as shown in Fig 5.20a; however, this can lead to questionable

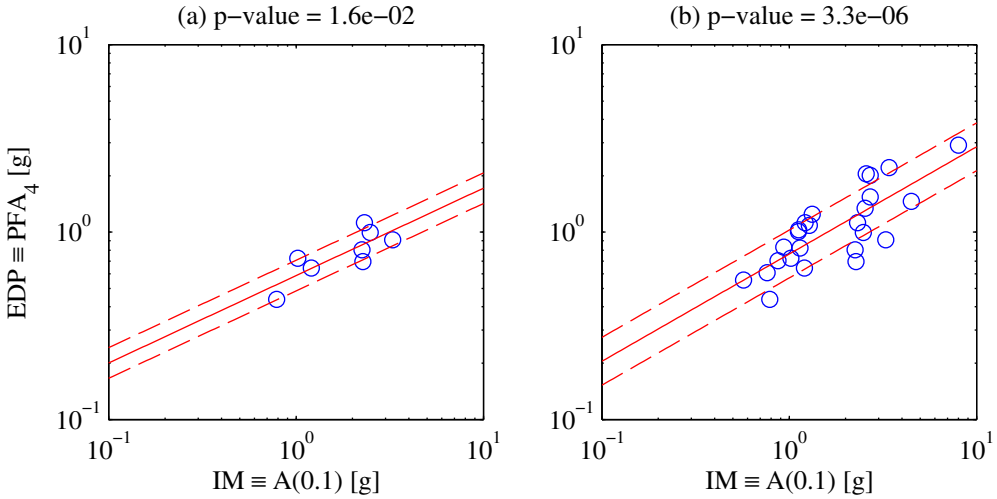

Figure 5.20: Output from applying t-tests (regression line in solid red and 68% CI of $\ln(EDP) \mid \ln(IM)$ in dashed red) to results from RHAs of the frame due to ground motions selected for $A(T^*)$ at 0.02% probability of exceedance in 50 years: (a) collapses excluded; and (b) collapses included (Rezaeian's model).

results as the number of collapses approaches the total number of ground motions selected for the particular intensity level, n (i.e., in the limit, no data would be available to construct the scattergram). Another option is to include the collapses, as shown in Fig 5.20b; however, this may also lead to questionable results because one is utilizing the numerical values of EDP corresponding to collapse. Third, the application of t-tests can become cumbersome as the number of EDPs considered increases (e.g., 14 EDPs are considered for the 4-story frame and 62 EDPs are considered for the 20-story frame) and as the number of IM consistencies increases (e.g., Fig 5.19a); therefore, it is advantageous to minimize the number of such inconsistencies from KS tests.

By reselecting ground motions at each intensity level up to $N_{Iter} = 10$ times, the selected motions for the 4-story frame with Rezaeian's model passed the majority of the KS tests. This is demonstrated in Fig 5.21a, where only three out of the $N_{IM^*} \times 24 = 288$ KS tests led to inconsistencies (shown in magenta); these three IMs, denoted by numbers 2, 4, and 6, correspond respectively to spectral accelerations at vibration periods 0.1, 0.25, and 0.5 sec. Among these three cases, only those corresponding to 0.02% probability of exceedance in 50 years led to statistically significant slopes from regression analyses for roof acceleration, as illustrated in Fig 5.21b. Therefore, 0.02% probability of exceedance in 50 years is the only intensity level in which ground motion reselection might be necessary; i.e., the selected motions for all other intensity levels is finalized at this point.

In order to determine whether or not ground motion reselection is necessary for the intensity level at 0.02% probability of exceedance in 50 years, the potential biases in PFA_4 caused

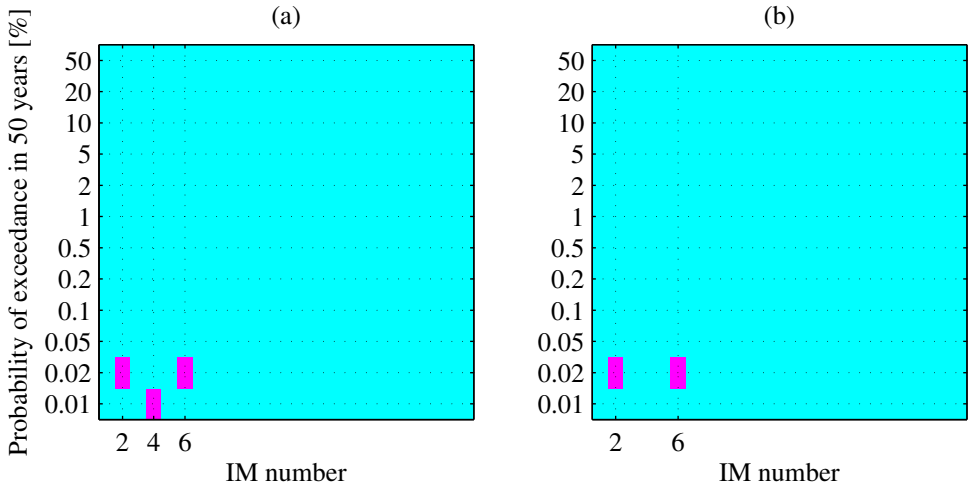

Figure 5.21: (a) Summary of results from KS tests for all 24 IMs employed in GCIM (magenta indicates inconsistency with respect to GCIM distribution), at all intensity levels of $A(T^*)$; (b) cases where IM is both inconsistent and influential to PFA_4, as measured by t-tests (magenta indicates slope from linear regression is statistically significant and IM is inconsistent). Results for Rezaeian's model.

by $A(0.1)$ or by $A(0.5)$ (Fig 5.21b) were estimated (Step 7(a)iii in Section 5.7). Fig 5.22a presents the potential bias in PFA_4 due to $A(0.1)$, as indicated by the discrepancy between the "uncorrected" (dashed black) and "corrected" (chained red) CDFs of roof acceleration, given $A(T^*) = 2.3$g. The "uncorrected" CDF was obtained by fitting a lognormal distribution (see Eq 2.3) to the values of EDP where collapse did not occur (solid grey); on the other hand, the "corrected" CDF was obtained by implementing Eq 17 in [47].

It is up to the analyst to decide whether or not such EDP biases are acceptable. In this study, we adopt an approach that is inspired by the KS tests shown in Fig 5.19. Specifically, the difference between the empirical CDF (solid grey) and the "corrected" CDF (chained red) was quantified by the KS test. Since the "corrected" CDF fell within the 10% KS bounds (Fig 5.22a), the bias in PFA_4 due to $A(0.1)$ was deemed acceptable and hence ground motions were not reselected. Because the treatment of collapse is unclear in the context of the bias-checking procedure, the bias in PFA_4 due to $A(0.1)$ was re-estimated without excluding collapses; as shown in Fig 5.22b, the estimated bias was again deemed acceptable. Note that the potential biases due to $A(0.5)$ were also estimated; however, these biases are not shown because they are even smaller than those presented in Fig 5.22.

Because the estimated biases in roof acceleration were deemed acceptable, the selected motions that were used to generate Fig 5.21 were also utilized to compute the SDHCs of the 4-story frame that are shown in Fig 5.18. Therefore, the preceding detailed illustration of the bias-checking procedure answers the question posed at the beginning of this section: *the biases in roof acceleration would not have been detected by implementing the bias-checking*

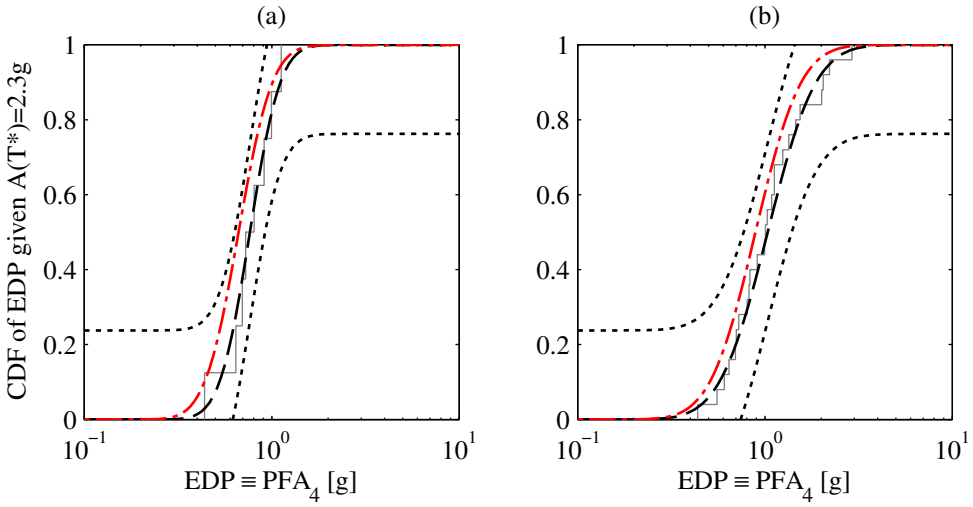

Figure 5.22: Estimates of bias in PFA_4 due to $IM \equiv A(0.1)$ from GCIM (empirical CDF in solid grey, lognormal estimate in dashed black, "corrected from $IM \equiv A(0.1)$" in chained red, and 10% KS "bounds" in dotted black) for $A(T^*)$ at 0.02% probability of exceedance in 50 years: (a) collapses excluded; and (b) collapses included (Rezaeian's model).

procedure in GCIM. Although the procedure can estimate potential EDP biases in a practical fashion, such bias estimates might be significantly different from the actual bias. For instance, the "corrected" CDF in Fig 5.22a indicates that the roof acceleration hazard curve from the current selection of ground motions will *overestimate* the 'true' roof acceleration hazard curve by a *slight* amount, because it is 'to the left' of the "uncorrected" CDF (see also Fig 4 in [87]). In contrast, the benchmark SDHC in Fig 5.18c demonstrates that the current SDHC estimate from GCIM *underestimates* the benchmark by a *significant* amount.

Since it is up to the analyst to decide whether or not EDP biases estimated from GCIM are acceptable, the discrepancy between conclusions from the two approaches – benchmark and GCIM – may have been a result of judgement employed in GCIM. To test whether this is the case or not, ground motions were deliberately reselected at the 0.02% probability of exceedance in 50 years level so that inconsistencies with respect to spectral accelerations at short vibration periods (Fig 5.19a) are eliminated altogether. To achieve this, a new weight vector was specified in the reselection where 85% is given to PGA, ASI, and spectral accelerations at periods from 0.05 to 0.95 sec, while 15% is given to the rest of the original 24 IMs. This weight vector led to ground motions that pass the KS tests for all spectral accelerations at short vibration periods, including $A(0.1)$ as shown in Fig 5.23a. In exchange however, inconsistencies are observed for $A(3)$ (Fig 5.23b) and for CAV (not shown).

Fortunately, the inconsistencies with respect to $A(3)$ and CAV are unimportant to roof acceleration, as one might expect. This is demonstrated in Fig 5.24, where the slopes are statistically insignificant in each of the two cases. Consequently, the new selection of ground

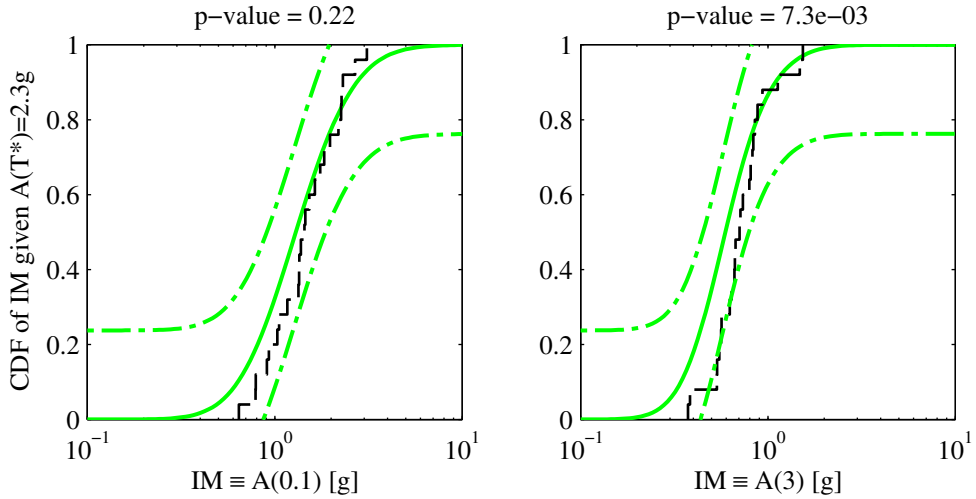

Figure 5.23: Results from applying KS tests (GCIM target in solid green, 10% KS bounds in chained green, and empirical CDF in dashed black) to ground motions reselected with a new weight vector for $A(T^*)$ at 0.02% probability of exceedance in 50 years: (a) $IM \equiv A(0.1)$; and (b) $IM \equiv A(3)$ (Rezaeian's model).

motions at the 0.02% probability of exceedance in 50 years level were employed to revise the SDHCs of the 4-story frame; these revised SDHCs are shown in Fig 5.25.

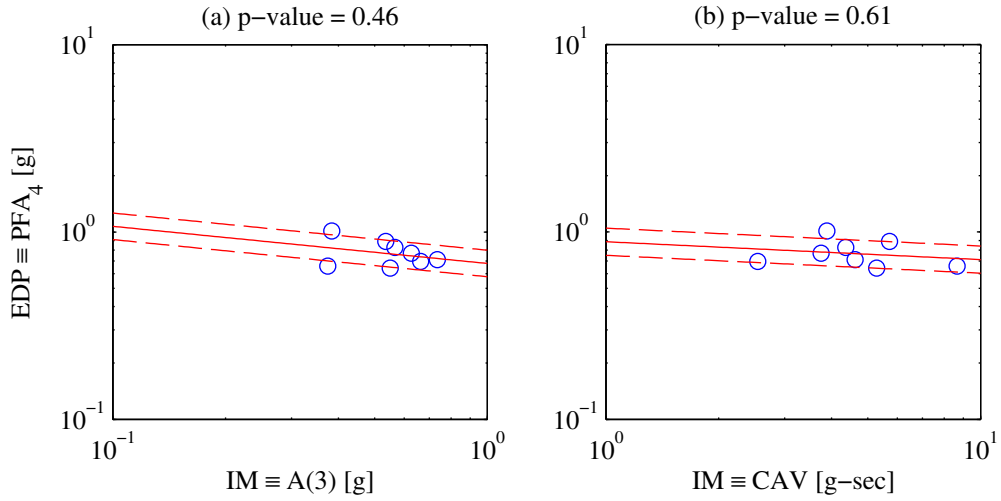

Figure 5.24: Output from applying t-tests (regression line in solid red and 68% CI of $\ln(EDP) \mid \ln(IM)$ in dashed red) to results from RHAs of the frame due to ground motions reselected with a new weight vector for $A(T^*)$ at 0.02% probability of exceedance in 50 years: (a) $IM \equiv A(3)$; and (b) $IM \equiv CAV$ (Rezaeian's model).

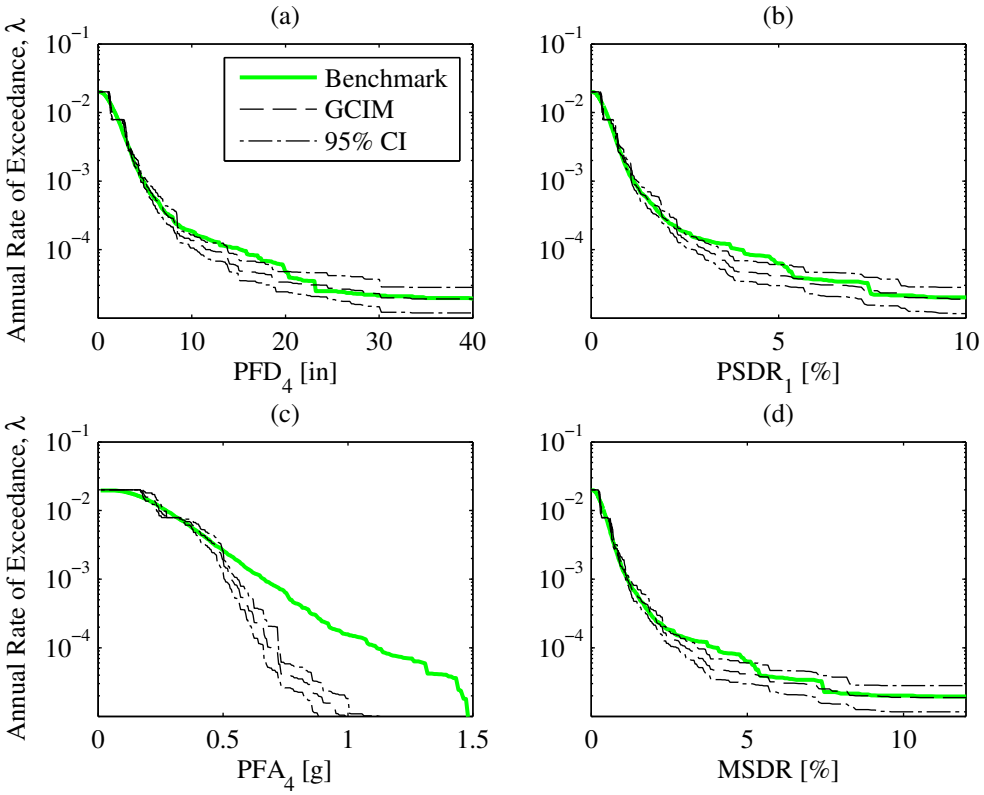

Figure 5.25: Comparison of SDHC estimates for several EDPs of the 4-story frame from ground motions reselected by GCIM with a new weight vector against benchmark (Rezaeian's model).

Comparing the revised SDHCs in Fig 5.25 against those shown in Fig 5.18 reveals several important observations. First, the SDHCs are nearly identical in the two cases because: (i) ground motions were reselected for only one out of $N_{IM^*} = 12$ intensity levels (specifically, 0.02% probability of exceedance in 50 years), (ii) the SDHCs for displacements and drift ratios at low exceedance rates are controlled by the annual rate of collapse, which is insensitive to the RHA results from the new selection of ground motions, and (iii) the SDHCs for floor accelerations are sensitive to the new RHA results only at exceedance rates less than 10^{-6}. Second and more importantly, the revised SDHCs demonstrate that the discrepancy between conclusions from the benchmark and from the bias-checking procedure in GCIM is *not* a consequence of the judgement exercised in determining whether or not estimated EDP biases are acceptable (Fig 5.22). Without the benchmark, which was obtained from 10^4 RHAs of the 4-story frame, one may draw erroneous conclusions from the bias-checking procedure in GCIM (see also Section 3 in [87]). Third, Figs 5.25c and 5.18c demonstrate that SDHCs from GCIM may still be biased, even after iteratively (i) selecting ground motions to be consistent with the GCIM targets (Figs 5.19 and 5.23), (ii) checking for dependencies

between all relevant combinations of EDPs and IMs (Figs 5.20 and 5.24), and (iii) estimating potential biases in EDPs caused by individual IMs (Fig 5.22). Such is the case because in many situations, we really don't know which IMs are insufficient for which EDPs of a complex, MDF system. For the 4-story frame considered herein, the benchmark reveals that the collection of 24 IMs employed in GCIM is *insufficient* with respect to roof acceleration, implying that this EDP depends on a feature of the ground motion time series that has not been considered thus far in the analysis.

20-story frame

The GCIM method was also implemented for the 20-story frame and for both stochastic models. In both stochastic models, ground motions were again carefully selected to ensure hazard consistency with respect to all 24 IMs (Step 4g in Section 5.7). Similar to the other systems considered, it was most difficult to satisfy all KS tests at the largest two intensity levels of $A(T^*)$ (i.e., 0.02% and 0.01% probability of exceedance in 50 years).

For such intensity levels, ground motions were examined for potential biases in EDPs (see Step 7, Fig 5.20, Fig 5.22) before SDHCs were computed and compared against the benchmark. Specifically, ground motions were iteratively selected and RHAs (of the 20-story frame) were iteratively performed until 'convergence' is achieved. Convergence is achieved when either the EDP was shown to not depend on the inconsistent IM (e.g., Fig 5.24), or the estimated EDP bias was deemed acceptable (e.g., Fig 5.22), *for all IMs that did not satisfy the KS test*. In order to avoid repeating Steps 7(a)ii-7(a)iii of the GCIM summary for all 62 EDPs of this 20-story frame, the latter steps were implemented for four salient EDPs: (i) roof displacement, PFD_{20}, (ii) first-story drift ratio, $PSDR_1$, (iii) roof acceleration, PFA_{20}, and (iv) maximum story drift ratio over all stories, $MSDR$. Fortunately, ground motions did not have to be re-selected with a different weight vector for the 20-story frame and for both stochastic models, because convergence was achieved for the initial selection of ground motions. For the 4-story frame however, convergence was not achieved for the initial selection and hence, ground motions were reselected once more with a different weight vector, after RHAs have already been conducted.

The GCIM-based SDHCs of the 20-story frame are shown in Figs 5.26 and 5.27, for Yamamoto's and Rezaeian's stochastic model, respectively. These results demonstrate that the agreement between the estimates from GCIM and the benchmark is excellent for all EDPs considered. This is expected because (i) a comparable level of good agreement was observed from CSexact for the same frame, and at the same time, (ii) GCIM captures even more aspects of the ground motion than in CSexact when selecting ground motions. As noted earlier in Section 5.6, such good agreement suggests, but does not imply, that the vector of IMs considered for selecting ground motions is sufficient for the EDPs of this 20-story frame.

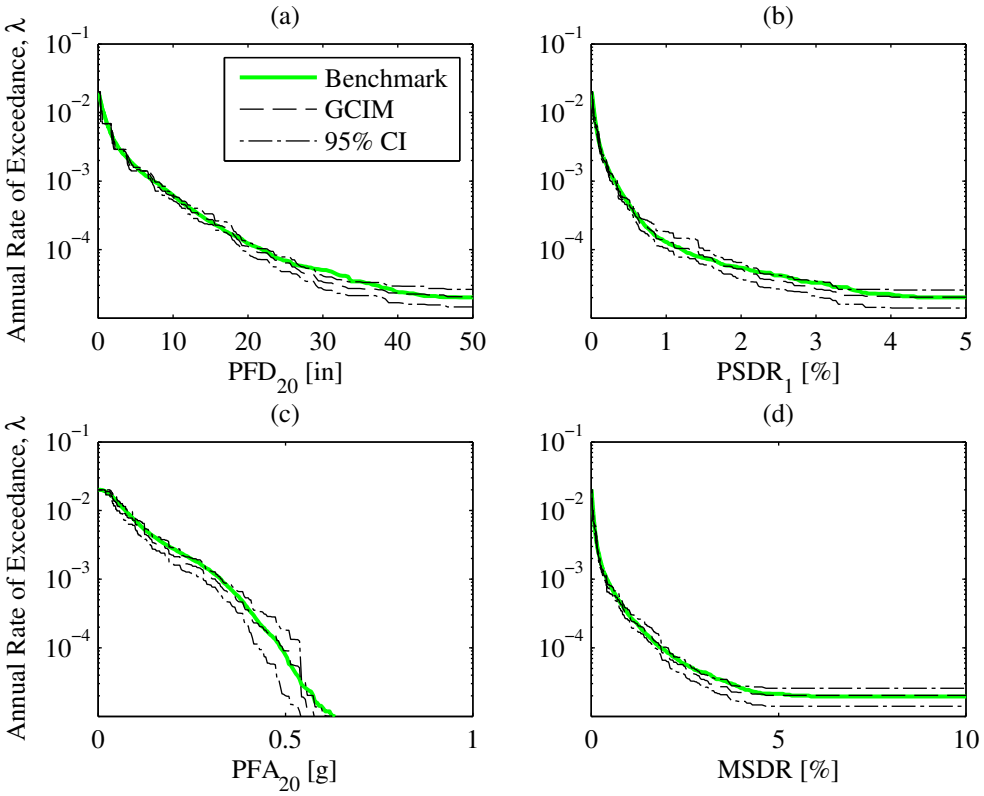

Figure 5.26: Comparison of SDHC estimates for several EDPs of the 20-story frame from GCIM against benchmark (Yamamoto's model).

5.9 Comparative summary of CSexact and GCIM

Table 5.1 summarizes the effort involved when implementing CSexact and GCIM in this study to compute SDHCs of a given structure at the specified site. The two procedures are similar in that (i) a conditioning IM is chosen to scale ground motions, (ii) a relatively large number of IMs is utilized to select ground motions, and (iii) KS tests are employed at each intensity level of IM^* to ensure hazard consistency of the selected motions. In addition, the two procedures are similar in that $N_{IM^*} = 12$ intensity-based assessments are conducted and hence $N_{IM^*} = 12$ deaggregations are performed, $N_{IM^*} = 12$ target multivariate distributions are computed, and $N_{IM^*} = 12$ sets of ground motions are selected when determining a single estimate of the SDHC.

Table 5.1 also highlights two major differences between CSexact and GCIM. First, other features of the ground motion time series in addition to spectral accelerations (e.g., cumulative effects, etc.) are incorporated in the ground motion selection process of GCIM whereas only spectral accelerations are incorporated in that of CSexact. As a result, scaling of ground motions in CSexact is limited by $SF_{max} = 4$ (based on personal communication with the

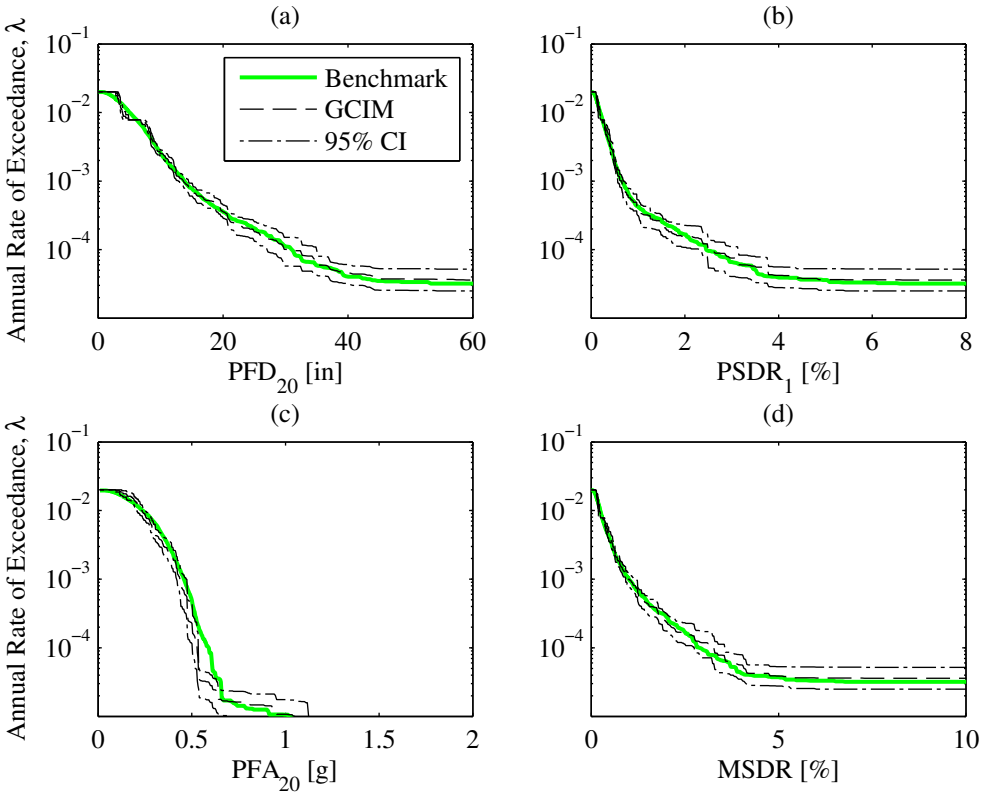

Figure 5.27: Comparison of SDHC estimates for several EDPs of the 20-story frame from GCIM against benchmark (Rezaeian's model).

author of CSexact) whereas the scale factors in GCIM are indirectly limited through a judicious choice of **IM**. Second, implementation of the bias-checking procedure is necessary in GCIM, because GCIM aims to select ground motions in a holistic fashion. The bias-checking procedure is an important step in GCIM because it offers analysts the ability to explicitly check for potential EDP biases caused by improper ground motion selection, before proceeding to compute SDHCs. As elaborated in Section 5.8 however, this step can become quite involved, depending on the level of accuracy desired by the analyst. More importantly, it is demonstrated in Section 5.8 that even after implementing the bias-checking procedure, for a wide range of IMs and EDPs (see Figs 5.19-5.22), the SDHCs resulting from the finalized set of ground motions may still be biased (see Fig 5.18c). This possibility of bias can be minimized by employing unscaled ground motions, through the method of Importance Sampling, as described in Chapter 4 and evaluated in Chapter 6.

Table 5.1: Summary of effort involved in using CSexact and GCIM in this study to compute SDHCs of a given structure at the specified site.

Attribute	CSexact	GCIM
Conditioning IM	$A(T^*) = A(T_1)$	$IM^* = A(T_1)$
Can all ground motions be unscaled?	No	No
Limits on scaling of ground motions	$SF_{max} = 4$	No threshold
Type of IMs considered	Spectral accelerations	Spectral accelerations, peak ground measures, spectrum intensities, cumulative effects
Number of IMs used to select ground motions	25 vibration periods	24 IMs
Total number of PSHA-based calculations for selecting ground motions	$N_{IM^*} = 12$ deaggregations and target spectra	$N_{IM^*} = 12$ deaggregations and GCIM distributions
Total number of ground motions used	$N_{IM^*} = 12$ sets of $n = 25$ ground motions	$N_{IM^*} = 12$ sets of $n = 25$ ground motions
How hazard consistency is enforced	KS tests and greedy optimization	KS tests
Is bias-checking procedure required?	No	Yes

5.10 Conclusions

In this study, two existing, contemporary GMSM procedures – CSexact and GCIM – are evaluated in their ability to accurately estimate seismic demand hazard curves (SDHCs) of a given structure at a specified site. A case study is chosen where rigorous benchmark SDHCs can be determined. The amount of effort involved in implementing these procedures to compute a single SDHC is summarized (Table 5.1). In essence N_{IM^*} intensity-based assessments are conducted where for each assessment, ground motions are scaled but selected to be consistent with respect to the target defined by PSHA for a user-specified collection of IMs. The results from implementing these procedures are compared against the benchmark, leading to the following conclusions:

1. Good agreement between the benchmark SDHC and the estimate from CSexact is observed for most of the SDF systems considered and for the 20-story frame. In some cases, the estimate from CSexact overestimates the annual rate of collapse and underestimates floor accelerations.

2. Good agreement between the benchmark SDHC and the estimate from GCIM is observed for all of the SDF systems considered, for the 20-story frame, and for most of the EDPs considered for the 4-story frame. Even with a large number of IMs employed to select ground motions, along with implementation of the bias-checking procedure, the estimate from GCIM underestimates some floor accelerations of the 4-story frame, which is likely caused by record scaling.

3. Whether or not the estimate from a particular GMSM procedure is biased depends on the particular problem, because the underlying cause of SDHC bias involves two important aspects of the particular selection of ground motions: (i) hazard consistency, and (ii) IM sufficiency. A GMSM procedure is only a tool for achieving hazard consistency with respect to a user-specified collection of IMs; whether or not the resulting SDHC is biased depends on how sufficient the vector of IMs is, relative to the EDP of interest.

4. Given hazard consistency with respect to an IM, the benchmark SDHCs enable us to identify IMs that are insufficient:

    a) The vector of spectral accelerations at vibration periods from 0.05 to 10 sec, is insufficient for estimating collapse of the 4-story frame and of the SDF system with $T_1 = 1$ sec, $R_y = 1$; for these cases, cumulative effects of the ground motion appear to be important.

    b) The vector of 24 IMs employed herein for GCIM, which captures amplitude, frequency content, and duration of the ground motion, is insufficient for estimating roof acceleration of the 4-story frame.

5. It is possible to obtain significantly biased SDHCs from GCIM, even after implementing the bias-checking procedure to approximate potential EDP biases arising from improper ground motion selection.

When interpreting the above conclusions, it should be borne in mind that a relatively simple site is studied.

Chapter 6

Evaluation of the Importance Sampling approach to estimating seismic demand hazard curves

6.1 Abstract

An Importance Sampling (IS) based ground motion selection procedure was proposed for estimating SDHCs of structures at a specified site (Chapter 4). This procedure enables us to take advantage of unscaled yet intense ground motions for estimating seismic demand hazard curves (SDHCs), through database-driven Importance Functions (IF). More importantly, it enables us to directly enforce hazard consistency of the selected motions with respect to a given set of IMs through different choices of the IF. In this study, we evaluate the IS procedure in its ability to accurately estimate SDHCs of structures at a specified site. We find that SDHCs from this procedure are typically unbiased, especially when ground motions are scaled minimally. The epistemic uncertainty in the SDHCs from the IS approach is controlled primarily by the IF, $g(\cdot)$, and secondarily by the sample size, n. The amount of effort involved in implementing the IS procedure is also summarized where we see that given a judiciously chosen IF, the procedure greatly simplifies the problem of selecting ground motions for estimating SDHCs. Finally, the possibility of estimating SDHCs for *multiple* systems from a *single* ensemble of ground motions selected by the IS approach seems promising.

6.2 Introduction

Seismic demand hazard curves (SDHCs) of a given structure at a given site, which play an important role in damage and loss estimation, are typically estimated in practice via probabilistic seismic demand analysis (PSDA) [15]. In essence, multiple intensity-based assessments [31, 3] of the structure are conducted and the results are combined with the hazard curve of the chosen conditioning intensity measure (IM), determined by probabilistic

seismic hazard analysis (PSHA) of the given site, in order to produce SDHCs of the structure. More details about PSDA can be found in Section 2 of [64], among others.

Since ground motions are scaled in PSDA, it is natural to ask whether the resulting SDHCs are biased and whether they provide useful information (e.g., [21]). As pointed out in Section 6 of [64] however, SDHC bias is not caused directly by record scaling but rather, by hazard inconsistencies of the selected ground motions with respect to IMs that are influential to the response quantity, or engineering demand parameter (EDP). In other words, the bias in a SDHC estimate is directly related to two important aspects of the specific selection of ground motions: (i) IM sufficiency, and (ii) hazard consistency.

For example, suppose the conditioning IM is defined as spectral acceleration at the fundamental vibration period of the structure, $A(T_1)$. By scaling ground motions to the hazard curve of $A(T_1)$, the motions are ensured to be consistent with the hazard curve for $A(T_1)$ that is determined by PSHA; such motions are said to be *hazard-consistent with respect to* $A(T_1)$. If the EDP is sensitive to *only* $A(T_1)$ and no other features of the ground motion (i.e., this IM is *sufficient* [12]), then (i) the resulting SDHC is unbiased at exceedance rates corresponding to those in which the selected ground motions are considered hazard-consistent, and (ii) such good agreement is independent of the level of record scaling.

In many situations however, the response of a structure is sensitive to many more features of the ground motion besides $A(T_1)$ alone and consequently, it is important to ensure that the selected ground motions are *also* hazard-consistent with respect to such features. This can be achieved with the Generalized Conditional Intensity Measure (GCIM) approach [47], where Kolmogorov-Smirnov (KS) tests are employed to select ground motions that are consistent with the GCIM distributions for a wide range of user-specified IMs. However, such KS tests do not necessarily ensure hazard consistency at low exceedance rates because low exceedance rates are occasionally controlled by the 'tails' of GCIM distributions (see Section 2 of [87]). Furthermore, the use of record scaling in PSDA suggests that hazard inconsistencies may still exist for IMs that have not been considered by the analyst in the selection of ground motions, which can be important for certain EDPs (e.g., see Fig 5.18). One possibility for minimizing such hazard inconsistencies is to employ a very large number of IMs to select ground motions. Since hazard inconsistencies appear to be more pronounced when ground motions are scaled (compare Fig 4.12 against Fig 4.9a), minimization of record scaling appears to be another alternative to minimize hazard inconsistencies.

Suppose we are interested in avoiding record scaling altogether when computing SDHCs. How can we best utilize a database of unscaled ground motions for this purpose? Moreover, can we directly enforce hazard consistency at user-specified exceedance rates? The Importance Sampling (IS) procedure, developed in Chapter 4, answers these questions. In this chapter, we evaluate this procedure using the same case study (i.e., site, stochastic models, structural systems, and EDPs) and methodology that were described in Section 5.3 and 5.4; in order to emphasize the main ideas regarding the IS procedure, only a subset of the results from Yamamoto's stochastic model are presented. Before doing so, we take a closer look at the IS procedure.

6.3 Step-by-step summary of the procedure

The Importance Sampling (IS) approach for estimating a SDHC is summarized as follows:

1. Specify a vector of IMs, **IM**, to be utilized for selecting ground motions.
2. Determine the target probability distribution of **IM** from PSHA of the site, using Eq 4.3.
3. Choose an Importance Function (IF) for selecting ground motions.
4. Randomly simulate n vectors of **IM** from the multivariate IF in Step 3, using the approach discussed in Section 4.4.
5. Select n ground motions whose computed values of **IM** most closely agree with those simulated from Step 4, using the approach discussed in Section 4.4.
6. Compute IS weights from the selected ground motions, using Eq 4.6.
7. Check hazard consistency of the selected ground motions with respect to any IM of interest (using Eq 4.5a); if deemed hazard-inconsistent, then reselect ground motions (Steps 4-6), following the guidance provided in Section 4.4.
8. Perform response history analyses (RHAs) of the structure due to the n selected ground motions.
9. Estimate the SDHC using the IS weights from Step 6, as outlined in Section 4.4.

When implementing Step 1 of the above summary, the number of IMs in **IM** should be relatively small (i.e., four to six) because a large number of IMs leads to large epistemic uncertainty in the resulting estimates of hazard curves (see Eqs 4.8-4.9), which is undesirable. In addition, a small number of IMs reduces the computational time involved in computing IS weights (Step 6); note that the evaluation of Eq 4.6 requires the evaluation of multiple multivariate lognormal PDFs (Eq 4.3). Since there is often a *finite* number of ground motions in the database to select from (Step 5), it is possible to obtain a selection of ground motions that does not closely agree with the randomly simulated values of **IM** and hence, it is very important to check hazard consistency of the selected motions (Step 7) before proceeding with any RHAs; if the selected motions are hazard-inconsistent, then ground motions should be reselected. Finally, the choice of IF (Step 3) is a critical step to the success of the IS procedure, which is discussed next.

6.4 Choice of Importance Function

In the IS procedure, hazard curves for IMs and EDPs are estimated from Eq 4.5 (Steps 7 and 9). Each implementation of the procedure leads to hazard curves that are, on average,

unbiased (Eq 4.7) [1]; in other words, the 95% confidence interval (CI) of the estimate covers the benchmark. The epistemic uncertainty of such hazard curve estimates are given by Eqs 4.8-4.9. For a given structure at a given site, all parameters in these two equations are fixed, except for the IF, $g(\cdot)$, and the sample size, n. Thus, for a given value of n, the IF controls the epistemic uncertainty of the hazard curve estimates.

Assuming an infinite number of ground motions is available for selection, a good IF is one that possesses two desirable attributes. First, it should be relatively easy to randomly simulate vectors of IMs from the IF (Step 4). For example, it is relatively easy to randomly simulate vectors of IMs from multivariate lognormal distributions (see e.g., Section 6.2 of [73]) or from mixtures of multivariate lognormal distributions. Second, the IF should lead to relatively small epistemic uncertainty in the SDHC estimates. This implies that the IF should be chosen by minimizing the integral in Eq 4.9; however, this cannot be done because the term $\Pr(EDP > z \mid \mathbf{IM} = \mathbf{s})$ is unknown. Consequently, we resort to another approach that will be described at the end of this section.

In practice, the range of possible IFs to choose from is restricted by the ground motions that are available for selection. For example, when the largest observed value of $A(1s)$ in the database is, say $1g$, there would be no point in specifying an IF whose mode is located at intensities greater than $1g$ (see Step 5). Consequently, we propose to develop IFs whose parameters are computed from the database of ground motions (Section 4.4).

The database of 10^4 synthetic ground motions from Yamamoto's stochastic model (Section 5.4) and the 4-story frame (Section 5.3) are chosen as an example to illustrate such database-driven IFs. Fig 6.1 illustrates two IFs that are multivariate lognormal: (i) $g_1(\cdot)$, and (ii) $g_2(\cdot)$. The mean vector and covariance matrix of $g_1(\cdot)$ are determined from the values of IMs corresponding to all 10^4 ground motions, using Eqs 4.10-4.11 (see Section 4.4). In this particular example, the mode of $g_1(\cdot)$ happens to be larger than the mode of the target PDF from PSHA, $f(\cdot)$, implying that ground motions selected using $g_1(\cdot)$ will be more intense than those selected using $f(\cdot)$. However, suppose one is interested in only unscaled ground motions where $A(T_1) \geq 1g$ and $A(2T_1) \geq 0.5g$. In this case, another possible IF would be to first filter the database of 10^4 ground motions according to the latter criteria before determining the mean vector and covariance matrix for the IF; this is depicted as $g_2(\cdot)$ in Fig 6.1.

Fig 6.1 also illustrates a third example of a database-driven IF, $g_3(\cdot)$. This IF is a mixture of the previous two IFs:

$$g_3(\mathbf{x}) = [1 - \eta] \cdot g_1(\mathbf{x}) + \eta \cdot g_2(\mathbf{x}) \tag{6.1}$$

where $0 \leq \eta \leq 1$ refers to the *mixing proportion*. Eq 6.1 is similar to Eq 4.12 except that the individual multivariate lognormal distributions in Eq 6.1 are derived from subsets of the database of *unscaled* ground motions. Similar to the two-component mixture IF in Eq 4.12, values of **IM** are randomly generated from $g_3(\cdot)$ via two steps: (i) identify one of the two components by randomly sampling from the Bernoulli distribution with probability η, and (ii) randomly generate a value of **IM** from the component identified.

[1] This may not be the case when **IM** is insufficient *and* ground motions are scaled (see Section 4.3).

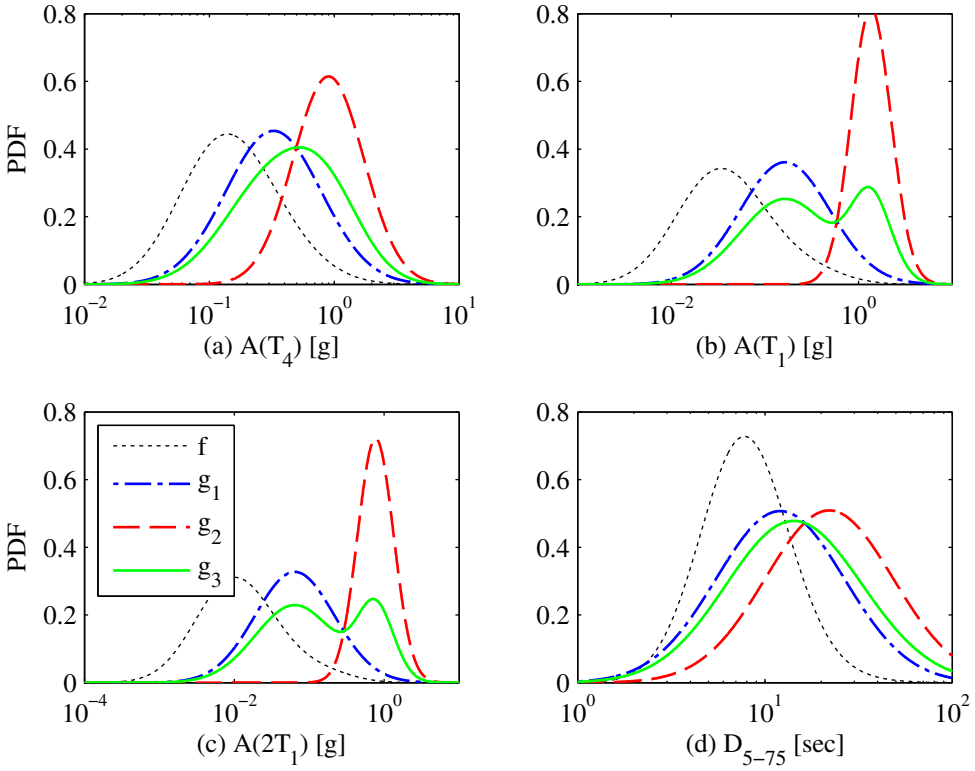

Figure 6.1: Examples of database-driven IFs with reference to target PDFs from PSHA, $f(\cdot)$ (dotted black): (i) $g_1(\cdot)$ (chained blue), (ii) $g_2(\cdot)$ (dashed red), (i) $g_3(\cdot)$ (solid green). Marginal distribution for (a) $A(T_4)$; (b) $A(T_1)$; (c) $A(2T_1)$; (d) D_{5-75}.

How can one identify a single IF to proceed with, given a range of possible choices for the IF (Fig 6.1)? First, we note that the "optimal" IF varies with both (i) the EDP considered and (ii) the level of seismic demand, z, because the epistemic uncertainty in the SDHC depends on $\Pr(EDP > z \mid \mathbf{IM} = \mathbf{s})$ in Eq 4.9. Second, we note that given an EDP and a level of seismic demand (or exceedance rate), the IF cannot be determined from minimizing Eq 4.9 because the term $\Pr(EDP > z \mid \mathbf{IM} = \mathbf{s})$ is unknown. Nevertheless, these observations suggest a practical approach for ranking a given collection of IFs.

For a given EDP and a level of seismic demand, we propose to choose the IF by minimizing the epistemic uncertainty in the hazard curves for each IM in **IM**, at exceedance rates that are deemed influential to the given level of seismic demand. The epistemic uncertainty in the hazard curves can be quantified by standard Monte Carlo simulation methods (see e.g., Chapter 5 of [89]). This approach is summarized as follows:

1. For each IF, do the following:

    a) Randomly generate n values of **IM** from the IF.

b) Compute the hazard curve for each IM in **IM**, by applying Eq 4.5a to the *simulated* values of **IM**.

c) Repeat the latter two steps until N_{Epi} hazard curves have been computed for each IM in **IM**.

d) Construct a 95% CI of the hazard curve for each IM in **IM**.

2. Choose the IF that leads to the narrowest CI for the IMs and exceedance rates of interest.

This approach is illustrated in Fig 6.2 for $g_1(\cdot)$ and $g_3(\cdot)$ from Fig 6.1. For each of the two IFs and for each IM, the 95% CI of the hazard curve is presented. As expected, the CI of the hazard curves for $A(T_1)$ and $A(2T_1)$ from $g_3(\cdot)$, at exceedance rates less than 10^{-5}, are narrower than those from $g_1(\cdot)$, because $g_3(\cdot)$ concentrates on the tail regions of $A(T_1)$ and $A(2T_1)$ more so than $g_1(\cdot)$ (Figs 6.1b-c). If one assumed that the response of the system at low exceedance rates is most sensitive to $A(T_1)$ and $A(2T_1)$, at exceedance rates less than 10^{-5}, then $g_3(\cdot)$ would be chosen over $g_1(\cdot)$. In summary, the IS procedure enables one to estimate SDHCs with unscaled yet intense ground motions, through different choices of the IF.

6.5 Estimating SDHCs without scaling ground motions

In this section, we evaluate the IS procedure in its ability to estimate SDHCs without scaling ground motions. In order to facilitate comparison between the results from this procedure against those from GCIM or CSexact (Chapter 5), where $12 \times 25 = 300$ ground motions were employed to estimate a single SDHC, $n = 300$ ground motions are selected for computing SDHCs of each system (SDF systems, 4-story frame, and 20-story frame). For each multistory frame, four IMs are chosen to select ground motions (Step 1): spectral accelerations at (i) the fundamental vibration period of the structure, $A(T_1)$, (ii) twice the fundamental period, $A(2T_1)$, (iii) the fourth-mode period, $A(T_4)$, and (iv) 5-75% significant duration, D_{5-75}. These four IMs are also chosen to select ground motions for each SDF system, except that $A(T_4)$ is replaced by $A(0.2T_1)$. Given these IMs for selecting ground motions, **IM**, the only input parameter that remains to be specified for the IS procedure is the IF.

The simplest IF is a multivariate lognormal distribution whose parameters are determined from all 10^4 unscaled, ground motions in the database; this is denoted by $g_u(\cdot)$ in Section 4.4 (i.e., $SF_{max} = 1$ or $\gamma = 0$) or equivalently, $g_1(\cdot)$ in Section 6.4. Using this IF, $n = 300$ values of **IM** are randomly generated (Step 4) and using Eq 4.13, $n = 300$ ground motions from the database are selected (Step 5). Applying Eqs 4.5a and 4.6 to the selected ground motions leads to estimates of hazard curves for any IM. For example, hazard consistency of the ground motions selected for the 4-story frame is examined in Fig 6.3, with respect to nine different IMs: (i) $A(T_4)$, (ii) $A(T_1)$, (iii) $A(2T_1)$, (iv) $A(4T_1)$, (v) peak ground acceleration (PGA),

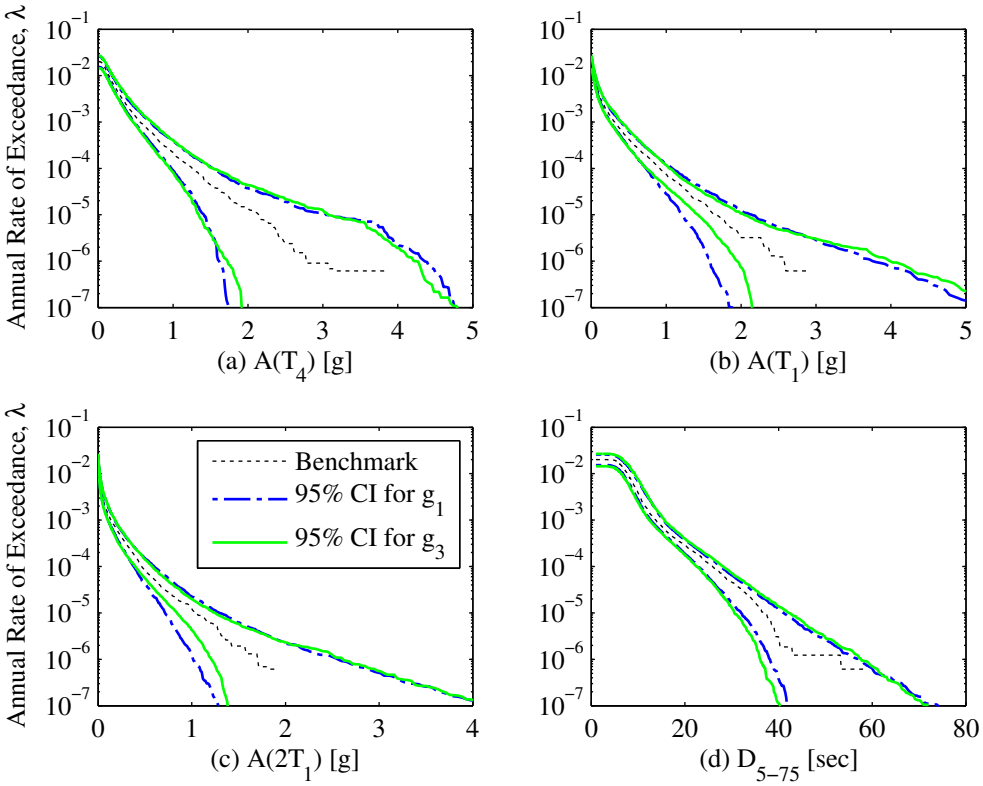

Figure 6.2: Proposed approach for choosing IF among several possibilities; $N_{Epi} = 10^3$. Hazard curves for (a) $A(T_4)$; (b) $A(T_1)$; (c) $A(2T_1)$; (d) D_{5-75}.

(vi) peak ground velocity (PGV), (vii) peak ground displacement (PGD), (viii) cumulative absolute velocity (CAV), and (ix) D_{5-75}.

Fig 6.3 demonstrates that the ground motions selected from the IS procedure, with $g_u(\cdot)$ as the IF, are hazard-consistent with respect to a wide range of IMs and exceedance rates, *even though only four IMs are chosen to select ground motions*. This is the case because (i) ground motions are *unscaled*, and (ii) the chosen **IM** is strongly correlated with many other features of the ground motion. Thus, the IS procedure offers a direct means (through various choices for **IM** and the IF) to achieve hazard consistency over a wide range of IMs and exceedance rates. As a result, SDHCs from the IS procedure are expected to be unbiased.

Fig 6.4 presents SDHCs of the 4-story frame, resulting from the ground motions summarized in Fig 6.3, for four EDPs: (i) roof displacement, PFD_4, (ii) first story drift ratio, $PSDR_1$, (iii) roof acceleration, PFA_4, and (iv) maximum story drift ratio (MSDR). As expected from theoretical considerations (Section 4.3) and from the hazard consistencies observed in Fig 6.3, the SDHCs are unbiased because the 95% CI of each SDHC covers the benchmark. Note that the roof acceleration hazard curve from the IS approach is unbiased (Fig 6.4c), whereas that from GCIM underestimates the benchmark (Fig 5.16c); however,

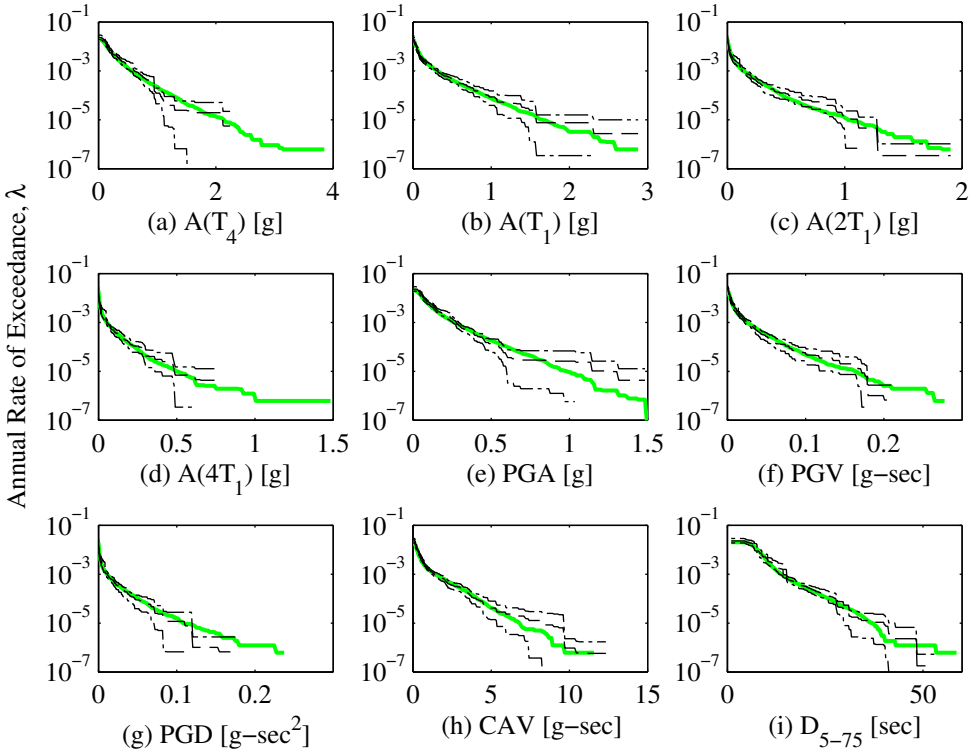

Figure 6.3: Hazard consistency of the motions selected with $g_u(\cdot)$ for the 4-story frame, with respect to: (a) $A(T_4)$; (b) $A(T_1)$; (c) $A(2T_1)$; (d) $A(4T_1)$; (e) PGA; (f) PGV; (g) PGD; (h) CAV; and (i) D_{5-75}. Benchmark in solid green, estimate from IS in dashed black, and 95% CI of estimate from IS in chained black.

the epistemic uncertainty in the SDHCs from the IS approach, at exceedance rates less than 10^{-3}, is larger than that from GCIM. Nonetheless, it is important to emphasize that the SDHCs from the IS approach are obtained from a *single* set of $n = 300$ ground motions that are selected using a total of *four* IMs.

Fig 6.5 presents SDHCs of the 20-story frame, resulting from ground motions selected by the IS approach with $g_u(\cdot)$ as the IF, for four EDPs: (i) roof displacement, PFD_{20}, (ii) first story drift ratio, $PSDR_1$, (iii) roof acceleration, PFA_{20}, and (iv) maximum story drift ratio (MSDR). The corresponding ground motions were again carefully selected to be hazard-consistent over a wide range of IMs and exceedance rates, by choosing the following four IMs for selection: (i) $A(T_4)$, (ii) $A(T_1)$, (iii) $A(2T_1)$, and (iv) D_{5-75}. As in the case of the 4-story frame, the SDHCs of the 20-story frame from the IS approach are again unbiased for all EDPs considered. Compared to the SDHCs of the 20-story frame from GCIM (Fig 5.26), the epistemic uncertainty in the displacement and drift ratio hazard curves from IS is larger than that from GCIM but the epistemic uncertainty in the acceleration hazard curves from IS is smaller than that from GCIM.

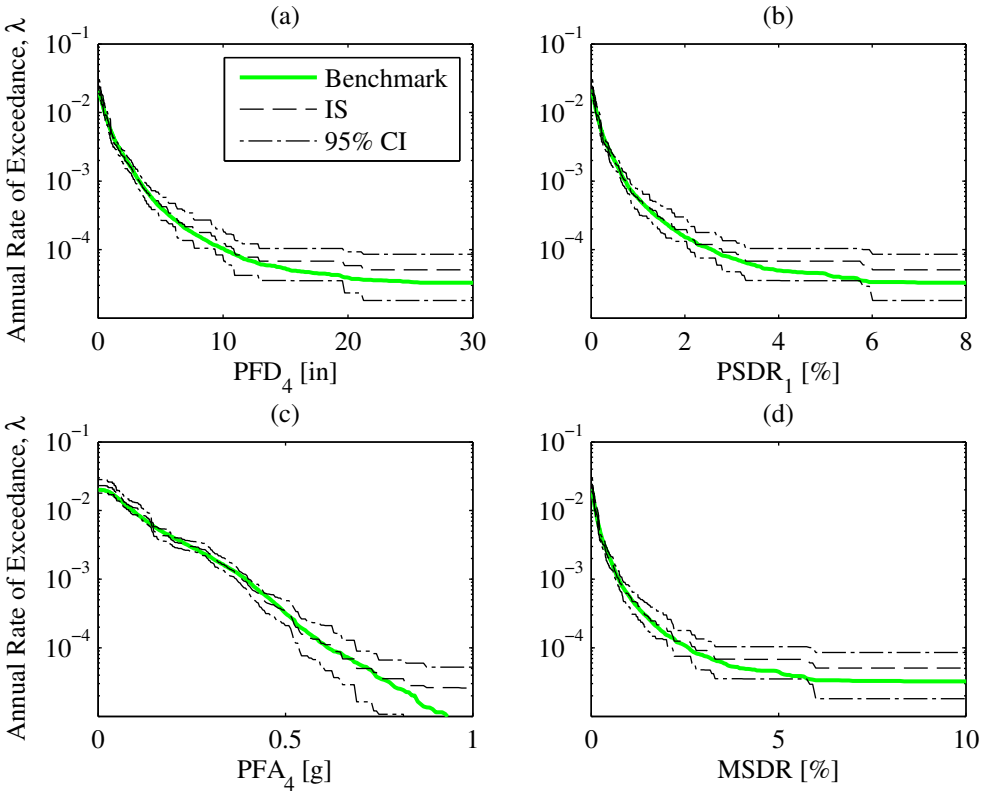

Figure 6.4: Comparison of SDHC estimates for several EDPs of the 4-story frame from IS, with $g_u(\cdot)$ as the IF, against benchmark.

Recall from Section 6.4 that for a given site, structure, and sample size n, the epistemic uncertainty in the SDHCs from IS is controlled by the IF. To verify this claim, ground motions for both frames are reselected from IS using IFs that strive to minimize the epistemic uncertainty of the displacement and drift ratio hazard curves at low exceedance rates. For this purpose, we choose $g_3(\cdot)$ (Eq 6.1) as the IF, where η and $g_2(\cdot)$ are chosen so that the resulting $g_3(\cdot)$ leads to lower epistemic uncertainty, at exceedance rates less than 10^{-4} of the hazard curves for $A(T_1)$ and $A(2T_1)$, compared to that from $g_u(\cdot)$ (see Fig 6.2).

Fig 6.6 examines hazard consistency of the ground motions selected from $g_3(\cdot)$ for the 4-story frame, with respect to the same nine IMs shown in Fig 6.3. As expected from the construction of $g_3(\cdot)$, we observe that the epistemic uncertainty in the hazard curves from $g_3(\cdot)$ for $A(T_1)$ and $A(2T_1)$, at exceedance rates less than 10^{-5}, (Fig 6.6b-c) is smaller than that from $g_1(\cdot)$ (Fig 6.3b-c). In fact, the same can be said for virtually all of the nine IMs considered. If the response of the 4-story frame at low exceedance rates is indeed sensitive to these IMs, then the reduction in epistemic uncertainty of the hazard curves in Fig 6.6 suggests that a similar reduction will be obtained for the SDHCs.

This hypothesis is confirmed in Figs 6.7-6.8, where SDHCs resulting from $g_3(\cdot)$ are pre-

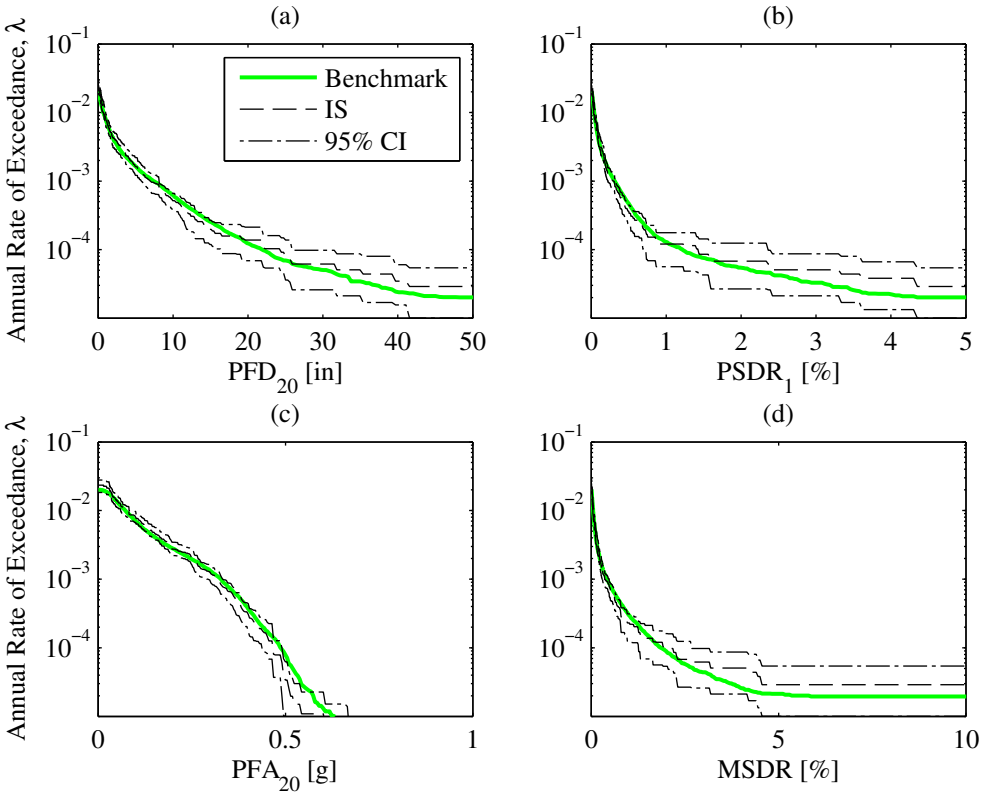

Figure 6.5: Comparison of SDHC estimates for several EDPs of the 20-story frame from IS, with $g_u(\cdot)$ as the IF, against benchmark.

sented for both frames. Compared to the SDHCs from $g_u(\cdot)$ (Figs 6.4-6.5), the epistemic uncertainty in the SDHCs from $g_3(\cdot)$ (Figs 6.7-6.8) is smaller, especially at low annual rates of exceedance. Furthermore, the SDHCs from $g_3(\cdot)$ remain essentially unbiased. In summary, accurate estimates of the SDHC can be obtained from the IS approach (e.g., compare Fig 6.7 against Fig 5.16) with less effort than existing procedures (i.e., 4 IMs and a single set of 300 ground motions in IS compared to 24 IMs and 12 sets of 25 ground motions in GCIM), as long as a large number of unscaled yet intense ground motions are available for selection, and a good IF is chosen.

6.6 Estimating SDHCs with partially scaled ground motions

In practice, ground motion records that are intense enough may be lacking. In this case, the mode of all database-driven IFs would be equal to or smaller than the mode of the target PDFs given by PSHA, $f(\cdot)$, unlike those shown in Fig 6.1. As a result, the hazard curve

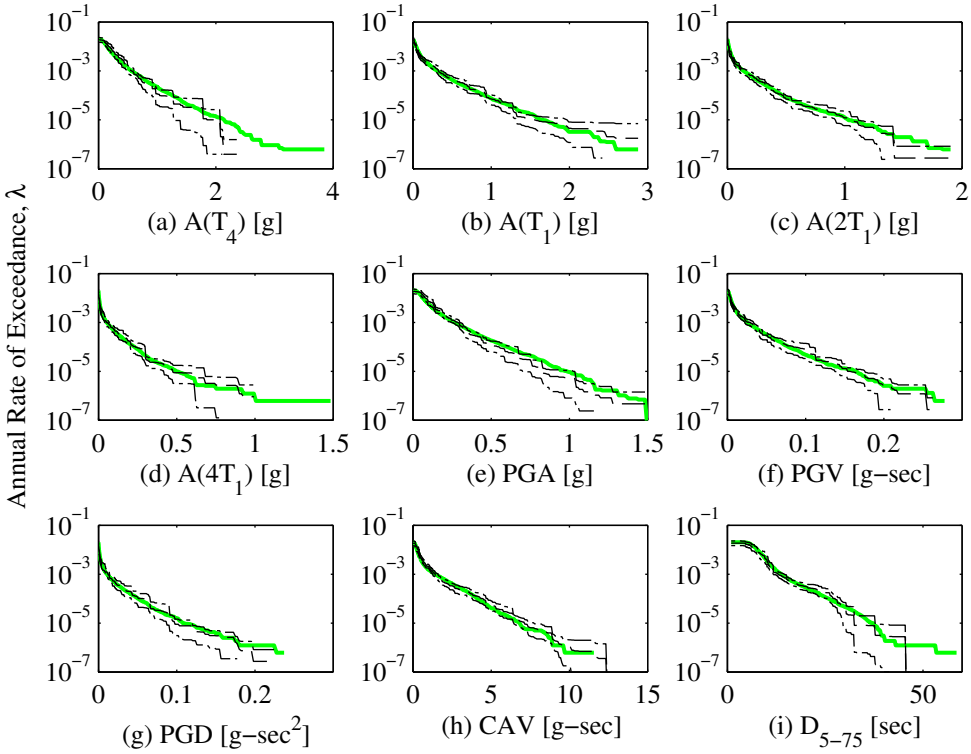

Figure 6.6: Hazard consistency of the motions selected with $g_3(\cdot)$ for the 4-story frame, with respect to: (a) $A(T_4)$; (b) $A(T_1)$; (c) $A(2T_1)$; (d) $A(4T_1)$; (e) PGA; (f) PGV; (g) PGD; (h) CAV; and (i) D_{5-75}. Benchmark in solid green, estimate from IS in dashed black, and 95% CI of estimate from IS in chained black.

estimates from the IS approach will contain a relatively large degree of epistemic uncertainty at low exceedance rates, despite the fact that they are unbiased. This issue can be overcome by either: (i) adding more unscaled, synthetic ground motions to the database, or (ii) scale the motions in the existing database; we investigate the latter option in this section.

By allowing ground motions to be scaled, the effective size of the database increases and hence, a wider range of IFs can be chosen. For instance, a two-component mixture of multivariate lognormals was introduced in Section 4.4 (Eq 4.12), where the IF is controlled by three inputs: (i) the specified database of unscaled ground motions, (ii) the maximum acceptable scale factor, SF_{max}, and (iii) a target fraction of scaled ground motions, γ. Through varying SF_{max} and γ, different IFs can be derived for minimizing epistemic uncertainty in the resulting estimates of hazard curves.

However, record scaling potentially introduces bias into the hazard curve estimates, depending on the sufficiency of **IM** relative to the EDP (and seismic demand level, z) of interest. Section 4.7 explored the relationship between various levels of record scaling and bias in SDHCs of the 4-story frame, leading to the recommendation that (i) SF_{max} should

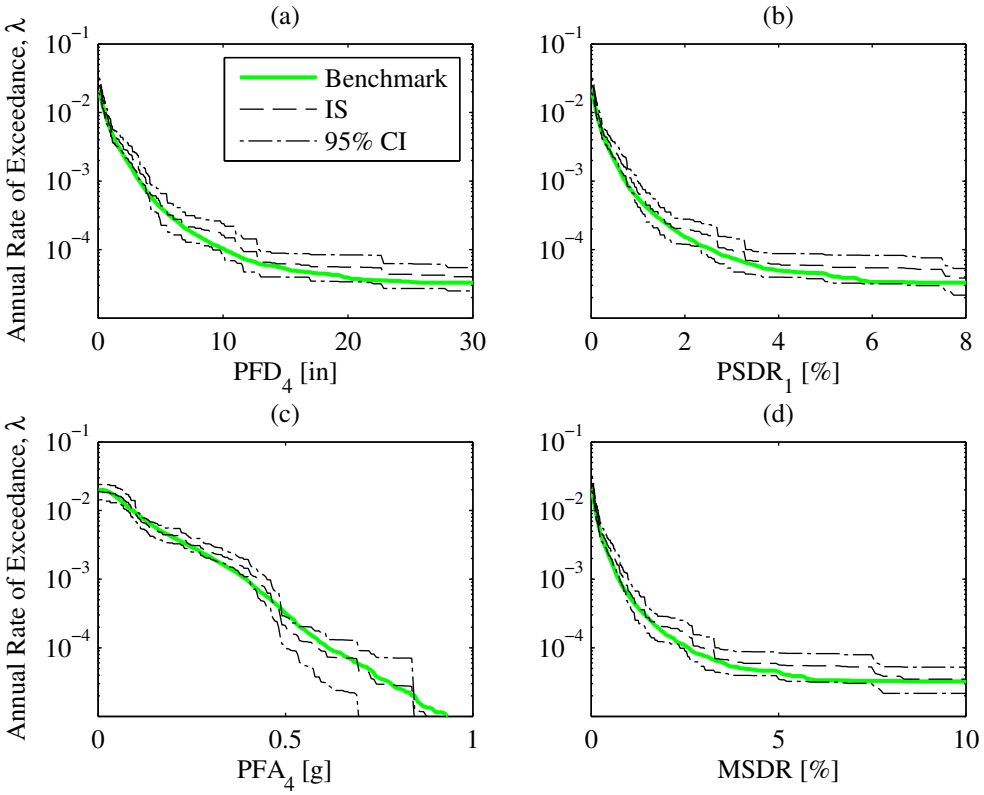

Figure 6.7: Comparison of SDHC estimates for several EDPs of the 4-story frame from IS, with $g_3(\cdot)$ as the IF, against benchmark.

be less than or equal to 5, and (ii) γ should be less than or equal to 0.5 [2]. To evaluate the IS procedure with scaled ground motions in this section, we specify $SF_{max} = 5$ and $\gamma = 0.5$. In order to minimize potential bias due to record scaling, **IM** is expanded in this section to include six IMs: (i) $A(T_4)$, (ii) $A(T_1)$, (iii) $A(3T_1)$, (iv) displacement spectrum intensity (DSI) [90], (v) CAV, and (vi) D_{5-75}. Note that $A(3T_1)$ and DSI are chosen because the results from Section 4.7 suggest that the inelastic response of the 4-story frame is sensitive to the long-period content of the ground motion (Fig 4.14). Thus, the IF in this section is defined by Eq 4.12, with $SF_{max} = 5$, $\gamma = 0.5$, and **IM** consisting of these six IMs.

Ground motions are selected from IS with the IF defined in the preceding paragraph, for both multistory frames. Fig 6.9 examines hazard consistency of these ground motions, with respect to the same nine IMs used in Figs 6.3 and 6.6. As in Figs 6.3 and 6.6 where ground motions are unscaled, the scaled motions are also hazard-consistent over a wide range of IMs and exceedance rates, despite the fact that only six IMs are chosen to select ground motions. Unlike the hazard curves from $g_u(\cdot)$ in Fig 6.3 however, those for scaled motions

[2] When **IM** consists of: (i) $A(T_1)$, (ii) $A(2T_1)$, (iii) $A(T_4)$, and (iv) D_{5-75}.

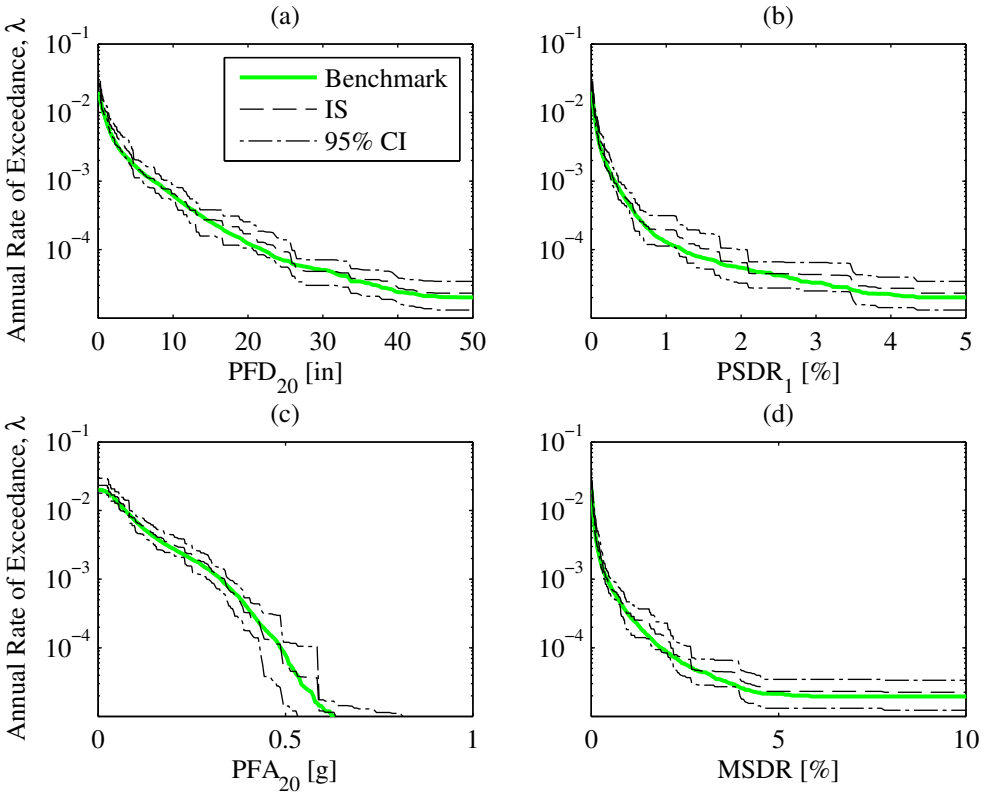

Figure 6.8: Comparison of SDHC estimates for several EDPs of the 20-story frame from IS, with $g_3(\cdot)$ as the IF, against benchmark.

in Fig 6.9 contain *less* epistemic uncertainty at low exceedance rates, which is desirable. This is expected because the IF with $SF_{max} = 5$ and $\gamma = 0.5$ puts more probability density at large values of the IMs (see Fig 4.5a). Although the hazard curves for IMs contain less epistemic uncertainty as a result of scaling, can the same be said for the hazard curves for EDPs? Further, are the resulting SDHCs biased?

Fig 6.10 answers these questions for the 4-story frame. Specifically, the SDHCs from IS with scaling (i) are indeed unbiased, and (ii) contain less epistemic uncertainty that those from unscaled motions (Fig 6.4). Such is the case because the ground motions, although scaled, were carefully selected to be hazard-consistent with respect to **IM**, and these six IMs are in turn correlated with a wide range of other IMs (Fig 6.9).

Ground motions were also selected for the 20-story frame, from the IF defined by $SF_{max} = 5$, $\gamma = 0.5$, and the same six IMs that were chosen for the 4-story frame (i.e., $A(T_4)$, CAV, etc.), such that hazard consistency is ensured for a wide range of IMs and exceedance rates through **IM**. The resulting SDHCs for the 20-story frame are presented in Fig 6.11. As in the case of the 4-story frame, the SDHCs of the 20-story frame are also unbiased. Unlike the 4-story frame however, the epistemic uncertainty in the SDHCs from scaled motions is

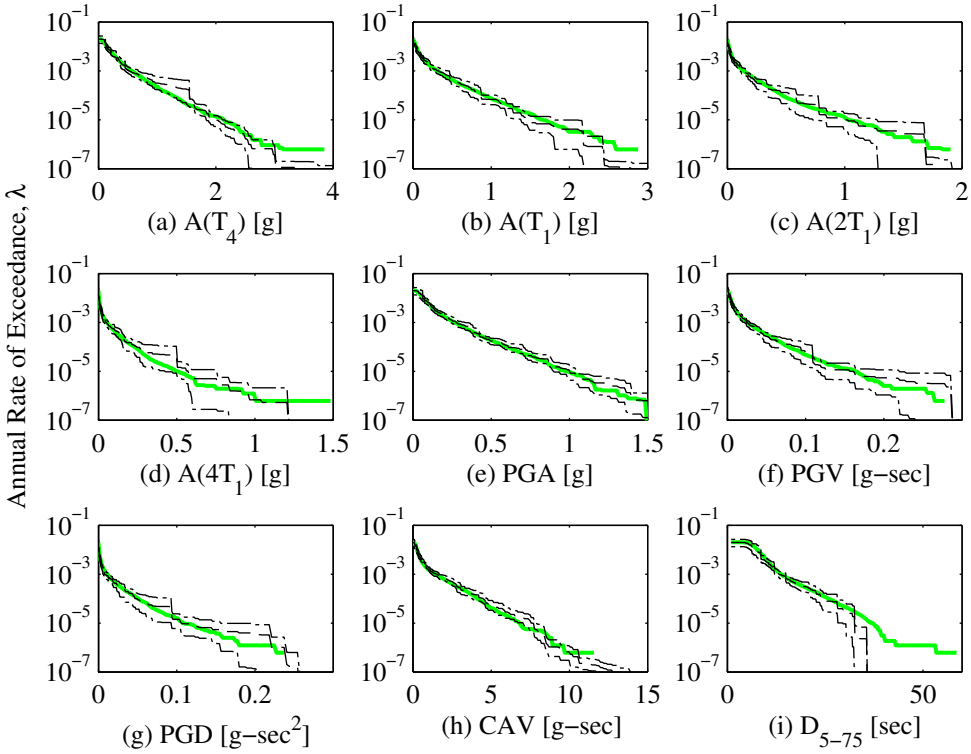

Figure 6.9: Hazard consistency of the motions selected with $SF_{max} = 5$ and $\gamma = 0.5$ for the 4-story frame, with respect to: (a) $A(T_4)$; (b) $A(T_1)$; (c) $A(2T_1)$; (d) $A(4T_1)$; (e) PGA; (f) PGV; (g) PGD; (h) CAV; and (i) D_{5-75}. Benchmark in solid green, estimate from IS in dashed black, and 95% CI of estimate from IS in chained black.

not less than that from unscaled motions (Fig 6.5). This is due to the fact that the IF for scaled ground motions is chosen herein out of convenience (i.e., by specifying $SF_{max} = 5$ and $\gamma = 0.5$ in Eq 4.12), instead of minimizing the epistemic uncertainty in hazard curves for IMs, as described at the end of Section 6.4 (see Fig 6.2).

The IS approach with scaling of ground motions, as described in this section, was also applied to nine SDF systems. For nearly all of the cases considered, the SDHCs from this approach are unbiased; for the cases where SDHCs from this approach are biased, the biases are relatively small and conservative. These results serve to remind us that the potential bias in any SDHC estimate is controlled directly by the hazard consistency of the particular set of ground motions with respect to sufficient IMs, and *not* by the GMSM procedure itself. Fortunately, the proposed IS procedure enables us to *directly* examine hazard consistency of the selected motions with respect to any IM of interest.

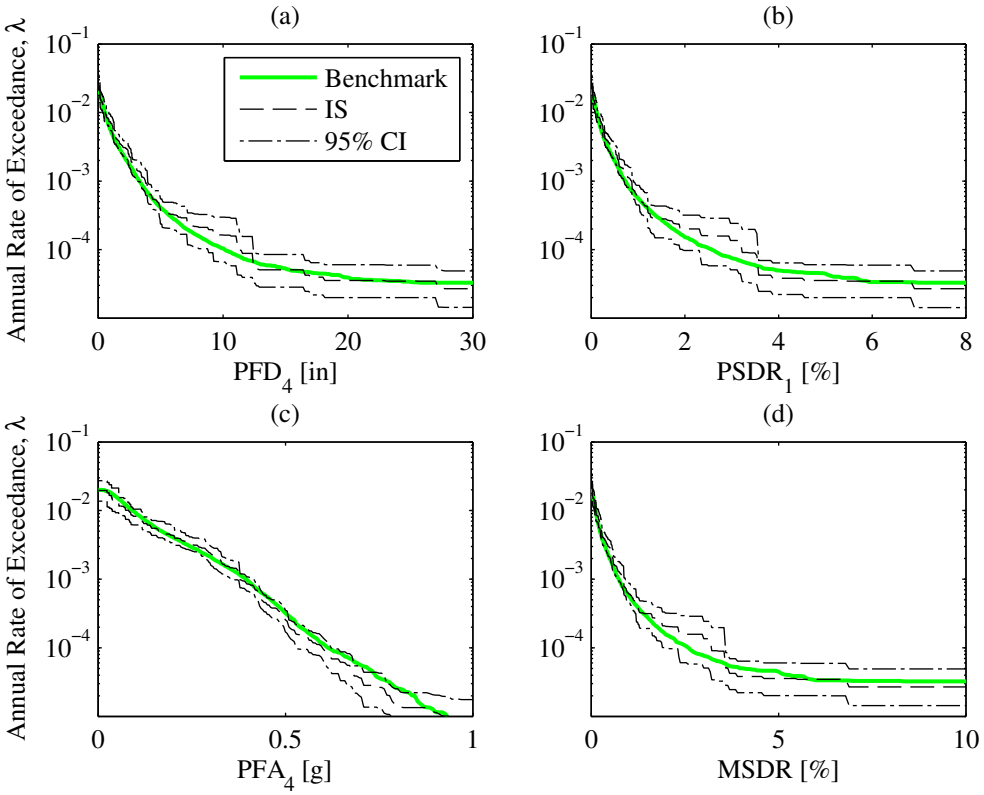

Figure 6.10: Comparison of SDHC estimates for several EDPs of the 4-story frame from IS, with $SF_{max} = 5$ and $\gamma = 0.5$, against benchmark.

6.7 Estimating SDHCs of multiple systems from a single ensemble of ground motions

In Section 6.5, we saw that ground motions selected from the IS approach can be hazard-consistent with respect to a wide range of IMs and exceedance rates, even though only four IMs were chosen to select ground motions. This was the case because (i) ground motions were unscaled, and (ii) the four IMs were judiciously chosen to correlate with many other features of the ground motion. In the limiting case where the selected motions are hazard-consistent with respect to an infinite number of IMs, the resulting SDHCs are guaranteed to be unbiased because a vector of an infinite number of IMs is sufficient for any EDP by definition (see Eq 5.1 in Section 5.2 and Section 6 in [64]). Thus, with hazard consistency enforced over a wide range of IMs and exceedance rates, it seems reasonable to expect the resulting SDHCs to be unbiased (see e.g., Figs 6.7 and 6.8). With these ideas in mind, can we somehow intelligently select a *single* ensemble of ground motions for estimating SDHCs of *multiple* systems – these could be alternate designs – at the same site?

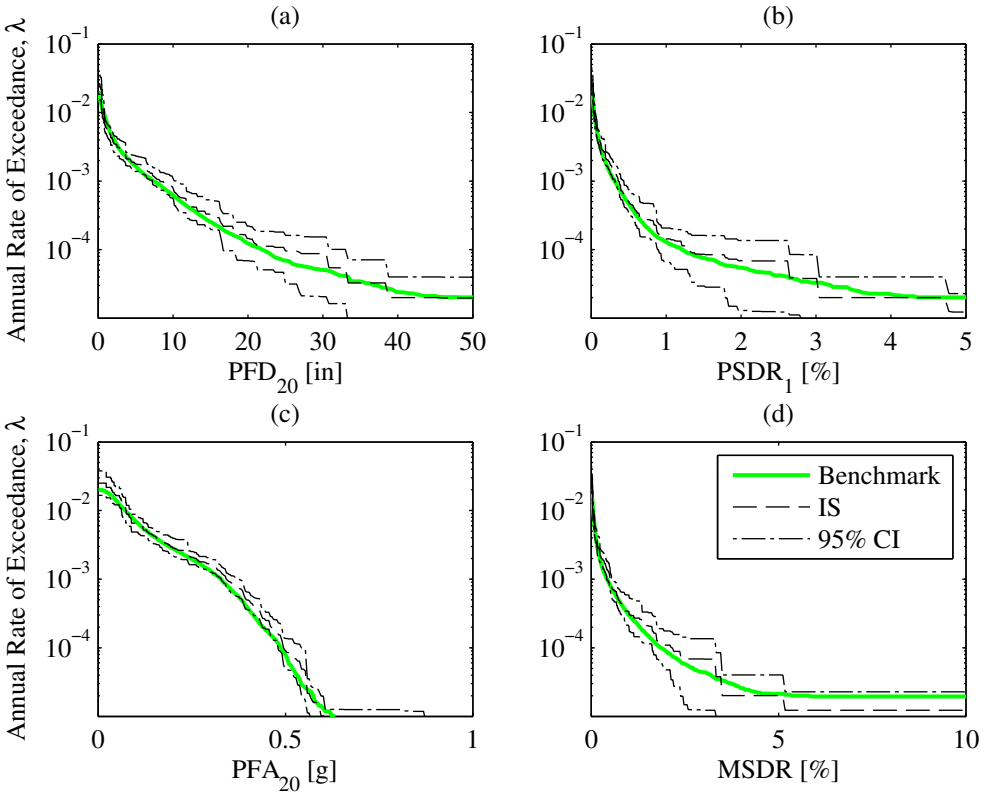

Figure 6.11: Comparison of SDHC estimates for several EDPs of the 20-story frame from IS, with $SF_{max} = 5$ and $\gamma = 0.5$, against benchmark.

To achieve this objective, one would perhaps need a vector of IMs that (i) covers virtually all aspects of the ground motion, and (ii) is not specific to a particular structure. In earthquake engineering, the three most important characteristics of ground motion are: (i) amplitude, (ii) frequency content, and (iii) duration [91]. Motivated by this idea, let us select ground motions with four non-structure specific IMs: (i) PGA, (ii) PGV, (iii) PGD, and (iv) D_{5-75}.

Using this vector of IMs and $g_1(\cdot)$ as the IF (Fig 6.1) in the IS approach, a single ensemble of $n = 300$ unscaled ground motions is selected. Fig 6.12 examines hazard consistency of these selected motions, with respect to nine IMs: (i) $A(0.1s)$, (ii) $A(1s)$, (iii) $A(5s)$, (iv) $A(10s)$, (v) PGA, (vi) PGV, (vii) PGD, (viii) CAV, and (ix) D_{5-75}. The motions are not only hazard-consistent with respect to the four IMs chosen for selection but *also* with respect to IMs such as CAV and spectral accelerations at various vibration periods. However, the hazard consistencies are occasionally limited to exceedance rates greater than 10^{-5} (e.g., Fig 6.12a) because $g_1(\cdot)$ is chosen as the IF (Fig 6.1); this suggests that the epistemic uncertainty in the resulting SDHCs may be large at low exceedance rates.

RHAs are performed for both multistory frames, subjected to the *same* set of $n = 300$

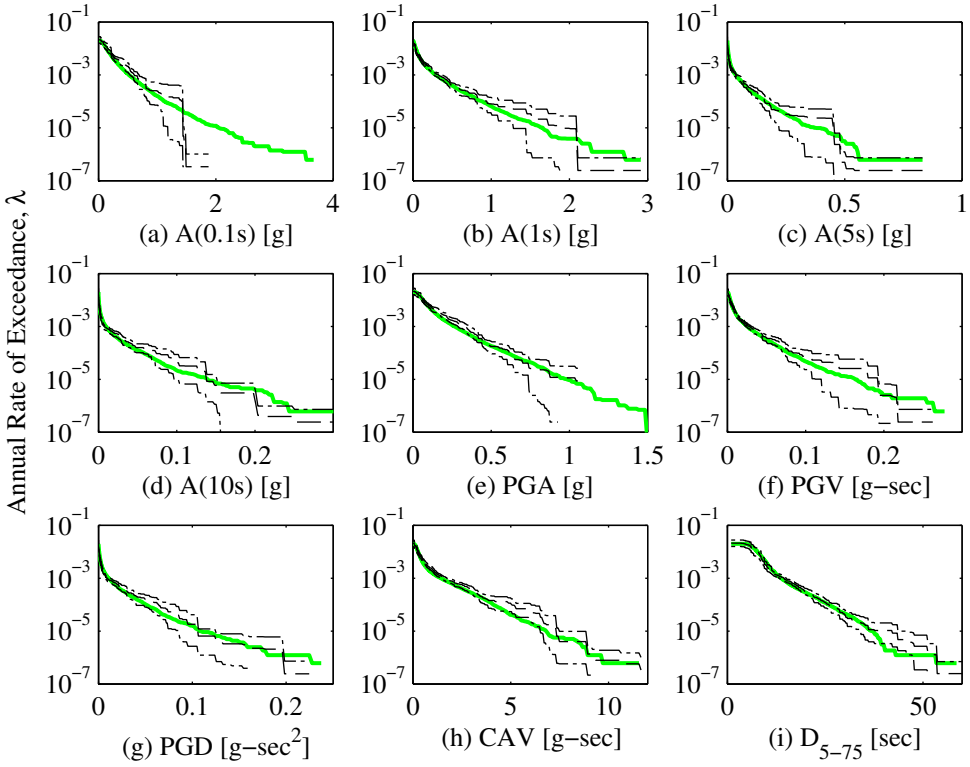

Figure 6.12: Hazard consistency of the motions selected from a non-structure specific **IM**, with respect to: (a) $A(0.1s)$; (b) $A(1s)$; (c) $A(5s)$; (d) $A(10s)$; (e) PGA; (f) PGV; (g) PGD; (h) CAV; and (i) D_{5-75}. Benchmark in solid green, estimate from IS in dashed black, and 95% CI of estimate from IS in chained black.

ground motions that are summarized in Fig 6.12. The resulting SDHCs of the 4-story and 20-story frames are presented in Figs 6.13 and 6.14, respectively. Based on these figures, the idea of selecting a *single* ensemble of ground motions for estimating SDHCs of *several* structures (and several EDPs for each structure) seems promising. Observe that the SDHCs of both frames are essentially unbiased for all EDPs considered. However, the epistemic uncertainty in the SDHCs at low exceedance rates is relatively large, compared to the results shown in Figs 6.4 and 6.5. This epistemic uncertainty can be reduced by increasing the sample size n and/or choosing a different IF (Fig 6.2).

6.8 Comparison with other GMSM procedures

Table 6.1 compares the effort involved when implementing IS in this study, without scaling ground motions, to compute SDHCs of a given structure at the specified site, against that from implementing GCIM (Chapter 5). The two procedures are similar in that a wide variety

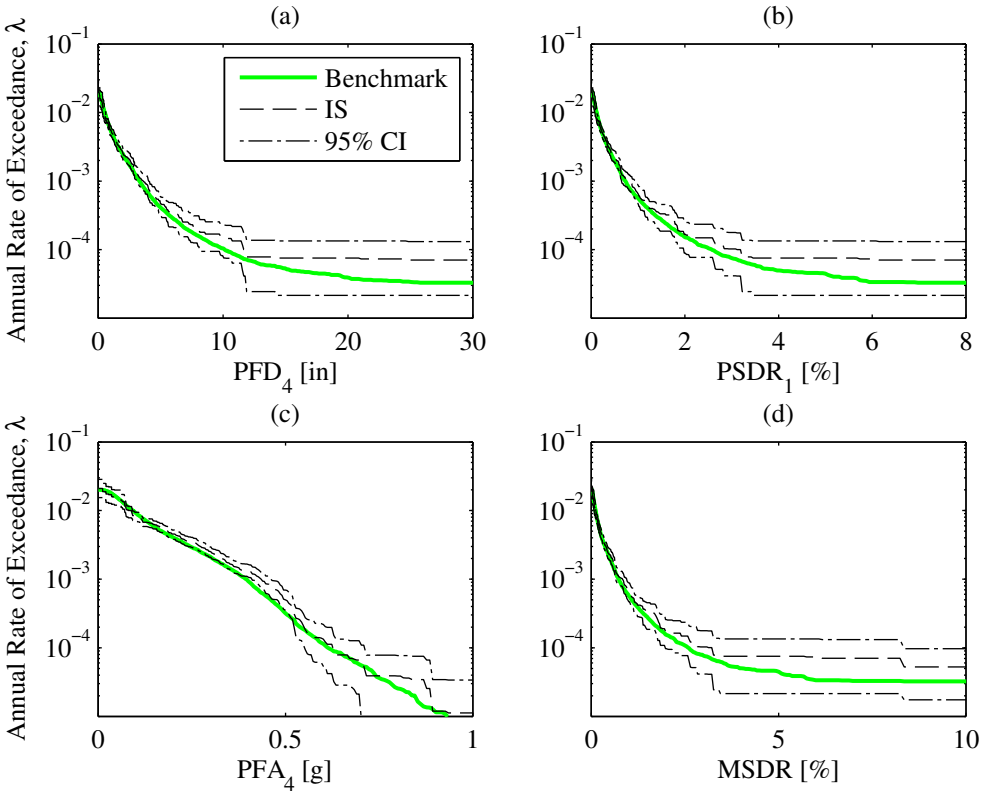

Figure 6.13: Comparison of SDHC estimates for several EDPs of the 4-story frame from a single non-structure specific set of ground motions, against benchmark.

of IMs can be chosen to select ground motions. Other than this attribute, the two procedures are very different.

Recall from Chapter 5 that the potential bias in a SDHC estimate is caused *directly* by hazard inconsistencies of the specific set of ground motions with respect to IMs that are influential to the response and *indirectly* by GMSM procedures; GMSM procedures are only tools to achieve hazard consistency with respect to a user-specified collection of IMs. For instance, GCIM aims to enforce hazard consistency by ensuring that the selected motions pass the KS tests at all intensity levels of the conditioning IM. Because hazard consistencies at low exceedance rates are occasionally controlled by the 'tail' of the GCIM distributions, the ground motions selected from GCIM may still remain hazard-inconsistent at low exceedance rates, despite passing all KS tests (see Figs 1-2 in [87]). In contrast (see Table 6.1 for how hazard consistency is enforced), the IS approach allows users to *directly* enforce hazard consistency through different choices of the IF, $g(\cdot)$.

In addition to hazard consistency, the other key issue that controls biases in SDHC estimates is IM sufficiency [12]. If a vector of IMs is known to be sufficient for the EDPs of interest, then *both* GCIM and IS may lead to unbiased SDHCs, as long as the resulting

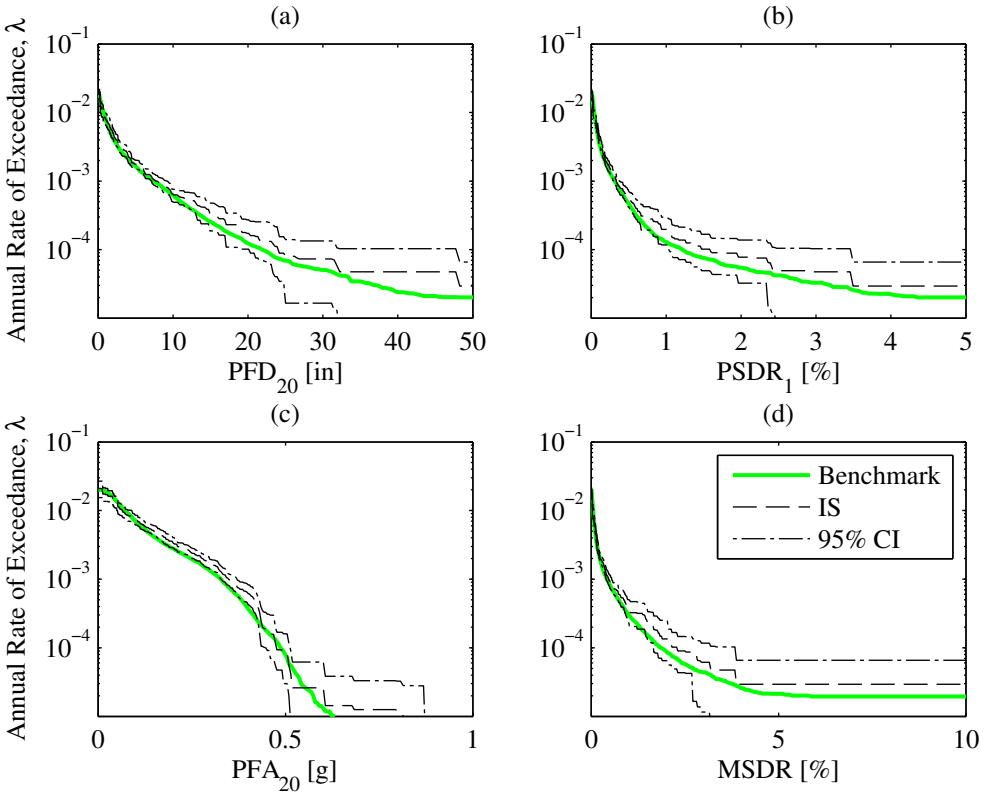

Figure 6.14: Comparison of SDHC estimates for several EDPs of the 20-story frame from the same set of ground motions utilized in Figs 6.12-6.13, against benchmark.

ground motions are hazard-consistent with respect to the sufficient IM. Unfortunately, it is difficult to identify IMs that are truly sufficient for complex, MDF systems and consequently, biases in the SDHC estimate may still exist despite achieving hazard consistency for a finite number of IMs. The GCIM approach strives to minimize such potential biases through two means: (i) by including a large number of 'orthogonal' IMs in the ground motion selection process, and (ii) by implementing the bias-checking procedure (Section 5.8). In contrast and as shown in Table 6.1, the IS approach strives to minimize potential SDHC biases by (i) minimizing the level of record scaling (including the possibility of no scaling at all), (ii) judiciously choosing the vector of IMs for ground motion selection, and (iii) carefully choosing the IF (Fig 6.2). Given that SDHCs from the IS approach are generally unbiased (e.g., Figs 6.7, 6.8, 6.10, 6.11, etc.), a procedure for checking bias does not appear to be necessary.

The IS approach simplifies the problem of selecting ground motions (for estimating SDHCs) in many ways. First, a *single* set of n ground motions is selected in IS to estimate SDHCs whereas in standard PSDA (Section 2.3), N_{IM^*} sets of n ground motions are selected. Instead of conducting N_{IM^*} deaggregations and computing N_{IM^*} different target

Table 6.1: Summary of effort involved in using GCIM and IS (without scaling ground motions) in this study to compute SDHCs of a given structure at the specified site.

Attribute	GCIM	IS
Conditioning IM	$IM^* = A(T_1)$	None
Can all ground motions be unscaled?	No	Yes
Limits on scaling of ground motions	No threshold	$SF_{max} = 1$, $\gamma = 0$
Type of IMs considered	Spectral accelerations, peak ground measures, spectrum intensities, cumulative effects	Spectral accelerations, peak ground measures, spectrum intensities, cumulative effects
Number of IMs used to select ground motions	24 IMs	4 IMs
Total number of PSHA-based calculations for selecting ground motions	$N_{IM^*} = 12$ deaggregations and GCIM distributions	1 target distribution for **IM**
Total number of ground motions used	$N_{IM^*} = 12$ sets of $n = 25$ ground motions	1 set of $n = 300$ ground motions
How hazard consistency is enforced	KS tests	Direct comparison of hazard curves
Is bias-checking procedure required?	Yes	May not be necessary
Can SDHCs for several systems be obtained from a single set of GMs?	No	Seems promising

distributions of **IM**, the target distribution of **IM** in IS is computed once (Eq 4.3). Second, good results can be obtained from the IS approach with just a small number of judiciously chosen IMs (four to six in this study, depending on the level of record scaling), whereas contemporary GMSM procedures often employ more than a dozen IMs (e.g., 17 IMs in [48], 20 IMs in [1], etc.). In exchange for unbiased SDHCs with low epistemic uncertainty from a small number of IMs however, the analyst must either (i) carefully choose the IF (Fig 6.2), or employ a very large number of unscaled ground motions. Third, a conditioning scalar IM does not need to be chosen in IS (see Table 6.1); in fact, the vector of IMs chosen in IS to select ground motions can be non-structure specific, suggesting the possibility of determining SDHCs of *multiple* systems, which may represent alternative designs at a fixed site, from a *single* ensemble of ground motions (Section 6.7).

6.9 Conclusions

An Importance Sampling (IS) based ground motion selection procedure was proposed for estimating SDHCs of structures at a specified site (Chapter 4). This procedure enables us to take advantage of unscaled yet intense ground motions for estimating SDHCs, through database-driven Importance Functions (IF). Moreover, it enables us to directly enforce hazard consistency of the selected motions with respect to a given set of IMs via various choices of the IF. In this study, we evaluate the IS procedure in its ability to accurately estimate SDHCs of multistory frames, leading to the following conclusions:

1. SDHCs from the IS approach are typically unbiased:
   a) When ground motions are unscaled, SDHCs from IS are unbiased for all EDPs, systems, and stochastic models considered.
   b) When ground motions are scaled (up to $SF_{max} = 5$), SDHCs from IS are unbiased for nearly all EDPs, systems, and stochastic models considered.
   c) The biased cases from scaling indicate that the vector of IMs chosen for ground motion selection is insufficient for those EDPs; i.e., hazard inconsistencies with respect to other IMs cause bias. The fact that no biases are observed when scaling is avoided implies that hazard inconsistencies with respect to other IMs are minimized when ground motions are unscaled.
2. The epistemic uncertainty in the SDHC estimates from the IS approach is controlled primarily by the IF and secondarily by the sample size, n.
3. Given a judiciously chosen IF, the IS approach greatly simplifies the problem of selecting ground motions to estimate SDHCs, by reducing the number of: (i) IMs chosen to select ground motions, (ii) target distributions of **IM** to be computed from PSHA, and (iii) sets of ground motions for RHAs.
4. With a non-structure specific vector of IMs and an appropriate choice of IF, the IS approach offers the ability to estimate SDHCs of *multiple* systems from a *single* ensemble of ground motions.

When interpreting the above conclusions, it should be borne in mind that a relatively simple site is studied. For a realistic site with many earthquake sources and uncertainty in source-to-site distance, the target probability distribution of **IM** (i.e., $f_{\mathbf{IM}}(\mathbf{x})$ from Eq 4.3) and the availability of recorded ground motions may collectively render it difficult to obtain a database-driven IF that covers the 'tail' of $f_{\mathbf{IM}}(\mathbf{x})$ (see Fig 4.1) while simultaneously avoiding record scaling. Furthermore, a realistic site may increase the computational time involved in computing IS weights (Eq 4.6), because Eq 4.3 must be evaluated for each of the n selected ground motions.

There are two limitations to the IS procedure:

1. The number of IMs chosen to select ground motions (Step 1) cannot be very large because a large number of IMs leads to two undesirable effects: (i) increase in epistemic uncertainty of the hazard curve estimates (Eqs 4.8-4.9), and (ii) increase in computational time involved in computing IS weights (see Eqs 4.6 and 4.3).

2. The potential bias and epistemic uncertainty of the hazard curve estimates are highly dependent on the choice of the IF (Section 6.4).

Chapter 7

Conclusions

In this dissertation, the issue of selecting and scaling ground motions for estimating seismic demand hazard curves (SDHCs) of structures is investigated. The key contributions are summarized as follows:

1. An approach to rigorously quantify potential biases in SDHC estimates from ground motion selection and modification (GMSM) procedures is developed, leading to the important notion of a *benchmark SDHC*.

2. Based on the concept of Importance Sampling, a novel ground motion selection procedure is developed that allows: (i) hazard consistency to be directly enforced for a user-specified collection of IMs, and (ii) SDHCs of a structure to be estimated from a single ensemble of ground motions, with the option of avoiding record scaling altogether.

3. Contemporary GMSM procedures are evaluated for a variety of structures and response quantities in their ability to accurately estimate SDHCs at a given site.

This investigation has led to the following major conclusions:

1. Biases in SDHC estimates are caused *directly* by hazard inconsistencies of the specific selection of ground motions with respect to intensity measures (IMs) that are influential to the response and *indirectly* by GMSM procedures; such procedures are only a means for enforcing hazard consistency of a particular selection of ground motions, with respect to a user-specified collection of IMs.

2. As long as ground motions are selected to be hazard-consistent with respect to an IM that is sufficient, the resulting estimates of the SDHC are unbiased, irrespective of the level of record scaling.

3. Given that a particular selection of ground motions is hazard-consistent with respect to a vector of IMs, any bias observed in the resulting estimate of the SDHC implies that

the vector of IMs is *insufficient* for that particular response quantity. The concept of a benchmark, developed in Chapters 2-3, enables such biases to be directly determined and hence, insufficient IMs to be identified.

4. Based on the evaluation of three contemporary GMSM procedures – (i) "exact" Conditional Spectrum (CSexact), (ii) Generalized Conditional Intensity Measure (GCIM), and (iii) Importance Sampling (IS) – the following can be concluded:

   a) The SDHCs from CSexact are unbiased for many systems and response quantities but in some cases, the annual rate of collapse is overestimated and floor accelerations are underestimated. The epistemic uncertainty in the SDHCs is relatively small.

   b) The SDHCs from GCIM are unbiased for many systems and response quantities but in few cases, the floor accelerations are underestimated. The epistemic uncertainty in the SDHCs is relatively small.

   c) The SDHCs from IS are unbiased for all systems and response quantities considered when record scaling is avoided altogether; however, the epistemic uncertainty in the SDHCs depends on the Importance Function chosen to select ground motions. When ground motions are scaled in IS, both the SDHC bias and epistemic uncertainty depend on the IMs and the Importance Function chosen to select ground motions.

The work in this dissertation is limited in that:

1. Only two multistory frames and nine SDF systems (with degrading hysteresis) are considered.

2. The site considered is relatively simple.

3. Only a single horizontal component of ground motion is studied herein.

4. Near-fault effects are not considered.

Future research should consider more structural systems and sites to confirm the generality of the conclusions presented herein.

Bibliography

[1] Nirmal Jayaram, Ting Lin, and Jack W Baker. A computationally efficient ground-motion selection algorithm for matching a target response spectrum mean and variance. *Earthquake Spectra*, 27(3):797–815, 2011.

[2] Keith Porter, Robert Kennedy, and Robert Bachman. Creating fragility functions for performance-based earthquake engineering. *Earthquake Spectra*, 23(2):471–489, 2007.

[3] Applied Technology Council. Seismic performance assessment of buildings, Volume 1 - Methodology, FEMA P-58-1. Technical report, Federal Emergency Management Agency, 2012.

[4] MC CHAPMAN. A probabilistic approach to ground-motion selection for engineering design. *Bulletin of the Seismological Society of America*, 85(3):937–942, JUN 1995. PT: J; NR: 5; TC: 26; J9: B SEISMOL SOC AM; PG: 6; GA: RC529; UT: WOS:A1995RC52900022.

[5] Jonathan P. Stewart and Pacific Earthquake Engineering Research Center. *Ground motion evaluation procedures for performance-based design*. Pacific Earthquake Engineering Research Center, Berkeley, 2001. ID: 48433559.

[6] ASCE. *Minimum design loads for buildings and other structures, ASCE Standard No. 7-10*. American Society of Civil Engineers: Structural Engineering Institute, Reston, VA, 2010.

[7] PK Malhotra. Strong-motion records for site-specific analysis. *Earthquake Spectra*, 19(3):557–578, AUG 2003. PT: J; UT: WOS:000186485900005.

[8] Albert Kottke and Ellen M. Rathje. A semi-automated procedure for selecting and scaling recorded earthquake motions for dynamic analysis. *Earthquake Spectra*, 24(4):911–932, NOV 2008. PT: J; UT: WOS:000264125600005.

[9] Jack W. Baker and C. Allin Cornell. Spectral shape, epsilon and record selection. *Earthquake Engineering & Structural Dynamics*, 35(9):1077–1095, JUL 25 2006. PT: J; UT: WOS:000239034000002.

[10] S Akkar and Ö Özen. Effect of peak ground velocity on deformation demands for sdof systems. *Earthquake engineering & structural dynamics*, 34(13):1551–1571, 2005.

[11] Rafael Riddell. On ground motion intensity indices. *Earthquake Spectra*, 23:147, 2007.

[12] Nicolas Luco and C Allin Cornell. Structure-specific scalar intensity measures for near-source and ordinary earthquake ground motions. *Earthquake Spectra*, 23:357, 2007.

[13] Dixiong Yang, Jianwei Pan, and Gang Li. Non-structure-specific intensity measure parameters and characteristic period of near-fault ground motions. *Earthquake Engineering & Structural Dynamics*, 38(11):1257–1280, 2009.

[14] E. Kalkan and A. K. Chopra. Modal-pushover-based ground-motion scaling procedure. *Journal of Structural Engineering*, 137:298, 2011.

[15] N. Shome, P. Bazzurro, and J. E. Carballo. Earthquakes, records, and nonlinear responses. *Earthquake Spectra*, 14:469, 1998.

[16] JJ Bommer and AB Acevedo. The use of real earthquake accelerograms as input to dynamic analysis. *Journal of Earthquake Engineering*, 8:43–91, 2004. PT: J; CT: 3rd International ROSE-School Seminar; CY: JUN 23-24, 2003; CL: Pavia, ITALY; SI: 1; UT: WOS:000223920600004.

[17] J. Watson-Lamprey and N. Abrahamson. Selection of ground motion time series and limits on scaling. *Soil Dynamics and Earthquake Engineering*, 26(5):477–482, MAY 2006. PT: J; UT: WOS:000236790500011.

[18] I. Iervolino and CA Cornell. Record selection for nonlinear seismic analysis of structures. *Earthquake Spectra*, 21(3):685–713, AUG 2005. PT: J; UT: WOS:000231277200004.

[19] Nicolas Luco and Paolo Bazzurro. Does amplitude scaling of ground motion records result in biased nonlinear structural drift responses? *Earthquake Engineering & Structural Dynamics*, 36(13):1813–1835, OCT 25 2007. PT: J; UT: WOS:000250650100002.

[20] Jack W Baker. Measuring bias in structural response caused by ground motion scaling. In *8th Pacific Conference on Earthquake Engineering, Singapore*, 2007.

[21] Mircea Grigoriu. To scale or not to scale seismic ground-acceleration records. *Journal of Engineering Mechanics*, 137(4):284–293, 2010.

[22] Anil K. Chopra. *Dynamics of structures : theory and applications to earthquake engineering*. Pearson Prentice Hall, Upper Saddle River, NJ, 4th edition, 2011.

[23] Jack W Baker and C Allin Cornell. Which spectral acceleration are you using? *Earthquake Spectra*, 22:293, 2006.

[24] Polsak Tothong and Nicolas Luco. Probabilistic seismic demand analysis using advanced ground motion intensity measures. *Earthquake Engineering & Structural Dynamics*, 36(13):1837–1860, 2007.

[25] Jack W. Baker. Conditional mean spectrum: Tool for ground-motion selection. *Journal of Structural Engineering-Asce*, 137(3):322–331, MAR 2011. PT: J; SI: SI; UT: WOS:000288523100006.

[26] Curt B. Haselton. Evaluation of ground motion selection and modification methods: Predicting median interstory drift response of buildings. Technical Report 01, 2009.

[27] Evangelos I Katsanos, Anastasios G Sextos, and George D Manolis. Selection of earthquake ground motion records: A state-of-the-art review from a structural engineering perspective. *Soil Dynamics and Earthquake Engineering*, 30(4):157–169, 2010.

[28] YeongAe Heo, Sashi K Kunnath, and Norman Abrahamson. Amplitude-scaled versus spectrum-matched ground motions for seismic performance assessment. *ASCE Journal of Structural Engineering*, 137(3):278–288, 2010.

[29] Jonathan Hancock, Julian J. Bommer, and Peter J. Stafford. Numbers of scaled and matched accelerograms required for inelastic dynamic analyses. *Earthquake Engineering & Structural Dynamics*, 37(14):1585–1607, NOV 2008. PT: J; UT: WOS:000260692500001.

[30] Jennie Anne Watson-Lamprey. *Selection and scaling of ground motion time series*. PhD thesis, University of California Berkeley, 2007.

[31] NEHRP Consultants Joint Venture. Selecting and scaling earthquake ground motions for performing response-history analyses, NIST GCR 11-917-15. Technical report, National Institute of Standards and Technology, 2011.

[32] Robin K. McGuire. *Seismic hazard and risk analysis*. Earthquake Engineering Research Institute, Oakland, Calif., 2004. ID: 56501500.

[33] Nilesh Shome. *Probabilistic seismic demand analysis of nonlinear structures*. PhD thesis, Stanford University, 1999.

[34] Brendon A Bradley. A comparison of intensity-based demand distributions and the seismic demand hazard for seismic performance assessment. *Earthquake Engineering & Structural Dynamics*, 42(15):2235–2253, 2013.

[35] B.A. Bradley. The seismic demand hazard and importance of the conditioning intensity measure. *Earthquake Engineering & Structural Dynamics*, 2012.

[36] JW Baker and CA Cornell. A vector-valued ground motion intensity measure consisting of spectral acceleration and epsilon. *Earthquake Engineering & Structural Dynamics*, 34(10):1193–1217, AUG 2005. PT: J; UT: WOS:000230977000001.

[37] Ting Lin, Curt B Haselton, and Jack W Baker. Conditional spectrum-based ground motion selection. part i: Hazard consistency for risk-based assessments. *Earthquake Engineering & Structural Dynamics*, 2013.

[38] Jack W Baker. Probabilistic structural response assessment using vector-valued intensity measures. *Earthquake Engineering & Structural Dynamics*, 36(13):1861–1883, 2007.

[39] Larry Wasserman. *All of statistics : a concise course in statistical inference*. Springer, New York, 2004. ID: 52901588.

[40] D. Vamvatsikos and CA Cornell. Applied incremental dynamic analysis. *Earthquake Spectra*, 20(2):523–553, MAY 2004. PT: J; UT: WOS:000230959900012.

[41] Edward H Field, Nitin Gupta, Vipin Gupta, Michael Blanpied, Philip Maechling, and Thomas H Jordan. Hazard calculations for the wgcep-2002 earthquake forecast using opensha and distributed object technologies. *Seismological Research Letters*, 76(2):161–167, 2005.

[42] Kenneth W Campbell and Yousef Bozorgnia. Nga ground motion model for the geometric mean horizontal component of pga, pgv, pgd and 5% damped linear elastic response spectra for periods ranging from 0.01 to 10 s. *Earthquake Spectra*, 24:139, 2008.

[43] David M Boore and Gail M Atkinson. Ground-motion prediction equations for the average horizontal component of PGA, PGV, and 5%-damped PSA at spectral periods between 0.01 s and 10.0 s. *Earthquake Spectra*, 24(1):99–138, 2008.

[44] Norman Abrahamson and Walter Silva. Summary of the Abrahamson & Silva NGA ground-motion relations. *Earthquake Spectra*, 24(1):67–97, 2008.

[45] BrianS-J Chiou and Robert R Youngs. An NGA model for the average horizontal component of peak ground motion and response spectra. *Earthquake Spectra*, 24(1):173–215, 2008.

[46] D. Vamvatsikos and CA Cornell. Incremental dynamic analysis. *Earthquake Engineering & Structural Dynamics*, 31(3):491–514, MAR 2002. PT: J; UT: WOS:000173870500002.

[47] Brendon A Bradley. A generalized conditional intensity measure approach and holistic ground-motion selection. *Earthquake Engineering & Structural Dynamics*, 39(12):1321–1342, 2010.

[48] B.A. Bradley. A ground motion selection algorithm based on the generalized conditional intensity measure approach. *Soil Dynamics and Earthquake Engineering*, 40:48–61, 2012.

[49] Applied Technology Council. Quantification of building seismic performance factors, FEMA P695. Technical report, Federal Emergency Management Agency, 2009.

[50] Maurice Power, Brian Chiou, Norman Abrahamson, Yousef Bozorgnia, Thomas Shantz, and Clifford Roblee. An overview of the NGA project. *Earthquake Spectra*, 24(1):3–21, 2008.

[51] Robin K McGuire. Probabilistic seismic hazard analysis and design earthquakes: Closing the loop. *Bulletin of the Seismological Society of America*, 85(5):1275–1284, 1995.

[52] Paolo Bazzurro and C Allin Cornell. Disaggregation of seismic hazard. *Bulletin of the Seismological Society of America*, 89(2):501–520, 1999.

[53] Nirmal Jayaram and Jack W Baker. Statistical tests of the joint distribution of spectral acceleration values. *Bulletin of the Seismological Society of America*, 98(5):2231–2243, 2008.

[54] Jack W Baker and C Allin Cornell. Correlation of response spectral values for multicomponent ground motions. *Bulletin of the Seismological Society of America*, 96(1):215–227, 2006.

[55] Jack W Baker and Nirmal Jayaram. Correlation of spectral acceleration values from nga ground motion models. *Earthquake Spectra*, 24:299, 2008.

[56] Andrew Edward Seifried. *Response spectrum compatibilization and its impact on structural response assessment*. PhD thesis, Stanford University, 2013.

[57] Ting Lin, Stephen C Harmsen, Jack W Baker, and Nicolas Luco. Conditional spectrum computation incorporating multiple causal earthquakes and ground-motion prediction models. *Bulletin of the Seismological Society of America*, 103(2A):1103–1116, 2013.

[58] Brian Carlton and Norman Abrahamson. Issues and approaches for implementing conditional mean spectra in practice. *Bulletin of the Seismological Society of America*, 104(1):503–512, 2014.

[59] Polsak Tothong and C Allin Cornell. An empirical ground-motion attenuation relation for inelastic spectral displacement. *Bulletin of the Seismological Society of America*, 96(6):2146–2164, 2006.

[60] Brendon A Bradley. Site-specific and spatially distributed ground-motion prediction of acceleration spectrum intensity. *Bulletin of the Seismological Society of America*, 100(2):792–801, 2010.

[61] Kenneth W Campbell and Yousef Bozorgnia. A ground motion prediction equation for the horizontal component of cumulative absolute velocity (CAV) based on the PEER-NGA strong motion database. *Earthquake Spectra*, 26(3):635–650, 2010.

[62] Julian J Bommer, Peter J Stafford, and John E Alarcón. Empirical equations for the prediction of the significant, bracketed, and uniform duration of earthquake ground motion. *Bulletin of the Seismological Society of America*, 99(6):3217–3233, 2009.

[63] John Douglas and Hideo Aochi. A survey of techniques for predicting earthquake ground motions for engineering purposes. *Surveys in geophysics*, 29(3):187–220, 2008.

[64] N. Simon Kwong, Anil K. Chopra, and Robin K. McGuire. A framework for the evaluation of ground motion selection and modification procedures. *Earthquake Engineering & Structural Dynamics*, 44(5):795–815, 2014. DOI: 10.1002/eqe.2502.

[65] Jack W Baker. Efficient analytical fragility function fitting using dynamic structural analysis. *Earthquake Spectra*, 2014. (in press).

[66] Sanaz Rezaeian and Armen Der Kiureghian. Simulation of synthetic ground motions for specified earthquake and site characteristics. *Earthquake Engineering & Structural Dynamics*, 39(10):1155–1180, 2010.

[67] Yoshifumi Yamamoto. *Stochastic model for earthquake ground motion using wavelet packets*. Stanford University, 2011.

[68] Robert R Youngs and Kevin J Coppersmith. Implications of fault slip rates and earthquake recurrence models to probabilistic seismic hazard estimates. *Bulletin of the Seismological society of America*, 75(4):939–964, 1985.

[69] Sanaz Rezaeian and Armen Der Kiureghian. A stochastic ground motion model with separable temporal and spectral nonstationarities. *Earthquake Engineering & Structural Dynamics*, 37(13):1565–1584, 2008.

[70] Yoshifumi Yamamoto and Jack W Baker. Stochastic model for earthquake ground motion using wavelet packets. *Bulletin of the Seismological Society of America*, 103(6):3044–3056, 2013.

[71] H. Bobadilla and Anil K. Chopra. Modal pushover analysis for seismic evaluation of reinforced concrete special moment resisting frame buildings. Technical report, Earthquake Engineering Research Center: University of California, Berkeley, 2007.

[72] Luis F Ibarra, Ricardo A Medina, and Helmut Krawinkler. Hysteretic models that incorporate strength and stiffness deterioration. *Earthquake engineering & structural dynamics*, 34(12):1489–1511, 2005.

[73] Sheldon M. Ross. *Simulation*. Elsevier, 2013.

[74] Bradley Efron and Robert Tibshirani. *An introduction to the bootstrap*, volume 57. Chapman & Hall/CRC, 1993.

[75] Norman Abrahamson, Gail Atkinson, David Boore, Yousef Bozorgnia, Kenneth Campbell, Brian Chiou, IM Idriss, Walter Silva, and Robert Youngs. Comparisons of the NGA ground-motion relations. *Earthquake Spectra*, 24(1):45–66, 2008.

[76] Jack W Baker. *Vector-valued ground motion intensity measures for probabilistic seismic demand analysis*. PhD thesis, 2006.

[77] Yousef Bozorgnia and Vitelmo V. Bertero. *Earthquake engineering : from engineering seismology to performance-based engineering*. CRC Press, Boca Raton, Fla., 2004. ID: 53306604.

[78] N. Simon Kwong, Anil K. Chopra, and Robin K. McGuire. Evaluation of ground motion selection and modification procedures using synthetic ground motions. *Earthquake Engineering & Structural Dynamics*, 2015. DOI: 10.1002/eqe.2558.

[79] CB Haselton and JW Baker. Ground motion intensity measures for collapse capacity prediction: Choice of optimal spectral period and effect of spectral shape. In *8th National Conference on Earthquake Engineering*, pages 18–22, 2006.

[80] Brendon A Bradley. Empirical correlations between cumulative absolute velocity and amplitude-based ground motion intensity measures. *Earthquake Spectra*, 28(1):37–54, 2012.

[81] Jack R. Benjamin and C. Allin Cornell. *Probability, Statistics and Decision for Civil Engineers*. McGraw Hill Book Company, 1970.

[82] A. D. Kiureghian. Nonergodicity and peer's framework formula. *Earthquake Engineering & Structural Dynamics*, 34(13):1643–1652, 2005.

[83] Christine A Goulet, Curt B Haselton, Judith Mitrani-Reiser, James L Beck, Gregory G Deierlein, Keith A Porter, and Jonathan P Stewart. Evaluation of the seismic performance of a code-conforming reinforced-concrete frame buildingfrom seismic hazard to collapse safety and economic losses. *Earthquake Engineering & Structural Dynamics*, 36(13):1973–1997, 2007.

[84] Silvia Mazzoni, Frank McKenna, Michael H Scott, Gregory L Fenves, et al. Opensees command language manual. *Pacific Earthquake Engineering Research (PEER) Center*, 2006.

[85] Brendon A Bradley. Seismic hazard epistemic uncertainty in the san francisco bay area and its role in performance-based assessment. *Earthquake Spectra*, 25(4):733–753, 2009.

[86] Armen Der Kiureghian and Kazuya Fujimura. Nonlinear stochastic dynamic analysis for performance-based earthquake engineering. *Earthquake Engineering & Structural Dynamics*, 38(5):719–738, 2009.

[87] N. Simon Kwong, Anil K. Chopra, and Robin K. McGuire. Authors reply to the discussion by brendon a. bradley of a framework for the evaluation of ground motion selection and modification procedures. *Earthquake Engineering & Structural Dynamics*, 44(5):823–828, 2015.

[88] Ting Lin. *Advancement of hazard-consistent ground motion selection methodology*. PhD thesis, Stanford University, 2012.

[89] AHS Ang and WH Tang. *Probability Concepts in Engineering: Emphasis on Applications to Civil and Environmental Engineering (v. 1)*. John Wiley Publishers, 2007.

[90] Brendon A Bradley. Empirical equations for the prediction of displacement spectrum intensity and its correlation with other intensity measures. *Soil Dynamics and Earthquake Engineering*, 31(8):1182–1191, 2011.

[91] Steven L Kramer. *Geotechnical earthquake engineering*, volume 1. Prentice-Hall Civil Engineering and Engineering Mechanics Series, Upper Saddle River, NJ: Prentice Hall,— c1996, 1996.

[92] Yousef Bozorgnia, Norman A Abrahamson, Linda Al Atik, Timothy D Ancheta, Gail M Atkinson, Jack W Baker, Annemarie Baltay, David M Boore, Kenneth W Campbell, Brian S-J Chiou, et al. Nga-west2 research project. *Earthquake Spectra*, 30(3):973–987, 2014.

Appendix A

Derivations for the proposed Importance Sampling procedure

A.1 Derivation for Eq 4.7a

Let a randomly generated vector of IMs from the Importance Function (IF), $g_{\mathbf{X}}(\mathbf{x})$, be denoted by $\mathbf{X}$ and let a random sample of n vector-valued IMs be denoted by $\{\mathbf{X}_1, \ldots, \mathbf{X}_n\}$. Let a single element of the vector $\mathbf{X}_i$ be denoted by X_i and the rest of its elements be denoted by $\mathbf{X}_i^c$; that is, $\mathbf{X}_i = \{X_i, \mathbf{X}_i^c\}$. The resulting estimate of the hazard curve for an IM [1] is given by Eq 4.5a, repeated here for convenience:

$$\widehat{\lambda}_{IM}(x) = \frac{\nu_0}{n} \sum_{i=1}^{n} [I(X_i > x) \cdot w(\mathbf{X}_i)] \tag{A.1}$$

where x_i is capitalized and w_i is replaced by $w(\mathbf{X}_i)$ to emphasize that the hazard curve estimate is random because the IMs generated from the IF are random.

[1] Only IMs included in **IM** are considered in this section.

Taking the expectation of $\widehat{\lambda}_{IM}(x)$ in Eq A.1 with respect to $g_{\mathbf{X}}(\mathbf{x})$ gives

$$\begin{aligned}
\mathbb{E}_{\mathbf{X}}\left[\widehat{\lambda}_{IM}(x)\right] &= \nu_0 \cdot \mathbb{E}_{\mathbf{X}}\left[I(X_1 > x) \cdot w(\mathbf{X}_1)\right] \\
&= \nu_0 \int_{\mathbf{s}} \left[I(s > x) \cdot w(\mathbf{s})\right] \, g(\mathbf{s}) \, \mathrm{d}\mathbf{s} \\
&= \nu_0 \int_{s} \int_{\mathbf{s}^c} \left[I(s > x) \, f(\mathbf{s})\right] \mathrm{d}\mathbf{s}^c \, \mathrm{d}s \\
&= \nu_0 \int_{s} I(s > x) \left(\int_{\mathbf{s}^c} f(\mathbf{s}) \, \mathrm{d}\mathbf{s}^c \right) \mathrm{d}s \\
&= \nu_0 \int_{x}^{\infty} f(s) \, \mathrm{d}s \\
&= \lambda_{IM}(x) \qquad \text{(A.2)}
\end{aligned}$$

where each transition is obtained from:

1. Each i^{th} vector, $\mathbf{X}_i$, is independent and identically distributed, with the joint distribution as $g_{\mathbf{X}}(\mathbf{x})$.
2. Rule of the lazy statistician.
3. Definition of Importance Sampling weight and rewriting domain of integration.
4. Indicator function does not depend on $\mathbf{s}^c$.
5. Definition of the indicator function and definition of the marginal distribution, $f_X(s)$, relative to the joint distribution, $f_{\mathbf{X}}(\mathbf{s})$.
6. Definition of the complementary cumulative distribution function (CCDF) and application of Eq 4.2.

A.2 Derivation for Eq 4.7b

Let a randomly generated vector of IMs from the Importance Function (IF), $g_{\mathbf{X}}(\mathbf{x})$, be denoted by $\mathbf{X}$ and let a random sample of n vector-valued IMs be denoted by $\{\mathbf{X}_1, \ldots, \mathbf{X}_n\}$. Each vector-valued IM corresponds to a ground motion time series and hence, a random sample of vector-valued IMs corresponds to an ensemble of n ground motions. Let an arbitrary EDP of the ith ground motion be denoted by Z_i. The resulting estimate of the hazard curve for an EDP is given by Eq 4.5b, repeated here for convenience:

$$\widehat{\lambda}_{EDP}(z) = \frac{\nu_0}{n} \sum_{i=1}^{n} \left[I(Z_i > z) \cdot w(\mathbf{X}_i)\right] \qquad \text{(A.3)}$$

where z_i is capitalized and w_i is replaced by $w(\mathbf{X}_i)$ to emphasize that the hazard curve estimate is random because the IMs generated from the IF are random. By introducing the IF, $g_{\mathbf{X}}(\mathbf{x})$, the joint probability distribution of Z and $\mathbf{X}$, denoted by $f_{Z,\mathbf{X}}(z,\mathbf{x}) = f_{Z|\mathbf{X}}(z \mid \mathbf{x}) \cdot f_{\mathbf{X}}(\mathbf{x})$ (see Fig 4.2), becomes $g_{Z,\mathbf{X}}(z,\mathbf{x}) = f_{Z|\mathbf{X}}(z \mid \mathbf{x}) \cdot g_{\mathbf{X}}(\mathbf{x})$.

Taking the expectation of $\widehat{\lambda}_Z(z)$ in Eq A.3 with respect to $g_{Z,\mathbf{X}}(z,\mathbf{x})$ gives

$$\begin{aligned}
\mathbb{E}_{Z,\mathbf{X}}\left[\widehat{\lambda}_{EDP}(z)\right] &= \nu_0 \cdot \mathbb{E}_{Z,\mathbf{X}}\left[I(Z_1 > z) \cdot w(\mathbf{X}_1)\right] \\
&= \nu_0 \int_t \int_{\mathbf{s}} \left[I(t > z) \cdot w(\mathbf{s})\right] \, g_{Z,\mathbf{X}}(t,\mathbf{s}) \, \mathrm{d}\mathbf{s} \, \mathrm{d}t \\
&= \nu_0 \int_t I(t > z) \int_{\mathbf{s}} w(\mathbf{s}) \left[f_{Z|\mathbf{X}}(t \mid \mathbf{s}) \, g(\mathbf{s})\right] \mathrm{d}\mathbf{s} \, \mathrm{d}t \\
&= \nu_0 \int_z^{\infty} \left(\int_{\mathbf{s}} f(\mathbf{s}) \, f_{Z|\mathbf{X}}(t \mid \mathbf{s}) \, \mathrm{d}\mathbf{s} \right) \mathrm{d}t \\
&= \nu_0 \int_z^{\infty} f_Z(t) \, \mathrm{d}t \\
&= \lambda_{EDP}(z) \qquad \text{(A.4)}
\end{aligned}$$

where each transition is obtained from:

1. Each i^{th} vector $(\mathbf{X}, Z)_i$ is independent and identically distributed, with the joint distribution as $g_{Z,\mathbf{X}}(t,\mathbf{s}) = f_{Z|\mathbf{X}}(t \mid \mathbf{s}) \cdot g(\mathbf{s})$.
2. Rule of the lazy statistician.
3. Indicator function does not depend on $\mathbf{s}$ and definition of joint distribution $g_{Z,\mathbf{X}}(t,\mathbf{s})$.
4. Definitions of the indicator function and of the Importance Sampling weight.
5. Marginal distribution $f_Z(t)$ from joint distribution $f_{Z,\mathbf{X}}(t,\mathbf{s}) = f(\mathbf{s}) \cdot f_{Z|\mathbf{X}}(t \mid \mathbf{s})$ (see Fig 4.2).
6. Definition of CCDF and use of Eq 4.2.

The expected values of the hazard curve estimates for IMs that are excluded from those chosen to select ground motions (i.e., $IM \notin \mathbf{IM}$) may be derived in a fashion similar to that presented in this section.

A.3 Derivation for Eq 4.8

The variance of $\widehat{\lambda}_{IM}(x)$ in Eq A.1, with respect to the joint distribution of $\mathbf{X}$, is

$$\begin{aligned}
\mathbb{V}_{\mathbf{X}}\left[\widehat{\lambda}_{IM}(x)\right] &= \frac{\nu_0^2}{n} \cdot \mathbb{V}_{\mathbf{X}}\left[I(X_1 > x) \cdot w(\mathbf{X}_1)\right] \\
&= \frac{\nu_0^2}{n}\left\{\mathbb{E}_{\mathbf{X}}\left[\left[I(X_1 > x) \cdot w(\mathbf{X}_1)\right]^2\right] - \left(\mathbb{E}_{\mathbf{X}}\left[I(X_1 > x) \cdot w(\mathbf{X}_1)\right]\right)^2\right\} \\
&= \frac{1}{n}\left\{\nu_0^2 \cdot \mathbb{E}_{\mathbf{X}}\left[\left[I(X_1 > x) \cdot w(\mathbf{X}_1)\right]^2\right] - \lambda_{IM}^2(x)\right\} \qquad \text{(A.5)}
\end{aligned}$$

where each transition is obtained from:

1. Each $\mathbf{X}_i$ is independent and identically distributed with the joint distribution as $g(\mathbf{x})$.
2. Computational formula for variance.
3. Recognizing that $\nu_0 \cdot \mathbb{E}_{\mathbf{X}}\left[I(X_1 > x) \cdot w(\mathbf{X}_1)\right] = \lambda_{IM}(x)$ (see Eq A.2 in Section A.1).

The term $\mathbb{E}_{\mathbf{X}}\left[\left[I(X_1 > x) \cdot w(\mathbf{X}_1)\right]^2\right]$ in Eq A.5 may be rewritten as follows:

$$\begin{aligned}
\mathbb{E}_{\mathbf{X}}\left[\left[I(X_1 > x) \cdot w(\mathbf{X}_1)\right]^2\right] &= \int_{\mathbf{s}} \left[I(s > x) \cdot w(\mathbf{s})\right]^2 \, g(\mathbf{s}) \, \mathrm{d}\mathbf{s} \\
&= \int_{\mathbf{s}} \left[I(s > x) \cdot w^2(\mathbf{s})\right] \, g(\mathbf{s}) \, \mathrm{d}\mathbf{s} \\
&= \int\limits_{\mathbf{s}:s>x} \frac{f^2(\mathbf{s})}{g(\mathbf{s})} \, \mathrm{d}\mathbf{s} \qquad \text{(A.6)}
\end{aligned}$$

where each transition is obtained from:

1. Rule of the lazy statistician.
2. Square of the indicator function is the indicator function.
3. Definitions of the indicator function and of the Importance Sampling weight.

Substituting Eq A.6 into Eq A.5 gives

$$\mathbb{V}_{\mathbf{X}}\left[\widehat{\lambda}_{IM}(x)\right] = \frac{1}{n}\left\{\nu_0^2 \int\limits_{\mathbf{s}:s>x} \frac{f^2(\mathbf{s})}{g(\mathbf{s})} \, \mathrm{d}\mathbf{s} - \lambda_{IM}^2(x)\right\} \qquad \text{(A.7)}$$

A.4 Derivation for Eq 4.9

The variance of $\widehat{\lambda}_{EDP}(z)$ in Eq A.3, with respect to the joint distribution of Z and $\mathbf{X}$, is

$$\begin{aligned}
\mathbb{V}_{Z,\mathbf{X}}\left[\widehat{\lambda}_{EDP}(z)\right] &= \frac{\nu_0^2}{n}\cdot\mathbb{V}_{Z,\mathbf{X}}\left[I(Z_1>z)\cdot w(\mathbf{X}_1)\right] \\
&= \frac{\nu_0^2}{n}\left\{\mathbb{E}_{Z,\mathbf{X}}\left[\left[I(Z_1>z)\cdot w(\mathbf{X}_1)\right]^2\right]-\left(\mathbb{E}_{Z,\mathbf{X}}\left[I(Z_1>z)\cdot w(\mathbf{X}_1)\right]\right)^2\right\} \\
&= \frac{1}{n}\left\{\nu_0^2\cdot\mathbb{E}_{Z,\mathbf{X}}\left[\left[I(Z_1>z)\cdot w(\mathbf{X}_1)\right]^2\right]-\lambda_{EDP}^2(z)\right\} \qquad \text{(A.8)}
\end{aligned}$$

where each transition is obtained from:

1. Each i^{th} vector $(\mathbf{X},Z)_i$ is independent and identically distributed, with the joint distribution as $g_{Z,\mathbf{X}}(t,\mathbf{s}) = f_{Z|\mathbf{X}}(t\mid\mathbf{s})\cdot g(\mathbf{s})$.
2. Computational formula for variance.
3. Recognizing that $\nu_0\cdot\mathbb{E}_{Z,\mathbf{X}}\left[I(Z_1>z)\cdot w(\mathbf{X}_1)\right]=\lambda_{EDP}(z)$ (see Eq A.4 in Section A.2).

The term $\mathbb{E}_{Z,\mathbf{X}}\left[\left[I(Z_1>z)\cdot w(\mathbf{X}_1)\right]^2\right]$ in Eq A.8 may be rewritten as follows:

$$\begin{aligned}
\mathbb{E}_{Z,\mathbf{X}}\left[\left[I(Z_1>z)\cdot w(\mathbf{X}_1)\right]^2\right] &= \int_{\mathbf{s}}\int_t \left[I(t>z)\cdot w(\mathbf{s})\right]^2 g_{Z,\mathbf{X}}(t,\mathbf{s})\,\mathrm{d}t\,\mathrm{d}\mathbf{s} \\
&= \int_{\mathbf{s}}\int_t \left[I(t>z)\cdot w^2(\mathbf{s})\right]\left[f_{Z|\mathbf{X}}(t\mid\mathbf{s})\,g(\mathbf{s})\right]\mathrm{d}t\,\mathrm{d}\mathbf{s} \\
&= \int_{\mathbf{s}}\int_t \left[I(t>z)\cdot\frac{f^2(\mathbf{s})}{g(\mathbf{s})}\right] f_{Z|\mathbf{X}}(t\mid\mathbf{s})\,\mathrm{d}t\,\mathrm{d}\mathbf{s} \\
&= \int_{\mathbf{s}}\left[\int_t I(t>z)\cdot f_{Z|\mathbf{X}}(t\mid\mathbf{s})\,\mathrm{d}t\right]\frac{f^2(\mathbf{s})}{g(\mathbf{s})}\,\mathrm{d}\mathbf{s} \\
&= \int_{\mathbf{s}}\Pr(Z>z\mid\mathbf{X}=\mathbf{s})\cdot\frac{f^2(\mathbf{s})}{g(\mathbf{s})}\,\mathrm{d}\mathbf{s} \qquad \text{(A.9)}
\end{aligned}$$

where each transition is obtained from:

1. Rule of the lazy statistician.
2. Square of the indicator function is the indicator function and definition of joint distribution $g_{Z,\mathbf{X}}(t,\mathbf{s})$.
3. Definition of the Importance Sampling weight.
4. The ratio $\frac{f^2(\mathbf{s})}{g(\mathbf{s})}$ does not depend on t.
5. Definition of conditional CCDF of $Z\mid X$.

Substituting Eq A.9 into Eq A.8 gives

$$\mathbb{V}_{Z,\mathbf{X}}\left[\widehat{\lambda}_{EDP}(z)\right] = \frac{1}{n}\left\{\nu_0^2 \int_{\mathbf{s}} \Pr(Z > z \mid \mathbf{X} = \mathbf{s}) \cdot \frac{f^2(\mathbf{s})}{g(\mathbf{s})}\, \mathrm{d}\mathbf{s} - \lambda_{EDP}^2(z)\right\} \tag{A.10}$$

The variance of the hazard curve estimates for IMs that are excluded from those chosen to select ground motions (i.e., $IM \notin \mathbf{IM}$) may be derived in a fashion similar to that presented in this section.

A.5 Derivation for Eq 4.15

Given an observed value of the vector-valued IM from the Importance Function, $\mathbf{IM}_{IF}$, and a computed value of the vector-valued IM from the scaled ground motion time series, $\mathbf{IM}_P$, the optimal scale factor can be derived by first rewriting Eq 4.13 to express Δ as a quadratic function of the scale factor, SF. Substituting Eq 4.14 into Eq 4.13 and rearranging terms gives

$$\Delta = \sum_{j=1}^{N_{IM}} \left[\frac{\ln\left(\frac{IM_{IF,j}}{IM_{U,j}}\right) - \alpha_j \ln(SF)}{\sigma_j}\right]^2 \tag{A.11}$$

Setting the first derivative of Δ with respect to SF to zero leads to the scale factor that minimizes Δ:

$$\frac{\partial \Delta}{\partial SF} = \sum_{j=1}^{N_{IM}} 2\left[\frac{\ln\left(\frac{IM_{IF,j}}{IM_{U,j}}\right) - \alpha_j \ln(SF)}{\sigma_j}\right]\left(\frac{-\alpha_j}{\sigma_j \cdot SF}\right) = 0 \tag{A.12}$$

Assuming SF is never zero, Eq A.12 is equivalent to:

$$\sum_{j=1}^{N_{IM}} \left[\frac{\ln\left(\frac{IM_{IF,j}}{IM_{U,j}}\right) - \alpha_j \ln(SF)}{\sigma_j}\right]\left(\frac{\alpha_j}{\sigma_j}\right) = 0 \tag{A.13}$$

Distributing the summation in Eq A.13 and rearranging terms gives

$$\sum_{j=1}^{N_{IM}} \left(\frac{\alpha_j}{\sigma_j^2}\right) \ln\left(\frac{IM_{IF,j}}{IM_{U,j}}\right) = \ln(SF)\left[\sum_{i=j}^{N_{IM}} \left(\frac{\alpha_j}{\sigma_j}\right)^2\right] \tag{A.14}$$

Finally, isolating SF in Eq A.14 leads to the desired optimal scale factor:

$$SF_{optimal} = \exp\left\{\frac{\sum_{j=1}^{N_{IM}} \left(\frac{\alpha_j}{\sigma_j^2}\right) \ln\left(\frac{IM_{IF,j}}{IM_{U,j}}\right)}{\sum_{j=1}^{N_{IM}} \left(\frac{\alpha_j}{\sigma_j}\right)^2}\right\} \tag{A.15}$$

Appendix B

Documentation of developing benchmark-consistent prediction models

This appendix documents the development of benchmark-consistent prediction models that are needed to select ground motions within a universe of synthetic ground motions generated from a stochastic model. For both stochastic models – Rezaeian's and Yamamoto's – a total of 120 intensity measures (IMs) were considered. These IMs include 5%-damped spectral accelerations at the same vibration periods utilized in the NGA West 2 project [92] (i.e., a total of 111 periods ranging from 0.01 to 20 sec), peak ground acceleration (PGA), peak ground velocity (PGV), peak ground displacement (PGD), cumulative absolute velocity (CAV), acceleration spectrum intensity (ASI), spectrum intensity (SI), displacement spectrum intensity (DSI), 5-95% significant duration (D_{5-95}), and 5-75% significant duration (D_{5-75}).

B.1 Functional forms

To facilitate the development of functional forms, the 120 IMs were partitioned into four categories: (i) spectral accelerations, (ii) peak ground parameters (PGA, PGV, and PGD), (iii) spectrum intensity related parameters (ASI, SI, and DSI), and (iv) cumulative based measures (CAV, D_{5-95}, and D_{5-75}). For each category and each stochastic model, a polynomial-based functional form (see Eq 3.13) was determined via the approach described in Section 3.6. In Rezaeian's model, the following functional forms were employed:

1. Spectral accelerations: linear
2. Peak ground parameters: linear
3. Spectrum intensity related parameters: linear

4. Cumulative based measures: cubic

In Yamamoto's model, the following functional forms were employed:

1. Spectral accelerations: purequadratic
2. Peak ground parameters: purequadratic
3. Spectrum intensity related parameters: purequadratic
4. Cumulative based measures: cubic

Fig 3.6 illustrated the linear and purequadratic functional forms; the cubic functional form is illustrated in Fig B.1. The determination of $\sigma_{optimal}$ is discussed next.

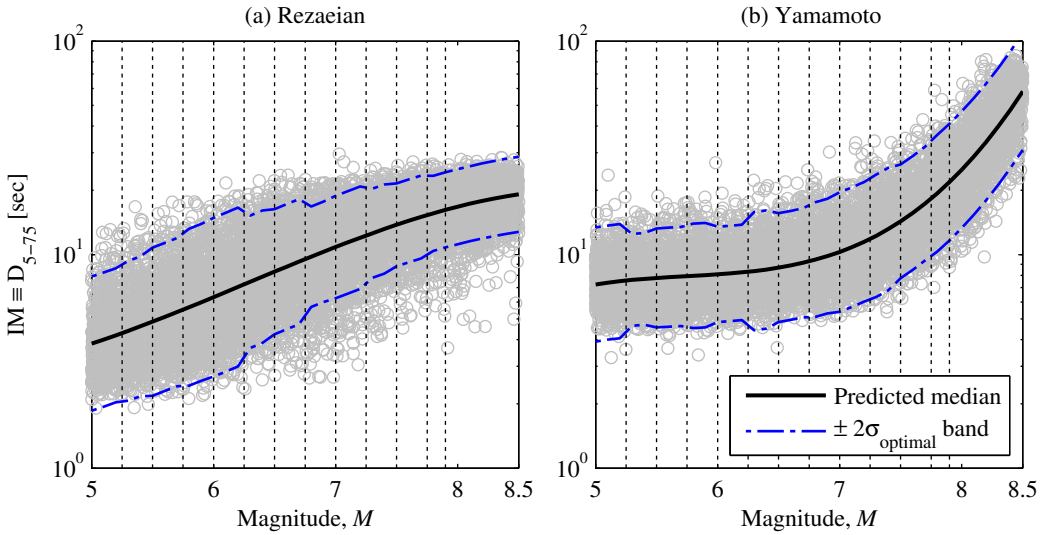

Figure B.1: Functional form for D_{5-75} under stochastic model from: (a) Rezaeian; (b) Yamamoto.

B.2 Benchmark consistency of ground motion prediction models

Once the functional forms for all 120 IMs are finalized via exploratory data analysis, the standard deviations, σ, of the ground motion prediction models (GMPMs) were further adjusted to achieve consistency with respect to the benchmark, as elaborated in Section 3.6. In essence, the standard deviation is modeled as a nonparametric function of magnitude and at each magnitude interval, the value of σ was adjusted so that the GMPM-based estimate of the hazard curve agrees closely with the benchmark hazard curve (see Fig 3.7a). Figs B.2-B.19 document such hazard-consistent GMPMs for IMs unrelated to spectral accelerations.

B.3 Correlations between IMs

The correlation between IMs (more precisely, between the residuals of the IMs) were discussed in Section 3.6. As mentioned therein, the correlations were occasionally found to depend on the earthquake magnitude. For generality, the correlation between a pair of IMs is modeled as a function of the magnitude by computing a correlation for each magnitude interval shown schematically by the dotted lines in Fig B.1. The correlations between spectral accelerations at various vibration periods were shown in Fig 3.8; correlations between IMs that are unrelated to spectral accelerations were also computed.

B.4 Figures for confirming benchmark consistency

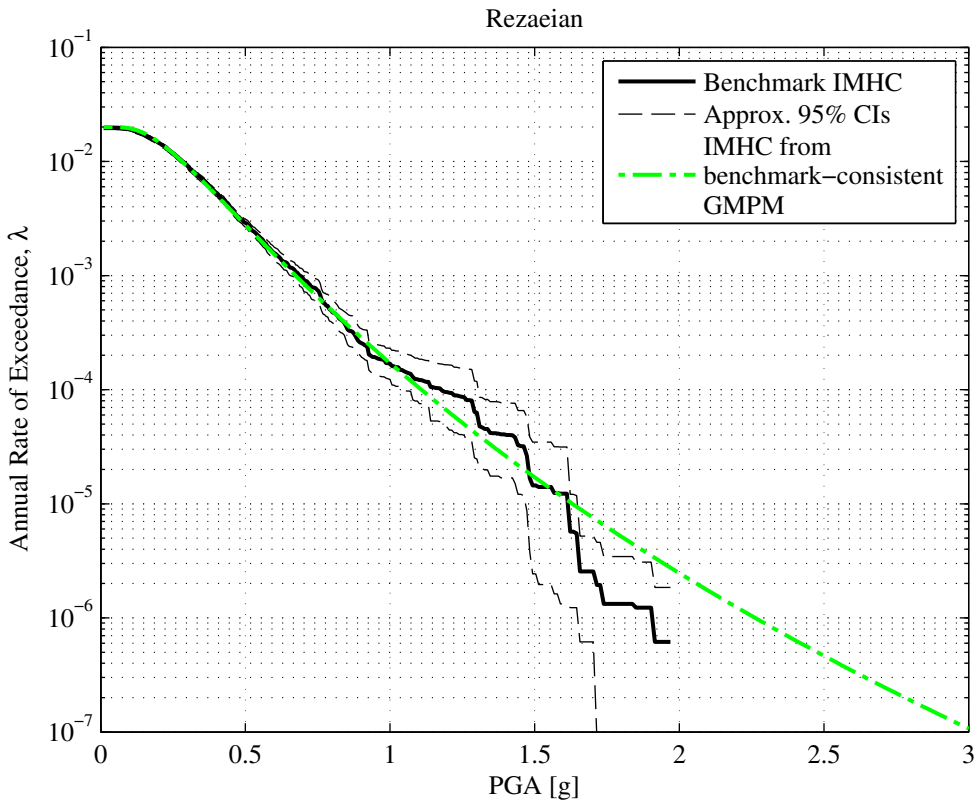

Figure B.2: Benchmark-consistency of GMPM for PGA under Rezaeian's stochastic model.

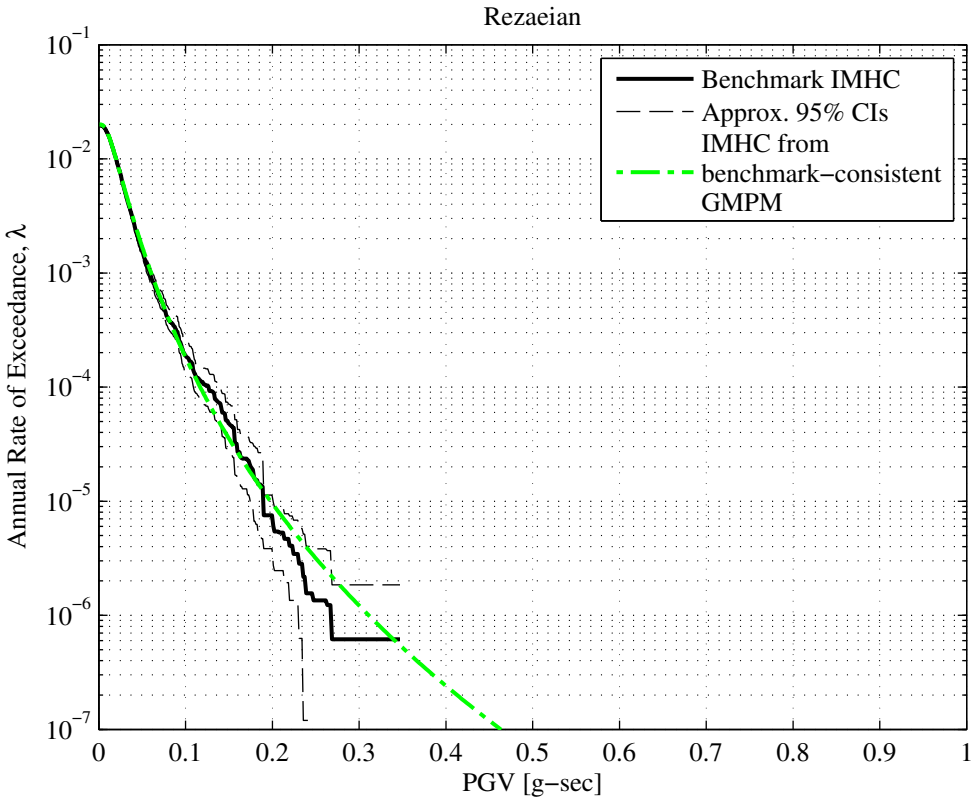

Figure B.3: Benchmark-consistency of GMPM for PGV under Rezaeian's stochastic model.

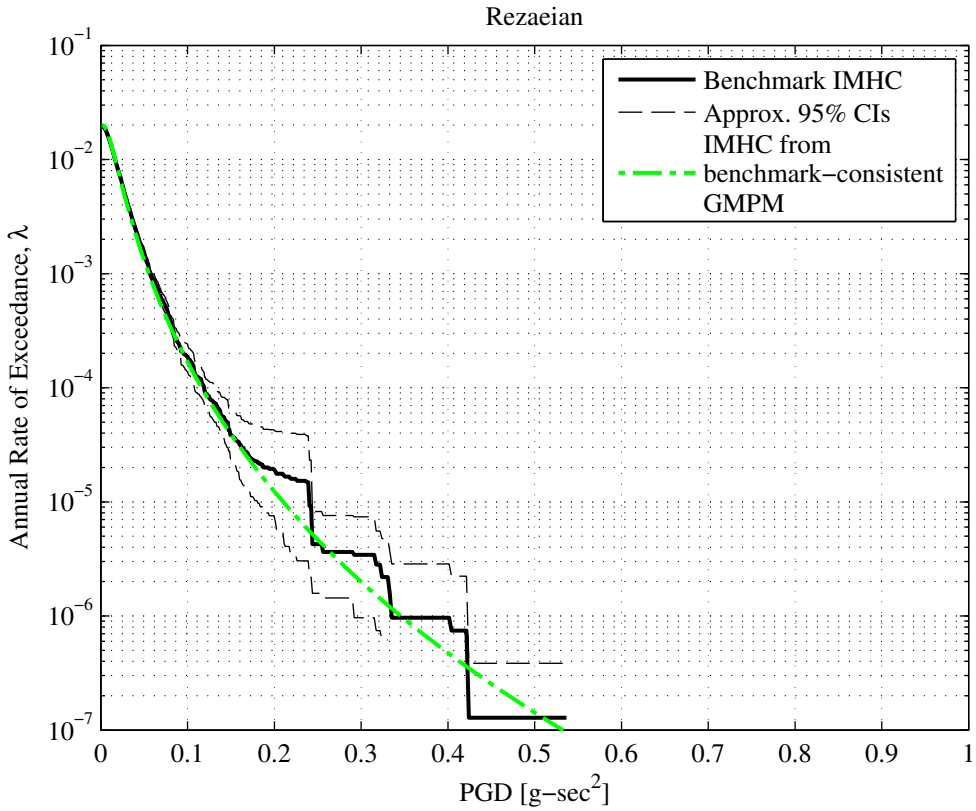

Figure B.4: Benchmark-consistency of GMPM for PGD under Rezaeian's stochastic model.

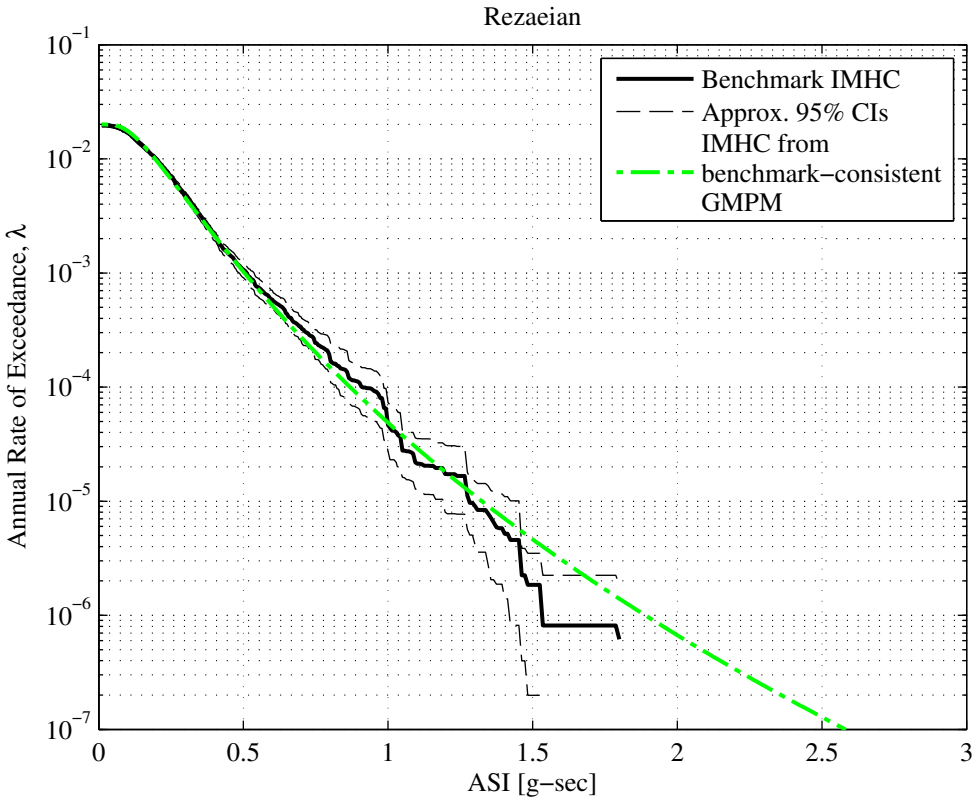

Figure B.5: Benchmark-consistency of GMPM for ASI under Rezaeian's stochastic model.

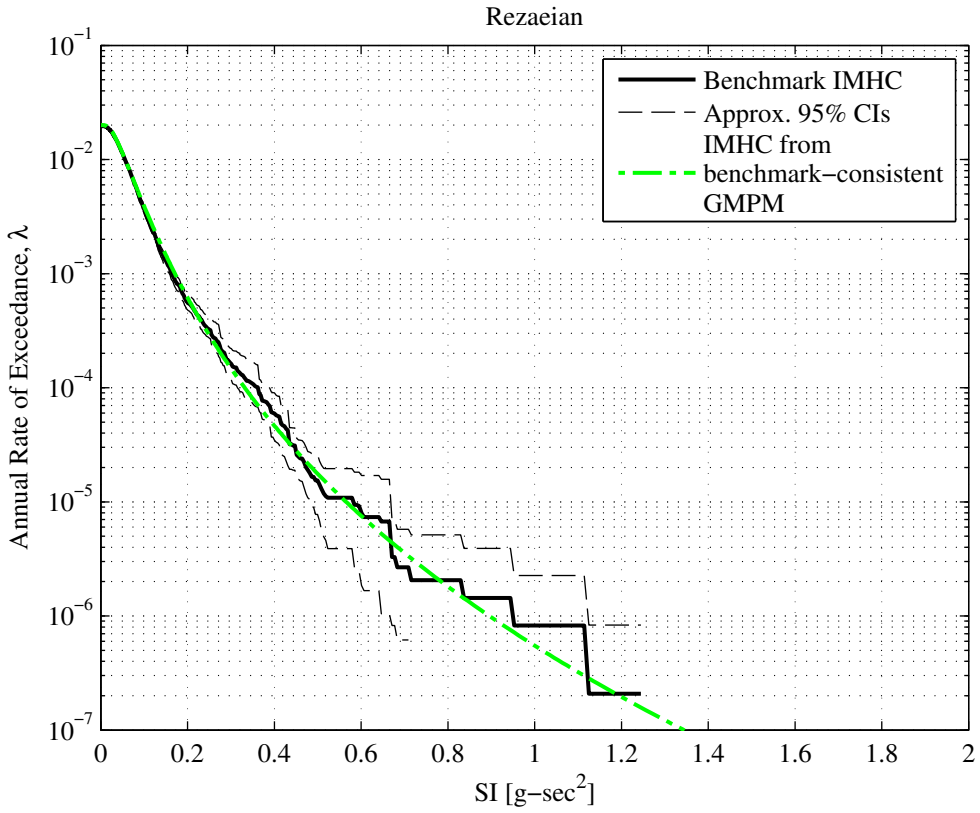

Figure B.6: Benchmark-consistency of GMPM for SI under Rezaeian's stochastic model.

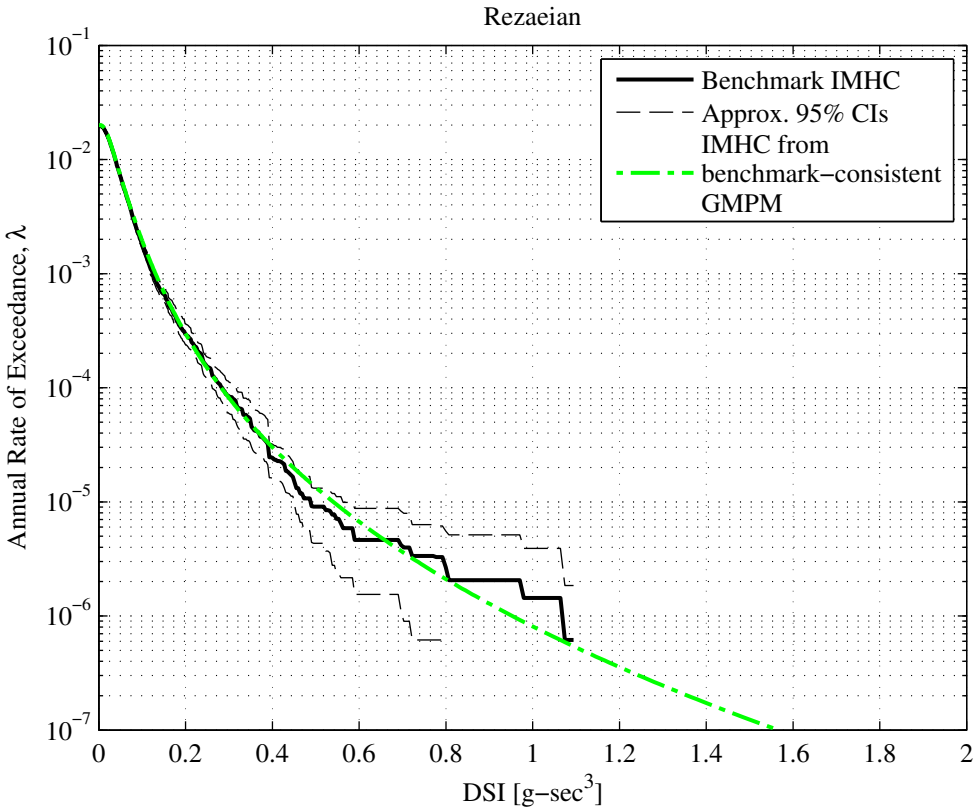

Figure B.7: Benchmark-consistency of GMPM for DSI under Rezaeian's stochastic model.

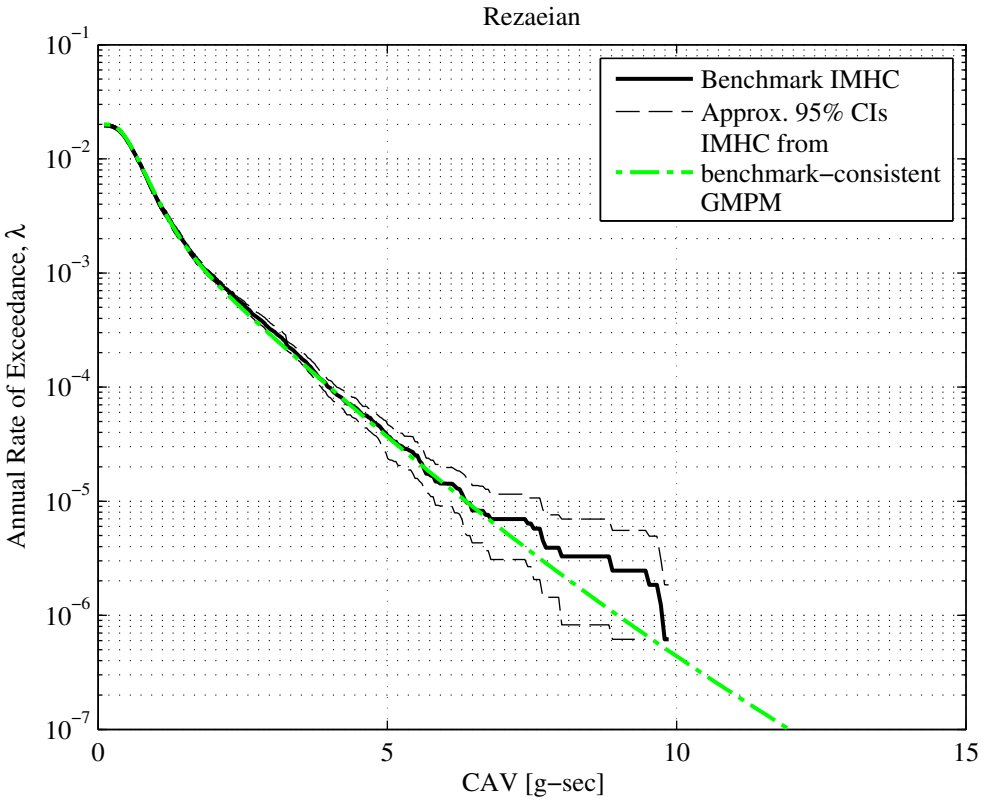

Figure B.8: Benchmark-consistency of GMPM for CAV under Rezaeian's stochastic model.

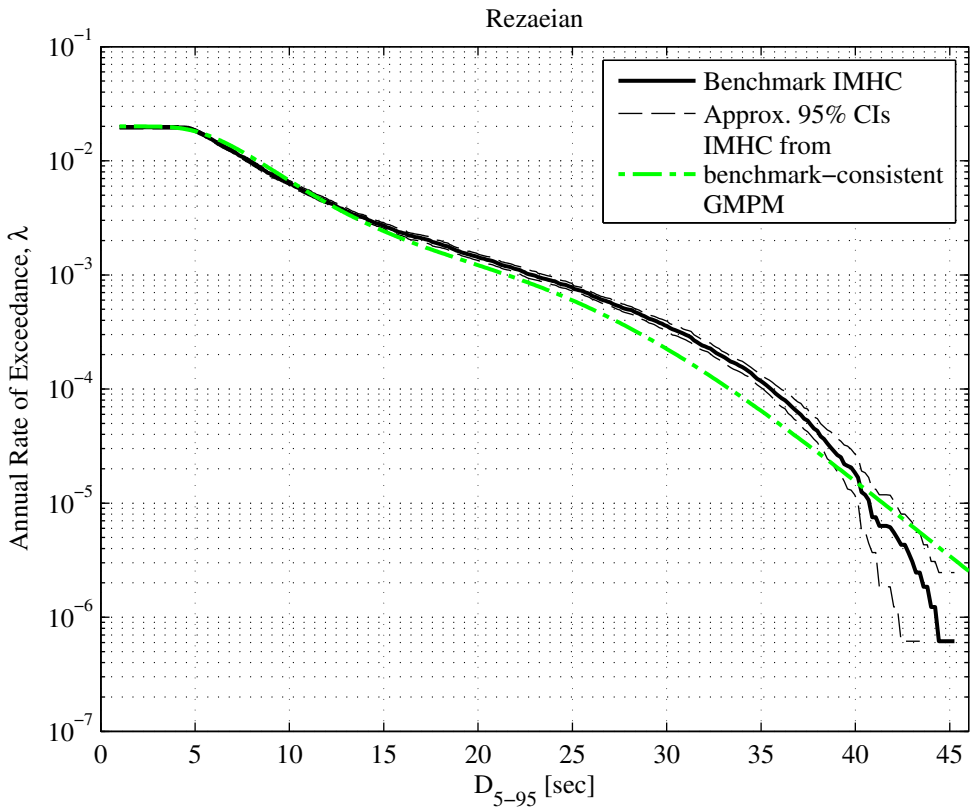

Figure B.9: Benchmark-consistency of GMPM for D_{5-95} under Rezaeian's stochastic model.

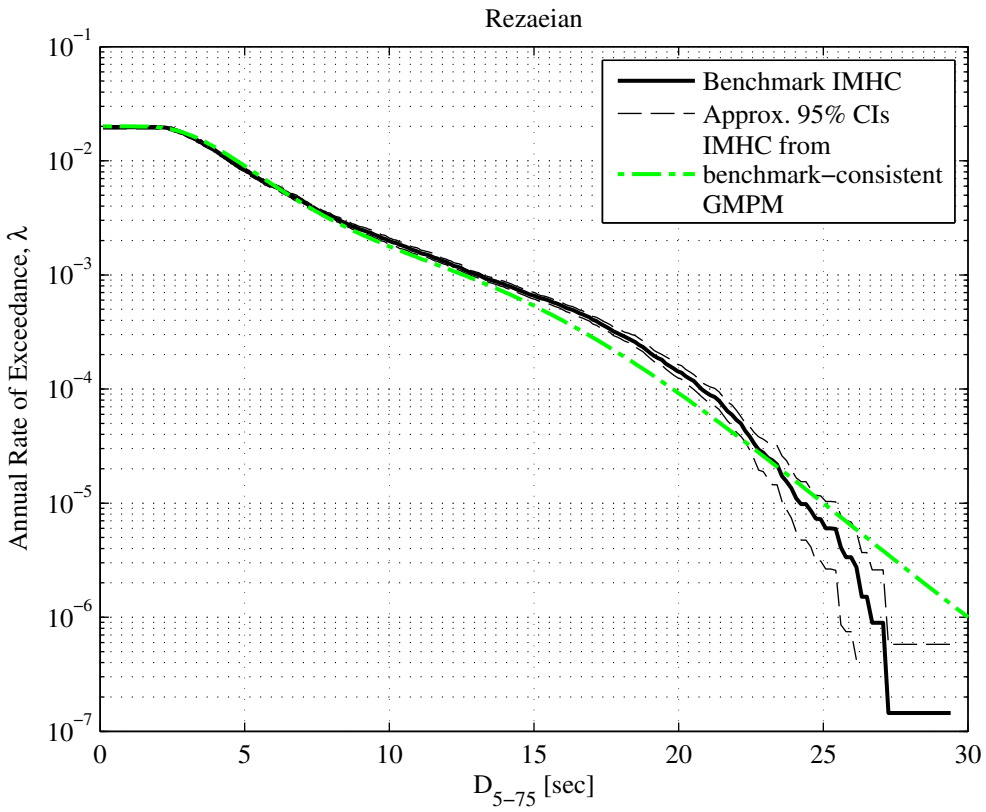

Figure B.10: Benchmark-consistency of GMPM for D_{5-75} under Rezaeian's stochastic model.

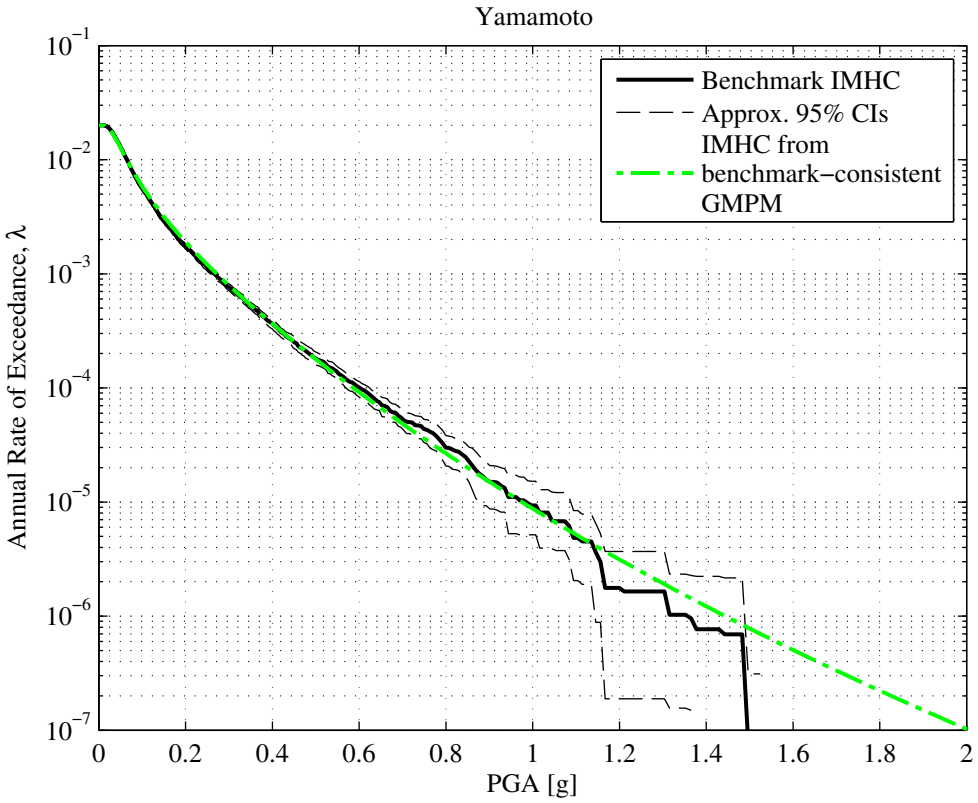

Figure B.11: Benchmark-consistency of GMPM for PGA under Yamamoto's stochastic model.

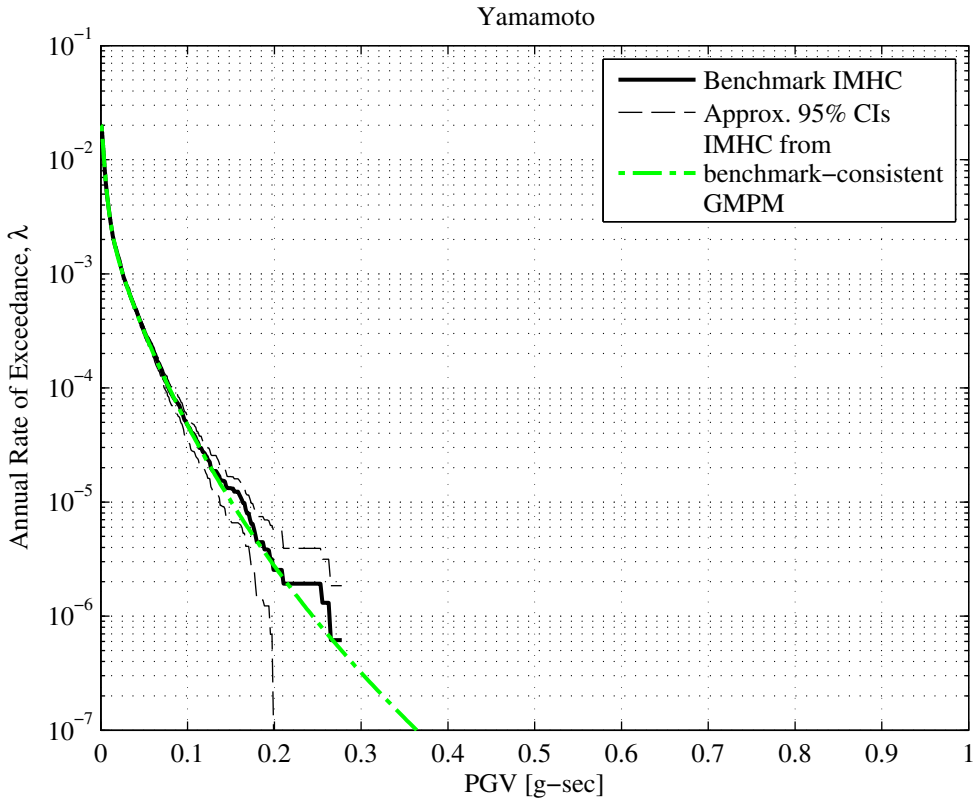

Figure B.12: Benchmark-consistency of GMPM for PGV under Yamamoto's stochastic model.

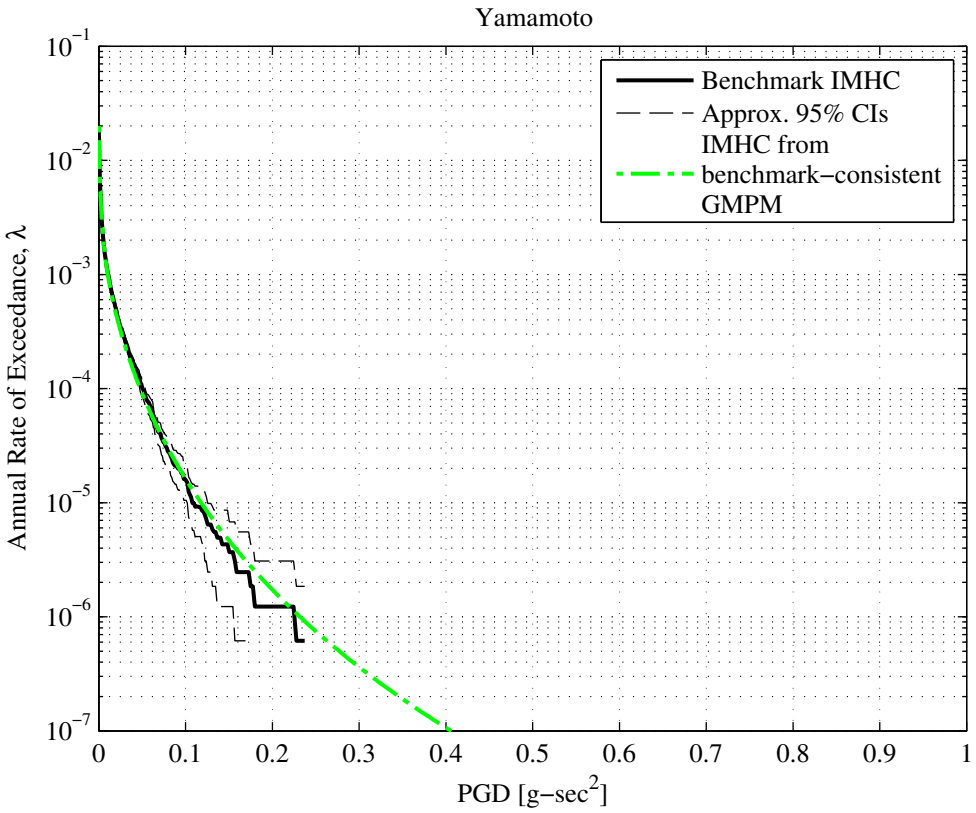

Figure B.13: Benchmark-consistency of GMPM for PGD under Yamamoto's stochastic model.

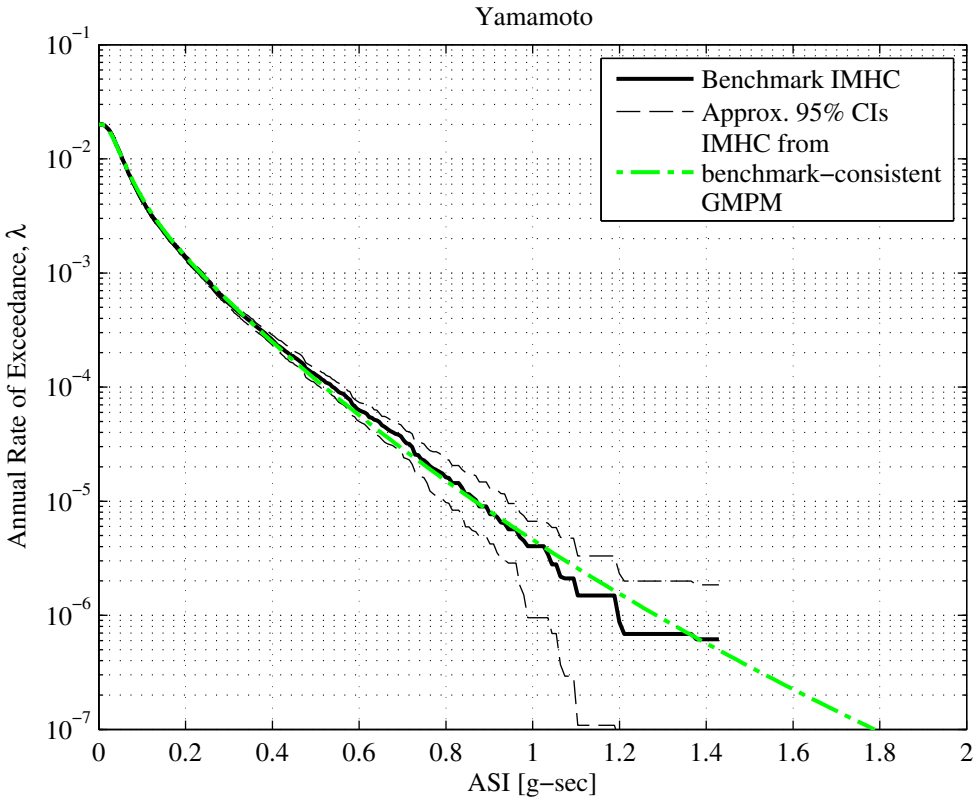

Figure B.14: Benchmark-consistency of GMPM for ASI under Yamamoto's stochastic model.

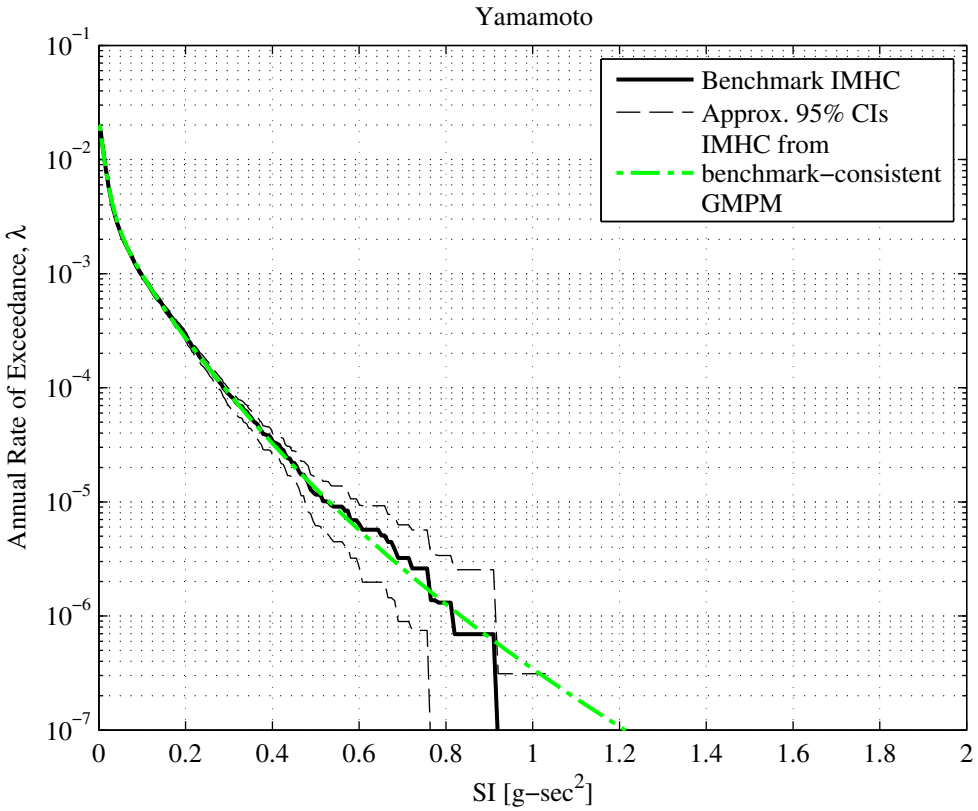

Figure B.15: Benchmark-consistency of GMPM for SI under Yamamoto's stochastic model.

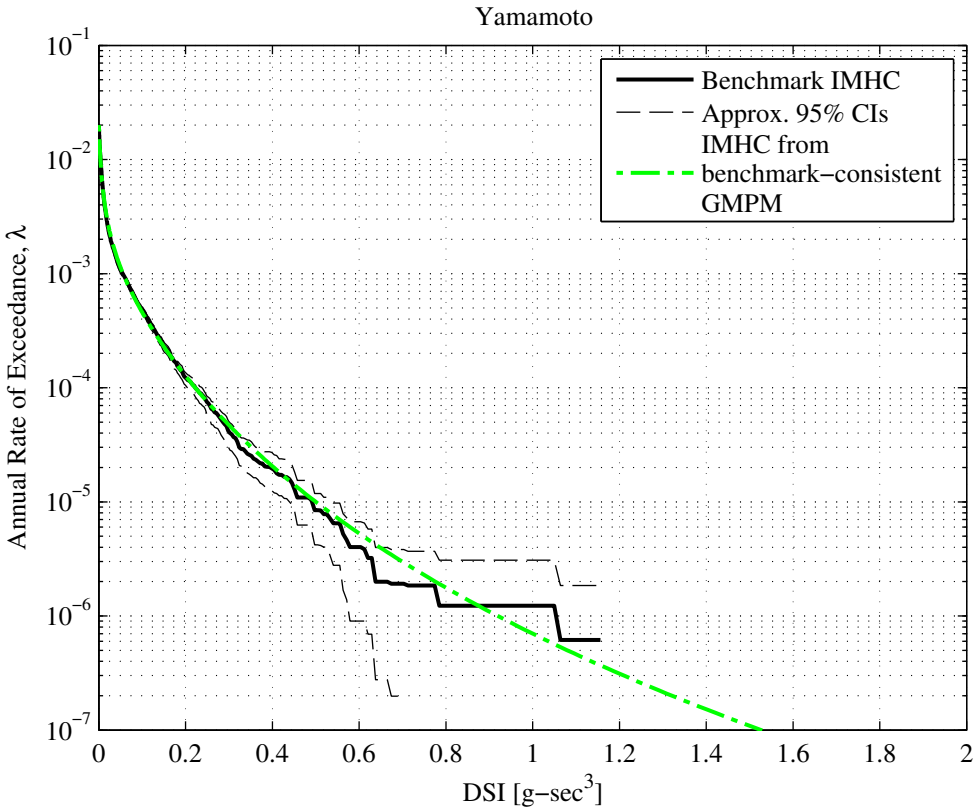

Figure B.16: Benchmark-consistency of GMPM for DSI under Yamamoto's stochastic model.

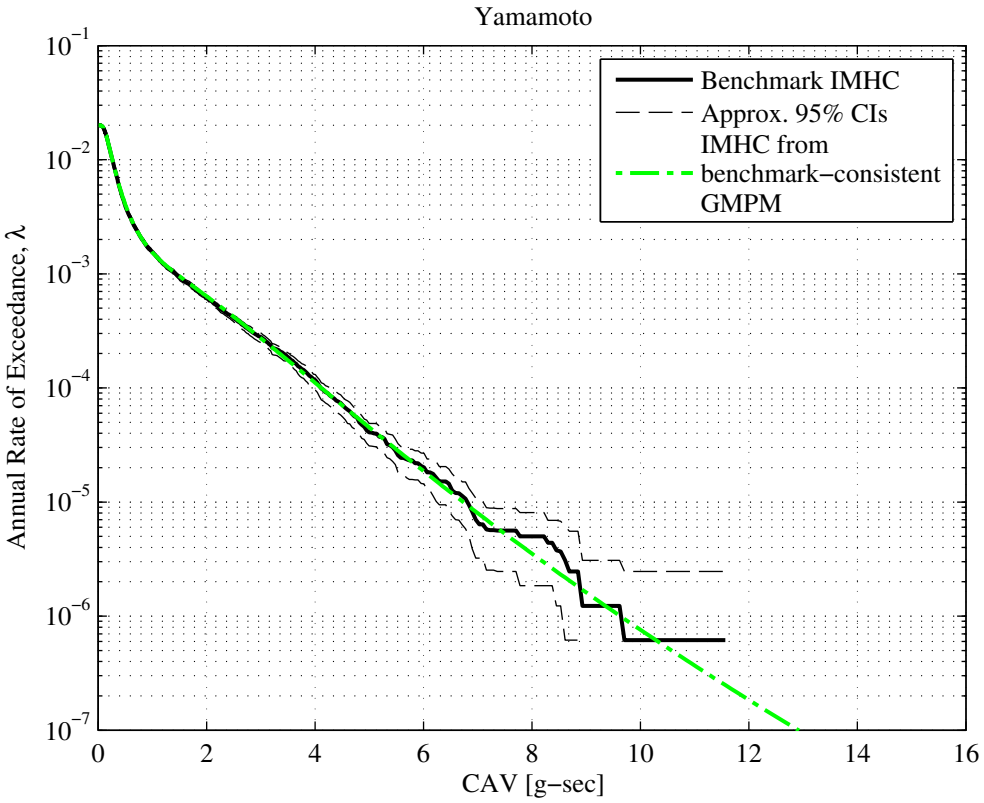

Figure B.17: Benchmark-consistency of GMPM for CAV under Yamamoto's stochastic model.

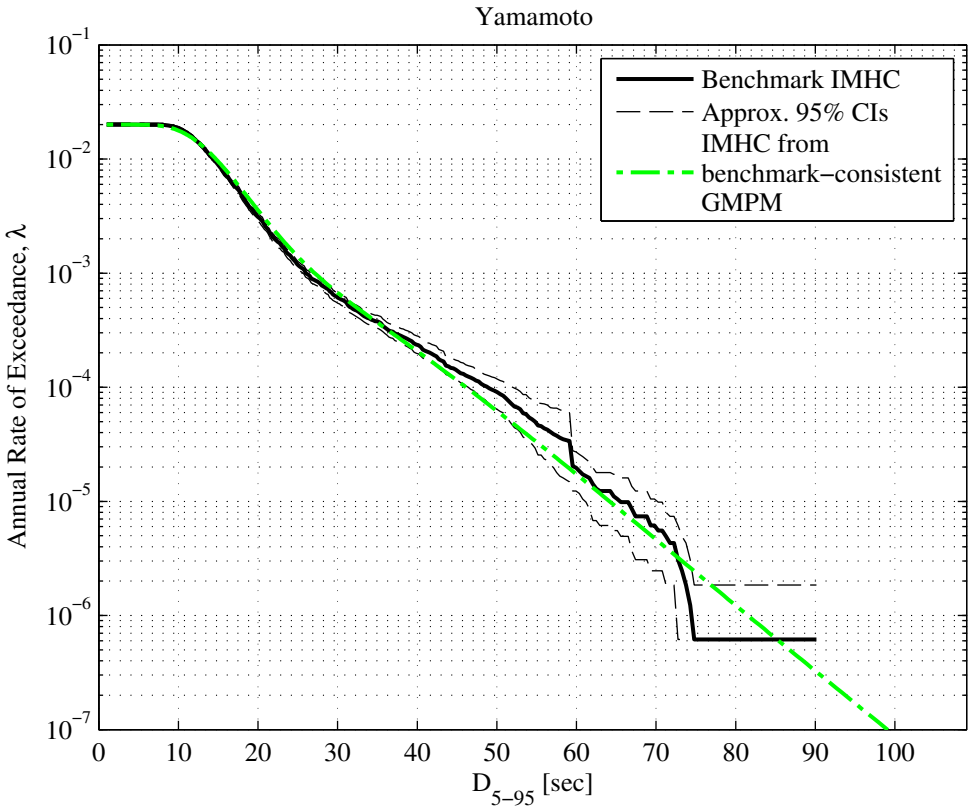

Figure B.18: Benchmark-consistency of GMPM for D_{5-95} under Yamamoto's stochastic model.

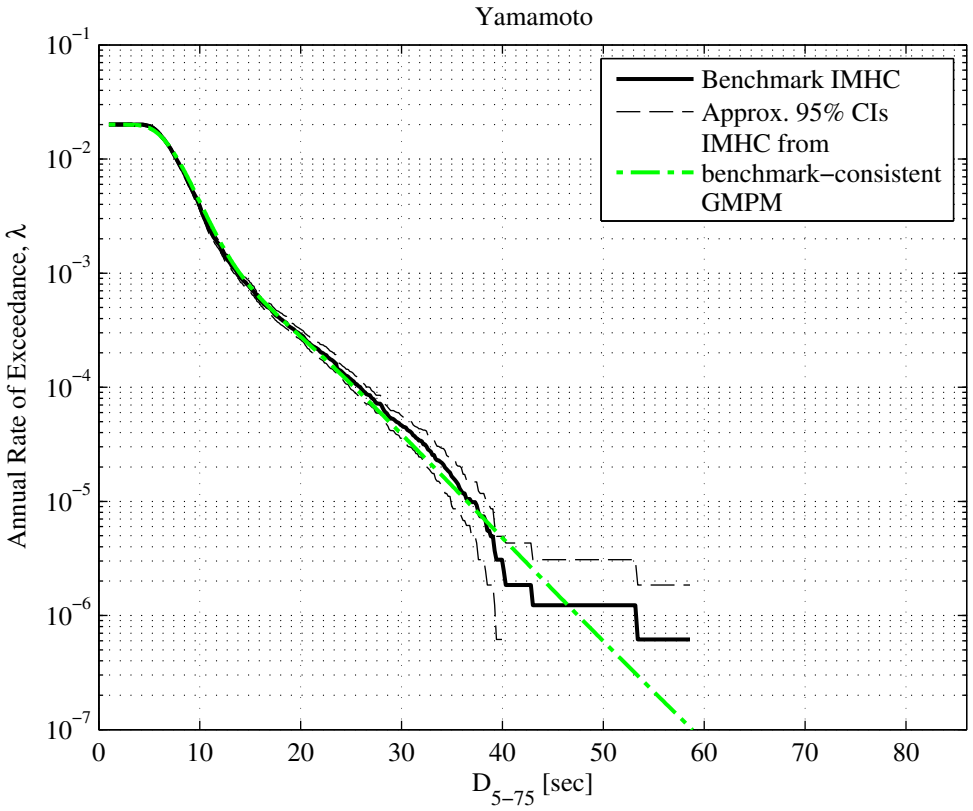

Figure B.19: Benchmark-consistency of GMPM for D_{5-75} under Yamamoto's stochastic model.